On the dynamics of the Trojan asteroids

Frederic Gabern Guilera

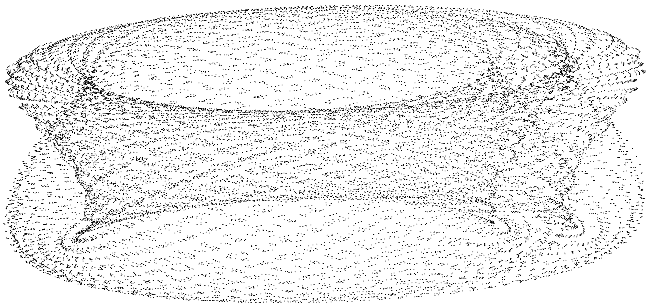

Departament de Matemàtica Aplicada i Anàlisi
Universitat de Barcelona

Programa de doctorat de Matemàtica Aplicada i Anàlisi.
Bieni 1997-99.

Memòria presentada per aspirar al grau de
Doctor en Matemàtiques per la Universitat
de Barcelona.

Certifico que la present memòria ha estat
realitzada per en Frederic Gabern Guilera
i dirigida per mi.

Barcelona, 3 de març de 2003

Àngel Jorba i Monte

Als meus pares, al meu germà i a la Maria

Preface

The Trojans are a group of asteroids that move in a neighbourhood of the triangular points of the Sun-Jupiter system. The goal of this thesis is to go deeply into the knowledge of the dynamical properties of their motion.

Some of the known results on this subject use, as the model for their dynamics, the well-celebrated Restricted Three Body Problem (RTBP). In this model, it is assumed that the Sun and Jupiter are punctual masses that revolve in circular orbits around their center of gravitation (following the Kepler laws), and that the motion of the asteroid is given by the gravitational attraction of these masses.

The first purpose of this work is to develop some other models for the motion of the asteroid. In these models, we take into account the main perturbations into the RTBP, that mainly come from the eccentricity of Jupiter's orbit and from the perturbation that other planets (such as Saturn and Uranus) causes to Jupiter's motion.

The second purpose is to make a semi-analytic study of the models. By means of standard (for simpler cases) techniques, such as normal forms or approximated first integrals, we describe the local non-linear dynamics around the triangular points. The main novel aspect of the application of these techniques to the developed models is the implementation of the symplectic reducibility of the (periodic and quasi-periodic) time-dependent equations. Another important application of these techniques is the computation of a zone of effective stability, that is a zone of the phase space where a particle remains at least the expected lifetime of the Solar System.

The third purpose is to redo a numerical study of the dynamical properties of the Trojan orbits in a more "realistic" model and to compare it with the semi-analytical models. We use, as most of astronomers do when they study this problem, the Outer Solar System (OSS). That is, the N-body problem formed by the Sun, Jupiter, Saturn, Uranus, Neptune and the massless particle. This study is based on the frequency analysis of long (about 5 Millions of years) integrations of the Trojan orbits. In order to produce such long integrations with a good accuracy, a symplectic integrator has been used.

The thesis has been organized as follows: in the first chapter, we give an extensive introduction to the problem. In chapter two, a periodic perturbation of the RTBP (that comes from introducing the effect of Saturn into the problem) is developed and studied in detail. In the third chapter, the eccentricity of Jupiter is taken into account giving rise to a model that is a periodic perturbation of the RTBP and that contains an intrinsic resonance, showing up new dynamical features. In chapter four, two quasi-periodic perturbations of the RTBP are presented. The first one is constructed in order to include both the effect of Saturn and the eccentricity of Jupiter's orbit. In the second one, the effect of Saturn and Uranus are taken into account. In the fifth chapter, we show the results of the frequency analysis of the orbits generated by a symplectic integration of the actual positions and velocities of 420 Trojans in the OSS, we also compute the proper frequencies of the asteroids in the semi-analytical models and we compare them with the results obtained in the former OSS study.

Acknowledgements

First of all, I want to sincerely thank my thesis advisor, Àngel Jorba, for the time and effort that he has spent with me during the achievement of this work. I wish also to emphasize his teaching capacity that has allowed me to get initialized in the exciting world of Celestial Mechanics and to learn several numerical techniques that are very helpful when studying dynamical systems.

I thank the Department of Applied Mathematics and Analysis of the University of Barcelona, for let me use the necessary resources in order this work to be achieved, and all the partners (actual and old ones) that have helped me somehow. I would like to specially mention the friends Gerard Albà, Miquel Àngel Andreu, Imma Baldomà, Heri Coll, Àlex Haro, Xavi Massaneda, Eva Miranda, Quim Ortega, Laura Prat, Javi Rodríguez, Xavi Tolsa i Joan Vidal.

I thank Josep Maria Mondelo to let me use his frequency analysis routine that has helped me to check some results.

I thank the "Institut de Mécanique Céleste et de Calcul des Éphémerides" of Paris, for welcoming me in two stays of research where I started to learn the techniques used in Chapter 5 and very specially to the person I worked with, Philippe Robutel.

I thank Nati, the Department's secretary, for the numerous bureaucratic tasks that she has done for me.

I want also to say two words of gratitude to the person who encouraged me to join the Department and, somehow, is in part responsible that this thesis has been carried out, but unfortunately he is not with us anymore, August Palanques.

Outside the work's context, I thank my Avinyonet's friends for all the funny moments that we have had together and my friends of "Efecte Bandwagon" and "BeatleStones" for the great "musical moments" that we have lived on the stages and, specially, out of them.

Finally, there are no words to thank my grandparents, my parents, my brother and Maria for everything that they have done for me. Without their support, this work would have never been done.

Contents

Chapter 1

Introduction

Let us start by introducing the well known Restricted Three Body Problem (from now on, RTBP). The RTBP models the motion of a particle under the gravitational attraction of Jupiter and Sun (also called primaries), under the following assumptions: i) the particle is so small that it does not affect the motion of Jupiter and Sun; and ii) Jupiter and Sun are point masses that revolve in circular orbits around their common centre of mass. It is usual to take a rotating reference frame with the origin at the centre of mass, and such that Sun and Jupiter are kept fixed on the x axis, the (x, y) plane is the plane of motion of the primaries, and the z axis is orthogonal to the (x, y) plane. These coordinates are sometimes called synodical. The usual (adimensional) units are chosen as follows: the unit of distance is the Sun–Jupiter distance, the unit of mass is the total Sun–Jupiter mass, and the unit of time is such that the period of Jupiter around the Sun equals 2π. With this selection of units, it turns out that the gravitational constant is also equal to 1. Defining momenta as $p_x = \dot{x} - y$, $p_y = \dot{y} + x$ and $p_z = \dot{z}$, the equations of motion for the particle can be written as an autonomous Hamiltonian system with three degrees of freedom. The corresponding Hamiltonian function is

$$H_{RTBP} = \frac{1}{2}(p_x^2 + p_y^2 + p_z^2) + yp_x - xp_y - \frac{1-\mu}{r_{PS}} - \frac{\mu}{r_{PJ}},$$

where μ the mass of Jupiter (in adimensional units), $r_{PS}^2 = (x-\mu)^2 + y^2 + z^2$ is the distance from the particle to the Sun, and $r_{PJ}^2 = (x-\mu+1)^2 + y^2 + z^2$ is the distance from the particle to Jupiter. The details can be found in almost any textbooks on Celestial Mechanics (for instance, see [MH92, Sze67]).

It is also well known that, in these –rotating– coordinates, the RTBP has five equilibrium points (see Figure 1.1): three of them lay on the x axis (they are called collinear points, Eulerian points, or simply $L_{1,2,3}$), and the other two form an equilateral triangle (in the (x, y) plane) with Sun and Jupiter (they are called triangular points, Lagrangian points or simply $L_{4,5}$).

It is not difficult to study the linear stability of these points. The collinear points are of the type centre×centre×saddle (for all μ), while the stability of the triangular points depends on the value of μ. If μ is lower than $\mu_R = \frac{1}{2}(1 - \sqrt{23/27})$ (this value is known as the Routh mass, or Routh critical value), these points are linearly stable. On the contrary, for $\mu_R < \mu < \frac{1}{2}$, these points are unstable. The usual cases in the solar system

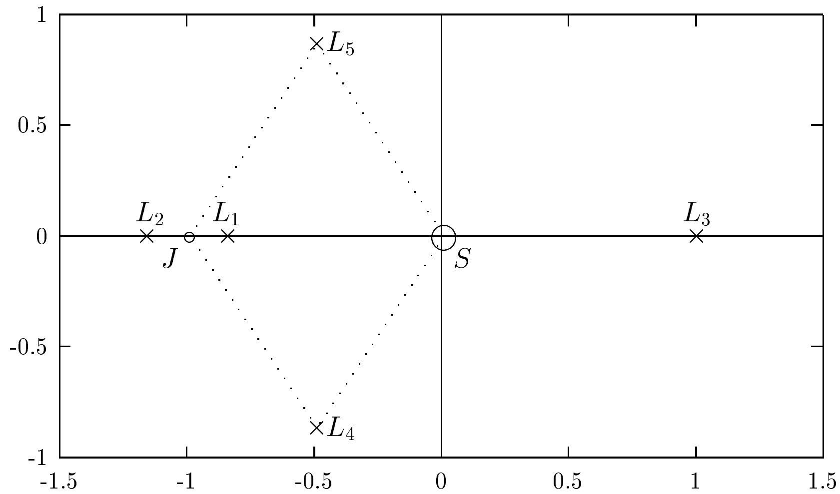

Figure 1.1: The five equilibrium points of the RTBP.

(like Sun–Jupiter or Earth–Moon) have a mass parameter lower than μ_R, so they are linearly stable ([Sze67]).

The nonlinear stability of elliptic points of conservative systems is a difficult problem. The case of two degrees of freedom is solved by the celebrated KAM theorem ([Kol54, Arn63, Mos62], see [AKN88] and [dlL01] for a survey, or [BHS96] for a presentation in a more general context), while the general case is still an open problem. On one side, a theorem by Lagrange and Dirichlet (see [AKN88], p. 271) shows that, if the Hessian of the Hamiltonian function at the equilibrium point is positive definite, then the elliptic point is stable, in the classical Lyapunov sense. On the other hand, there is also a well-known example (see [Dou88]) of a C^∞ –and not analytic– system with a linearly stable equilibrium point that is unstable for the complete system (see also [FM01] for the analytic case).

Under very general conditions, the KAM theorem can be applied to the neighbourhood of the Lagrangian points of the RTBP [Leo62, DDB67, Mar71, Mar73, MS86] to ensure the existence of many quasi-periodic motions. Each quasi-periodic trajectory fills densely a compact manifold diffeomorphic to a torus. The union of these invariant tori is a set with positive Lebesgue measure, and empty interior. In the planar case (the motion of the particle is restricted to the $z = p_z = 0$ plane, so the system only has two degrees of freedom), each torus is a two-dimensional manifold that separates the 3-D energy surface, so it acts as a confiner for the motion –this is the key point in the stability proof for two degrees of freedom Hamiltonian systems–. In the spatial case, the tori are now 3-D and the energy manifold is 5-D, so the tori cannot act as a barrier for the motion. Hence, it is possible to have trajectories that wander between these tori and escape from any vicinity of an elliptic point. The existence of such trajectories is believed to happen generically in non-integrable Hamiltonian systems. This phenomenon is known as Arnol'd diffusion since it was first conjectured by V.I. Arnol'd in [Arn64].

A different approach to the stability of Hamiltonian systems was introduced by N.N. Nekhoroshev in [Nek77]. The idea is to derive an upper bound on the diffusion velocity on an open domain of the phase space, and to show that the (possible) instability is so slow, that it does not show up in practical applications. This leads to the concept of effective stability of a given physical system: A system is considered effectively stable if the time needed to "observe" significant changes is longer than the expected lifetime of the system itself. For instance, [GDF+89] shows, among other things, the effective stability of a neighbourhood of the triangular points of the RTBP in the Sun-Jupiter case, for a time span of the order of the estimated age of the Solar system. Remarkable works in this direction are also [Sim89, CG91, BFG98]. For an application to a more general situation, see [Nie96].

We can summarise both approaches by saying that KAM theory ensures true stability (i.e., for all times) on a set of initial conditions of large Lebesgue measure but with empty interior –this set is completely filled up with quasi-periodic motions– while Nekhoroshev theory ensures the effective stability (i.e., for a finite but very long time) of an open set of initial conditions. A formal presentation of these ideas in a more general setting can be found in [JV97a].

A natural question is the persistence of these stability regions near the Lagrangian points of the Sun-Jupiter system in the real Solar system. With regard to this question it is remarkable that, in 1906, Max Wolf discovered (photographically) an asteroid (named 588 Achilles) moving near the Lagrangian point L_4 of the Sun-Jupiter system. Within a year, August Kopff had discovered two more: 617 Patroclus, located near the L_5 point, and 624 Hector near the L_4 point. It was later decided to name such asteroids after the participants in the Trojan War as given in *The Iliad* and, furthermore, to name those near the preceding (L_4) point after the Greek warriors and those near the following (L_5) point after the Trojan warriors (see Figure 1.2). With the exception of two previously named "spies" (Hector, the lone Trojan in the Greek camp, and Patroclus, the lone Greek in the Trojan camp), this tradition has been maintained. Up to now, as many as 180 Trojans had been given permanent names following this tradition (a point that taxes the efforts of those who search the pages of *The Iliad* and other works for suitable names!). At the moment (February 15th, 2003), 962 Trojan asteroids have been observed near the L_4 point and 602 near the L_5 one, and 667 have been given a permanent number. For a complete list of an (updated daily) list of the Trojan asteroids visit the URL `http://cfa-www.harvard.edu/iau/lists/JupiterTrojans.html`.

The term Trojan has been applied to any object moving near the equilateral Lagrangian points of other pairs of bodies. Searches have been made for Trojans of the Earth, Mars, Saturn and Neptune, as well as the Earth-Moon system, but so far none have been found with the exception of the Martian and Neptunian cases. It was long considered doubtful whether truly stable orbits could exist near these Lagrangian points because of perturbations by the major planets. However, in 1990 an asteroid librating the following Lagrange (L_5) point of Mars was discovered by the American astronomers David H.Levy and Henry E. Holt (see [BLH90]), thus reopening this question. Up to now, 6 Martian Trojans and 1 Neptunian Trojan (see [PMW+03]) have been observed.

The Jovian Trojan asteroids (or, at least, some of them) seem to move in a stable zone near the equilateral points. There have been many attempts to rigorously prove the stability of the motion of some of these asteroids in the RTBP, with little success (see Section 1.1). We note that, given a proof of effective stability in the RTBP, the (effective) stability of the Trojan asteroids is still an open problem, since the RTBP is not an accurate

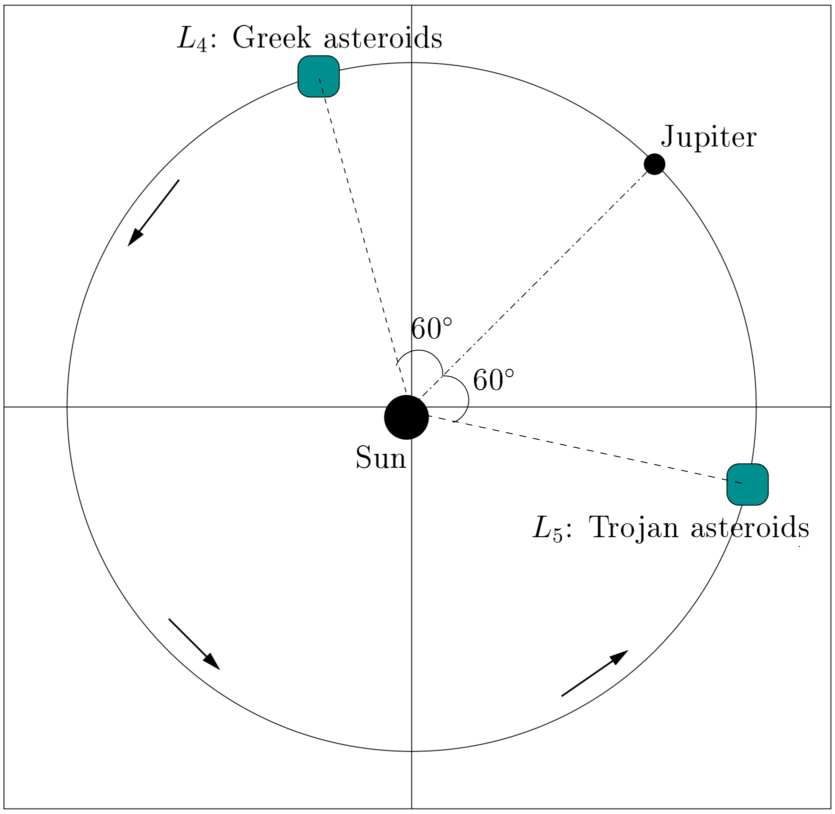

Figure 1.2: Projection into Jupiter's orbital plane of motion of the two swarms of Trojan asteroids. The Greek group (the one near the L_4 point) precedes Jupiter in their turning motion around the Sun in 60° and the Trojan group (the one near the L_5 point) follows Jupiter's orbit 60° behind.

model for the dynamics of an asteroid in the real Solar system (see Section 2.2.1).

One of the most accurate models for the dynamics of the Solar system is given by the so-called JPL ephemeris (see [JPL]). Essentially, this model is a computer file storing a sequence of interpolating polynomials for the position of all the planets; these polynomials have been derived from suitable numerical integrations of a very sophisticated model –it includes, for instance, relativistic corrections–. So, this is a numerical model, only defined for a limited time span –the longest version is only valid for 6,000 years–. Hence, it is not difficult to integrate numerically the motion of a particle in the JPL model, but it seems extremely difficult to derive theoretical results for such a complex model.

On the other hand, most of the numerical studies of the dynamical properties of the Trojan asteroids have been done by simulating their motion in the so-called Outer Solar System (OSS, from now on). This model concerns to the motion of a massless particle (an asteroid, for instance) in the gravitational field of the Sun and the four major planets of the Solar System (Jupiter, Saturn, Uranus and Neptune). Even though it is very easy to write the equations of this model, it is not so easy to obtain semi-analytical (theoretical) results for such a model. See [BJ87, SB87, Mil93, LSS97, PLDB99, TDPL00] for some numerical results for the Jovian Trojan problem in the OSS.

It seems then natural to look for a scaffolding of increasingly accurate (and increasingly complicated) models, starting at the RTBP and approaching the OSS (or the JPL) model. In each of these models we focus on some dynamical structures that we study in detail. This detailed study of features of one model can be taken as the starting point of another study in the next model in our hierarchy of accuracy. At each stage new phenomena appear. At the end we uncover some phenomena present in the most realistic model but not present (even in a qualitative form) in the most simplified one.

There are several ways to introduce intermediate models, and we will summarise some of them in the following sections. One of the goals of this work is to introduce several intermediate models, trying to take into account the effect of some other planets (such as Saturn and Uranus). These models are based on the numerical computations of true periodic and quasi-periodic orbits for the (planar) three and four body problems Sun-Jupiter-Saturn and Sun-Jupiter-Saturn-Uranus, close to the real orbit of these bodies in the Solar system. Using these orbits, it is not difficult to write the equations of motion of a particle under the gravitational attraction of the main bodies. In suitable coordinates, these equations are written as a time-dependent perturbation of the RTBP, where the time-dependence accounts for the effect of the other planets (in a periodic or quasi-periodic way). These models allow us to perform a semi-analytic study of them by means of normal form or first integrals techniques.

1.1 The restricted three body problem

As it has been explained before, this is the simplest model to study this problem. Hence, it has been used by several authors to try to show the stability of the Trojan asteroids for this model. The usual techniques are based in normal form calculations (see [GDF$^+$89, Sim89]) or first integrals ([CG91]). The first stability calculation for a Trojan can be found in [GS97], although the authors use a planar model instead of a three-dimensional one. Hence, they show the stability for the projection, on the plane of motion of Jupiter, of the position of a real Trojan. In [SD00], we can find the first stability result for the 3-D RTBP case. Although [GS97] and [SD00] papers are strongly based on numerical calculations and for this reason cannot be regarded as standard mathematical proofs, they are, in our opinion, quite close to rigorous computer-assisted proofs.

1.2 Periodic perturbations of the RTBP

The first attempt in order to build a more complex model is to include a periodic time-dependent perturbation. This one can be introduced by taking into account the eccentricity of Jupiter's orbit, or from trying to account for the main effect of Saturn on the system. In the former case, we have a (periodic time-dependent) restricted three body problem (called Elliptic RTBP) and, in the latter one, a (periodic time-dependent) restricted four body problems As we will see, there are several ways of introducing the effect of Saturn in a periodic way: the Bicircular Problem (in which the motion of Sun, Jupiter and Saturn are not supposed to be a true solution of the three body problem) or the Bicircular Coherent Problem (in which we ask the motion of Sun, Jupiter and Saturn to be coherent, that is, to be a true solution of the three body problem).

1.2.1 The elliptic restricted three body problem

An improvement over the RTBP can be done by assuming that the two main bodies revolve not on a circular orbit but on an elliptic one. This is what is known as the elliptic RTBP (see [Sze67]). In suitable coordinates, this model can be seen as a periodic time-dependent perturbation of the RTBP. The linearization of the flow around the triangular points of the RTBP model for the Sun-Jupiter case is described by the direct product of three linear oscillations, two of them are contained in the $z = p_z = 0$ plane and the third one is contained in the $x = p_x = y = p_y = 0$ plane. It is remarkable that the vertical oscillation has a frequency exactly equal to 1, for all the values of the mass parameter μ ([Sze67]). This frequency 1 corresponds to a period of 2π that is also the period of revolution of the primaries in the synodic reference system. If we look at the effect of a small eccentricity on the motion of the primaries as a periodic time-dependent perturbation of the RTBP, then the period of this perturbation will be exactly 2π –the elliptic motion of the primaries is exactly repeated after one revolution–. In other words, we have an exact 1:1 resonance between one of the linear modes around $L_{4,5}$ of the RTBP and the perturbation coming from the eccentricity of Jupiter. However, this resonance does not play any role in the linearised system, since the perturbation is uncoupled –at first order– from the “vertical mode” with frequency 1. The linear dynamics near the Lagrangian points of the elliptic RTBP has been studied by several authors (see [Dan64, Sze67]).

When one considers the nonlinear dynamics around the triangular points of the elliptic problem, the above-mentioned resonance becomes relevant, giving rise to hyperbolic, lower dimensional tori near the point. It is also worth to mention that these hyperbolic tori are not an obstruction to the existence of regions of effective stability. See [JS94] for more details.

In Chapter 3, we rebuild this model using as independent variable the physical adimensional time. This is done in order to make comparisons of the Trojan orbits with the other models. We make also a study of the non-linear dynamics by means of a truncated normal form of the Hamiltonian and we compute an approximated first integral. In this way, we are also able to compute regions of effective stability.

1.2.2 The Bicircular model

As far as we know, it was first introduced in [CRR64] to include the effect of the Sun in the Earth–Moon RTBP. This model assumes that Earth and Moon are moving as in the RTBP, but also that the centre of mass of this RTBP is moving in a circular orbit around the Sun. The three bodies are assumed to move in the same plane. Then, once the motion of these three massive bodies has been prescribed (using very simple trigonometric expressions), it is not difficult to write the force acting on an infinitesimal particle and to derive the equations of motion for such a particle. It is usual to use the same reference frame as in the RTBP: the origin is taken at the Earth-Moon barycentre, with the same axis as in the RTBP. Hence, in these coordinates, the Sun is turning (clockwise) around the origin. For recent results on this model in the Earth-Moon case, see [GJMS93, SGJM95, Jor00b, CJ00, Jor00a].

We can apply a similar approach to introduce the effect of Saturn into the model: we can assume that Sun and Jupiter move as in the RTBP, and that Saturn also moves in circular orbit around the Jupiter-Sun barycentre, and that the three bodies move in the same plane. Then, as in the Earth-Moon case, it is not difficult to derive the equations of motion of a fourth infinitesimal particle under the Newtonian attraction of these bodies. Defining momenta as $p_x = \dot{x} - y$, $p_y = \dot{y} + x$ and $p_z = z$, the Hamiltonian for this Bicircular model is given by

$$\begin{aligned} H &= \frac{1}{2}(p_x^2 + p_y^2 + p_z^2) + yp_x - xp_y - \\ &\quad - \frac{1-\mu}{r_s} - \frac{\mu}{r_j} - \frac{m_{sat}}{r_{sat}} - \frac{m_{sat}}{a^2}(y\sin(\theta-\theta_0) - x\cos(\theta-\theta_0)), \end{aligned}$$

where $r_s^2 = (x-\mu)^2 + y^2 + z^2$, $r_j^2 = (x-\mu+1)^2 + y^2 + z^2$, $r_{sat}^2 = (x-x_{sat})^2 + (y-y_{sat})^2 + z^2$, $x_{sat} = a\cos(\theta-\theta_0)$, $y_{sat} = -a\sin(\theta-\theta_0)$, $\theta = \omega_{sat}t$, being m_{sat}, ω_{sat} and a the mass, frequency and semi-major axis of the orbit of Saturn, in the RTBP units.

1.2.3 The Bicircular coherent model

A characteristic of the Bicircular model is that the motion of the three massive bodies is not coherent, in the sense that they do not follow Newton's law. This lack of coherence is due to the selection of circular trajectories for the bodies, to avoid a too complex model.

To derive a coherent model, we need first to compute a true periodic solution of the general Three Body Problem (from now on, TBP), close to the real motion of Sun, Jupiter and Saturn. Although this is already a difficult problem, it can be solved by means of numerical methods. Then, it is not difficult to write the equations of motion for a particle under the gravitational attraction of these three bodies. Finally, using a suitable change of coordinates –in which Sun and Jupiter are kept fixed on the x-axis, as in the RTBP–, these equations of motion are written as a periodic time-dependent perturbation of the RTBP. In what follows, we will refer to these kind of models as Bicircular Coherent Periodic Models or BCCP, and they can be seen as the simplest restricted (coherent) four body models.

A coherent model for the Earth-Moon-Sun problem has been developed in [And98, AS00], to study the dynamics near the collinear points $L_{1,2}$ of the Earth-Moon system (see also [And02]). Here we will focus on the Sun-Jupiter-Saturn case and, although we will roughly follow the methods developed in [And98], we will also introduce a few changes to simplify the technicalities of the method.

In Chapter 2, we derive the BCCP model for the Sun-Jupiter-Saturn case, we compare it with the RTBP and JPL models, we numerically estimate the stability region around the L_5 point, and we build a normal form and a formal first integral (both up to order 16) and compute regions of effective stability by using estimates on the remainders of the series.

1.3 Quasi-periodic perturbations of the RTBP

Assume we are given a model for the motion of the bodies of the Solar system (for instance, the JPL ephemeris), and that we are interested in the dynamics near the triangular points of the Sun-Jupiter system. Then, we can proceed as follows:

a) Write the vector field acting on a particle under the gravitational attraction of all the planets.

b) Take coordinates (a time dependent reference frame) such that Sun and Jupiter are kept fixed on the x axis. As in the RTBP, we will refer to these coordinates as synodical. Write the vector field defined in a) in these coordinates.

Now we have a vector field that can be seen as a perturbation of the RTBP, but with more terms that depend on the transformation used –that is, of the real position of Sun and Jupiter– plus the position of the bodies of the Solar system. Note that these extra terms depend on the positions of Sun and planets and that, for a model like the JPL ephemeris, there are no "simple closed formulas" for these terms. Then, we can apply the following steps:

c) Perform a frequency analysis on these terms, and detect the dominant frequencies. As the motion of the Solar system seems to be quasi-periodic (at least for moderate time spans), it turns out that the part of these perturbing terms that depend on the positions of Sun and planets can be well approximated by Fourier series.

d) We substitute the dependence of the positions of the bodies by these truncated Fourier series.

e) The frequencies detected in c) can be written as a linear combination of a few of them, that correspond to the mean motion of the elements of the orbits of the bodies. We will refer to them as basic frequencies.

f) It is not necessary to take into account all the basic frequencies. In fact, the frequencies selected can be used as a control on the complexity (and the accuracy) of the model.

As far as we know, these models were first introduced in [GLMS85, GJMS91b, GJMS93] (see also [GMM02]) to apply dynamical systems tools to the transfer and control of space missions (see also [DJS91, GJMS91a, CGJ$^+$96]). Theoretical results for these kind of models can be found in [JS96] and [JV97b].

In this work, we construct two models that depend quasi-periodically (with two frequencies) on time and they can be written as (small) perturbations of the RTBP. They are natural improvements of the ERTBP and BCCP models. The first one is based on the computation of a 2-D invariant torus of the Sun-Jupiter-Saturn (planar) TBP. In some sense, it can be seen as a mixing of the Elliptic and Bicircular coherent problems, because this solution of the TBP tries to simulate the effect of Saturn on the system as well as the eccentricity of Jupiter's orbit. We have called this model, the Bianular Problem (because of the TBP solution's shape). In the second model, we compute a quasi-periodic solution of the four-body problem Sun-Jupiter-Saturn-Uranus and use it as the basis for a restricted five-body model. This model can be seen as the simplest restricted (coherent) five body problem and a natural improvement (by adding a massive body) of the BCCP. We have named this model as the Tricircular Coherent Problem.

1.3.1 The Bianular Problem

The periodic solution of the BCCP is used as the starting point of the computation of a 2-D invariant torus for which the osculating eccentricity of Jupiter's orbit is the actual one. In this sense, the Sun-Jupiter relative motion is better simulated by this quasi-periodic solution of the planar three body problem.

First, we reduce the Hamiltonian of the planar three body problem written in the Jacobi coordinates in a uniformly rotating reference frame from 4 to 3 degrees of freedom via a canonical change of variables that uses the angular momentum first integral (see [Whi52] for a general statement of this kind of reductions).

Then, we use the method developed by [CJ00] in order to compute a quasi-periodic solution (with two frequencies) of the reduced equations. The method, basically, consists in computing an invariant curve of a suitable Poincaré map. This invariant curve is seen as a truncated Fourier series and our aim is to compute its rotation number and a Fourier representation of it. At the end, the problem is reduced to a nonlinear system of equations, which is solved by means of a Newton method. As a first guess for this Newton method, the normal modes of the Bicircular Coherent solution of the TBP described in 1.2.3 are used.

Due to the Hamiltonian character of the problem, invariant tori are not isolated. In fact, an invariant torus with r basic frequencies belongs to a r-dimensional (Cantor) family of r-dimensional invariant tori. Thus, we "move" inside this family in order to find an invariant torus for which the motion of Jupiter is a prescribed one. We use a continuation method (using the angular momentum as the parameter) and we find a quasi-periodic solution of the reduced problem for which Jupiter's eccentricity, at a given moment, is the actual one. Then, it is not difficult (by means of a Fourier analysis) to write this 2-D invariant torus in the non-reduced coordinates.

Finally, the equations of motion of a massless particle that moves under the attraction of these three main bodies (supposing that they move in the previously computed quasi-periodic solution) are easily derived. This is a restricted four body problem and we call it the Bianular Problem (BAP, for short).

1.3.2 The Tricircular Coherent Problem

The second quasi-periodic model is based on the computation of a quasi-periodic solution (with two basic frequencies) of the planar four body problem Sun, Jupiter, Saturn and Uranus (SJSU). We adapt the method shortly described in the preceding section for computing invariant curves of maps to this case.

First, we also use the angular momentum first integral in order to reduce the four body problem (written in the generalised Jacobi coordinates) in one degree of freedom. Thus, we build a Hamiltonian reduction from 6 to 5 degrees of freedom.

Second, we suppose that the mass of Uranus is equal to zero. A good approximation of the initial point used in the Newton method for computing an invariant curve is given by the periodic orbit of the BCCP for the three inner bodies (Sun, Jupiter and Saturn) and the Kepler solution for the (Sun + massless-Uranus) problem. During the computations, the extra frequency is fixed (equal to Uranus's frequency) by forcing the rotation number to be a concrete value. Thus, we are able to obtain a quasi-periodic solution in the case that Uranus has no mass.

Thirdly, by means of a continuation method (taking the mass of Uranus as the parameter), we compute a quasi-periodic solution of the SJSU planar problem. Due to the smallness of the relative mass of Uranus, no visible bifurcations occur during the continuation process.

A restricted five body model (that will be called Tricircular Coherent Problem, or TCCP for short) can be constructed by writing the equations of a massless particle that moves under the influence of the four bodies. The system's intrinsic frequencies are Saturn's and Uranus'.

1.4 Study of the semi-analytical models

We will focus on the dynamics near the Lagrangian point L_5. The same results will hold for L_4, due to the symmetries of the models.

For the study of the dynamics near L_5 , we have followed a similar scheme in all the cases (periodic and quasi-periodic perturbations of the RTBP). In the quasi-periodic case, we have chosen the TCCP as the guiding model (the techniques work in a similar way for any (small) quasi-periodic perturbation of the RTBP).

1.4.1 Periodic and quasi-periodic orbits as replacements of $L_{4,5}$

Due to the effect of the different perturbations, the equilateral points are not longer equilibrium points (in the phase space) in any of the time-dependent models developed in this work. A simple application of the Implicit Function Theorem shows that, under generic hypotheses of non-resonance and smallness of the perturbations, the equilibrium points of the RTBP are replaced by a periodic orbit in the BCCP case. In the TCCP case, a KAM-like argument (see [JS96]) shows that, under generic conditions, the equilibrium point is replaced by a quasi-periodic orbit with the same frequencies as the perturbation. In both cases, these orbits tend to the respective equilibrium points when the perturbations go to zero.

In the BCCP case, the first step is to compute the periodic orbit that is replacing L_5, and to study its linear normal behaviour. In our case, as all the eigenvalues of the monodromy matrix corresponding to this periodic orbit have modulus 1, the orbit is linearly stable. This information will be used to compute an affine transformation that brings the Hamiltonian into linear normal form. We note that the case of a periodic orbit of an autonomous system is much more involved, since this transformation cannot be taken as affine, see [JV98] for more details.

For the quasi-periodic model, we firstly compute the 2-D invariant torus that replaces L_5 in the TCCP system. This torus will have Saturn's and Uranus's frequencies (the same frequencies as the perturbations) as intrinsic frequencies. Let us call them ω_{sat} and ω_{ura}, respectively. We will also study the normal linear behaviour around it by computing the three normal modes. That is, the basic frequencies (let them be ω_1, ω_2 and ω_3) of the three harmonic oscillators that correspond to the linearised system around the 2-D invariant torus.

The method used for the computation of the linearised normal behaviour of the invariant curve is due to À. Jorba (see [Jor01]) and is based in solving a generalised eigenvalue problem of the type $A(\theta)\Psi(\theta) = \lambda\Psi(\theta+\omega)$, where ω is the rotation number of the invariant curve.

1.4.2 Normal forms and first integrals

Next step is to compute a complete (and integrable) normal form around these orbits up to a high order (typically, we will use order 16 in the periodic cases and order 12 in the TCCP system). This means that we will expand the Hamiltonians in power series (of the 6 phase space coordinates) up to degree 16 (or 12). Note that the coefficients of the corresponding monomials depend on time in a periodic (BCCP and ERTBP cases) or quasi-periodic (TCCP case) way. Hence, we will handle them as truncated Fourier series with double precision coefficients. The truncation has been selected to only drop terms whose contribution is less than a given tolerance. In the BCCP and ERTBP cases, this tolerance has been selected as 10^{-16}, the truncation error of the computer arithmetic. In the TCCP, the chosen value was 10^{-10} (we note that the number of Fourier coefficients grows very rapidly every time we add a new Fourier variable).

We note that we could also have truncated the Fourier series, that define the different models, asking for a much bigger tolerance (for instance, 10^{-5} or 10^{-6}). This is due to the fact that, even though we are trying to construct models that simulates the real system, this tolerance is much smaller than the actual difference between any of the models presented here and the real system.

We stress that we are using truncated formal Fourier-Taylor expansions for the Hamiltonians, but with double precision coefficients. The use of the standard floating point arithmetic instead of a symbolic (and exact) arithmetic allows huge savings both in memory and computer time for the programs. This, jointly with an efficient implementation of the algorithms, is the key that allows to reach high orders in a standard PC.

The integrability of the normal form (in the BCCP and TCCP cases) can be achieved since the frequencies ω_j ($j = 1, 2, 3$), ω_{sat} and ω_{ura} have no exact resonances, at least up to order 16 (or 12). Hence, it is possible to introduce action-angle variables such that the truncated normal form, to degree 16 (12), only depends on the actions. Then, it is not difficult to describe approximately the dynamics around the periodic or quasi-periodic orbits that replace L_5. In a similar way it is possible to compute approximate first integrals, as power expansions with periodic or quasi-periodic time-dependent coefficients. These functions (sometimes called "quasi integrals" [Mar80]) can be used to derive estimates of the diffusion time near the orbit ([CG91, GG78]).

The computational process is based on the use of generating functions and Lie series. The algorithms used for the normal form computations are modifications of the classical Lie series method (see [Jor99] for the details of this modified method), to deal with periodic (see [GJMS93, JS94, SGJM95]) and quasi-periodic time-dependent Hamiltonians. The main advantage of the method presented in [Jor99] is to avoid dealing with the Lie triangle (it would require too much memory). These algorithms have been coded in C++ (C or FORTRAN would have also been a good choice), since the use of general purpose packages of algebraic manipulation requires a prohibitive amount of computer memory and time. The computer programs are enlargements of the ones presented in [Jor99].

1.4.3 Dynamical implications

The normal forms will provide two kinds of information. From one side, we can use them to compute invariant tori of dimensions ranging from 2 to 4 (in the BCCP and ERTBP cases) and of dimensions 3, 4 and 5 (in the TCCP case); this will give a description of the kind of motions near the periodic and quasi-periodic orbits that replace L_5. On the other side, in the periodic cases, we have bound (numerically) the remainder of the normal form and we have produced estimates of the time needed by a particle (like an asteroid) to escape from a neighbourhood of the periodic orbit. We have also used the first integrals to derive the region of effective stability.

A more direct method to estimate the region of effective stability near the triangular points is by means of a direct numerical integration: given a sufficiently fine mesh of points, we use them as initial conditions for a long numerical integration, to discard those points whose subsequent evolution is not confined near the Lagrangian points. The main advantage of a direct numerical simulation is that we obtain a quite realistic estimate of the size of the stability region, and the main inconveniences are that the number of initial conditions in the mesh grows exponentially with the dimension of the mesh, and that the integration time cannot be arbitrarily long. For these reasons, in the simulations of Section 2.2.2 we have restricted ourselves to a two dimensional mesh (so we have obtained a slice of the region) and the time span has been restricted to 10^6 years.

On the other hand, the estimation of the region by means of normal forms and/or first integrals is much less affected by the stability time or the dimension of the phase space, and the results can be converted in mathematical proofs, provided that the computations are done using an exact arithmetic, like the intervalar one. The main weakness of these methods is that the regions obtained are much smaller than the real region of effective stability. Examples of this are shown in 2.4.4, 2.5.2 and 3.4.2.

1.5 The Outer Solar System

In the last part of this work (Chapter 5), we perform a purely numerical study of the dynamics of the Trojan asteroids orbits by means of the frequency analysis method. We use, as the basis model, the more “realistic” Outer Solar System. As we have already mentioned before, this model consists in the gravitational attraction of the Sun, the four main planets of the Solar System (Jupiter, Saturn, Uranus and Neptune) and one (or more) massless particle (the asteroid).

The orbit of each asteroid is generated by numerically integrating its actual positions and velocities (that are taken from the database [Bow]) for a time span of millions of years. The method of integration used is due to J. Laskar and P. Robutel (see [LR01]) and it belongs to the family of symplectic integrators. The usage of a symplectic method in such a long-term integrations is advisable since other (non-symplectic) methods could insert numerical noise to the system and have an artificial drift on the values of the frequencies. One of the standard ways to look at the accuracy of such a long integration is given by the preservation of the energy (in an autonomous Hamiltonian system it should be constant): symplectic methods integrate exactly (provided that there is no roundoff errors) a Hamiltonian system that is very close to the one that we want to integrate, and, thus, the exactly conservation of a very close energy (the characteristic differences are about 10^{-13}) is obtained. This phenomenon does not appear, normally, in other integration methods. Even though, a very accurate (with a very good local error) integrator is given, what typically occur is that, after a long integration, a drift on the energy appears.

Normally, when performing such a study for an asteroid, several basic frequencies appear. In one hand, there are three basic frequencies for each planetary orbit. The fast one that is due to the periodic motion around the Sun and two secular (or slowly) ones that are due to the motion of planets's perihelion and nodes. On the other hand, each Trojan asteroid has three proper frequencies: the libration (fast) frequency around the corresponding triangular point and two secular frequencies that come from the proper perihelion and node motions. Thus, we have to deal with 14 (that is $15-1$, because Jupiter's secular frequency corresponding to the motion of the node can be set to zero, see [Las90]) basic frequencies in the analysis of each Trojan orbit.

Finally, we also perform a frequency analysis of the Trojan orbits in the RTBP and the semi-analytic models that are built and studied in chapters 2, 3 and 4, and we compare them with the results obtained with the OSS.

Chapter 2

The Bicircular Coherent Problem

The first intermediate model that we present is a periodic perturbation of the RTBP that tries to take into account the effect of Saturn. This model is based on the numerical computation of a periodic orbit for the (full) planar three body problem Sun-Jupiter-Saturn, close to the (non periodic) orbit of these bodies in the real Solar system. Using this orbit, it is not difficult to write the equations of motion of a particle under the gravitational attraction of these bodies. In suitable coordinates, these equations are written as a periodic time-dependent perturbation of the RTBP, where the time-dependence accounts for the effect of Saturn. The remaining part of this chapter is focused on the study of this model. We have also included some comparisons with the real Solar system, by means of the JPL ephemeris [JPL].

The chapter has been structured as follows: Section 2.1 describes the details on the derivation of the four-body model, Section 2.2 contains some numerical integrations comparing the model obtained with the RTBP and JPL model plus a numerical estimation of the stability region around the orbit. Section 2.3 deals with the preparation and initial expansion of the Hamiltonian of the restricted four-body problem, Section 2.4 is devoted to the computation of a normal form of order 16 around a periodic orbit near the triangular point, and to the computation of a region of effective stability around this orbit using estimates on the remainder of the normal form, Section 2.5 deals with the computation of formal first integrals (up to high order) and the use of these integrals to again estimate the stability region around the periodic orbit.

2.1 Construction of the model

This section is devoted to the construction of the BCCP model. First, we compute a periodic solution of the planar three body problem close to the Sun-Jupiter-Saturn case; then we will use this solution to derive the equations for the BCCP model as a perturbation of the RTBP. A BCCP model for the Sun-Earth-Moon system has already been constructed in [And98, AS00].

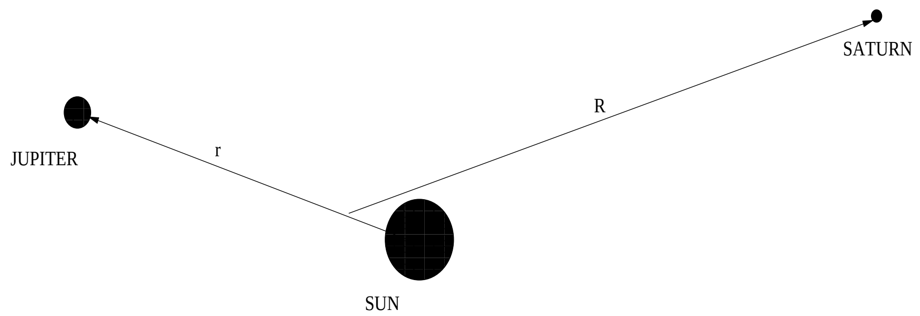

Figure 2.1: Jacobi coordinates for the TBP.

2.1.1 A periodic solution of the general three body problem

Our first purpose is to obtain (numerically) a periodic solution of the planar three body problem (TBP). We will use the Jacobi formulation of the TBP, where we deal with two position vectors: one going from the Sun to Jupiter, and another one from the Sun-Jupiter barycentre to Saturn. This second vector contains the barycentre of the three masses (see Figure 2.1).

Taking units such that the total mass of Sun and Jupiter is equal to 1 and the gravitational constant is also 1, the equations of motion for the three massive bodies are (see [Mar90]):

$$\begin{aligned} \ddot{\vec{r}} &= -\frac{\vec{r}}{r^3} + m_{sat}\left[\frac{\vec{R}-(1-\mu)\vec{r}}{|\vec{R}-(1-\mu)\vec{r}|^3} - \frac{\vec{R}+\mu\vec{r}}{|\vec{R}+\mu\vec{r}|^3}\right], \\ \ddot{\vec{R}} &= -(1+m_{sat})\left[\mu\frac{\vec{R}-(1-\mu)\vec{r}}{|\vec{R}-(1-\mu)\vec{r}|^3} + (1-\mu)\frac{\vec{R}+\mu\vec{r}}{|\vec{R}+\mu\vec{r}|^3}\right], \end{aligned} \tag{2.1}$$

where $\mu = 0.95387536 \times 10^{-3}$ and $m_{sat} = 0.285515017438987 \times 10^{-3}$. We will look for a solution in which the three bodies start on a line –Saturn, Jupiter and Sun, from left to right– and that they repeat this configuration (including speeds) after T units of time. Of course, the value of T has to be selected appropriately to obtain a solution as close as possible to the real motion of Sun, Jupiter and Saturn. Here, T is taken as the period of Saturn in the RTBP coordinates for the Sun-Jupiter system, assuming that both Jupiter and Saturn move on circular orbits. The associated frequency $\omega_{sat} = \frac{2\pi}{T}$ is then 0.597039074021947.

The procedure for the numerical computation of this periodic orbit is as follows: first, we apply the change of variables

$$\begin{aligned} r_x &= \xi_x \cos t - \xi_y \sin t, & R_x &= \eta_x \cos t - \eta_y \sin t, \\ r_y &= \xi_x \sin t + \xi_y \cos t, & R_y &= \eta_x \sin t + \eta_y \cos t, \end{aligned}$$

to equation (2.1). This is a uniform (counterclockwise) rotation with frequency 1, the frequency of Jupiter in the RTBP. Then, defining the momenta as usual,

$$\begin{aligned} p_x &= \dot{\xi}_x - \xi_y, & P_x &= \dot{\eta}_x - \eta_y, \\ p_y &= \dot{\xi}_y + \xi_x, & P_y &= \dot{\eta}_y + \eta_x, \end{aligned}$$

and renaming the variables ξ and η as r and R respectively (we hope the reader will not be confused by this), equations (2.1) become:

$$
\begin{aligned}
\dot{r_x} &= p_x + r_y, \\
\dot{r_y} &= p_y - r_x, \\
\dot{R_x} &= P_x + R_y, \\
\dot{R_y} &= P_y - R_x, \\
\dot{p_x} &= p_y - \frac{r_x}{r^3} - \frac{m_{sat}}{r_{Ssat}^3}(R_x + \mu r_x) + \frac{m_{sat}}{r_{Jsat}^3}(R_x - (1-\mu)r_x), \\
\dot{p_y} &= -p_x - \frac{r_y}{r^3} - \frac{m_{sat}}{r_{Ssat}^3}(R_y + \mu r_y) + \frac{m_{sat}}{r_{Jsat}^3}(R_y - (1-\mu)r_y), \\
\dot{P_x} &= P_y - (1+m_{sat})\left[\frac{1-\mu}{r_{Ssat}^3}(R_x + \mu r_x) + \frac{\mu}{r_{Jsat}^3}(R_x - (1-\mu)r_x)\right], \\
\dot{P_y} &= -P_x - (1+m_{sat})\left[\frac{1-\mu}{r_{Ssat}^3}(R_y + \mu r_y) + \frac{\mu}{r_{Jsat}^3}(R_y - (1-\mu)r_y)\right],
\end{aligned}
$$

where $r^2 = r_x^2 + r_y^2$, $r_{Ssat}^2 = (R_x + \mu r_x)^2 + (R_y + \mu r_y)^2$ and $r_{Jsat}^2 = (R_x - (1-\mu)r_x)^2 + (R_y - (1-\mu)r_y)^2$. The numerical computation of the periodic orbit is done by means of a Newton method, looking for an initial condition such that the vectors $\vec{r}$, $\vec{R}$ (see Figure 2.1) and their derivatives are periodic with period T. The initial conditions are kept on the x axis, so the bodies are always on the same line at the beginning of the orbit. We have also used a continuation scheme on the masses starting with $\mu = \mu_{sat} = 0$ (where the solution can be easily found by hand).

Let us describe this periodic solution. In an inertial frame, Jupiter and Saturn are turning counterclockwise. In the rotating frame, Jupiter is librating around the point $(\mu - 1, 0)$ while Saturn is turning clockwise (see Figure 2.2). A more geometrical view can be obtained by computing, for each instant of time, the orbital elements of the orbits of Jupiter and Saturn: Figure 2.3 displays the variation of the instantaneous eccentricity and argument of the perihelion along a period. As the eccentricities are very small (we recall that the eccentricities of Jupiter and Saturn in the real Solar system are 0.048 and 0.054, respectively), we can conclude that the motion of Jupiter and Saturn around the Sun is very close to circular. Moreover, the averaged Sun-Saturn distance for this solution (1.8333) is very close to the real one (1.8315, in RTBP units).

Finally, we note that there are other options for the construction of the BCCP. Here we have used the synodic frequency of Saturn as a reference for selecting the periodic orbit of the TBP, but it is possible to use other elements of Saturn as a reference (for instance, its mean distance to the Sun). The differences between the results of these selections are very small.

2.1.2 The Hamiltonian of the BCCP model

Here we will derive the equations of motion of a fourth massless particle under the attraction of the three primaries moving in the periodic orbit found in the previous section. One of the main goals is to write the model as a periodic time-dependent perturbation of the Sun-Jupiter RTBP.

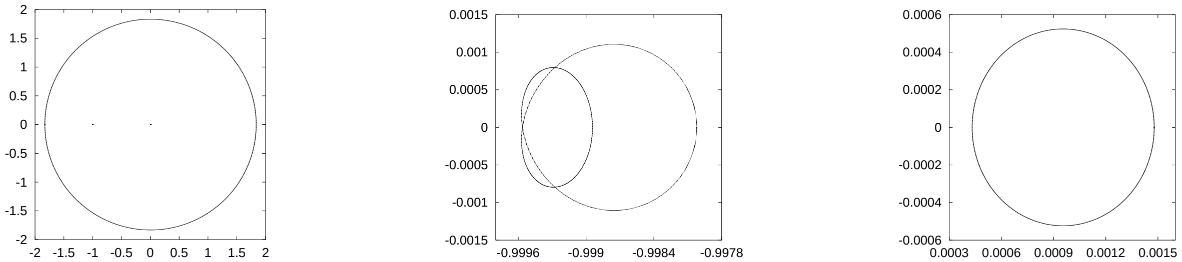

Figure 2.2: Periodic orbits of, respectively, Saturn, Jupiter and the Sun in the rotating reference frame. In fact, the plots for Jupiter and Sun are also displayed in Saturn's plot; they are seen as two small dots inside Saturn's orbit.

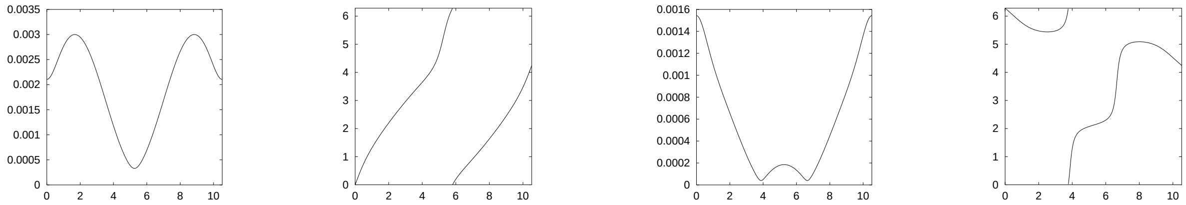

Figure 2.3: Orbital elements of Jupiter and Saturn for a full period of the BCCP. They correspond, from left to right, to the eccentricity and the perihelion argument of Jupiter (first and second plot) and Saturn (third and fourth plot).

We start from the periodic solution for Sun, Jupiter and Saturn, written in an inertial reference system, and let $\vec{\rho}$ be the position vector of the particle in this inertial reference frame. We are going to use the change of variables obtained from the composition of the following three transformations.

a) Translation of the origin from the global barycentre to the Sun-Jupiter barycentre.
b) Periodic time-dependent rotation to fix Sun and Jupiter on the x-axis.
c) Scaling to force the distance between Sun and Jupiter to be one.

In this "rotating-pulsating" reference frame, the three main bodies and the particle have the coordinates:

$$\begin{aligned} S &: \vec{Q}_s = (\mu, 0, 0)^t \\ J &: \vec{Q}_j = (\mu - 1, 0, 0)^t \\ sat &: \vec{Q}_{sat} = \frac{1}{r} C^T \vec{R} \\ part &: \vec{q} = \frac{1}{r} C^t (\vec{\rho} + \frac{m_{sat}}{1 + m_{sat}} \vec{R}) \end{aligned}$$

where S, J, sat and $part$ stands for Sun, Jupiter, Saturn and particle, respectively, and $r = \|\vec{r}\|$ (note that $\vec{r}$ and $\vec{R}$ depend periodically on time). The matrix C is defined as

$$C = \begin{pmatrix} -\frac{r_x}{r} & \frac{r_y}{r} & 0 \\ -\frac{r_y}{r} & -\frac{r_x}{r} & 0 \\ 0 & 0 & 1 \end{pmatrix}$$

where $\vec{r} = (r_x, r_y, 0)$ and $\vec{R} = (R_x, R_y, 0)$ are the periodic solution of the TBP embedded in the three dimensional space. The inverse change is given by

$$\vec{\rho} = -\frac{m_{sat}}{1+m_{sat}}\vec{R} + B\vec{q},$$

where $B = rC$. Defining the conjugate momentum as

$$\vec{p} = r^2\dot{\vec{q}} + B^t\dot{B}\vec{q},$$

the equations for the particle become Hamiltonian, and the Hamiltonian is:

$$H = \frac{1}{2r^2}\langle\vec{p},\vec{p}\rangle - \frac{1}{r^2}\vec{p}B^t\dot{B}\vec{q} - \frac{m_{sat}}{1+m_{sat}}\ddot{\vec{R}}^t B\vec{q} + U,$$

where U, the potential energy, is given by

$$U = -\frac{1-\mu}{r||\vec{Q}_s - \vec{q}||} - \frac{\mu}{r||\vec{Q}_j - \vec{q}||} - \frac{m_{sat}}{r||\vec{Q}_{sat} - \vec{q}||}.$$

To write the Hamiltonian in a more suitable way, we look at the vectors $\vec{r}$ and $\vec{R}$ as if they were in the complex plane

$$\begin{aligned} z &= r_x + ir_y, \\ Z &= R_x + iR_y, \end{aligned}$$

and we define the (T-periodic) functions:

$$\begin{aligned}
\alpha_1 &= \frac{1}{r^2}, & \alpha_2 &= \frac{\mathrm{Re}\,(\dot{z}\bar{z})}{r^2}, & \alpha_3 &= \frac{\mathrm{Im}\,(\dot{z}\bar{z})}{r^2}, \\
\alpha_4 &= \frac{m_{sat}}{1+m_{sat}}\mathrm{Re}\,(\ddot{Z}\bar{z}), & \alpha_5 &= \frac{m_{sat}}{1+m_{sat}}\mathrm{Im}\,(\ddot{Z}\bar{z}), & \alpha_6 &= \frac{1}{r}, \\
\alpha_7 &= -\frac{1}{r^2}\mathrm{Re}\,(Z\bar{z}), & \alpha_8 &= -\tfrac{1}{r^2}\mathrm{Im}\,(Z\bar{z}).
\end{aligned}$$

From a numerical tabulation of the values of $\vec{r}$ and $\vec{R}$ we can easily compute the Fourier coefficients for α_j, $j = 1, \ldots, 8$, up to a finite order (in fact, all the coefficients with modulus larger than 10^{-13} have been kept). Due to the parity properties of these functions (see Figure 2.4), we can write them as

$$\begin{aligned}
\alpha_j(t) &= \sum_{k\geq 0}\alpha_{jk}\cos(k\omega_{sat}t), \qquad j = 1, 3, 4, 6, 7 \\
\alpha_j(t) &= \sum_{k\geq 1}\alpha_{jk}\sin(k\omega_{sat}t), \qquad j = 2, 5, 8.
\end{aligned}$$

It is then possible to write the Hamiltonian of the BCCP problem as:

$$\begin{aligned}
H &= \frac{1}{2}\alpha_1(t)(p_x^2 + p_y^2 + p_z^2) + \alpha_2(t)(xp_x + yp_y + zp_z) + \alpha_3(t)(yp_x - xp_y) \\
&\quad + \alpha_4(t)x + \alpha_5(t)y - \alpha_6(t)\left[\frac{1-\mu}{q_S} + \frac{\mu}{q_J} + \frac{m_{sat}}{q_{sat}}\right], \qquad (2.2)
\end{aligned}$$

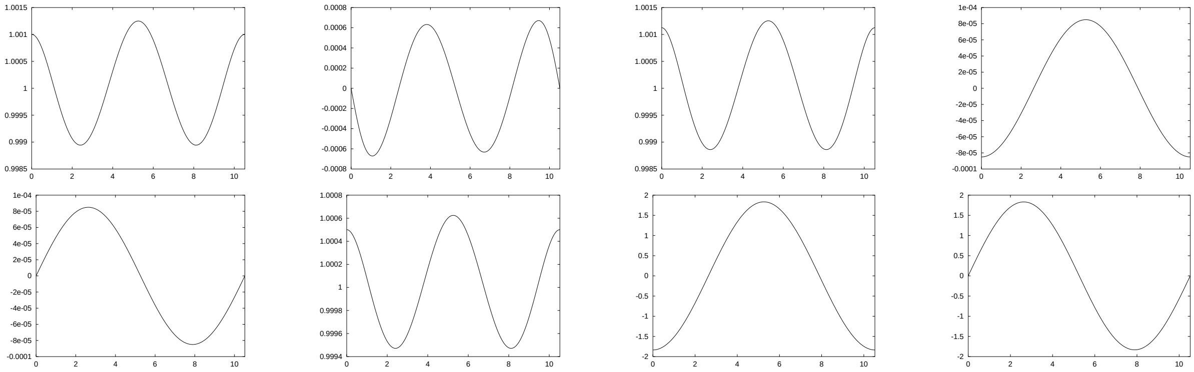

Figure 2.4: Plot of one period of the α_j functions. They are consecutively displayed from top-left (α_1) to bottom-right (α_8).

where $q_S^2 = (x-\mu)^2 + y^2 + z^2$, $q_J^2 = (x-\mu+1)^2 + y^2 + z^2$ and $q_{sat}^2 = (x-\alpha_7(t))^2 + (y-\alpha_8(t))^2 + z^2$. We recall that, for $t = 0$, Saturn is on the negative part of the x axis. Due to the symmetries of the periodic solution of the TBP, this Hamiltonian has the symmetry $(t, x, y, z, \dot{x}, \dot{y}, \dot{z}) \mapsto (-t, x, -y, z, -\dot{x}, \dot{y}, -\dot{z})$. This implies that, to study the triangular points, it is enough to focus on one of them.

We want to make some comparisons between the derivation of the BCCP done here and the method used in [And98, AS00] to compute a similar model for the Sun-Earth-Moon case. There, the authors compute the periodic solution of the TBP by means of an (specially built) algebraic manipulator to find a Fourier series that satisfies, up to a prescribed order, equation (2.1). Then, this truncated Fourier series is manipulated to obtain the functions α_j, $j = 1, \ldots, 8$.

The concrete values for the coefficients of the periodic functions (α_j), $j = 1, \ldots, 8$, are displayed in Table A.1 of Appendix A.1 and the files containing them can be downloaded from the web site `http://www.maia.ub.es/dsg/2001/index.html/`.

2.1.3 Tests

To check the results obtained in the preceding calculations, we have compared numerical integrations of the obtained model (2.2) with a restricted four body problem: we have randomly selected initial conditions for the particle, and we have computed the subsequent orbit for a period of Saturn. Then, each of these orbits has been sent to the initial coordinates of the Jacobi formulation (2.1). Finally, adding the equation of the infinitesimal particle to (2.1), using the initial condition for the periodic orbit of the TBP and integrating the four particles at once, it is not difficult to test the accuracy of the initial orbit. We note that this not only tests the equations obtained, but also the changes of coordinates used. The differences between the two integrations are of the order of 10^{-12}. We note that, in the computation of the Fourier coefficients of the functions α_j we discarded all the coefficients whose absolute value were lower than 10^{-13}.

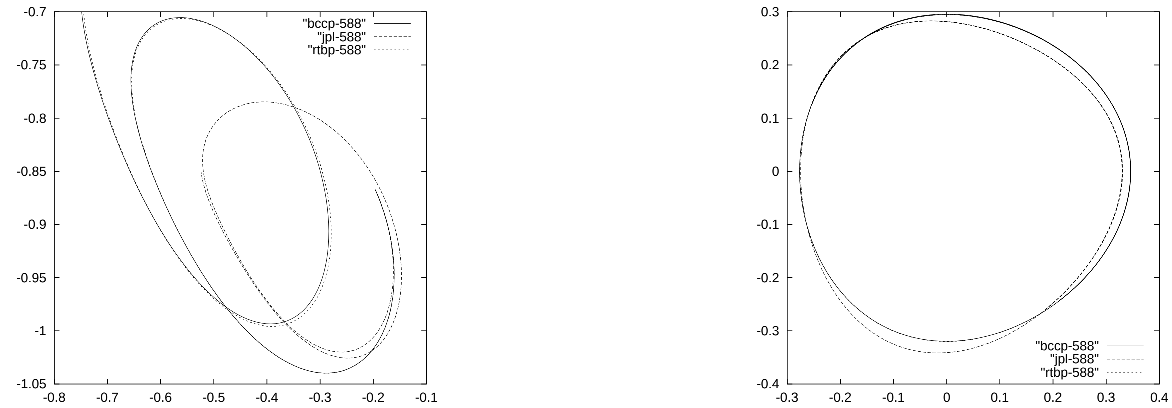

Figure 2.5: (x, y) and $(z, \dot{z})$ projections of the orbit of 588 Achilles for the RTBP, BCCP and JPL models, during 20 years.

2.2 Numerical simulations

Here we have included some numerical simulations for the BCCP model, as well as some comparisons with the results for the RTBP and the JPL model for the real Solar system.

2.2.1 Trajectories of some Trojan asteroids

To compare the accuracies of the models RTBP and BCCP against the JPL ephemeris, we have integrated numerically the motion of the Trojan asteroids 588 Achilles and 624 Hektor (both are near L_4) and 1870 Glaukos (near L_5), in these three models. We have selected Achilles and Hektor because they are two well-known members of the Trojan family, and Glaukos because is one of the four Trojans whose effective stability has been shown in [GS97], but for the planar RTBP. The initial conditions have been taken at December 22nd, 2000 (i.e., Julian day 2451900.5), from the database [Bow], and the total integration time has been chosen to be 20 years –enough for our actual purposes–. Of course, for the integration in the BCCP we need to take into account the initial position of Saturn with respect to Jupiter, to select the right initial phase for the time variable. The results are displayed in Figures 2.5, 2.6 and 2.7.

Let us comment on these plots. First, note the proximity between the RTBP and the BCCP integrations. In fact, this is not surprising because of the construction of the BCCP: among all the solutions of the TBP, we have selected the simplest one, in the sense that the motion of Jupiter and Saturn is nearly circular. So, if we look at the gravitational forces acting on the asteroid in the RTBP and BCCP models, we see that the force coming from Jupiter is very similar for the two models, and the main difference is the effect of Saturn, which is small since it is far away. Note that, in the real system, Saturn has little effect on the asteroid but it has a strong effect on Jupiter. In other words, the main difference –we are looking at the forces acting on the asteroid– between RTBP and the real system is the different motion of Jupiter. The main point in constructing the BCCP by introducing Saturn is to take into account the effect of Saturn on the orbit of Jupiter and, in second place, to account for the less important effect of Saturn on the

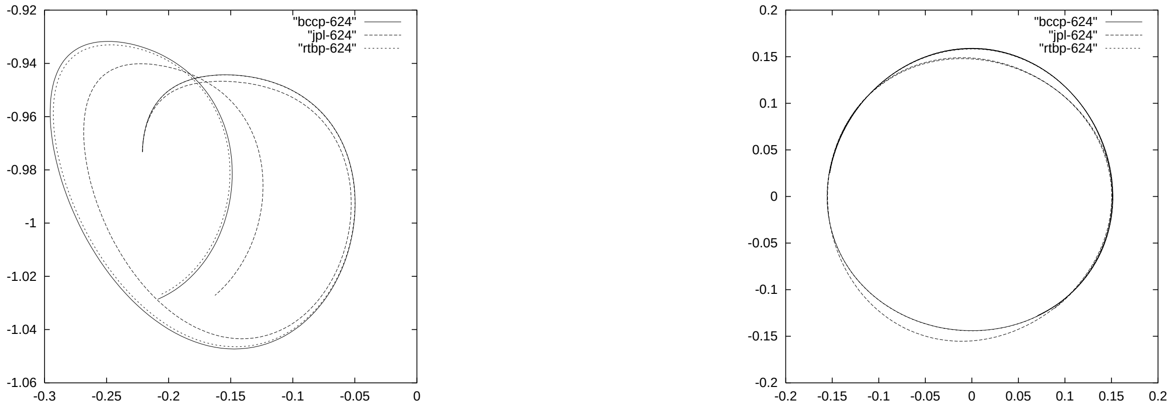

Figure 2.6: (x, y) and $(z, \dot{z})$ projections of the orbit of 624 Hektor for the RTBP, BCCP and JPL models, during 20 years.

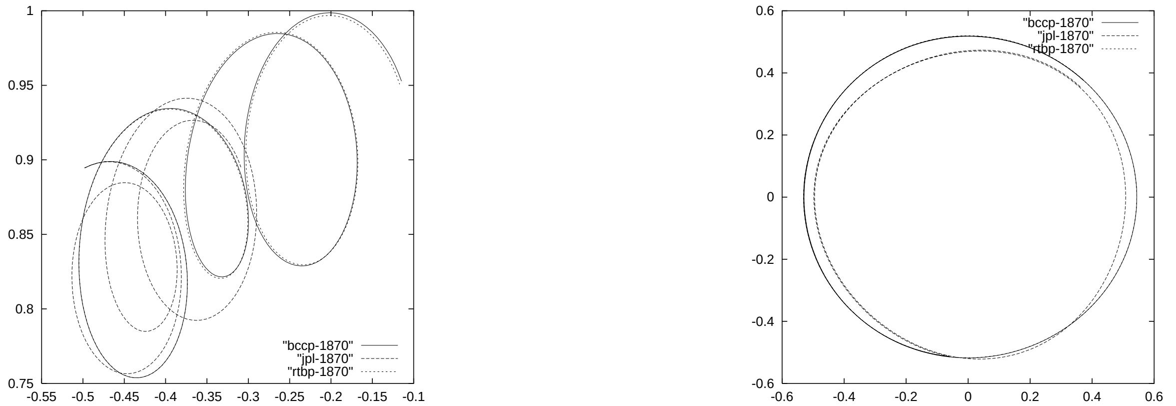

Figure 2.7: (x, y) and $(z, \dot{z})$ projections of the orbit of 1870 Glaukos for the RTBP, BCCP and JPL models, during 20 years.

asteroid. As we have explained, our particular –and simple– selection of solution for the TBP is not close enough to the motion of Jupiter in the real system. Hence, a natural improvement to the BCCP model is to look for a solution (of the TBP) not periodic but quasi-periodic, in which the motion of Jupiter is closer to the real one. This is actually work in progress.

Although, from these considerations, it could seem that the BCCP is so close to the RTBP that it is not worth to study, we think that the BCCP contains very interesting features. One of the most important is that, as the equilibrium point is replaced by a periodic orbit (see Section 2.3.1), the stability region is not located around the geometrical triangular point but it moves along the periodic orbit. As we will see in the following sections, this motion is wide enough such that we can show effective stability for points in the space that are outside of previously computed regions for the RTBP. Of course, these points are inside these regions only for certain times (i.e., for certain positions of Saturn). See Section 2.5.3.2 for more details.

Finally, as a side comment, we want to note the simplicity of the $(z, \dot{z})$ projection of the motion: it looks like a mildly perturbed linear oscillator. This can be already explained using the RTBP: the linearization of the flow around L_5 in synodical coordinates contains a linear oscillator (of frequency 1) fully contained in the $(z, \dot{z})$ direction. When we take into consideration the nonlinear terms, we see that they have little influence in the vertical direction so the dynamics in this $(z, \dot{z})$ direction is close to an harmonic oscillator. Hence, for the full Solar system, we expect to have a similar behaviour.

2.2.2 Numerical estimation of a stability region

Figure 2.8 contains an estimation of the stability region of the BCCP for $t = 0$. This region has been obtained by the following procedure: a) selecting a grid of values (x, y) and taking the remaining coordinates from the position of the periodic orbit that substitutes L_5 (see Section 2.3.1) at time $t = 0$; b) using the previous values as initial conditions, we start a numerical integration of the BCCP model; and c) the trajectories that go away before the final integration time (10^6 years) are discarded. Hence, in Figure 2.8 we have drawn a black dot for each couple (x, y) giving rise to a trajectory that stays near the Lagrangian points for 10^6 years. The explored area is also displayed, enclosed with a semi-circular box. Of course, we can compute a similar region for each value of t along a period of Saturn in the BCCP coordinates.

We note the big size of the region (we recall that the unit of distance is the Sun-Jupiter distance). In the following sections, we will also obtain regions of effective stability using truncated normal forms and approximated first integrals. These regions will be much smaller than the one obtained here, as it is usual for this kind of computations.

2.3 Preliminary transformations and expansions

Before starting with the normal form or first integral computations, we will put the initial Hamiltonian (2.2) into a more suitable form. First, we compute the periodic orbit that replaces the equilibrium point L_5, since the (time-dependent) translation of the origin of

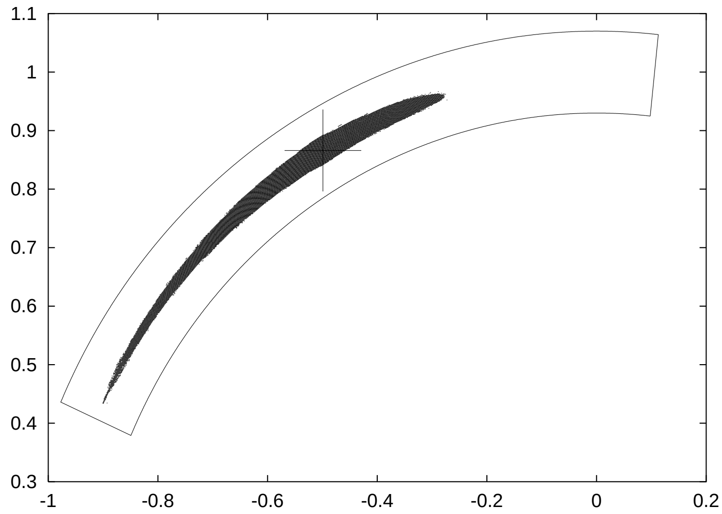

Figure 2.8: Numerical estimation of the stability region for the BCCP, for $t = 0$. The axis are the x and y synodical coordinates.

coordinates to this orbit cancels the first order terms in the Hamiltonian. Then, we will compute the linear transformation that reduces the linear variational equations along the orbit to constant coefficients. This (canonical) transformation reduces the second degree terms in the Hamiltonian to constant coefficients. Moreover, this reducing transformation can be taken such that the Hamiltonian is put in (complex) normal form up to second degree. Finally, we will expand, up to high order, the Hamiltonian in these coordinates. The resulting expansion will be used in Sections 2.4 and 2.5. This procedure has already been used in [GJMS93, JS94].

2.3.1 The periodic orbit that replaces L_5

As it has been mentioned before, the equilibrium points of the RTBP are no longer equilibrium solutions for the BCCP. A straightforward application of the Implicit Function Theorem shows that, under suitable conditions (essentially, they are a non-resonance condition involving the perturbing frequencies and the linear modes around the point, and a smallness condition on the size of the perturbation), the equilibrium points are replaced with periodic orbits with the same period as the perturbation; these orbits go to the corresponding point when the perturbation goes to zero.

To compute this periodic orbit, we will consider the time period-of-Saturn map associated to the flow of the BCCP, and we will look for a fixed point. Note that this map can be easily evaluated by numerical integration of the flow associated to (2.2), and its differential is also obtained integrating the variational flow. Hence, it is not difficult to apply a Newton method to look for a fixed point. Due to the smallness of the perturbation, it is enough to use, as initial condition, the coordinates of the triangular point L_5. The (x, y) projection of the resulting periodic orbit is shown in Figure 2.9.

To check for possible bifurcations of this orbit when the size of the perturbation increases from zero to its actual value, we have introduced a perturbing parameter in the

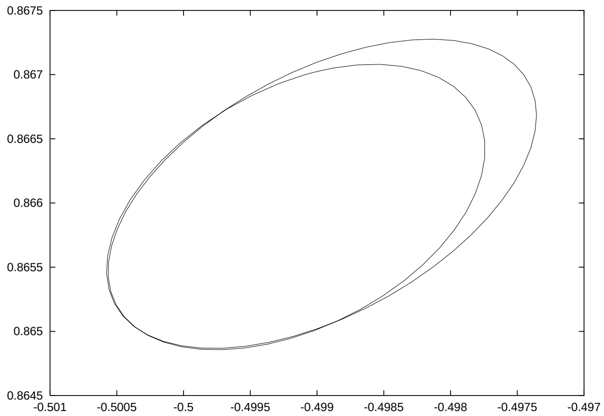

Figure 2.9: (x, y)-projection of the periodic orbit near L_5

j	Re (λ_j)	$\pm$Im (λ_j)	$\lvert\lambda_j\rvert$	$\pm$Arg (λ_j)
1	0.662312812634	0.749227427569	1.0	0.846894831435
2	-0.485147270414	0.874432459375	1.0	2.077327904892
3	-0.453737377106	0.891135451330	1.0	2.041751159215

Table 2.1: Eigenvalues of the monodromy matrix of the periodic orbit near L_5.

Hamiltonian of the BCCP,

$$\begin{aligned} H_\varepsilon &= \frac{1}{2}(1+\varepsilon(\alpha_1(t)-1))(p_x^2+p_y^2+p_z^2)+\varepsilon\alpha_2(t)(xp_x+yp_y+zp_z) \\ &\quad +(1+\varepsilon(\alpha_3(t)-1))(yp_x-xp_y)+\varepsilon\alpha_4(t)x+\varepsilon\alpha_5(t)y \\ &\quad -(1+\varepsilon(\alpha_6(t)-1))\left[\frac{1-\mu}{q_S}+\frac{\mu}{q_J}\right]-\varepsilon\alpha_6(t)\frac{m_{sat}}{q_{sat}}. \end{aligned}$$

Hence, $\varepsilon = 0$ corresponds to the RTBP, while $\varepsilon = 1$ corresponds to the BCCP. By means of a continuation procedure, we have computed the periodic orbit for ε ranging from 0 to 1, showing a continuous behaviour of the periodic orbit w.r.t. ε. We note that this is not the case in similar models (with a larger perturbation), like the Bicircular problem for the Sun-Earth-Moon system (see [SGJM95, CJ00]).

The linearized normal behaviour is given by the eigenvalues of the monodromy matrix of the periodic orbits, shown in Table 2.1. As these eigenvalues have modulus 1, the orbit is linearly stable.

2.3.2 Second order normal form

In the previous section we have derived a time-dependent translation that cancels the first order terms in the Hamiltonian. Here we will derive a linear change of variables (that depends on time in a periodic way) that puts the second degree terms of the Hamiltonian into a more convenient form. This is, essentially, the Floquet transformation for the variational flow along the periodic orbit, but taking into account the symplectic structure of the problem. To simplify further steps in the normalizing process, we also apply a complexifying change of variables that put the second degree terms of the Hamiltonian in the so-called diagonal form.

2.3.2.1 Implementation of the Floquet change

The linear flow around the periodic orbit that replaces L_5 is described by a linear system of differential equations, that depends periodically on time, with period T:

$$\dot{u} = Q(t)u. \tag{2.3}$$

Our goal is to find a symplectic and T-periodic change of variables, $u = P(t)v$, such that $P(t)^{-1}(Q(t)P(t) - \dot{P}(t)) \equiv A$ does not depend on time. Then, using this transformation, (2.3) becomes autonomous:

$$\dot{v} = Av.$$

The existence of such a change is ensured by the classical Floquet theorem. Here, as we want to work not with the flow but with the Hamiltonian, we want this transformation to be canonical.

The construction of the transformation $P(t)$ as well as of the reduced matrix A follows from the proof of the Floquet theorem. Here we will give the details of the calculation of $P(t)$ and A for the BCCP case. In what follows we will denote by J the matrix of the standard symplectic form of $\mathbb{R}^6$,

$$J = \begin{pmatrix} 0 & I \\ -I & 0 \end{pmatrix},$$

where I stands for the 3×3 identity matrix. We note that, with this definition of J, the first three coordinates (of $\mathbb{R}^6$) correspond to the positions while the last three are the momenta.

We start with the computation of the monodromy matrix M of (2.3), by integrating the fundamental matrix over a period T. In this case, all the eigenvalues of this matrix are different and of modulus 1, so M can be reduced to diagonal form $D_M = \mathrm{diag}(\lambda_1, \lambda_2, \lambda_3, \overline{\lambda}_1, \overline{\lambda}_2, \overline{\lambda}_3)$. Let S be the diagonalizing transformation, $M = SD_MS^{-1}$ (due to the Hamiltonian structure of the problem, the columns of S can be scaled such that $S^tJS = -iJ$; this makes easier the computation of the inverse of S, $S^{-1} = -iJS^tJ$). Next, we can compute values ω_j, $j = 1, 2, 3$, such that $\lambda_j = \exp(i\omega_jT)$. Note that these values are not uniquely defined: if ω_j is one of them, then any of the values $\pm(\omega_j + \frac{2k\pi}{T})$, $\forall\, k \in \mathbb{Z}$, is also admissible. Here, we have selected the values of k and the sign such that value $\pm(\omega_j + \frac{2k\pi}{T})$ is the closest to the frequencies of the (unperturbed) RTBP. This is the natural selection from a perturbative point of view, since the matrix $P(t)$ is then close to the identity. So, defining $D_B = \mathrm{diag}(i\omega_1, i\omega_2, i\omega_3, -i\omega_1, -i\omega_2, -i\omega_3)$ and $B = SD_BS^{-1}$, we have that B is a real matrix such that $M = \exp(BT)$. Then, it is not difficult to check that the matrix $P(t)$ that solves the initial value problem,

$$\dot{P}(t) = Q(t)P(t) - P(t)B, \qquad P(0) = I,$$

is a T-periodic transformation that brings (2.3) into the reduced form $\dot{v} = Bv$.

Therefore, we have derived constructively the existence of the reducing transformation. However, we will first introduce a small modification on the scheme above to obtain a simpler reduced matrix B, and we then discuss the canonical character of the transformation $u = P(t)v$.

We want to compute a real transformation R such that $A = R^{-1}BR$ have a very simple form. Hence, we define R as the matrix whose first three columns are the real parts of the eigenvectors of M, and the last three columns are the corresponding imaginary parts (as before, due to the Hamiltonian structure of the problem, it is possible to scale the columns of R such that R becomes symplectic, $R^tJR = J$, and then the computation of R^{-1} becomes trivial). Then, it can be checked that the matrix $A = R^{-1}BR$ takes the form

$$A = \left(\begin{array}{ccc|ccc} 0 & 0 & 0 & \omega_1 & 0 & 0 \\ 0 & 0 & 0 & 0 & \omega_2 & 0 \\ 0 & 0 & 0 & 0 & 0 & \omega_3 \\ \hline -\omega_1 & 0 & 0 & 0 & 0 & 0 \\ 0 & -\omega_2 & 0 & 0 & 0 & 0 \\ 0 & 0 & -\omega_3 & 0 & 0 & 0 \end{array}\right).$$

Finally, it is not difficult to see that the solution of the initial value problem,

$$\dot{P}(t) = Q(t)P(t) - P(t)A, \qquad P(0) = R,$$

is a T-periodic matrix that reduces (2.3) to

$$\dot{v} = Av.$$

Finally, to ensure that the transformation is canonical, we only need to check that $P(t)$ is a symplectic matrix. This can be proved analytically (see [GJMS93]) but here, to also check the correctness of the software, we have tested numerically this condition for a mesh of values of t, with good agreement.

We also want to note that the selection of sign for the ω_j plays an essential role in the canonical character of the transformation. For instance, changing the sign of one of the ω_j when computing the logarithm of the monodromy matrix would end up in a non-symplectic matrix $P(t)$. If the reader is not familiar with these properties, we recommend the papers [GDF+89], [Sim89] or [Jor99] for a similar discussion for an autonomous system (as the Hamiltonian considered in these papers is simpler and the calculations can be carried out by hand, the discussion is probably much clearer).

Implementing this (time depending) change of variables, the second degree terms of the Hamiltonian become:

$$H_2 = \frac{1}{2}\omega_1(x_1^2 + y_1^2) + \frac{1}{2}\omega_2(x_2^2 + y_2^2) + \frac{1}{2}\omega_3(x_3^2 + y_3^2), \tag{2.4}$$

where the frequencies are $\omega_1 = -0.08047340341466$, $\omega_2 = 0.99668687782956$ and $\omega_3 = 1.00006744139040$. Due to the different signs for the values of the ω_j, the Hessian of H_2 is not positive definite. Hence, we cannot use the Lagrange-Dirichlet theorem to derive the nonlinear stability of the periodic orbit that replaces L_5.

2.3.2.2 Complexification

To simplify the subsequent steps in the normalizing process, it is very convenient to bring (2.4) into diagonal form. This can be achieved by means of a complexifying change of variables,

$$x_j = \frac{q_j + ip_j}{\sqrt{2}}, \quad y_j = \frac{iq_j + p_j}{\sqrt{2}}, \quad j = 1, 2, 3. \tag{2.5}$$

It is trivial to check that this defines a symplectic transformation that casts (2.4) into the form:

$$H_2 = i\omega_1 q_1 p_1 + i\omega_2 q_2 p_2 + i\omega_3 q_3 p_3. \tag{2.6}$$

This complexification is composed with the above-defined real matrix $P(t)$, to produce a (now complex) transformation, $P_c(t)$, that puts the second degree terms of the Hamiltonian into the form (2.6).

2.3.3 Expansion of the Hamiltonian

We need to produce a power expansion of the Hamiltonian (2.2), in the complex coordinates described before,

$$H = \sum_{n=2}^{N} H_n(q, p, \theta) + R_{N+1}(q, p, \theta),$$

where H_n, $n \geq 2$, denotes an homogeneous polynomial of degree n in the variables q and p, and H_2 is (2.6). To describe how to produce such expansion, we focus first on the terms

$$\frac{1}{s_l} = \frac{1}{\sqrt{(x - x_l(\theta))^2 + (y - y_l(\theta))^2 + z^2}}, \tag{2.7}$$

where l stands for S (the Sun), J (Jupiter) or sat (Saturn). If we write

$$\frac{1}{s_l} = \sum_{n\geq 0} A_n^l(x, y, z, \theta),$$

where A_n^l denotes an homogeneous polynomial of degree n whose coefficients are 2π periodic functions of θ. The expressions A_n^l can be easily written in terms of the Legendre polynomials, as it is explained in [Jor99] (see also [JS94]). Then, the recurrence of the Legendre polynomials allows to prove that

$$A_{n+1}^l = \frac{1}{x_l^2(\theta) + y_l^2(\theta)} \left[\frac{2n+1}{n+1}(x_l(\theta)x + y_l(\theta)y)A_n^l - \frac{n}{n+1}(x^2 + y^2 + z^2)A_{n-1}^l \right],$$

for $n \geq 1$. The recurrence can be started using the values

$$A_0^l = \frac{1}{\sqrt{x_l^2(\theta) + y_l^2(\theta)}}, \qquad A_1^l = \frac{x_l(\theta)x + y_l(\theta)y}{(x_l^2(\theta) + y_l^2(\theta))^{3/2}}.$$

As the derivation of these formulas is a straightforward modification of the autonomous case (explained in [Jor99]), we are convinced that the interested reader will not have any difficulty in proving them.

Now, the process to obtain the desired expansion for the Hamiltonian is the following. We first apply the translation that puts the periodic orbit that replaces L_5 at the origin. For simplicity, we call again to the new coordinates x, y, and z. After this translation, the terms $\frac{1}{s_l}$ still have the form (2.7). Next, we substitute the values of the variables x, y and z in the A_n^l, $n \geq 0$, by their expressions in terms of the variables q and p used in (2.6) –these expressions are given by the Floquet transformation $P_c(t)$ obtained before–. Then, we use the recurrence for the A_n^l up to a given degree $n = N$. In this way, we produce the expansion for the terms $\frac{1}{s_l}$ directly in the coordinates q, p (note that expanding first in the (x, y, z) coordinates and then substituting the Floquet transformation in this expansion requires much more work). Once the expansions for the three terms $\frac{1}{s_l}$ $(l = S, J, sat)$ are obtained, we only need to insert these transformations in the remaining terms of (2.2). Due to the simplicity of these terms –they are all of second degree–, this insertion is done directly. Finally, once all these operations have been finished, we can check that we have obtained a power expansion, with periodic time-dependent coefficients, starting at degree two, in coordinates such that the second degree terms have the diagonal form (2.6).

2.3.4 Bounds on the expansion

Here we will include two lemmas that will be used later to estimate the size of the truncated terms in the expansion. To simplify the notation, we will denote by m_l the masses of the three bodies: $m_S = 1 - \mu$ (Sun), $m_J = \mu$ (Jupiter), and m_{sat} (Saturn).

2.3.4.1 Norms

Let $f_n(u, v, \theta)$ be an homogeneous polynomial of degree n in the variables $(u, v) = (u_1, u_2, u_3, v_1, v_2, v_3)$, with periodic time-dependent coefficients,

$$f_n(u, v, \theta) = \sum_{|k|=n} \sum_{j \in \mathbb{Z}} f_{n,j}^k e^{ij\theta} u^{k^1} v^{k^2}, \quad k = (k^1, k^2) \in \mathbb{Z}^3 \times \mathbb{Z}^3, \quad f_{n,j}^k \in \mathbb{C},$$

where, if $k^1 = (k_1, k_2, k_3)$ and $k^2 = (k_4, k_5, k_6)$, we denote $|k| = |k_1| + \cdots + |k_6|$. For further use, we define the norms

$$\begin{aligned} ||f_n|| &= \sum_{|k|=n} \sum_{j \in \mathbb{Z}} |f_{n,j}^k|, \\ ||f_n||_\rho &= \sup_{(u,v) \in B_\rho,\, \theta \in \mathbb{T}^1} |f_n(u, v, \theta)|, \end{aligned}$$

where B_ρ denotes the ball of radius ρ –with respect to the Euclidean metric– centred at the origin.

2.3.4.2 Lemmas

The following lemmas are slight modifications of lemmas contained in [CG91] (see also [GDF$^+$89]), in order to include the periodic time dependence.

Lemma 2.3.1 *Assume that*

$$\begin{aligned} \|\alpha_6\| \sum_l m_l \|A^l_{n-1}\| &\leq S_{n-1}, \\ \|\alpha_6\| \sum_l m_l \|A^l_{n}\| &\leq S_{n}, \end{aligned}$$

for some $n \geq 2$ and positive constants S_{n-1} and S_n. Then, for $k > n$ one has $\|H_k\| \leq S_k$, where $\{S_k\}_{k>n}$ is a sequence of positive numbers recursively defined by

$$S_{k+1} = c_1 \left(\frac{2k+1}{k+1} c_2 S_k + \frac{k}{k+1} c_3 S_{k-1} \right), \qquad k \geq n,$$

where

$$\begin{aligned} c_1 &= \max_l c_1^l \quad \textit{where} \quad c_1^l = \left\| \frac{1}{x_l^2(\theta) + y_l^2(\theta)} \right\|, \\ c_2 &= \max_l c_2^l \quad \textit{where} \quad c_2^l = \|x_l(\theta)x + y_l(\theta)y\|, \\ c_3 &= \|x^2 + y^2 + z^2\|, \end{aligned}$$

where x, y and z are linear functions of q and p with coefficients that depend periodically on time, and the norms have been taken with respect to the variables p and q.

Proof For all $n \geq 2$ one has $H_{n+1} = -\alpha_6(\theta) \sum_l m_l A^l_{n+1}$, where

$$A^l_{n+1} = \frac{1}{x_l^2(\theta) + y_l^2(\theta)} \left(\frac{2n+1}{n+1} (x_l(\theta)x + y_l(\theta)y) A^l_n - \frac{n}{n+1} (x^2 + y^2 + z^2) A^l_{n-1} \right).$$

If we take norms,

$$\|A^l_{n+1}\| \leq c_1^l \left(\frac{2n+1}{n+1} c_2^l \|A^l_n\| + \frac{n}{n+1} c_3 \|A^l_{n-1}\| \right).$$

Thus,

$$\|H_{n+1}\| \leq \|\alpha_6\| \sum_l m_l \|A^l_{n+1}\| \leq c_1 \left(\frac{2n+1}{n+1} c_2 S_n + \frac{n}{n+1} c_3 S_{n-1} \right) = S_{n+1}.$$

■

Lemma 2.3.2 *Let us suppose that*

$$\begin{aligned} \|\alpha_6\| \sum_l m_l \|A^l_{n-1}\| &\leq S_{n-1}, \\ \|\alpha_6\| \sum_l m_l \|A^l_{n}\| &\leq S_{n}, \end{aligned}$$

for any $n \geq 2$ and positive constants S_{n-1} and S_n. Then, for $k > n$, one has $\|H_k\| \leq h^{k-n+1} E$, with

$$\begin{aligned} E &= S_{n-1}, \\ h &= max \left(\frac{S_n}{S_{n-1}}, c_1 c_2 + \sqrt{c_1^2 c_2^2 + c_1 c_3} \right), \end{aligned}$$

where c_1, c_2 and c_3 are defined in Lemma 2.3.1.

Proof We use induction. If $k = n-1$, then $\|H_{n-1}\| \le S_{n-1} = E$. If $k = n$, it follows that $\|H_n\| \le S_n = hE$ and, hence,

$$h \ge \frac{S_n}{S_{n-1}}. \tag{2.8}$$

For the case $k > n$, we assume that the result is true for k and we will show that it also holds for $k+1$.

$$\begin{aligned} S_{k+1} &= c_1\left(\frac{2k+1}{k+1}c_2 S_k + \frac{k}{k+1}c_3 S_{k-1}\right) \\ &\le c_1\left(\frac{2k+1}{k+1}c_2 h^{k-n+1}E + \frac{k}{k+1}c_3 h^{k-n}E\right). \end{aligned}$$

Imposing the right part of the inequality to be smaller than $h^{k-n+2}E$ we obtain

$$\frac{2k+1}{k+1}c_1c_2h + \frac{k}{k+1}c_1c_3 \le h^2. \tag{2.9}$$

Both inequalities (2.8) and (2.9) are satisfied by h.

■

2.4 Truncated normal form

Here we will compute a high order normal form for the expansion of the Hamiltonian obtained in the previous section. This initial expansion is already a normal form of degree 2, so here we will directly focus on the explicit computation to higher orders, as well as on obtaining explicit expansions for the change of variables.

2.4.1 Normal form of order higher than 2

For the computation of the normal form, we use the Lie series method as described in [Jor99] –to avoid using the Lie triangle–, but with the modifications introduced in [GJMS93] (see also [JS94, SGJM95]) to deal with the periodic time-dependence. The purpose of the normalizing transformation is to suppress the maximum number of terms in the Hamiltonian.

Let us start by describing a general step of the normalizing process. Suppose that the Hamiltonian is already in normal form up to degree $r-1$:

$$H = \omega_{sat}p_\theta + H_2(q,p) + \sum_{j=3}^{r-1} H_j(q,p) + H_r(q,p,\theta) + H_{r+1}(q,p,\theta) + \cdots$$

where $H_r(q,p,\theta) = \sum_{|k|=r} h_r^k(\theta) q^{k^1} p^{k^2}$, $h_r^k(\theta) = \sum_j h_{r,j}^k e^{ji\theta}$ and $k = (k^1, k^2) \in \mathbb{Z}^3 \times \mathbb{Z}^3$ is a multi-index.

We want to make a change of variables that removes the θ-dependence in H_r and suppress the maximum number of monomials of H_r. Let us call G_r the generating function of the canonical transformation we are looking for,

$$G_r = G_r(q,p,\theta) = \sum_{|k|=r} g_r^k(\theta) q^{k^1} p^{k^2}, \qquad g_r^k(\theta) = \sum_j g_{r,j}^k e^{ji\theta}. \tag{2.10}$$

If we apply the transformation defined by the time 1 flow of the Hamiltonian G_r (for more details, see the Appendix A of [Jor99]), we easily see that the terms of degree r of the transformed Hamiltonian, H_r', are given by

$$H_r' = H_r + \{\omega_{sat} p_\theta, G_r\} + \{H_2, G_r\} \equiv H_r + \omega_{sat}\frac{\partial G_r}{\partial \theta} + \{H_2, G_r\}.$$

We select the Fourier coefficients $g_{r,j}$ of (2.10) such that H_r' has the simplest possible form:

$$g_r^k(\theta) = \begin{cases} \dfrac{i h_{r,0}^k}{\langle \omega, k^2 - k^1\rangle} + \displaystyle\sum_{j\neq 0} \dfrac{h_{r,j}^k}{ij\omega_{sat} - i\langle \omega, k^2-k^1\rangle} e^{ji\theta} & \text{if} \quad k^1 \neq k^2, \\ \displaystyle\sum_{j\neq 0} \dfrac{h_{r,j}^k}{ij\omega_{sat}} e^{ji\theta} & \text{if} \quad k^1 = k^2, \end{cases}$$

Of course, we are assuming that the frequencies $\omega = (\omega_1, \omega_2, \omega_3)$ and ω_{sat} satisfy a non-resonance condition, $ij\omega_{sat} - i\langle\omega, k\rangle \neq 0$, $j \in \mathbb{Z}$, $k \in \mathbb{Z}^3$. In fact, as we will only apply this process up to a finite order in the variables (q,p), and the Fourier series are truncated to a finite order, this condition is only needed up to suitable values of $|j|$ and k. In fact, it is automatically checked before computing the function G_r, for each r. In our case, this non-resonance condition is satisfied up to the orders we have worked with.

The H_r' obtained with such a G_r does not depend on time, and it only depends on monomials of the form $q^{k^1}p^{k^2}$, with $k^1 = k^2$. The new Hamiltonian obtained with this change of variables is

$$H' = H + \{H, G_r\} + \frac{1}{2!}\{\{H, G_r\}, G_r\} + \cdots,$$

and satisfies that

$$H' = \omega_{sat} p_\theta + H_2(q,p) + \sum_{j=3}^{r-1} H_j(q,p) + H_r'(q,p) + H_{r+1}'(q,p,\theta) + \cdots,$$

is in normal form up to degree r. Hence, we can rename the Hamiltonian as H, and repeat the same process as before and compute the normal form for the terms of degree $r+1$.

After performing all this changes up to a suitable degree $n = N$, the Hamiltonian takes the form

$$H = \omega_{sat} p_\theta + \mathcal{N}(q_1p_1, q_2p_2, q_3p_3) + \mathcal{R}(q_1, q_2, q_3, p_1, p_2, p_3, \theta), \tag{2.11}$$

k_1	k_2	k_3	Re (h_k)	Im (h_k)
1	0	0	-8.0473403414658348e-02	0.0000000000000000e+00
0	1	0	9.9668687782955701e-01	0.0000000000000000e+00
0	0	1	1.0000674413904136e+00	0.0000000000000000e+00
2	0	0	5.6007414394589805e-01	-1.8705256953566430e-13
1	1	0	-1.5540007094294600e-01	-9.3830451518209680e-15
0	2	0	5.5094910495712413e-03	1.0717280513316625e-16
1	0	1	5.4161643846023226e-02	-6.2140551599726659e-15
0	1	1	6.6064951514490360e-03	1.2257344054847067e-16
0	0	2	-3.4086514191576233e-04	9.5191394827757230e-22
3	0	0	1.7076591917555746e+01	-7.8087823960270605e-09
2	1	0	2.5312327640336463e+00	5.9890652038702482e-09
1	2	0	1.2040133893299085e+00	7.5183303416244784e-10
0	3	0	-1.7301900678281523e-03	4.4060011855097767e-12
2	0	1	-2.0884087969793064e-01	-3.6110568734989503e-10
1	1	1	1.3097674563771786e+00	1.6810633045057165e-10
0	2	1	-8.8065932627078847e-03	1.8072038419138380e-12
1	0	2	-3.8394202697275989e-02	-6.8093926120365380e-12
0	1	2	-8.1760590356997620e-03	-1.9530188730672947e-13
0	0	3	4.8057053869314466e-04	-3.8350420390170530e-14

Table 2.2: Coefficients of the normal form, up to degree 3 in the actions. The first three columns contain the exponents of the actions, and the fourth and fifth columns are the real and imaginary part of the coefficients. Imaginary parts must be zero, but they are not due to the roundoff errors of the floating point arithmetic.

where $\mathcal{N}$ denotes the normal form (that only depends on the products $q_j p_j$) and $\mathcal{R}$ is the remainder. Finally, we will write the normal form $\mathcal{N}$ again in real action-angle coordinates. This can be easily achieved by using the (canonical) transformation,

$$q_j = I_j^{1/2} \exp(i\varphi_j), \quad p_j = -iI_j^{1/2} \exp(-i\varphi_j), \quad j = 1, 2, 3. \tag{2.12}$$

It is not difficult to see that $\mathcal{N}$, in these coordinates, does not depend on the angles φ_j but only on the actions I_j,

$$\mathcal{N} = \sum_{|k|=1}^{[N/2]} h_k I_1^{k_1} I_2^{k_2} I_3^{k_3}, \qquad k \in \mathbb{Z}^3, \quad h_k \in \mathbb{R}.$$

Values for the coefficients h_k can be found in Table 2.2.

Later, we will also use this normalized Hamiltonian in the real coordinates (x, y), defined as

$$I_j = \frac{1}{2}(x_j^2 + y_j^2), \qquad j = 1, 2, 3.$$

These coordinates can also be defined from the coordinates (q, p) of (2.11) by

$$q_j = \frac{x_j - iy_j}{\sqrt{2}}, \quad p_j = \frac{-ix_j + y_j}{\sqrt{2}}, \quad j = 1, 2, 3. \tag{2.13}$$

Note that this is the inverse of (2.5).

2.4.2 Changes of variables

With a similar process based on the use of Lie series, we have also computed explicit expressions for the transformation from the initial variables of (2.6) to the final variables (see [GJMS93, Jor99] for more details). This change of variables is also a truncated power series up to degree N, that will be used in the forthcoming sections to send information from the normal form coordinates to the initial ones.

2.4.3 Invariant tori

In the previous sections we have obtained a change of variables that brings the initial Hamiltonian (2.2) into the form $H = \omega_{sat} p_\theta + \mathcal{N} + \mathcal{R}$, where $\mathcal{N}$ is an autonomous, integrable Hamiltonian system, and $\mathcal{R}$ is a remainder of order 17 with respect to the distance to the periodic orbit. Hence, we can neglect the term $\mathcal{R}$ and the (trivial) dynamics given by the rotator $\omega_{sat} p_\theta$, and take $\mathcal{N}$ as a good approximation for the dynamics, at least near the periodic orbit.

The dynamics of the integrable normal form $\mathcal{N}$ is very simple: as $\mathcal{N}$ only depends on the action coordinates, the equations of motion are

$$\dot{I} = -\nabla_\varphi \mathcal{N}(I) \equiv 0, \qquad \dot{\varphi} = \nabla_I \mathcal{N}(I) \equiv \Omega(I), \quad I \in \mathbb{R}^3, \quad \varphi \in \mathbb{T}^3. \tag{2.14}$$

These equation can be easily integrated:

$$I = I_0, \qquad \varphi = \Omega(I_0)t + \varphi_0, \tag{2.15}$$

Therefore, the phase space is completely foliated by a 3-parametric family of invariant tori (I_0 is the parameter) and, on each torus $I = I_0$, there is a linear flow with frequency $\Omega(I_0)$. If the frequencies (i.e., the components of the vector $\Omega(I_0)$) are linearly independent over the rationals then the torus $I = I_0$ is filled densely by any trajectory starting on it. If the frequencies are linearly dependent over the rationals, then the orbits on this torus are not dense: if there are ℓ_i independent frequencies, the torus $I = I_0$ contains a $(3 - \ell_i)$-parametric family of ℓ_i dimensional tori, being each one densely filled by any trajectory starting on it. These tori of dimension ℓ_i are known as lower dimensional tori, while the tori of dimension 3 are called maximal dimensional ones.

The effect of the remainder $\mathcal{R}$ on these tori is studied by the KAM theory. Essentially, the KAM theorem ensures that the tori whose frequencies satisfy a suitable Diophantine condition of the kind,

$$\langle k, \Omega(I_0) \rangle \geq \frac{c}{|k|^\tau},$$

are not destroyed by the perturbation, but only slightly deformed. Under generic conditions, it can be proved that the measure of the tori not preserved by the effect of the remainder is bounded by an exponentially small quantity with respect to the periodic orbit ([JV97b, JV97a, JV01]). This implies that, from a practical point of view, the phase space of the complete system $\mathcal{N} + \mathcal{R}$ seems, near the origin, foliated by invariant tori, since the measure of the set of non quasi-periodic motions is too small to be seen with the standard floating point arithmetic of the computer.

Let us now consider the frequency map of the normal form,

$$\Omega : B \subset \mathbb{R}^3 \to \mathbb{R}^3,$$

where $\Omega \equiv \nabla_I \mathcal{N}$, and B is an open neighbourhood of the origin such that the remainder $\mathcal{R}$ is sufficiently small or, in other words, such that the normal form provides a sufficiently good approximation to the dynamics (later, in Section 2.4.4, we will discuss how to estimate such a domain). The vector $\Omega(0)$ is the vector of normal frequencies of the periodic orbit (the values $(\omega_1, \omega_2, \omega_3)$ obtained in Section 2.3.2). Consider the line $I_\lambda = (\lambda, 0, 0)$, $|\lambda| \leq \lambda_0$, and the values $\Omega(I_\lambda)$. For any value of λ, the corresponding trajectory in (2.14) is sent by (2.12) into a periodic orbit in the (q,p) coordinates; the frequency of this orbit is $\Omega_1(I_\lambda)$, and the normal frequencies are $\Omega_2(I_\lambda)$ and $\Omega_3(I_\lambda)$. Similar families can be obtained using $I_\lambda = (0, \lambda, 0)$ and $I_\lambda = (0, 0, \lambda)$. These families of periodic orbits can be seen as the Lyapunov families (of periodic orbits) around the origin of the normal form. When these families are sent (through the changes we have computed before) to the coordinates of the BCCP Hamiltonian (2.2), they "gain" the frequency of the periodic orbit and become quasi-periodic orbits –with two basic frequencies– near the periodic orbit replacing L_5. Of course, this does not prove the existence of these families of quasi-periodic solutions around the periodic orbit because, during the computations, we have neglected the remainders. The proof of persistence requires a KAM theorem adapted to the lower-dimensional case, see [JV97b].

We can also consider two-parametric families $I_{\lambda_1,\lambda_2} = (\lambda_1, \lambda_2, 0)$. This will produce a two-parametric family of two-dimensional tori on the normal form, with frequencies $\Omega_1(I_{\lambda_1,\lambda_2})$ and $\Omega_2(I_{\lambda_1,\lambda_2})$, and normal frequency $\Omega_3(I_{\lambda_1,\lambda_2})$. This family gives rise, in the initial BCCP coordinates, to a two-parametric family of quasi-periodic orbits with three basic frequencies. Finally, we can use three non-zero parameters $\lambda_{1,2,3}$ to obtain three dimensional tori in the normal form, that correspond to four dimensional tori for the BCCP problem. Therefore, the normal form gives a complete description of the kind of quasi-periodic orbits we can find near the periodic orbit replacing L_5.

Finally, we will use this normal form to compute some quasi-periodic motions near the periodic orbit. The process will be as follows. First, we will select a value $I_0 \in \mathbb{R}^3$ –later we will discuss this selection with more detail– and we will compute the vector $\Omega(I_0) = \nabla_I \mathcal{N}(I_0)$ (we recall that $\mathcal{N}$ is a polynomial in I). Given a phase φ_0 (for these examples, we have simply taken $\varphi_0 = 0$), it is then not difficult to use (2.15) to tabulate points of the corresponding trajectory on the torus $I = I_0$. Finally, using the changes of variables, we can send these points to the initial (synodical) coordinates of the BCCP model.

Figures 2.10, 2.11 and 2.12 are examples of these computations. More concretely, Figure 2.10 displays two different projections of a two dimensional torus of the vertical family –the family that "grows" in the (z, p_z) direction–. Figure 2.11 are projections of two different two dimensional tori contained in the $z = p_z = 0$ plane. Finally, Figure 2.12 displays the projections of a three and a fourth dimensional torus. All these graphics have been obtained computing 10,000 points, with a time step of 0.1 units. See the captions for more details.

We also note that, in this way, it is possible to compute quasi-periodic orbits with prescribed set of frequencies Ω_0, provided that Ω_0 belongs to the domain B where the

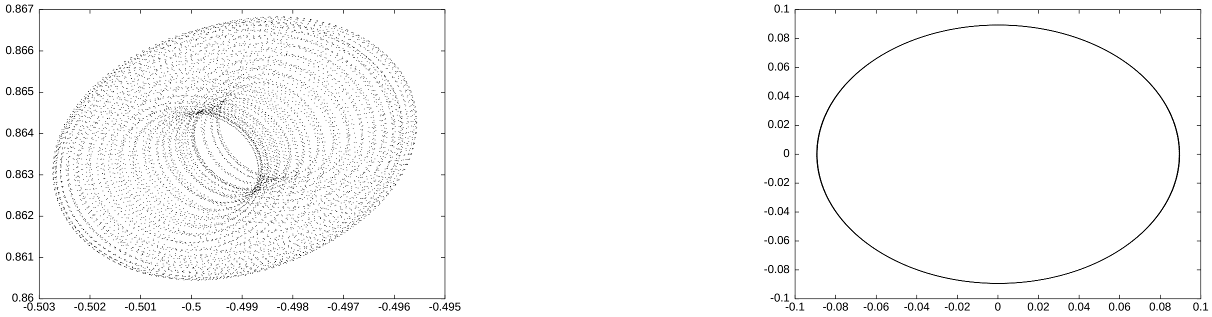

Figure 2.10: Projection on the (x, y) (left) and on the (z, p_z) (right) planes of an elliptic two-dimensional invariant torus of the vertical family near the periodic orbit that replaces L_5. The intrinsic frequencies are ω_{sat} and $\omega_3 = 1.000064737$. The normal ones are $\omega_1 = -0.08025736934$ and $\omega_2 = 0.9967131749$.

Figure 2.11: Projections on the (x, y) plane of two tori, belonging to the two planar two-dimensional invariant tori families near the periodic orbit that replaces L_5. The intrinsic frequencies of the left figure one are ω_{sat}, $\omega_1 = -0.08042851476$ and the normal ones are $\omega_2 = 0.9966806656$, $\omega_3 = 1.000069607$. For the right figure one the intrinsic frequencies are ω_{sat}, $\omega_2 = 0.9966912842$ and the normal ones $\omega_1 = -0.08053537024$, $\omega_3 = 1.000070082$.

normal form is accurate.

2.4.4 A lower bound on the diffusion time

As it has been explained in the previous section, the dynamics described by the normal form is quasi-periodic. This means that, for the normal form, the origin is Lyapunov stable. Of course, this picture can be changed by the effect of the remainder $\mathcal{R}$. For this reason, in this section we will focus on the determination of a region B in the actions space, such that any trajectory starting inside B remains near B for a time of the order of the age of the Solar system. The method to compute such a region is based on bounding the remainder $\mathcal{R}$, and it is based on the procedures used in [GDF+89], [Sim89] and [JS94].

2.4.4.1 Norms

We will use the norms defined in Section 2.3.4.1. Here, the sup norm $\|.\|_\rho$ will be always taken for real values of the variables. If $f_n(x, y, \theta)$ and $g_m(x, y, \theta)$ denote homogeneous

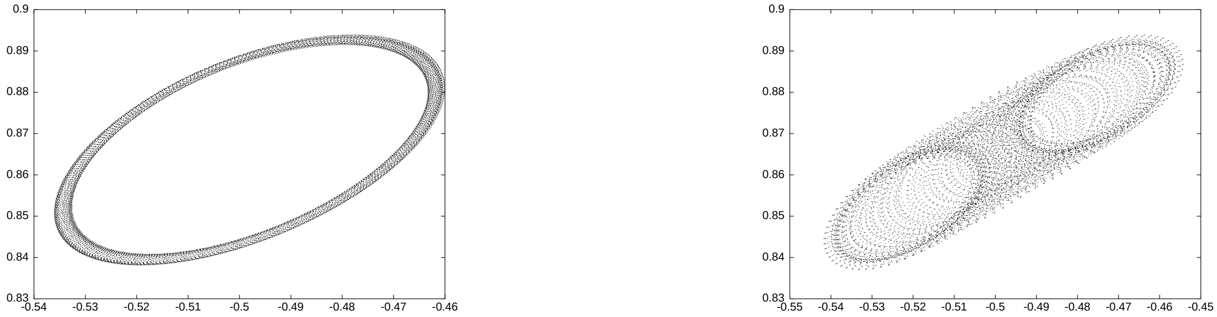

Figure 2.12: Left: Projection on the (x, y) plane of an elliptic three-dimensional invariant torus of the vertical family near the periodic orbit that replaces L_5. The intrinsic frequencies are ω_{sat}, $\omega_2 = 0.9966904013$ and $\omega_3 = 1.000068625$. The normal one is $\omega_1 = -0.08049355163$. Right: Projection on the (x, y) plane of an elliptic fourth-dimensional invariant torus of the vertical family near the periodic orbit that replaces L_5. The frequencies are ω_{sat}, $\omega_1 = -0.08045369737$, $\omega_2 = 0.9966878607$ and $\omega_3 = 1.000068109$.

polynomial of degrees n and m, we have that

$$\begin{aligned} || \{f_{n_1}, g_{n_2}\} || &\leq n_1 n_2 ||f_{n_1}|| ||g_{n_2}||, \\ ||f_n||_\rho &\leq \rho^n ||f_n||. \end{aligned}$$

The proof is a straightforward generalisation of the autonomous case ([Gio88]).

2.4.4.2 Bounding the effect of the remainder

Let us consider a trajectory $(x(t), y(t))$ for the Hamiltonian (2.11) in the coordinates (x, y) defined by (2.13). We define the quantity $\rho(t)$ as the distance of the trajectory to the origin,

$$\rho(t)^2 = \sum_{j=1}^{3} (x_j(t)^2 + y_j(t)^2).$$

As $I_j(t) = \frac{1}{2}(x_j(t)^2 + y_j(t)^2)$, $j = 1, 2, 3$, we have that

$$\frac{1}{2}\rho(t)^2 = \sum_{j=1}^{3} I_j(t).$$

Then,

$$\rho\dot{\rho} = \sum_{j=1}^{3} \dot{I}_j = \sum_{j=1}^{3} \{I_j, H\} = \sum_{j=1}^{3} \{I_j, \mathcal{R}\}, \tag{2.16}$$

where we have used that $H = \mathcal{N} + \mathcal{R}$, and that $\mathcal{N}$ only depends on the actions I_j. To continue with this process, we will make use of the following estimation.

Lemma 2.4.1 *Let $f_n(x,y,\theta)$ be an homogeneous polynomial of degree n in (x,y) coordinates with time dependent coefficients and $I_j = \frac{1}{2}(x_j^2 + y_j^2)$ with $j = 1,2,3$. Then,*

$$\left\| \left\{ \sum_{j=1}^{3} I_j, f_n \right\} \right\| \leq n \|f_n\|.$$

Proof It is based on Lemma A.3 in [Gio88]. As we have

$$\left\{ \sum_{j=1}^{3} I_j, f_n \right\} = \sum_{|k^1|+|k^2|=n} \left(\sum_{j=1}^{3} (k_j^2 \frac{x_j}{y_j} - k_j^1 \frac{y_j}{x_j}) \right) \left(\sum_l f_{n,l}^k(\theta) \right) x^{k^1} y^{k^2},$$

taking bounds, we obtain

$$\begin{aligned} \left\| \left\{ \sum_{j=1}^{3} I_j, f_n \right\} \right\| &\leq \sum_{|k^1|+|k^2|=n} \left(\sum_{j=1}^{3} (k_j^1 + k_j^2) \right) \left(\sum_l |f_{n,l}^k(\theta)| \right) \\ &= n \sum_{|k^1|+|k^2|=n} \sum_l |f_{n,l}^k(\theta)|. \end{aligned}$$

■

Now we can continue from formula (2.16). If we write $\mathcal{R} = \sum_{k>N} \mathcal{R}_k$ ($\mathcal{R}_k$ denotes an homogeneous polynomial of degree k), we can take absolute values in both sides of (2.16) and, using the bound in Lemma 2.4.1 we have that (2.16) becomes

$$|\dot{\rho}| \leq \sum_{k>N} k \|\mathcal{R}_k\| \rho^{k-1}.$$

Now we define the function

$$z(\rho) = \sum_{k>N} k \|\mathcal{R}_k\| \rho^{k-1},$$

and, therefore, to estimate the diffusion speed (given by $\dot{\rho}$) we need to produce bounds on this function. Of course, the main problem is that, in the normal form process, we have not obtained the terms $\mathcal{R}_k$ for $k > N$. As we cannot compute those terms for all $k > N$, we will try to derive bounds on these terms. So, we start by computing the norms of the initial expanded Hamiltonian up to degree N and, with the recurrence given in Lemma 2.3.1, we compute explicit bounds on the terms of the Hamiltonian up to a given degree $\widehat{N}$. Then, we transform (numerically) these norms using the sequence of changes given by the generating functions used to put the Hamiltonian in normal form up to degree N. For example, in step r ($r = 3, \dots, N$) we have the exact norms of the terms 2 to N of the Hamiltonian in normal form up to degree $r-1$ and a bound on the norms of the terms $N+1$ to $\widehat{N}$ of the same Hamiltonian. To obtain bounds of the norms of the Hamiltonian in normal form up to degree r, we use the same process as described in Section 2.4.1, but only using norms in the formulas:

$$\begin{aligned} \|\bar{H}_k\| &\leq \|H_k\| + \|\{H_{k-r+2}, G_r\}\| + \frac{1}{2!} \| \{ \{ H_{k-2(r-2)}, G_r \}, G_r \} \| + \cdots \\ &\leq \|H_k\| + (k-r+2) r \|H_{k-r+2}\| \|G_r\| \\ &\quad + \frac{1}{2!} (k - 2(r-2))(k-r+2) r^2 \|H_{k-2(r-2)}\| \|G_r\|^2 + \cdots , \end{aligned}$$

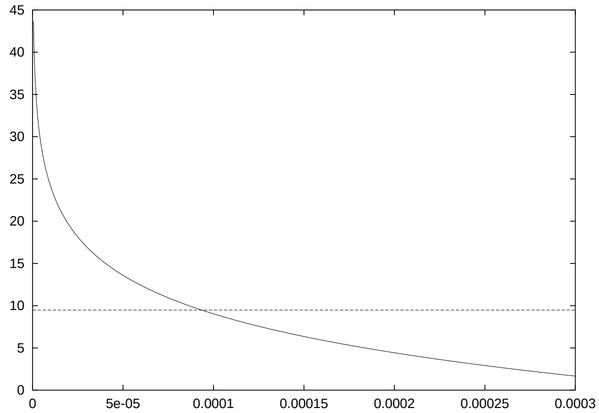

Figure 2.13: Plot of the function $\log(T_{\rho_0})$ and the estimated age of the Solar System $\log(T_S) = 9.4771213$ is marked with an horizontal line.

for $N < k \leq \widehat{N}$. After the last step ($r = N$), we have obtained an array of bounds of the norms of the terms from degree $N+1$ to $\widehat{N}$ of the Hamiltonian in normal form up to degree N. These are the bounds we were looking for.

Then, we can approximate the function $z(\rho)$:

$$z(\rho) \approx \sum_{k=N+1}^{\widehat{N}} k\|\mathcal{R}_k\|\rho^{k-1}. \tag{2.17}$$

Note that, if $\widehat{N}$ is sufficiently large, the effect of the remainder $\sum_{k>\widehat{N}} k\|\mathcal{R}_k\|\rho^{k-1}$ can be neglected. For the final calculations, in this paper we have used the values $N = 16$ and $\widehat{N} = 99$.

2.4.4.3 Region of effective stability

Assume that we select an initial condition inside a ball B_{ρ_0} and that we want the orbit to remain inside B_ρ ($\rho > \rho_0$) during a time span of length T. Then, the values ρ_0, ρ and T satisfy

$$T = \int_{\rho_0}^{\rho} \frac{du}{z(u)}. \tag{2.18}$$

So, if we write $\rho = \sigma\rho_0$ and we select a value $\sigma > 1$, equation (2.18) defines a function $T = T(\rho_0)$. This function can be tabulated numerically, and it is plotted in Figure 2.13. In this paper, we have used the value $\sigma = 2.1861$. This value of σ is chosen to compare these results with the ones obtained using a first integral. See Section 2.5.3.2 for more details.

Then, if we choose $T = T_S \equiv 3 \times 10^9$ as an estimation of the age of the Solar system (we recall that 2π is the period of the orbit of Jupiter), we can easily find the initial radius ρ_0 for which any orbit starting in the ball B_{ρ_0} lies inside the ball $B_{\sigma\rho_0}$ for this time span T_S. The result obtained here is $\rho_0 = 9.3539 \times 10^{-5}$.

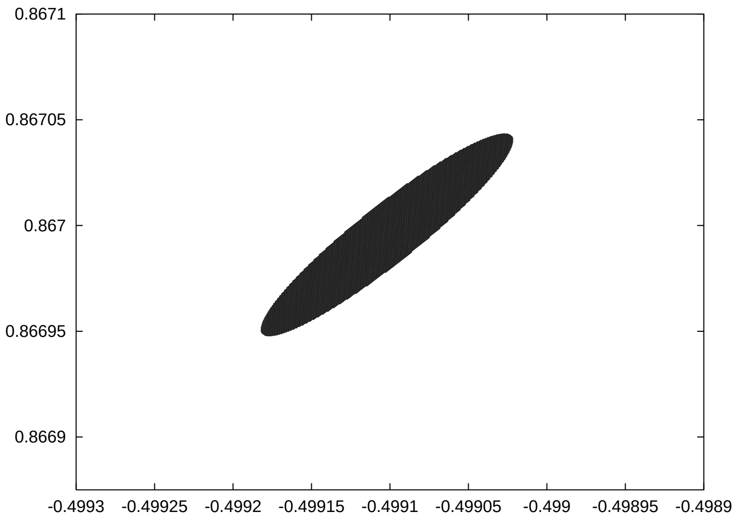

Figure 2.14: Region of effective stability from the normal form computation. The region has been computed around the position for $t = 0$ of the periodic orbit replacing L_5. The axis are the x and y synodical coordinates of the BCCP used in (2.2) and in Figure 2.8.

2.4.4.4 Going back to synodical coordinates

The last step is to send this ball to the initial coordinates of the BCCP. We first note that, due to the time dependence, the resulting stability region moves around the periodic orbit substituting L_5. Here, in order to compare the results obtained with the normal form, first integrals and direct numerical simulation, we will use the following scheme:

a) Compute a 2-D mesh of points, in the synodical BCCP coordinates x and y, around the position of the periodic orbit for $t = 0$.

b) Each point (x, y) of this mesh is completed to a 6-D point by adding the z, p_x, p_y and p_z coordinates of the periodic orbit for $t = 0$.

c) These points are sent to the real normal form coordinates, so we can test whether the point is inside the ball B_{ρ_0} or not.

d) The initial (x, y) coordinates of the points that are mapped into B_{ρ_0} are plotted.

The result of this procedure is shown in Figure 2.14 where each point of d) has been marked with a black dot. More comments in Section 2.5.3.2.

2.5 Approximate first integrals

This section is devoted to the computation of an approximate first integral for the BCCP Hamiltonian (2.2). Then, we will use this approximate first integral for computing a region of effective stability around the periodic orbit replacing L_5. This process is based on the methods used in [Gio88, CG91], with the necessary modifications to include the periodic time-dependence of the Hamiltonian. This is an alternative procedure to the normal form computations for estimating regions of effective stability.

2.5.1 Numerical computation

We start with the Hamiltonian expanded in complex coordinates, as it has been explained in Section 2.3,

$$H(q,p,\theta,p_\theta) = \omega_{sat} p_\theta + H_2(q,p) + \sum_{n\geq 3} H_n(q,p,\theta),$$

where H_2 is in the diagonal form (2.6), and H_n are homogeneous polynomials of degree n. As before, we have introduced p_θ as the conjugate variable of θ, so the Hamiltonian is now autonomous. We look for an approximate first integral as a truncated Taylor-Fourier expansion,

$$F(q,p,\theta) = \sum_{n=2}^{N} F_n(q,p,\theta),$$

where, as usual, F_n stands for an homogeneous polynomial of degree n in the variables (q,p), with coefficients that are (truncated) Fourier series in the angle θ. Note that F does not depend on p_θ; the reasons for this selection will be clear later on.

It is known that, if F is a first integral for the flow of the Hamiltonian H, then $\{H,F\} = 0$ (for a summary of basic properties of Hamiltonian systems, see Appendix A of [Jor99]). This equation gives a recursive way of computing the coefficients of the expansion of F: taking into account the form of H, we have

$$\{\omega_{sat} p_\theta, F\} + \{H_2, F\} = -\left\{\sum_{n\geq 3} H_n, F\right\}. \tag{2.19}$$

Now we use the expansion for F, and we select

$$F_2 = i\sum_{j=1}^{3} q_j p_j. \tag{2.20}$$

As $\{H_2, F_2\} = 0$, equation (2.19) reads "0=0" for $n = 2$. So, we will focus on the case $n > 2$. Assume now that we know the values F_m for $2 < m < n$, and we want to compute F_n. From (2.19), we have

$$\sum_{n=3}^{N} -\omega_{sat}\frac{\partial F_n}{\partial \theta} + \sum_{n=3}^{N}\{H_2, F_n\} = -\sum_{n\geq 3}\sum_{j=3}^{n}\{H_j, F_{n-j+2}\}$$

In this equation, we select all the terms of degree n to obtain

$$-i\omega_{sat}\sum_{|k|=n}\left(\sum_j j f_{n,j}^k e^{ij\theta}\right) q^{k^1} p^{k^2} + \{H_2(q,p), F_n(q,p,\theta)\} = C_n(q,p,\theta), \tag{2.21}$$

where $f_{n,j}^k$ is the j-Fourier coefficient of $f_n^k(\theta)$, $F_n(q,p,\theta) = \sum_{|k|=n} f_n^k(\theta) q^{k^1} p^{k^2}$ and

$$C_n(q,p,\theta) = -\sum_{j=3}^{n}\{H_j(q,p,\theta), F_{n-j+2}(q,p,\theta)\}$$

Note that C_n only depends on values of F_m that are known. Hence, we can write it as

$$C_n(q,p,\theta) = \sum_{|k|=n} \left(\sum_j c^k_{n,j} e^{ij\theta} \right) q^{k^1} p^{k^2},$$

where the coefficients $c^k_{n,j}$ are known. Then, equation (2.21) can be easily solved to find F_n:

$$f^k_{n,j} = \frac{ic^k_{n,j}}{j\omega_{sat} - \langle k^2 - k^1, \omega \rangle}. \tag{2.22}$$

Hence, we have derived a recurrent procedure to generate the formal expansion of the first integral. This process is very similar to the one used in [CG91], but with the necessary modifications to take into account the periodic time dependence.

The reason for selecting F_2 as (2.20) is that, in real coordinates, it corresponds to a positive definite quadratic form,

$$F_2 = \sum_{j=1}^{3} \frac{1}{2}(x_j^2 + y_j^2). \tag{2.23}$$

We will show that, using this positive definite character of F_2 on a suitable domain, F has a bounded drift for a time of $T_S = 3 \times 10^9$ and that, on the same domain, the level surfaces of F still act as a barrier to the diffusion. Note that, in [CG91], the authors use three independent first integrals, corresponding to the selection

$$F_2^{(j)} = \frac{1}{2}(x_j^2 + y_j^2), \qquad j = 1, 2, 3,$$

and they bound the drift of these three integrals. Hence, each integral is used to bound the diffusion in the corresponding direction (x_j, y_j). Here, we use a single integral, that is a positive definite combination of these three. In this way, we only need to compute and control a single first integral. Finally, note that the integral does not contain the variable p_θ, so we do not obtain bounds on the diffusion of this variable. We note that p_θ has been introduced to autonomize the Hamiltonian, and has no physical meaning, so there is no need in bounding the drift of such variable. In fact, the diffusion in this variable can be seen as a diffusion respect to the initial phase taken for the angular variable θ, which is irrelevant for our purposes.

As a side comment, we want to note that the formal existence of these integrals to all orders is not a trivial question. Looking at (2.22) it is clear that the following two conditions are required:

a) ω_{sat} and ω must satisfy that

$$j\omega_{sat} - \langle k, \omega \rangle \neq 0, \quad \forall\, j \in \mathbb{Z}, \quad \forall\, k \in \mathbb{Z}^3 \text{ such that } |j| + |k| \neq 0,$$

b) if $j = 0$ and $k^1 = k^2$, the value $c^k_{n,j}$ must vanish.

If ω_{sat} and ω are known, condition a) can be in principle verified. Condition b) is, however, much more involved. See [CG91] for a discussion.

2.5.2 Bounding the diffusion

We will start using the expansion of the Hamiltonian in complex coordinates obtained in 2.3. Thus, the Hamiltonian looks like:

$$H = \omega_{sat} p_\theta + \sum_{j=1}^{3} i\omega_j q_j p_j + \sum_{n\geq 3} H_n(q,p,\theta).$$

We will assume that we have computed a truncation F (to degree N) of a formal first integral. Then, both this Hamiltonian and F can be put again into real form using (2.13). Hence, they will have the form

$$\begin{aligned} H &= \omega_{sat} p_\theta + \sum_{j=1}^{3} \frac{\omega_j}{2}\left(x_j^2+y_j^2\right) + \sum_{n\geq 3} H_n(x,y,\theta), \\ F &= \sum_{j=1}^{3} \frac{1}{2}\left(x_j^2+y_j^2\right) + \sum_{n=3}^{N} F_n(x,y,\theta). \end{aligned}$$

Note that the variation of the values of F on a given trajectory of the Hamiltonian is not constant –F is not an exact first integral–, and that this variation can be written as

$$\dot F = \{F(q,p,\theta), H(q,p,\theta,p_\theta)\}\,.$$

From the equations in Section 2.5.1, it is easy to see that

$$\dot F = \sum_{n>N}\sum_{l=3}^{N} \{F_l, H_{n-l+2}\} + \sum_{n>N} \{F_2, H_n\}\,. \tag{2.24}$$

We will follow the same scheme as in [CG91]. So, we will use Lemmas in Section 2.3.4.2 to estimate the size of the terms in the Hamiltonian that have not been numerically computed. The idea is the following: we have computed F (and the expansion of H) up to degree $N=16$. Then, we will select a second degree $\widehat N$ (we have used $\widehat N = 99$) and we will use Lemma 2.3.1 to bound the norms of the expansion of the Hamiltonian from $n = N+1$ to $n=\widehat N$. Finally, the terms of the Hamiltonian of degree $n>\widehat N$ will be bounded by means of Lemma 2.3.2. There are no reasons for the particular selection of $\widehat N = 99$; we could have chosen an even larger value, but the results do not change in a significant way. The results of applying this procedure to (2.24) are summarized in the following lemma.

Lemma 2.5.1 *Let N and $\widehat N$ be integers such that $3\leq N\leq \widehat N$ and*

$$\begin{aligned} \|H_k\| &\leq S_k & 3\leq k\leq \widehat N, \\ \|H_k\| &\leq h^{k-\widehat N+1}E & k>\widehat N, \\ \|F_k\| &\leq Q_k & 3\leq k\leq N. \end{aligned}$$

Then, if $h\rho<1$,

$$\|\dot F\|_\rho \leq \mathcal{R}(\rho),$$

where

$$\begin{aligned}
\mathcal{R}(\rho) &= \sum_{j=1}^{N-2}(j+2)\rho^j Q_{j+2} \sum_{N-j<l\leq\widehat{N}} l\rho^l S_l \\
&\quad + \sum_{j=1}^{N-2}(j+2)\rho^j Q_{j+2}\frac{E}{h^{\widehat{N}}}h\frac{(\widehat{N}+1)(h\rho)^{\widehat{N}+1}-\widehat{N}(h\rho)^{\widehat{N}+2}}{(1-h\rho)^2} + \\
&\quad + \sum_{N<l\leq\widehat{N}} l\rho^l S_l + \frac{E}{h^{\widehat{N}}}h\frac{(\widehat{N}+1)(h\rho)^{\widehat{N}+1}-\widehat{N}(h\rho)^{\widehat{N}+2}}{(1-h\rho)^2}.
\end{aligned}$$

Proof See [CG91].

2.5.3 A lower bound on the diffusion time

Assume now that we have an initial condition $(x(0), y(0))$ inside the ball B_{ρ_0}. We are interested in values $\rho > \rho_0$ such that the orbit $(x(t), y(t))$ is contained in B_ρ for all $t \in [0, T_S]$. A sufficient condition to achieve this is that

$$|F_2(x(t), y(t)) - F_2(x(0), y(0))| \leq \frac{1}{2}(\rho^2 - \rho_0^2), \quad 0 \leq t \leq T_S, \tag{2.25}$$

where F_2 is given by (2.23). Let us now define

$$\Delta_N(\rho_0, \rho) = \frac{1}{2}(\rho^2 - \rho_0^2) - \sum_{j=3}^{N} \|F_j\|(\rho^j + \rho_0^j).$$

It is easy to see that, if $\Delta_N(\rho_0, \rho) \geq 0$ and

$$|F(x(t), y(t)) - F(x(0), y(0))| \leq \Delta_N(\rho_0, \rho),$$

then, (2.25) holds. The function $\Delta_N(\rho_0, \rho)$ is used to bound the maximum variation of $F(x, y, \theta)$ on the interval of time $[0, T_S]$ because (2.25) is a sufficient condition for the trajectory to be inside the ball B_ρ. Note that, due to the particular form of Δ_N, the values ρ_0 and ρ have to be selected sufficiently small to achieve $\Delta_N(\rho_0, \rho) \geq 0$ but, on the other hand, we want Δ_N to be as large as possible, to allow a large variation of F with a controlled variation of ρ. Hence, we will carefully select the values ρ_0 and ρ to obtain the largest region of effective stability for time T_S.

So, if $\Delta_N(\rho_0, \rho) \geq 0$ (later we will study this condition in detail), we can bound the escape time as a function of the initial radius,

$$T(\rho_0) = \sup_\rho \frac{\Delta_N(\rho_0, \rho)}{\mathcal{R}(\rho)}. \tag{2.26}$$

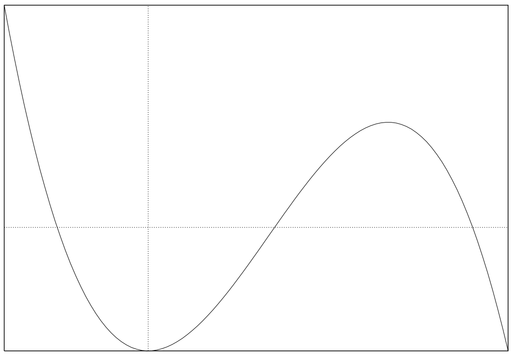

Figure 2.15: Heuristic plot of $\Delta_N(\rho_0, \rho)$ versus ρ for a fixed ρ_0

2.5.3.1 Study of the condition $\Delta_N(\rho_0, \rho) \geq 0$

As we are interested in values ρ_0 for which $T(\rho_0)$ is large (and positive), we will only focus on the study of values ρ and ρ_0 such that

$$\Delta_N(\rho_0, \rho) = \frac{1}{2}(\rho^2 - \rho_0^2) - \sum_{j=3}^{N} \|F_j\|(\rho^j + \rho_0^j) \geq 0. \tag{2.27}$$

If we fix ρ_0 and study Δ_N as a function of ρ, we observe that there is always a local minimum at $\rho = 0$, and a local maximum at $\rho = \hat{\rho}$ such that

$$\sum_{j=3}^{N} j||F_j||\hat{\rho}^{j-2} = 1.$$

If we increase the value of ρ_0, there is only a change in the values of Δ_N at the local extrema, but not in the points they are achieved. There is just a closed interval, in the positive part of the ρ axis, where the condition holds true (see Figure 2.15).

Increasing ρ_0, this interval shrinks to one point $\hat{\rho}$. After that, for $\rho_0 > \rho_0^{crit}$ where ρ_0^{crit} is such that $\Delta_N(\rho_0^{crit}, \hat{\rho}) = 0$, the condition is false.

2.5.3.2 Final results

In order to find the supreme in equation (2.26), we fix ρ_0 and we look for a zero of the equation

$$\frac{\partial \Delta_N}{\partial \rho}(\rho_0, \rho)\mathcal{R}(\rho) - \Delta_N(\rho_0, \rho)\mathcal{R}'(\rho) = 0.$$

We use a Newton method with $\rho = \hat{\rho}$ as initial guess, and this allows to find the supreme in (2.26). Thus, we solve equation (2.26) for different ρ_0's and plot T versus ρ_0, see Figure 2.16.

Afterwards, using inverse interpolation we find the initial radius ρ_0 for which an orbit does not leave the ball B_ρ in a time span of length $T_S = 3 \times 10^9$. The result obtained here is $\rho_0 = 1.9136 \times 10^{-4}$ and the maximal final radius is $\rho = 4.1835 \times 10^{-4}$. We note that the value of σ used in Section 2.4.4.3 is precisely the ratio ρ/ρ_0.

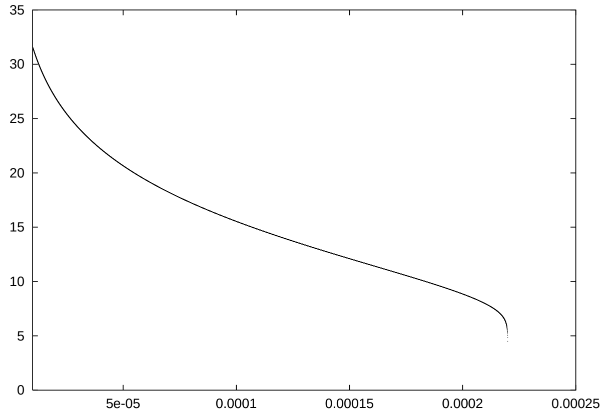

Figure 2.16: Plot of $\log(T(\rho_0))$ versus ρ_0

We can proceed as in Section 2.4.4.3 and plot the region of effective stability around the periodic orbit of L_5 in the (x, y)-plane of the RTBP space coordinates, see Figures 2.17 and 2.18.

Thus, we see that the first integral produces a slightly larger region of stability than the one computed with the normal form technique. As we have used the same estimates for both approaches, it seems that first integrals are more suitable than normal forms for estimating practical stability regions, but normal forms give a complete description of the dynamics inside the region. If we compare the stability region here for $t = 0$ with previous results on the RTBP, we see that the region here (Figure 2.17) is smaller than that of the RTBP. This is an expected result since the BCCP is more complex and contains more resonances than the RTBP.

However, when we consider the time dependence, we have that the position in the physical space (by physical space we mean positions and velocities, without the time) of the region of effective stability depends (periodically) on time. Let us call $S(t) \subset \mathbb{R}^6$ to this region and, as the one obtained using the first integral is larger, we will focus on that one. Now, let us consider the region $S \subset \mathbb{R}^6$ of physical space "swept" by the regions $S(t)$, $S = \cup_t S(t)$. For instance, Figure 2.17 shows a section of $S(0)$, and Figure 2.18 shows a slice of S. If we denote by R the region of effective stability for the RTBP obtained in [CG91] we have that this region does not cover the region S: if we look at Figure 2.18, R is centred at the triangular point and S is following the periodic orbit leaving R in the middle. This means that the region S that we have obtained, although is smaller, is not contained in R. Unfortunately, there are no Trojan asteroids inside S, mainly due to the large component in the z direction (we recall Figures 2.5, 2.6 and 2.7).

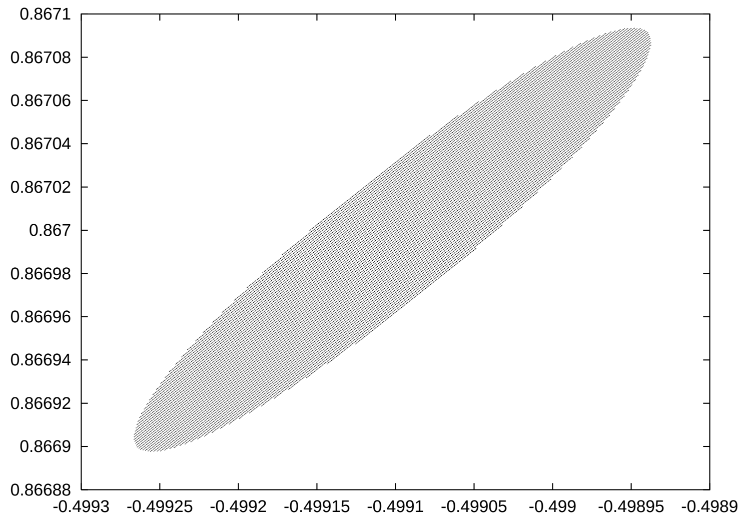

Figure 2.17: Region of effective stability around the point $t = 0$ of the periodic orbit replacing L_5. To compare this region with the one obtained in the normal form, we have used the same window as in Figure 2.14.

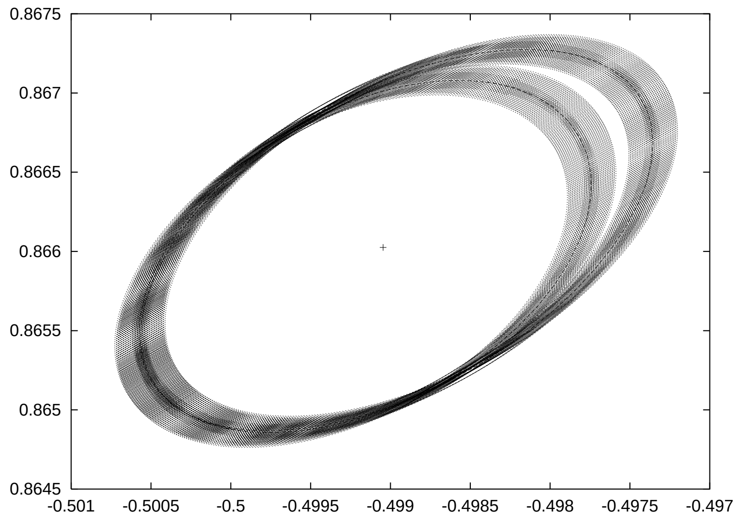

Figure 2.18: Region of effective stability around the periodic orbit replacing L_5. The triangular point is marked at the centre of the graphic.

Chapter 3

The Elliptic Restricted Three Body Problem

The elliptic RTBP is a classical model for studying the dynamics of a small particle in the Sun-Jupiter system, where the two primaries are supposed to move on an elliptic orbit. This elliptic orbit can be described by the vector $\vec{r}$ (see Figure 3.1):

$$\vec{r} = \frac{a(1-e^2)}{1+e\cos v}(\cos v, \sin v, 0), \tag{3.1}$$

where a is the semi-major axis of the orbit, e the eccentricity and v is the true anomaly (angle measured in the direction in which the orbit is described, starting from the perihelion).

In order to write the equations of motion in dimensionless variables, the common procedure (see [Sze67]) consists in dividing the distances and dimensional coordinates by $||\vec{r}||$ and to change the coordinate system to a one that rotates with an angular velocity

$$\frac{dv}{dt} = \frac{(1+e\cos v)^2}{a^{3/2}(1-e^2)^{3/2}}. \tag{3.2}$$

That is, the equations are written in a rotating and pulsating reference system with the origin at the center of masses. As usual, the sum of the masses of Sun and Jupiter and the gravitational constant are supposed to be one.

Thus, in adimensional coordinates, the equations of motion of the elliptic RTBP are:

$$\begin{aligned} \ddot{x} - 2\dot{y} &= \frac{\partial \omega}{\partial x} \\ \ddot{y} + 2\dot{x} &= \frac{\partial \omega}{\partial y} \\ \ddot{z} + z &= \frac{\partial \omega}{\partial z} \end{aligned}$$

where

$$\omega = \frac{\Omega}{1+e\cos v}, \quad \Omega = \frac{1}{2}(x^2+y^2+z^2) + \frac{1-\mu}{r_1} + \frac{\mu}{r_2} + \frac{\mu(1-\mu)}{2},$$

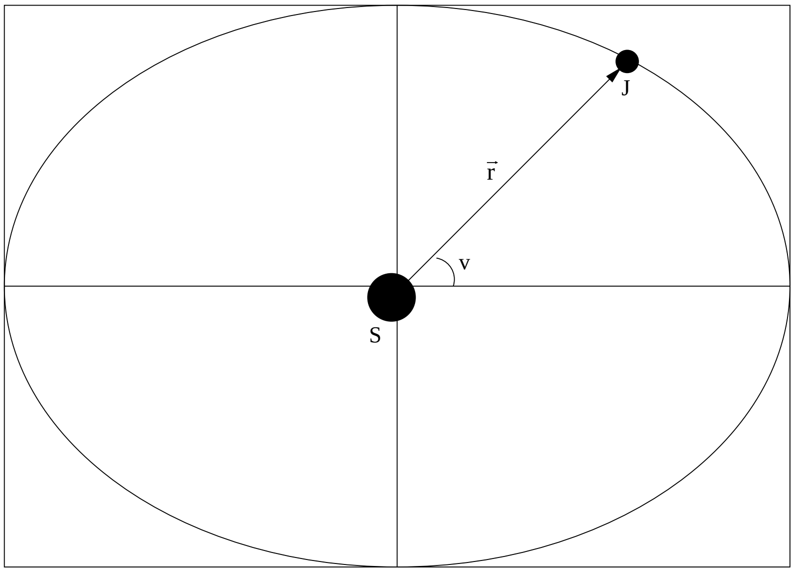

Figure 3.1: An elliptic solution of the Sun-Jupiter two body problem.

and $r_1^2 = (x-\mu)^2 + y^2 + z^2$, $r_2^2 = (x-\mu+1)^2 + y^2 + z^2$. The true anomaly v is taken as the independent variable, thus $\dot{}$ stands for the derivative with respect to v.

Several dynamical results concerning this model are given in [JS94]. There, a description of the non linear dynamics around the Lagrangian point L_5 is performed by means of the computation of a local normal form of the Hamiltonian. A region of effective stability (i.e. a region where an orbit will stay for a long time span) is also computed around the L_5 point.

As this representation of the model uses the true anomaly v as independent variable, the description of orbits are related to this variable and not to the (physical) time. This makes difficult the direct comparison of such orbits with the ones given by other models that use the time as independent variable, such as the Circular Restricted Three Body Problem, the Bicircular Problem, the Bicircular Coherent Problem, JPL and others.

In order to avoid this problem, in Section 3.1, we rewrite the elliptic spatial restricted three body problem (from now on, ERTBP) in such a way that the dimensional time is the independent variable. This is done, as usual, by defining a rotating-pulsating reference frame and by introducing some auxiliary periodic time-dependent functions that, basically, contain the perturbation of Jupiter's elliptic motion in this special system of coordinates.

In this representation of the ERTBP model, the Lagrangian $L_{4,5}$ points are viewed as periodic orbits in the phase space (although in the configuration space, (x, y, z), they are still fixed points). In Section 3.2, we compute these orbits and study the linear dynamics around them.

The non linear dynamics of a neighbourhood of these periodic orbits that substitute the $L_{4,5}$ RTBP points is also studied in this chapter by means of the computation of a truncated normal form (see Section 3.3) and an approximate first integral (see Section 3.4).

3.1 Construction of the model

Let us suppose that Sun and Jupiter move in the elliptic solution of the two body problem described by (3.1) and that we choose the origin of time ($t = 0$) such that the true anomaly is $v = -\pi$. Let $\vec{\rho}$ be the position vector of a massless particle that moves under the gravitational attraction of the Sun-Jupiter system in a barycenter-centered inertial reference frame and let us take the following numerical values for the mass parameter and the eccentricity: $\mu = 0.95387536 \times 10^{-3}$ and $e = 0.04839266$, respectively.

We are going to make a change of variables to a rotating-pulsating reference frame that will fix the positions of Sun and Jupiter in the following two points: $\vec{Q}_s = (\mu, 0, 0)^t$ and $\vec{Q}_j = (\mu - 1, 0, 0)^t$. The new set of coordinates for the particle ($\vec{q}$) is given from the old ones ($\vec{\rho}$) by

$$\vec{q} \;=\; \frac{1}{r} C^t \vec{\rho} \tag{3.3}$$

where

$$C = \begin{pmatrix} -\frac{r_x}{r} & \frac{r_y}{r} & 0 \\ -\frac{r_y}{r} & -\frac{r_x}{r} & 0 \\ 0 & 0 & 1 \end{pmatrix},$$

$r = ||\vec{r}||$ and $\vec{r} = (r_x, r_y, 0)$ is the equation of the elliptic orbit (3.1).

The inverse change can easily be stated as

$$\vec{\rho} \;=\; B\vec{q}, \tag{3.4}$$

where $B = rC$. We have used the (easy to check) equality $CC^t = Id$.

Defining the conjugate momentum as

$$\vec{p} = r^2 \dot{\vec{q}} + B^t \dot{B} \vec{q},$$

the equations for the particle become Hamiltonian, and the Hamiltonian is:

$$H = \frac{1}{2r^2}(\vec{p}, \vec{p}) - \frac{1}{r^2} \vec{p} B^t \dot{B} \vec{q} + U,$$

where U, the potential energy, is given by

$$U = -\frac{1-\mu}{r||\vec{Q}_s - \vec{q}||} - \frac{\mu}{r||\vec{Q}_j - \vec{q}||}.$$

To write the Hamiltonian in a more suitable way, we define the following (2π-periodic) functions:

$$\begin{aligned} \alpha_1 &= \frac{1}{r^2}, & \alpha_2 &= \frac{r_x \dot{r}_x + r_y \dot{r}_y}{r^2}, \\ \alpha_3 &= \frac{r_x \dot{r}_y - r_y \dot{r}_x}{r^2}, & \alpha_4 &= \frac{1}{r}. \end{aligned} \tag{3.5}$$

From (3.1) and (3.2) it is possible to numerically tabulate the values of $\vec{r}$ in an equidistant sequence of points in the $(0, 2\pi)$ time interval. Then, we can easily compute the Fourier coefficients for α_j, $j = 1, 2, 3, 4$, up to a finite order (in fact, all the coefficients with modulus larger than 10^{-15} have been kept). Due to the parity properties of these functions, we can write them as

$$\begin{aligned} \alpha_j(\theta) &= \sum_{k\geq 0} \alpha_{jk}\cos(k\theta), \qquad j = 1, 3, 4 \\ \alpha_2(\theta) &= \sum_{k\geq 1} \alpha_{2k}\sin(k\theta), \end{aligned}$$

where $\theta = t + \theta^{(0)}$ and $\theta^{(0)}$ is a phase. The numerical values of the Fourier coefficients, α_{jk}, are shown in Appendix A.2.

Finally, it is possible to write the Hamiltonian of the ERTBP problem, using the time as independent variable, as:

$$\begin{aligned} H &= \frac{1}{2}\alpha_1(\theta)(p_x^2 + p_y^2 + p_z^2) + \alpha_2(\theta)(xp_x + yp_y + zp_z) \\ &\quad + \alpha_3(\theta)(yp_x - xp_y) - \alpha_4(\theta)\left[\frac{1-\mu}{q_S} + \frac{\mu}{q_J}\right], \end{aligned} \tag{3.6}$$

where $q_S^2 = (x-\mu)^2 + y^2 + z^2$ and $q_J^2 = (x - \mu + 1)^2 + y^2 + z^2$.

This Hamiltonian has the following two symmetries:

$$(t, x, y, z, p_x, p_y, p_z) \mapsto (t, x, y, -z, p_x, p_y, -p_z), \tag{3.7}$$

$$(t, x, y, z, p_x, p_y, p_z) \mapsto (-t, x, -y, z, -p_x, p_y, -p_z). \tag{3.8}$$

The first one (3.7) implies that some monomials of the Hamiltonian expansion are zero (and this will be used in the computations in order to save computer memory and time). The second symmetry (3.8) implies that it is equivalent to study the Lagrangian point L_4 or the L_5 one.

3.1.1 Tests

To check the results obtained in the preceding calculations, we have compared numerical integrations of the obtained model (3.6) with a numerical restricted three body problem: we have randomly selected initial conditions for the particle, and we have computed the subsequent orbit for 2π units of time. Then, each of these orbits has been sent to the initial coordinates via the change (3.4).

Finally, we have integrated the equations

$$\begin{aligned} \ddot{\vec{r}} &= -\frac{\vec{r}}{r^3}, \\ \ddot{\vec{\rho}} &= -(1-\mu)\frac{\vec{\rho} + \mu\vec{r}}{||\vec{\rho} + \mu\vec{r}||^3} - \mu\frac{\vec{\rho} - (1-\mu)\vec{r}}{||\vec{\rho} - (1-\mu)\vec{r}||^3}, \end{aligned}$$

corresponding to the two body problem and to the infinitesimal particle, respectively; using the initial condition for the elliptic orbit of the two body problem and integrating the three particles at once. Then, it is easily checked the accuracy of the initial orbit. We note that this not only tests the equations obtained, but also the changes of coordinates used. The differences between the two integrations are of the order of 10^{-15}.

3.2 Local study of the L_5 point

In this section, we make an analogous study of the RTBP L_5 point's neighbourhood to the one we did in 2.3 for the BCCP model.

First of all, we note that the L_5 point becomes a periodic orbit in the phase space. Second, we study the linear dynamics around that periodic orbit. Later, we derive a (time-dependent) change of variables (via the Floquet Theorem) that autonomizes and diagonalizes the second order terms of the Hamiltonian. And, finally, we expand this Hamiltonian (using the same procedure than in the BCCP model) up to a high degree. This expansion will be used in Sections 3.3 and 3.4 in order to construct, respectively, a truncated normal form of the Hamiltonian and an approximate first integral.

3.2.1 Transformation of L_5 to a periodic orbit

The object that substitutes the L_5 point in the ERTBP is a periodic orbit. In order to compute it, we look for a fixed point of the time 2π-map associated to the flow of the ERTBP

$$
\begin{aligned}
\dot{x} &= \alpha_1(\theta)p_x + \alpha_2(\theta)x + \alpha_3(\theta)y, \\
\dot{y} &= \alpha_1(\theta)p_y + \alpha_2(\theta)y - \alpha_3(\theta)x, \\
\dot{z} &= \alpha_1(\theta)p_z + \alpha_2(\theta)z, \\
\dot{p_x} &= -\alpha_2(\theta)p_x + \alpha_3(\theta)p_y - \alpha_4(\theta)\left(\frac{(1-\mu)(x-\mu)}{q_S^3} + \frac{\mu(x-\mu+1)}{q_J^3}\right), \\
\dot{p_y} &= -\alpha_2(\theta)p_y - \alpha_3(\theta)p_x - \alpha_4(\theta)\left(\frac{(1-\mu)y}{q_S^3} + \frac{\mu y}{q_J^3}\right), \\
\dot{p_z} &= -\alpha_2(\theta)p_z - \alpha_4(\theta)\left(\frac{(1-\mu)z}{q_S^3} + \frac{\mu z}{q_J^3}\right),
\end{aligned}
$$

with a Newton method, taking as initial condition the RTBP L_5 point. The solution is

x	-0.4990461246398	p_x	$\bar{p_x}(\theta)$
y	0.8660254037841	p_y	$\bar{p_y}(\theta)$
z	0.0	p_z	0.0

where $\bar{p_x}(\theta)$ and $\bar{p_y}(\theta)$ are the 2π-periodic functions displayed in Figure 3.2.

The linearised normal behaviour is given by the eigenvalues of the monodromy matrix of the periodic orbit, shown in Table 3.1. As we can see, these eigenvalues have modulus 1. Thus, the orbit is linearly stable.

3.2.2 Normal Form of H_2

In order to obtain a normal form of the Hamiltonian up to order 2, what we are going to do is to cancel the first order of the Hamiltonian and to autonomize and diagonalize the order two.

Order one is cancelled by making a time dependent translation of the origin from the Sun-Jupiter barycenter to the periodic orbit found in 3.2.1. Then, the Floquet Theorem

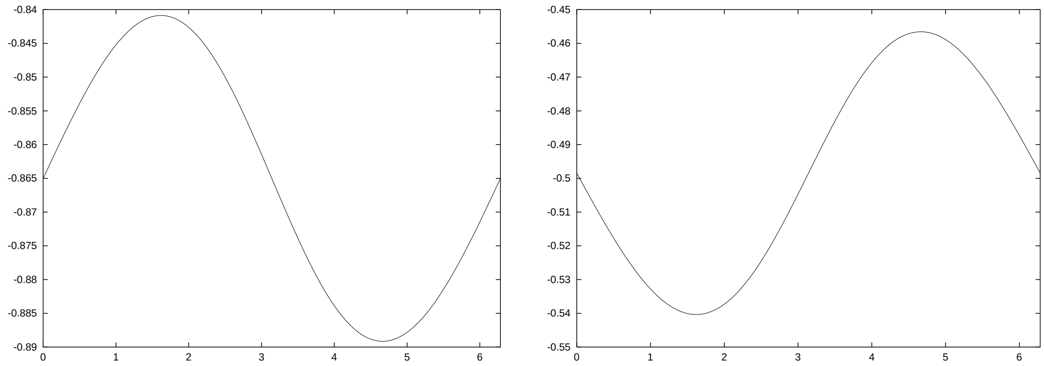

Figure 3.2: Periodic functions $\bar{p_x}(\theta)$ and $\bar{p_y}(\theta)$

j	$\mathrm{Re}\,(\lambda_j)$	$\pm\mathrm{Im}\,(\lambda_j)$	$\lvert\lambda_j\rvert$	$\pm\mathrm{Arg}\,(\lambda_j)$
1	0.873862933497	-0.486172370111	1.0	-0.507704262739
2	0.999792646328	-0.0203633088732	1.0	-0.0203647164589
3	1.0	0.0	1.0	0.0
4	0.873862933497	0.486172370111	1.0	0.507704262739
5	0.999792646328	0.0203633088732	1.0	0.0203647164589
6	1.0	0.0	1.0	0.0

Table 3.1: Eigenvalues of the monodromy matrix of the periodic orbit replacing L_5.

gives us a linear periodic time dependent change of variables (it can be chosen in a symplectic way) that autonomizes the second order of the Hamiltonian (the linear part of the differential equations).

The process that we follow is exactly the same as in Section 2.3.2 for the BCCP case. See there for the details.

Afterwards, we compose these two changes (translation + symplectic Floquet change) with a complexification of the variables in order to have a diagonal normal form of order two:

$$\mathcal{H}_2 = i\omega_1 q_1 p_1 + i\omega_2 q_2 p_2 + i\omega_3 q_3 p_3, \tag{3.9}$$

where

$$\begin{aligned} \omega_1 &= -0.08080364304385, \\ \omega_2 &= 0.99675885471089, \\ \omega_3 &= 1.0, \end{aligned}$$

and i stands for $\sqrt{-1}$.

Note that the frequency corresponding to the (q_3, p_3) direction (ω_3) is exactly equal to 1. Thus, in the elliptic problem, we have a resonance between this vertical frequency and the frequency of the periodic forcing. This fact implies, for example, that the normal form will not be autonomous.

3.2.3 Expansion of the Hamiltonian

We want to compute the expansion of the Hamiltonian (3.6) in homogeneous polynomials with the coefficients being truncated Fourier series. For this purpose, we need to expand $\frac{1}{q_l}$, where $q_l^2 = (x - x_l)^2 + (y - y_l)^2 + z^2$ and l stands for S or J, in terms of homogeneous polynomials. We will denote them in the following way:

$$\frac{1}{q_l} = \sum_{n=0}^{N} A_n(x, y, z, \theta).$$

It is easy, then, to obtain a recurrence for computing the A_n's from the Legendre polynomials recurrence:

$$A_0 = \frac{1}{\sqrt{x_l^2 + y_l^2}}, \qquad A_1 = \frac{x_l x + y_l y}{(x_l^2 + y_l^2)^{3/2}},$$

$$A_{n+1} = \frac{1}{x_l^2 + y_l^2}\left[\frac{2n+1}{n+1}(x_l x + y_l y)A_n - \frac{n}{n+1}(x^2 + y^2 + z^2)A_{n-1}\right].$$

Using this recurrence in the last two terms of (3.6) and applying the changes of variables mentioned in 3.2.2, the expanded Hamiltonian, ready to enter the process that will bring it to the desired normal form, is:

$$H = p_\theta + i\omega_1 q_1 p_1 + i\omega_2 q_2 p_2 + i\omega_3 q_3 p_3 + \sum_{n\geq 3} H_n(q, p, \theta), \tag{3.10}$$

where p_θ is the momentum corresponding to the time, it has been added to obtain an autonomous Hamiltonian.

3.3 Truncated normal form

In this section, we use the expansion (3.10) as a starting point of the computation of a truncated normal form of the Hamiltonian (3.6) up to a high order N. The used technique is the same as in 2.4.1. However, the presence of the 1:1 resonance between the vertical frequency ω_3 and the frequency of the periodic forcing implies some changes in the construction of the normal form (in this case, for example, it is not possible to suppress the dependence in time) and, also, in the non linear dynamics around the triangular points $L_{4,5}$.

3.3.1 Normal Form of order higher than 2

As it is commonly known, the goal of the process of normalization is to suppress the maximum number of terms of the Hamiltonian.

If we follow step by step the method described in 2.4.1, we realize that in this case the generating function of the canonical transformation (2.10) must be selected such that its Fourier coefficients have the form:

$$g_r^k(\theta) = \begin{cases} \dfrac{ih_{r,0}^k}{\langle \omega, k^2 - k^1 \rangle} + \displaystyle\sum_{j \notin \mathcal{J}_k} \dfrac{h_{r,j}^k}{ij - i\langle \omega, k^2 - k^1 \rangle} e^{ji\theta} & \text{if} \quad k^1 \neq k^2, \\[2ex] \displaystyle\sum_{j \neq 0} \dfrac{h_{r,j}^k}{ij} e^{ji\theta} & \text{if} \quad k^1 = k^2, \end{cases}$$

where the set $\mathcal{J}_k$ is defined as: $j \in \mathcal{J}_k \Longleftrightarrow j - \langle \omega, k^2 - k^1 \rangle = 0$.

After performing all the changes given by this generating functions up to order $n = N$, the transformed Hamiltonian have the following form:

$$H = \mathcal{N}(q_1p_1, q_2p_2, q_3, p_3, \theta) + \mathcal{R}(q_1, q_2, q_3, p_1, p_2, p_3, \theta). \tag{3.11}$$

$\mathcal{N}(\cdot)$ denotes the normal form: $\mathcal{N}(q, p, \theta) = p_\theta + \sum_{j=1}^3 i\omega_j q_j p_j + \sum_{n=3}^N \mathcal{H}_n$, where

$$\mathcal{H}_n = \begin{cases} 0 & \text{if} \quad n \neq \dot{2}, \\[2ex] \displaystyle\sum_{\substack{2a+2b+c_1+c_2=n \\ k=(a,a,b,b,c_1,c_2)}} h_{n,c_2-c_1}^k (q_1p_1)^a (q_2p_2)^b q_3^{c_1} p_3^{c_2} e^{i(c_2-c_1)\theta} & \text{if} \quad n = \dot{2}, \end{cases}$$

and $\mathcal{R}(\cdot)$ is the remainder.

As an intermediate step, it is useful to rewrite the normal form in real action-angle variables by means of the following canonical transformation:

$$\begin{aligned} q_j &= \sqrt{I_j} e^{i\varphi_j}, & j = 1, 2, 3 \\ p_j &= -i\sqrt{I_j} e^{-i\varphi_j}, & j = 1, 2, 3 \\ p_\theta &= I_\theta. \end{aligned}$$

The transformed normal form still depends on time, but in a very particular manner:

$$\mathcal{N}(I_\theta, I, \theta) = I_\theta + \sum_{j=1}^{3} \omega_j I_j + \sum_{\substack{n\geq 4 \\ n=\dot{2}}}^{N} \mathcal{H}_n(I,\theta),$$

where $I = (I_1, I_2, I_3)$,

$$\mathcal{H}_n(I,\theta) = \sum_{k_1^1+k_2^1+k_3^1=n/2} h^k_{n,0} I_1^{k_1^1} I_2^{k_2^1} I_3^{k_3^1} + \sum_{\substack{|k|=n \\ k_1^1=k_1^2 \\ k_2^1=k_2^2 \\ k_3^1\neq k_3^2}} h^k_{n,k_3^2-k_3^1} I_1^{k_1^1} I_2^{k_2^1} I_3^{\frac{k_3^1+k_3^2}{2}} e^{-i(k_3^2-k_3^1)(\varphi_3-\theta)}$$

and the multiindex $k \in \mathbb{N}^6$ is $k = (k^1, k^2) = (k_1^1, k_2^1, k_3^1, k_1^2, k_2^2, k_3^2)$. Obviously, the coefficients $h^k_{n,k_3^2-k_3^1} \in \mathbb{C}$ are such that $\mathcal{H}_n(I,t)$ is a real expansion.

In order to write the normal form of the Hamiltonian in a more convenient way, a last change of variables is implemented:

$$\begin{array}{rclrclrclrcl} I_\theta &=& J_0 - J_3, & I_1 &=& J_1, & I_2 &=& J_2, & I_3 &=& J_3, \\ \theta &=& \psi_0, & \varphi_1 &=& \psi_1, & \varphi_2 &=& \psi_2, & \varphi_3 &=& \psi_3 + \psi_0. \end{array}$$

Thus, the final Hamiltonian (with the coefficients up to degree 2 in the actions explicitly given) can be written as:

$$\begin{aligned} \mathcal{N} \;=\;& J_0 + \omega_1 J_1 + \omega_2 J_2 + \alpha_{1,1} J_1^2 + \alpha_{1,2} J_1 J_2 + \alpha_{2,2} J_2^2 + \\ & J_3[aJ_1 + dJ_2 + (bJ_1 + eJ_2)\cos(2\psi_3) + (cJ_1 + fJ_2)\sin(2\psi_3)] + \\ & J_3^2[g + h\cos(2\psi_3) + k\sin(2\psi_3) + j\cos(4\psi_3) + l\sin(4\psi_3)] + O_3(J), \end{aligned} \tag{3.12}$$

where the concrete values of the coefficients are given in Table 3.2.

3.3.2 Changes of variables

In a similar way as it was done in 2.4.2, we have computed a change of variables (written as a truncated power series up to a high degree N) in order to transport points from the initial space (the one in which the Hamiltonian is in normal form up to degree 2 (3.10)) to the final one (in which the normal form (3.12) is written). The inverse change of variables is also computed.

In order to obtain the complete change that takes points from the space in which the Hamiltonian of the ERTBP (3.6) is written to the final one (and vice versa), we compose this change of variables with the linear translation and the Floquet transformation computed in 3.2.2. In this way, the total inverse change is also obtained.

The software corresponding to the computation of the normal form and to the changes of variables is tested by integrating several random points near L_5 in the ERTBP and the corresponding points in the normal form space and checking (via the change of variables) that the differences behave in the correct way (see [Jor99], pages 172 and 173).

ω_1	-8.0803643043855636e-02	0.0000000000000000e+00
ω_2	9.9675885471089010e-01	0.0000000000000000e+00
ω_3	1.0000000000000000e+00	0.0000000000000000e+00
$\alpha_{1,1}$	5.8484519701809745e-01	-5.1103099961609840e-14
$\alpha_{1,2}$	-1.5529520931135821e-01	5.2069599000177628e-14
$\alpha_{2,2}$	5.6485205021129178e-03	2.8025706811703887e-15
a	5.4452703310267969e-02	-7.4985295169742308e-16
b	2.3242830996417219e-05	3.4347524824340780e-16
c	-2.1553181184676487e-04	3.3306690738754696e-16
d	5.8004534402251035e-03	1.3094197361733700e-15
e	-1.2048847340499595e-05	-2.3852447794681098e-18
f	7.7290056410439945e-06	1.7347234759768071e-18
g	-1.7896972086516028e-04	2.0214831819728854e-20
h	4.1961077661394758e-07	6.7762635780344027e-20
j	-1.2295791857182469e-10	-2.1175823681357508e-22
k	-2.2086812359514013e-13	-8.6736173798840355e-19
l	-6.6911208849675845e-16	2.1175823681357508e-22

Table 3.2: Coefficients of the normal form, up to degree 2 in the actions. The second and third columns show, respectively, the real and imaginary parts of the coefficients. The imaginary part should be zero, but it is not due to roundoff errors.

3.3.3 Local non-linear dynamics

If we take as an approximation to the dynamics near the periodic orbit that replaces L_5, the one given by the computed normal form (3.12), the description of the local phase space around the periodic orbit becomes much clearer.

For instance, we have that $J_1 = c_1$ and $J_2 = c_2$ are first integrals of the system, because $\dot{J}_1 = \dot{J}_2 = 0$. Thus, what is left is a one degree of freedom Hamiltonian that is essentially a perturbed pendulum depending on the parameters J_1 and J_2.

In particular, near the periodic orbit replacing L_5 we have normally hyperbolic invariant tori of dimensions 2 and 3. Figures 3.3, 3.4 and 3.5 show three examples of them. They are computed by setting $J_3 = 0$ and $\psi_3 = 0$, integrating with some different initial conditions for J_1 and J_2 and finally transporting these orbits to the initial space (the one in which the Hamiltonian of the ERTBP (3.6) is written) by the change computed in Section 3.3.2.

These invariant tori are usually called whiskered tori. That is, the hyperbolic tori have (in our case) 4-D unstable and stable manifolds (whiskers) in the 8-D extended phase space and they can be easily obtained from the normal form of the Hamiltonian. The procedure is as follows: we fix J_1 and J_2 to the constant values corresponding to a concrete hyperbolic torus (3.3, for instance) and we plot different energy levels of the Hamiltonian (3.12). These would be (an approximation to) the whiskers in the normal form space (see Figure 3.6, for an heuristic representation). Then, we would transport these manifolds, via the change of coordinates (who adds 2 dimensions to the objects), to

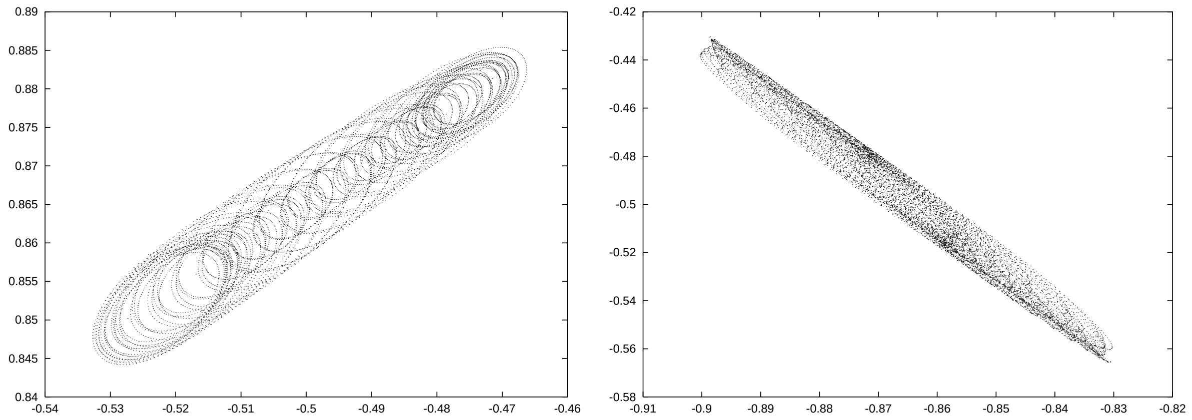

Figure 3.3: Projection on the (x, y) (left) and on the (p_x, p_y) (right) planes of a normally hyperbolic three-dimensional invariant torus near the periodic orbit that replaces L_5. The intrinsic frequencies are $\omega_t = 1$, $\omega_1 = -0.0807934933058347$ and $\omega_2 = 0.996757415227295$.

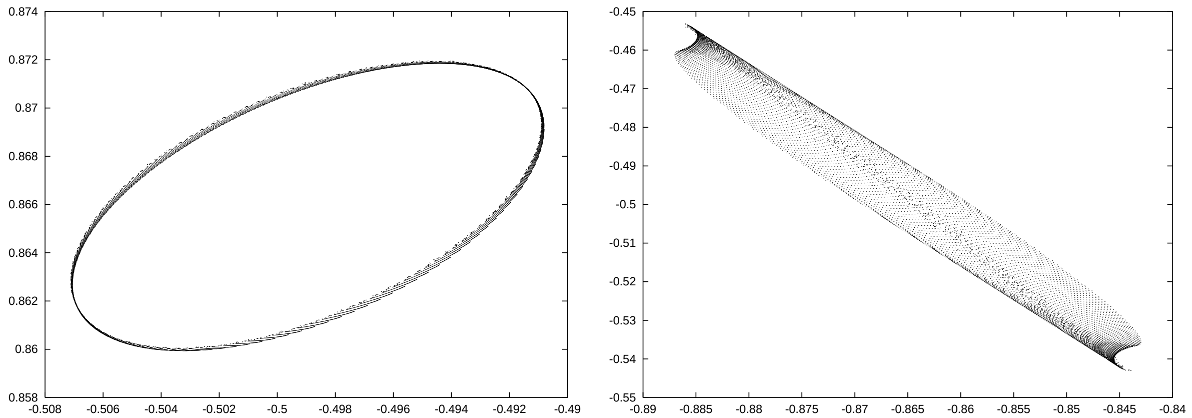

Figure 3.4: Projection on the (x, y) (left) and on the (p_x, p_y) (right) planes of a normally hyperbolic two-dimensional invariant torus near the periodic orbit that replaces L_5. The intrinsic frequencies are $\omega_t = 1$ and $\omega_2 = 0.996758967680182$.

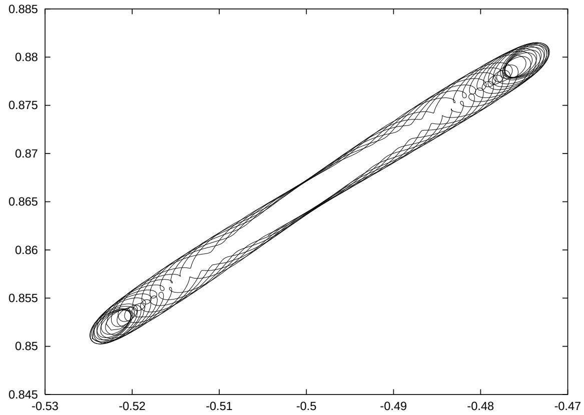

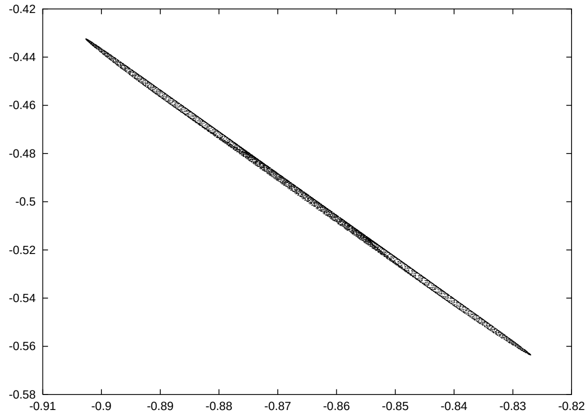

Figure 3.5: Projection on the (x, y) (left) and on the (p_x, p_y) (right) planes of a normally hyperbolic two-dimensional invariant torus near the periodic orbit that replaces L_5. The intrinsic frequencies are $\omega_t = 1$ and $\omega_1 = -0.0807919409926114$.

the extended initial phase space.

3.4 Approximate first integrals

This section is devoted to the computation of an approximate first integral for the ERTBP Hamiltonian (3.6). This process is based on the direct method used in [GG78], with the necessary modifications to include the periodic time-dependence of the Hamiltonian. Recall that in this problem we have a 1:1 resonance between the vertical mode (ω_3) and the proper frequency of the problem (Jupiter is orbiting around the Sun with frequency equal to one). This will make us to study in detail when the homological equation is solvable.

3.4.1 Numerical computation

We start the computation with the Hamiltonian (3.10) expanded in complex coordinates,

$$H(q, p, \theta, p_\theta) = p_\theta + H_2(q, p) + \sum_{n \geq 3} H_n(q, p, \theta),$$

where H_2 is in the diagonal form (3.9), and H_n are homogeneous polynomials of degree n. We look for an approximate first integral as a truncated Fourier-Taylor expansion,

$$F(q, p, \theta) = \sum_{n=2}^{N} F_n(q, p, \theta),$$

where, as usual, F_n stands for an homogeneous polynomial of degree n in the variables (q, p), with coefficients that are (truncated) Fourier series in the time variable.

It is known that, if F is a first integral for the flow of the Hamiltonian H, then $\{H, F\} = 0$. This equation gives a recursive way of computing the coefficients of the

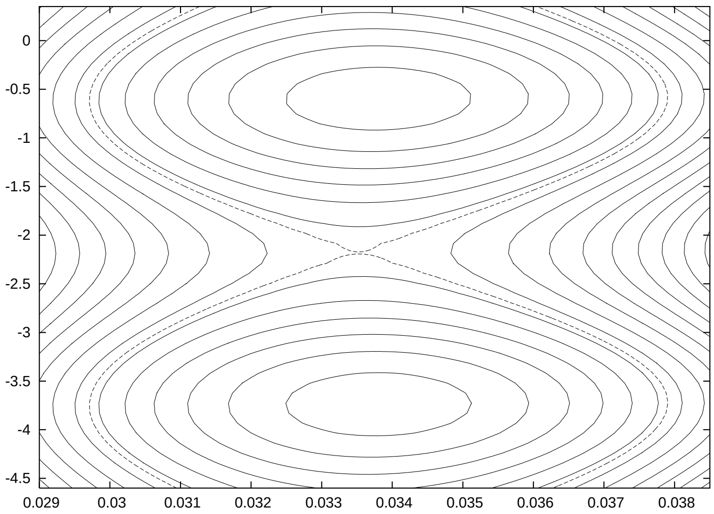

Figure 3.6: Energy levels of the Hamiltonian (3.12) when we fix the values of J_1 and J_2 that correspond to the hyperbolic torus in Figure 3.3. They can be seen as the whiskers of this invariant torus in the normal form space.

expansion of F:

$$-\frac{\partial F}{\partial \theta} + \{H_2, F\} = -\left\{\sum_{n\geq 3} H_n, F\right\}. \tag{3.13}$$

On the other hand, if Π denotes the vector space of the formal power series in (q,p) variables with $\mathcal{C}^\infty$ coefficients that depend periodically on time (with period 2π), we can define a linear operator $D : \Pi \longrightarrow \Pi$ as:

$$D(\cdot) = -\frac{\partial\,\cdot}{\partial \theta} + \{H_2, \cdot\}.$$

Thus, using this linear operator, it is possible to write equation (3.13) order by order in the following manner:

$$\begin{aligned} DF_2 &= 0, \\ DF_n &= -\sum_{m=3}^{n} \{H_m, F_{n-m+2}\}, \qquad n \geq 3. \end{aligned} \tag{3.14}$$

In order to recursively solve these equations, it is useful to make previously an elementary study of some algebraic properties of the operator D.

3.4.1.1 Study of the operator D

If we take the following Π generators:

$$\{e^{ij\theta} q^{k^1} p^{k^2}\}_{j\in\mathbb{Z},\, k=(k^1,k^2)\in\mathbb{N}^3\times\mathbb{N}^3},$$

where $k^1 = (k^1_1, k^1_2, k^1_3)$ and $k^2 = (k^2_1, k^2_2, k^2_3)$; then, the operator D is trivially diagonal:

$$D(e^{ij\theta} q^{k^1} p^{k^2}) = (-ij + i < \omega, k^2 - k^1 >) e^{ij\theta} q^{k^1} p^{k^2}. \tag{3.15}$$

On the other hand, if the null (N) and the image (R) spaces of D are defined as usual:

$$\begin{aligned} N &= \{f \in \Pi \quad s.t. \quad D(f) = 0\}, \\ R &= D(\Pi), \end{aligned}$$

it is immediate to see that $R \cap N = 0$ and $R \cup N = \Pi$.

Thus, if we denote P_N and P_R the projections to the null and image spaces of D, respectively, every element of Π can be decomposed in a direct sum of elements of N and R: $f \in \Pi \Rightarrow f = f^{(N)} + f^{(R)}$, where $f^{(N)} = P_N f \in N$ and $f^{(R)} = P_R f \in R$.

Moreover, the Poisson bracket $\{\cdot,\cdot\}$ gives to Π the structure of a Lie algebra and its action on the subsets N and R can be summarized in the next table:

	N	R
N	N	R
R	R	Π

It is also interesting to characterize the null space N in the former basis of Π. From (3.15), we see that an element of the basis $(e^{ij\theta}q^{k^1}p^{k^2})$ belongs to N iff $-j + < \omega, k^2 - k^1 >= 0$.

In the case of the ERTBP, as $\omega_3 = 1$, the subspace N is called the **resonant nucleus** and its characterisation is given by combinations of monomials of Π with the following Fourier-Taylor exponents:

$$\begin{aligned} k_1^1 &= k_1^2, \\ k_2^1 &= k_2^2, \\ k_3^2 - k_3^1 &= j. \end{aligned}$$

In the literature, it is also usual to define the non-resonant nucleus, $N_0 \subset N$, for a generic non-resonant vector of frequencies ω. In this case, the characterisation of the Fourier-Taylor exponents is given by

$$\begin{aligned} k_1^1 &= k_1^2, \\ k_2^1 &= k_2^2, \\ k_3^1 &= k_3^2. \end{aligned}$$

On the other hand, it is still possible to define a third type of null space, the **commutant** of N (denoted by N'), as the following set:

$$g \in N' \Longleftrightarrow \{g, f\} = 0 \quad \forall f \in N.$$

Its characterisation, in the case of the ERTBP, is given by

$$\begin{aligned} k_1^1 &= k_1^2, \\ k_2^1 &= k_2^2, \\ k_3^1 &= k_3^2 = 0. \end{aligned}$$

Thus, we have built a scale of three null spaces of D,

$$N' \subset N_0 \subset N,$$

that will be useful in the following construction of the approximate first integral.

3.4.1.2 Formal construction

Now, we are going to discuss how to solve recursively equations (3.14). The first one can be solved by choosing any $F_2 \in N$. For the second one, it is very useful to project it to the subspaces N and R:

$$D(F_n^{(N)} + F_n^{(R)}) = -\sum_{m=1}^{n-2} \left\{ H_{m+2}^{(N)} + H_{m+2}^{(R)}, F_{n-m}^{(N)} + F_{n-m}^{(R)} \right\}, \quad \forall n \geq 3.$$

Using the table that gives us the action of the Poisson bracket in the subspaces N and R, we can split this equation in two:

$$\sum_{k=1}^{n-2} \left\{ H_{2+k}^{(N)}, F_{n-k}^{(N)} \right\} = -\sum_{k=1}^{n-2} P_N \left\{ H_{2+k}^{(R)}, F_{n-k}^{(R)} \right\}, \tag{3.16}$$

$$DF_n^{(R)} = -\sum_{k=1}^{n-2} \left\{ H_{2+k}^{(R)}, F_{n-k}^{(N)} \right\} - \sum_{k=1}^{n-2} \left\{ H_{2+k}^{(N)}, F_{n-k}^{(R)} \right\} - \sum_{k=1}^{n-2} P_R \left\{ H_{2+k}^{(R)}, F_{n-k}^{(R)} \right\}. \tag{3.17}$$

It is very convenient, for the latter construction, to choose $F_2 \in N'$. So, we will assume in the further computations that $F_2 = F_2^{(N)} \in N'$ and, thus, $\{F_2, f\} = 0 \; \forall f \in N$.

Let's solve now, order by order, equations (3.16) and (3.17) up to order 5:

- **order n=3**:

  Equation (3.16):

  $$\left\{ H_3^{(N)}, F_2^{(N)} \right\} = -P_N \left\{ H_3^{(R)}, F_2^{(R)} \right\}.$$

  As $F_2 \in N' \subset N$, this equation is trivially accomplished.

  Equation (3.17):

  $$DF_3^{(R)} = -\left\{ H_3^{(R)}, F_2^{(N)} \right\} - \left\{ H_3^{(N)}, F_2^{(R)} \right\} - P_R \left\{ H_3^{(R)}, F_2^{(R)} \right\}.$$

  As $F_2^{(R)} = 0$, this equation can be rewritten as

  $$DF_3^{(R)} = -\left\{ H_3^{(R)}, F_2^{(N)} \right\}.$$

  Then, it is easy to compute $F_3^{(R)}$ in function of known things (note that the operator D is invertible in the space R):

  $$F_3^{(R)} = -D^{-1} \left\{ H_3^{(R)}, F_2^{(N)} \right\}.$$

- **order n=4**:

  Equation (3.16):

  $$\left\{ H_3^{(N)}, F_3^{(N)} \right\} = -P_N \left\{ H_3^{(R)}, F_3^{(R)} \right\}.$$

Note that $H_3^{(N)} = 0$, because of the special symmetry of the ERTBP Hamiltonian in the vertical variables (3.7) and the characterisation of the null space N. It is also possible to see that $P_N \left\{ H_3^{(R)}, F_3^{(R)} \right\} = 0$ (see [GG78] for the proof). Thus, this equation does not give us any restriction on $F_3^{(N)}$. We choose then $F_3^{(N)} = 0$.

Equation (3.17):

$$DF_4^{(R)} = -\left\{ H_3^{(R)}, F_3^{(N)} \right\} - \left\{ H_4^{(R)}, F_2^{(N)} \right\} - P_R \left\{ H_3^{(R)}, F_3^{(R)} \right\}.$$

From this second equation, we can write $F_4^{(R)}$ in a more convenient way:

$$F_4^{(R)} = \left\{ F_2, D^{-1} \left(H_4^{(R)} - \frac{1}{2} P_R \left\{ H_3^{(R)}, D^{-1} H_3^{(R)} \right\} \right) \right\} + \frac{1}{2} P_R \left\{ F_3^{(R)}, D^{-1} H_3^{(R)} \right\},$$

where we have used the following properties of the operators $D(\cdot)$ and $\{F_2, \cdot\}$:

1. $\{F_2, \{f, g\}\} = \{\{F_2, f\}, g\} + \{f, \{F_2, g\}\}$, $\forall f, g \in \Pi$.
2. $\{F_2, D(f)\} = D(\{F_2, f\})$, $\forall f \in \Pi$.
3. $\{F_2, D^{-1}(f)\} = D^{-1}(\{F_2, f\})$, $\forall f \in R$.
4. $\{F_2, P_N(f)\} = P_N(\{F_2, f\}) = 0$, $\forall f \in \Pi$.
5. $\{F_2, P_R(f)\} = P_R(\{F_2, f\}) = \{F_2, f\}$, $\forall f \in \Pi$.

- **order n=5**:

  Equation (3.16):

$$\left\{ H_3^{(N)}, F_4^{(N)} \right\} = -P_N \left\{ H_3^{(R)}, F_4^{(R)} \right\} - P_N \left\{ H_4^{(R)}, F_3^{(R)} \right\}.$$

  By a straightforward computation (see [GG78]), this equation turns out to be

$$\left\{ H_3^{(N)}, F_4^{(N)} \right\} = \left\{ H_3^{(N)}, \eta \right\},$$

  where η is a known function. As $H_3^{(N)} = 0$, we can choose any $F_4^{(N)} \in N$; for instance, $F_4^{(N)} = 0$.

  Equation (3.17): It is possible to see that in this case we have a solvable equation and to write $F_5^{(R)}$ in function of known terms (see [GG78], for the details).

A rigorous proof that a formal integral can be constructed using this method and the details of the lasts computations can be found in [GG78].

Hence, it is possible to solve recursively equations (3.14) up to a high order M, provided that we choose $F_2 \in N'$ and any $F_n^{(N)} \in N$, $\forall n \geq 3$. For instance, in our case, the choices have been $M = 16$ and $F_n^{(N)} = 0$, $\forall n = 3 \div 16$.

3.4.1.3 On the selection of F_2

As we have just seen, it is necessary to choose the second degree of the approximated first integral in the commutant space of N (N'): $F_2 \in N'$.

Thus, we select the second degree of the approximated first integral as

$$F_2 = iq_1p_1 + iq_2p_2.$$

This choice will be a very convenient choice when we bound the diffusion (in Jupiter's plane of motion) of the approximate first integral F in Section 3.4.2.

In real coordinates, the second degree of the formal first integral takes the form:

$$F_2 = \frac{1}{2}\left(x_1^2 + y_1^2\right) + \frac{1}{2}\left(x_2^2 + y_2^2\right), \tag{3.18}$$

and the truncation of the Fourier-Taylor expansion of the first integral can be written as:

$$F(x, y, \theta) = \frac{1}{2}\left(x_1^2 + y_1^2\right) + \frac{1}{2}\left(x_2^2 + y_2^2\right) + \sum_{n=3}^{16} F_n(x, y, \theta). \tag{3.19}$$

3.4.2 Bounding the diffusion on the Jupiter's plane

We use this approximate first integral to find an effective stability region in the plane of motion of Jupiter's orbit. The diffusion in the vertical direction for the ERTBP is bounded in [JS94]. There, the authors use the computation of a high-order normal form and are able to find an effective stability region by asking the radius of the final ball to be twice the value of the initial's one (in this way, the whiskers of the hyperbolic invariant tori of the "small" ball around L_5 are kept inside the "big" one).

The procedure that we follow is almost the same as the one given in Section 2.5.2 for the BCCP case. The only difference is that all the expansions, norms and Poisson brackets are performed in the $x_3 = y_3 = 0$ plane (let us call this plane $\mathcal{P}_J$).

If we define the ball of radius ρ in the plane $\mathcal{P}_J$

$$D_\rho = \{(x, y) \in \mathbb{R}^4 \; ; \; (x_1^2 + y_1^2) + (x_2^2 + y_2^2) \le \rho^2\},$$

then, we are able to find two values for the radius of this ball, ρ and ρ_0, for which the following holds: if the projection into $\mathcal{P}_J$ of a particle lies inside the domain D_{ρ_0} in a given moment, it will stay inside D_ρ for, at least, a span of time of $T_S = 3 \times 10^9$ (the expected lifetime of the Solar System in adimensional units). The concrete values of the radii are $\rho_0 = 1.6777 \times 10^{-4}$, for the initial ball, and $\rho = 3.4524 \times 10^{-4}$, for the final one.

Unfortunately, no projection into $\mathcal{P}_J$ of any Trojan asteroid lies inside the domain of effective stability D_{ρ_0}. This fact has been checked by taking the projection of the synodical coordinates of 432 Trojans in a given date (October 18th, 2001 – 2452200.5 Julian day), transporting them to the coordinates in which the approximate first integral is computed and finally checking if the value $r = \sqrt{(x_1^2 + y_1^2) + (x_2^2 + y_2^2)}$ is smaller than ρ_0.

Chapter 4

The Bianular and Tricircular Coherent Problems

In this chapter, we derive two new models for studying the dynamics around the Lagrangian points L_4 and L_5 of the Sun-Jupiter system.

In the first model, we find quasi-periodic solutions (with two frequencies) of the planar three body problem Sun-Jupiter-Saturn (SJS) and adjust some of the Jupiter's orbital elements to the actual ones. Thus, our goal is to simulate in a more realistic way the Sun-Jupiter relative motion.

The second one is a restricted five body model and its construction is based on a computation of a quasi-periodic solution with two frequencies (that lies on a 2-D torus) of the planar four body problem Sun, Jupiter, Saturn and Uranus (SJSU). This model can be seen as the simplest (coherent) restricted five body model and a natural improvement of the BCCP when adding a massive body to the system.

First, we describe the N-planetary problem in the Jacobi coordinates and we see how to perform a reduction of one degree of freedom of the Hamiltonian by using the angular momentum first integral. Then, we review a method, first developed by [CJ00], for computing 2-D invariant tori. Afterwards, we adapt this method to the SJS and SJSU problems. In the first case, we look for a torus for which Jupiter's osculating eccentricity is close to the real one. In the second case, a quasi-periodic orbit of the SJSU with the actual masses of the planets is found. Due to the shape of these solutions, we have called these quasi-periodic orbits as Bianular and Tricircular solutions of the three and four body problems. Finally, we give a general way of obtaining models for the motion of a massless particle in a field that comes from any N-planetary solution and we adapt it to our two cases. In this way, the Bianular and Tricircular Coherent Problems are defined.

The last section of this chapter (4.6) is devoted to a local semi-analytical study of the Tricircular Coherent Problem. First, we compute a (high-order) truncated normal form of the Hamiltonian around the invariant object (a 2-D torus) that substitutes the triangular point L_5. We use the normal form in order to give a description of the (local) non-linear dynamics around it. Later, we also compute an approximate first integral of the system and we use it to bound the diffusion around the invariant object. That is, we compute a zone of effective stability by estimating a bound of the remainder part of this quasi-integral.

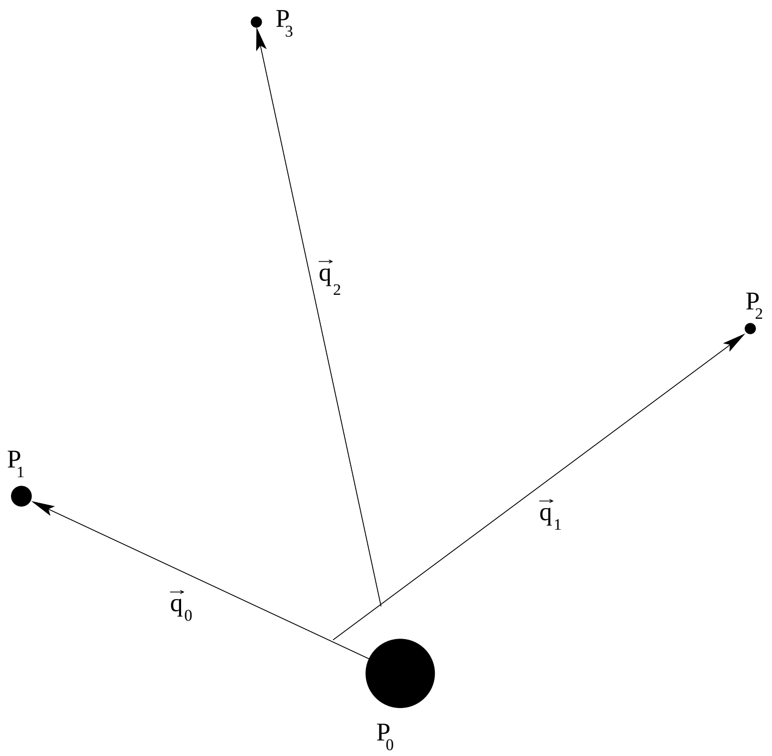

Figure 4.1: Jacobi coordinates for the N-planetary Problem.

4.1 The planar N-planetary problem

The planar N-planetary problem is the problem of N+1 bodies moving in a plane under their mutual gravitational attraction, but supposing that there is a bigger body around which the rest N bodies (planets) move in quasi-Kepler orbits.

4.1.1 Rotating Jacobi coordinates

In this section, we describe the generalized Jacobi formulation for the N-planetary problem, where we deal with a relatively big body P_0 (for instance, the Sun) with mass m_0 and N planets P_i with masses m_i, $i = 1, \ldots, N$. The idea is based in referring every planetary body P_i to the barycenter B_{i-1} of the i preceding bodies $P_0, \ldots, P_{i-1}$. Thus, we work with N position vectors $\vec{q}_i$, $i = 1, \ldots, N$, each one going from the barycenter B_{i-1} to the body P_i. Obviously, the vector $\vec{q}_N$ contains the barycentre of the system (see Figure 4.1). In this way, we can easily have a Hamiltonian formulation of the problem that includes the reduction of the linear momentum first integral.

In [Las89], the interested reader can find a more complete description of these and other useful coordinates to describe a N-planetary problem, as well as its Hamiltonian in an inertial reference frame in Jacobi coordinates:

$$H = \sum_{i=1}^{N} \frac{1}{2\alpha_i} ||\vec{p}_i||^2 - \sum_{0 \le i < j \le N} G \frac{m_i m_j}{||\vec{r}_{ij}||}, \tag{4.1}$$

where $\alpha_i = \frac{m_i \eta_{i-1}}{\eta_i}$, $\eta_i = \sum_{j=0}^{i} m_j$, $\vec{p}_i = \alpha_i \dot{\vec{q}}_i$ and the distances between the bodies are given by the modulus of the vectors

$$\begin{aligned}
\vec{r}_{0i} &= \vec{q}_i + \sum_{j=1}^{i-1} \frac{m_j}{\eta_j} \vec{q}_j, \qquad && i = 1, \ldots, N\,, \\
\vec{r}_{ij} &= \vec{q}_j + \sum_{k=1}^{j-1} \frac{m_k}{\eta_k} \vec{q}_k - \frac{\eta_{i-1}}{\eta_i} \vec{q}_i, \qquad && 0 < i < j \leq N.
\end{aligned} \tag{4.2}$$

We take the Hamiltonian (4.1) as the starting point of our study. First of all, we implement a uniform counterclockwise rotation of frequency 1 to a N-planetary system with the origin in the center of masses: $\vec{q}_i = \mathcal{R}(t)\vec{Q}_i$, for $i = 1, \ldots, N$, where

$$\mathcal{R}(t) = \begin{pmatrix} \cos(t) & -\sin(t) \\ \sin(t) & \cos(t) \end{pmatrix}.$$

Defining new momenta as usual,

$$\begin{aligned}
P_i^{(x)} &= \alpha_i (\dot{Q}_i^{(x)} - Q_i^{(y)}), \\
P_i^{(y)} &= \alpha_i (\dot{Q}_i^{(y)} + Q_i^{(x)}),
\end{aligned}$$

where $\vec{Q}_i = (Q_i^{(x)}, Q_i^{(y)})$, $\vec{P}_i = (P_i^{(x)}, P_i^{(y)})$, and renaming the new variables $(\vec{Q}, \vec{P})$ as before $(\vec{q}, \vec{p})$, we can write the Hamiltonian of the N-planetary problem in a uniformly rotating reference frame as:

$$H = \sum_{i=1}^{N} \frac{1}{2\alpha_i} ||\vec{p}_i||^2 + \sum_{i=1}^{N} (q_i^{(y)} p_i^{(x)} - q_i^{(x)} p_i^{(y)}) - \sum_{0 \leq i < j \leq N} G \frac{m_i m_j}{||\vec{r}_{ij}||}, \tag{4.3}$$

where, of course, the distances between the bodies, $||\vec{r}_{ij}||$, are still given by the Euclidean norm of the vectors (4.2).

4.1.2 Reduction of one degree of freedom

Now, we proceed to make a canonical change of variables that will reduce the Hamiltonian from $2N$ to $2N-1$ degrees of freedom. The idea is very well known (see, for example, [Whi52]) and consists on making use of the classical first integral of the angular momentum.

The change of variables that we perform can be written as:

$$\vec{q}_i = \frac{\partial G}{\partial \vec{p}_i}, \quad \vec{P}_i = \frac{\partial G}{\partial \vec{Q}_i}, \qquad i = 1, \ldots, N,$$

where $(Q_i, P_i)_i$ are the new variables and $G(Q, p)$ is the following generating function:

$$\begin{aligned}
G(Q,p) &= Q_1^{(x)} (p_1^{(x)} \cos Q_1^{(y)} + p_1^{(y)} \sin Q_1^{(y)}) \\
&\quad - \sum_{i=2}^{N} \Big(p_i^{(x)} (Q_i^{(x)} \cos Q_1^{(y)} + Q_i^{(y)} \sin Q_1^{(y)}) + p_i^{(y)} (Q_i^{(x)} \sin Q_1^{(y)} - Q_i^{(y)} \cos Q_1^{(y)}) \Big).
\end{aligned}$$

Hence, the equations that define the change and its inverse are:

$$
\begin{array}{rclrcl}
Q_1^{(x)} &=& \sqrt{(q_1^{(x)})^2+(q_1^{(y)})^2}, & q_1^{(x)} &=& Q_1^{(x)}\cos Q_1^{(y)},\\
Q_1^{(y)} &=& \arctan(q_1^{(y)}/q_1^{(x)}), & q_1^{(y)} &=& Q_1^{(x)}\sin Q_1^{(y)},\\
Q_i^{(x)} &=& \frac{-1}{Q_1^{(x)}}(\vec{q}_1\cdot\vec{q}_i), & q_i^{(x)} &=& -(Q_i^{(x)}\cos Q_1^{(y)}+Q_i^{(y)}\sin Q_1^{(y)}),\\
Q_i^{(y)} &=& \frac{1}{Q_1^{(x)}}(q_1^{(x)}q_i^{(y)}-q_1^{(y)}q_i^{(x)}), & q_i^{(y)} &=& -(Q_i^{(x)}\sin Q_1^{(y)}-Q_i^{(y)}\cos Q_1^{(y)}),\\
P_1^{(x)} &=& \frac{1}{Q_1^{(x)}}(\vec{q}_1\cdot\vec{p}_1), & p_1^{(x)} &=& P_1^{(x)}\cos Q_1^{(y)}-\frac{A}{Q_1^{(x)}}\sin Q_1^{(y)},\\
P_1^{(y)} &=& \sum_{i=1}^N(q_i^{(x)}p_i^{(y)}-q_i^{(y)}p_i^{(x)}), & p_1^{(y)} &=& P_1^{(x)}\sin Q_1^{(y)}+\frac{A}{Q_1^{(x)}}\cos Q_1^{(y)},\\
P_i^{(x)} &=& \frac{-1}{Q_1^{(x)}}(\vec{q}_1\cdot\vec{p}_i), & p_i^{(x)} &=& -(P_i^{(x)}\cos Q_1^{(y)}+P_i^{(y)}\sin Q_1^{(y)}),\\
P_i^{(y)} &=& \frac{1}{Q_1^{(x)}}(q_1^{(x)}p_i^{(y)}-q_1^{(y)}p_i^{(x)}), & p_i^{(y)} &=& -(P_i^{(x)}\sin Q_1^{(y)}-P_i^{(y)}\cos Q_1^{(y)}),
\end{array}
$$

where $i=2,\dots,N$ and $A=\sum_{i=2}^N(Q_i^{(x)}P_i^{(y)}-Q_i^{(y)}P_i^{(x)})+P_1^{(y)}$.

Note that $Q_1^{(x)}$ is the distance between the bodies P_0 and P_1, that $Q_i^{(x)}$, $Q_i^{(y)}$ for $i=2,\dots,N$, are, respectively, the projections of the vector $\vec{q}_i$ into the P_0P_1 direction and its orthogonal one and that $Q_1^{(y)}$ is the angle between the vector $\vec{q}_1$ and the "old" x axis. Also, $P_i^{(x)}$, $i=1,\dots,N$, are the projections of $\vec{p}_i$ into the P_0P_1 direction, $P_i^{(y)}$, $i=2,\dots,N$ into the orthogonal one and, finally, $P_1^{(y)}$ is the angular momentum of the system.

Implementing this change of variables, the Hamiltonian (4.3) becomes:

$$
H=\frac{1}{2\alpha_1}\left((P_1^{(x)})^2+\frac{A^2}{(Q_1^{(x)})^2}\right)-P_1^{(y)}+\sum_{i=2}^N\frac{1}{2\alpha_i}||\vec{P}_i||^2-\sum_{0\le i<j\le N}G\frac{m_im_j}{||\vec{r}_{ij}||},
$$

where $||\vec{r}_{ij}||$ is a scalar function of $Q_1^{(x)},Q_2^{(x)},Q_2^{(y)},\dots,Q_N^{(x)},Q_N^{(y)}$. This can be easily derived from the following relations: $||\vec{q}_1||=Q_1^{(x)}$, $||\vec{q}_i||^2=||\vec{Q}_i||^2$, $\vec{q}_1\cdot\vec{q}_i=-Q_1^{(x)}Q_i^{(x)}$ and $\vec{q}_i\cdot\vec{q}_j=\vec{Q}_i\cdot\vec{Q}_j$ for $i,j=2,\dots,N$.

As the Hamiltonian does not depend on $Q_1^{(y)}$, this is an ignorable coordinate and the corresponding integral is $P_1^{(y)}=K$ (where K is a constant real number). This integral of motion is the angular momentum. Therefore, the equation of motion corresponding to $Q_1^{(y)}$ can be integrated independently when the rest of the system has been solved.

Thus, the equations corresponding to $Q_1^{(y)}$ and $P_1^{(y)}$ can be skipped from the system of equations giving rise to the following $2N-1$ degrees of freedom Hamiltonian:

$$
H=\frac{1}{2\alpha_1}\left((P_1^{(x)})^2+\frac{A^2}{(Q_1^{(x)})^2}\right)-K+\sum_{i=2}^N\frac{1}{2\alpha_i}||\vec{P}_i||^2-\sum_{0\le i<j\le N}G\frac{m_im_j}{||\vec{r}_{ij}||}, \tag{4.4}
$$

where $A = \sum_{i=2}^{N}(Q_i^{(x)}P_i^{(y)} - Q_i^{(y)}P_i^{(x)}) + K$ and

$$\begin{aligned}
||\vec{r}_{01}||^2 &= (Q_1^{(x)})^2, \\
||\vec{r}_{0i}||^2 &= (Q_i^{(x)} - \frac{m_1}{\eta_1}Q_1^{(x)})^2 + (Q_i^{(x)})^2 - 2\sum_{j=2}^{i-1}\frac{m_1 m_j}{\eta_1\eta_j}Q_1^{(x)}Q_j^{(x)} \\
&\quad + \sum_{k,j=2}^{i-1}\frac{m_k m_j}{\eta_k\eta_j}\vec{Q}_k\cdot\vec{Q}_j + 2\sum_{j=2}^{i-1}\frac{m_j}{\eta_j}\vec{Q}_i\cdot\vec{Q}_j \qquad i>1, \\
||\vec{r}_{1j}||^2 &= (Q_j^{(x)} - \frac{\eta_0}{\eta_1}Q_1^{(x)})^2 + (Q_j^{(x)})^2 - 2\sum_{k=2}^{j-1}\frac{m_k\eta_0}{\eta_1\eta_k}Q_1^{(x)}Q_k^{(x)} \\
&\quad + \sum_{k,l=2}^{j-1}\frac{m_k m_l}{\eta_k\eta_l}\vec{Q}_k\cdot\vec{Q}_l + 2\sum_{k=2}^{j-1}\frac{m_k}{\eta_k}\vec{Q}_j\cdot\vec{Q}_k \qquad j>1, \\
||\vec{r}_{ij}||^2 &= ||\vec{Q}_j - \frac{\eta_{i-1}}{\eta_i}\vec{Q}_1||^2 - 2\sum_{k=i+1}^{j-1}\frac{m_k\eta_{i-1}}{\eta_k\eta_i}\vec{Q}_i\cdot\vec{Q}_k \\
&\quad + \sum_{k,l=i+1}^{j-1}\frac{m_k m_l}{\eta_k\eta_l}\vec{Q}_k\cdot\vec{Q}_l + 2\sum_{k=i+1}^{j-1}\frac{m_k}{\eta_k}\vec{Q}_j\cdot\vec{Q}_k \quad 1<i<j. \qquad (4.5)
\end{aligned}$$

4.1.3 Equations of motion for $N = 2$ and $N = 3$

The main part of these chapter is concerned in dealing with the two and three planetary problems Sun-Jupiter-Saturn (SJS) and Sun-Jupiter-Saturn-Uranus (SJSU). In this section, the equations of motion for these two cases ($N = 2$ and $N = 3$) are derived from Hamiltonian (4.4).

As usual, we use units such that the total mass of Sun and Jupiter is equal to 1 and the gravitational constant G is also 1. In these adimensional units, the masses of the bodies involved in the two and three planetary problems take the following values:

Body	Mass parameter	Mass value
Sun	$m_0 = 1 - \mu$	$9.990461246 \times 10^{-1}$
Jupiter	$m_1 = \mu$	$9.538753600 \times 10^{-4}$
Saturn	$m_2 = m_{sat}$	$2.855150174 \times 10^{-4}$
Uranus	$m_3 = m_{ura}$	$4.361228581 \times 10^{-5}$

The vector fields are computed using some normalized coordinates,

$(x_1, x_2, \dots, x_{2N-1}, y_1, y_2, \dots, y_{2N-1})$, that are defined by the following relations:

$$\begin{aligned} x_1 &= Q_1^{(x)}, \\ x_{2k-2} &= Q_k^{(x)}, \quad k = 2 \div N, \\ x_{2k-1} &= Q_k^{(y)}, \quad k = 2 \div N, \\ y_1 &= \frac{P_1^{(x)}}{\alpha_1}, \\ y_{2k-2} &= \frac{P_k^{(x)}}{\alpha_k}, \quad k = 2 \div N, \\ y_{2k-1} &= \frac{P_k^{(y)}}{\alpha_k}, \quad k = 2 \div N, \end{aligned}$$

where, recall that, $\alpha_k = \frac{m_k \eta_{k-1}}{\eta_k}$ and $\eta_k = \sum_{j=0}^{k} m_j$.

4.1.3.1 The SJS planar problem

The vector field of the reduced Sun-Jupiter-Saturn planar problem is a three degrees of freedom Hamiltonian system and can be written depending on six variables, $(x_1, x_2, x_3, y_1, y_2, y_3)$ and on the parameter angular momentum K:

$$\begin{aligned} \dot{x_1} &= y_1, \\ \dot{x_2} &= y_2 - \frac{x_3 A}{\alpha x_1^2}, \\ \dot{x_3} &= y_3 + \frac{x_2 A}{\alpha x_1^2}, \\ \dot{y_1} &= \frac{A^2}{\alpha^2 x_1^3} - \frac{1}{x_1^2} - m_{sat} \left(\frac{\mu x_1 - x_2}{r_{13}^3} + \frac{(1-\mu)x_1 + x_2}{r_{23}^3} \right), \\ \dot{y_2} &= -\frac{y_3 A}{\alpha x_1^2} + (1 + m_{sat}) \left((1-\mu) \frac{\mu x_1 - x_2}{r_{13}^3} - \mu \frac{(1-\mu)x_1 + x_2}{r_{23}^3} \right), \\ \dot{y_3} &= \frac{y_2 A}{\alpha x_1^2} - (1 + m_{sat}) \left(\frac{(1-\mu)x_3}{r_{13}^3} + \frac{\mu x_3}{r_{23}^3} \right), \end{aligned} \tag{4.6}$$

where $A = \beta(x_2 y_3 - x_3 y_2) + K$, $r_{13}^2 = (\mu x_1 - x_2)^2 + x_3^2$, $r_{23}^2 = ((1-\mu)x_1 + x_2)^2 + x_3^2$ and

$$\begin{aligned} \alpha &= \alpha_1 = \mu(1-\mu) = 9.52965481797585 \times 10^{-4}, \\ \beta &= \alpha_2 = \frac{m_{sat}}{1 + m_{sat}} = 2.85433521882010 \times 10^{-4}. \end{aligned}$$

In Section 4.3, we compute a quasi-periodic solution of this vector field for which the relative Sun-Jupiter motion has a prescribed characteristic.

4.1.3.2 The SJSU planar problem

We can also write the vector field of the reduced planar four body Sun-Jupiter-Saturn-Uranus problem depending on ten variables, $x_1, \dots, x_5, y_1, \dots, y_5$ and on the parameter angular momentum K. This is a five degrees of freedom Hamiltonian problem and the equations are:

$$
\begin{aligned}
\dot{x_1} &= y_1, \\
\dot{x_2} &= y_2 - \frac{x_3 A}{\alpha x_1^2}, \\
\dot{x_3} &= y_3 + \frac{x_2 A}{\alpha x_1^2}, \\
\dot{x_4} &= y_4 - \frac{x_5 A}{\alpha x_1^2}, \\
\dot{x_5} &= y_5 + \frac{x_4 A}{\alpha x_1^2}, \\
\dot{y}_1 &= \frac{A^2}{\alpha^2 x_1^3} - \frac{1}{x_1^2} - m_{sat}\left(\frac{\mu x_1 - x_2}{r_{13}^3} + \frac{(1-\mu)x_1 + x_2}{r_{23}^3}\right), \\
&\quad + m_{ura}\left(\frac{x_4 + \beta x_2 - \mu x_1}{r_{14}^3} + \frac{x_4 + \beta x_2 + (1-\mu)x_1}{r_{24}^3}\right), \\
\dot{y}_2 &= -\frac{y_3 A}{\alpha x_1^2} + (1 + m_{sat})\left((1-\mu)\frac{\mu x_1 - x_2}{r_{13}^3} - \mu\frac{(1-\mu)x_1 + x_2}{r_{23}^3}\right), \\
&\quad - m_{ura}\left((1-\mu)\frac{x_4 + \beta x_2 - \mu x_1}{r_{14}^3} + \mu\frac{x_4 + \beta x_2 + (1-\mu)x_1}{r_{24}^3} - \frac{x_4 - (1-\beta)x_2}{r_{34}^3}\right), \\
\dot{y}_3 &= \frac{y_2 A}{\alpha x_1^2} - (1 + m_{sat})\left(\frac{(1-\mu)x_3}{r_{13}^3} + \frac{\mu x_3}{r_{23}^3}\right), \\
&\quad - m_{ura}\left((1-\mu)\frac{x_5 + \beta x_3}{r_{14}^3} + \mu\frac{x_5 + \beta x_3}{r_{24}^3} - \frac{x_5 - (1-\beta)x_3}{r_{34}^3}\right), \\
\dot{y}_4 &= -\frac{y_5 A}{\alpha x_1^2} - \delta\left((1-\mu)\frac{x_4 + \beta x_2 - \mu x_1}{r_{14}^3} + \mu\frac{x_4 + \beta x_2 + (1-\mu)x_1}{r_{24}^3} + m_{sat}\frac{x_4 - (1-\beta)x_2}{r_{34}^3}\right), \\
\dot{y}_5 &= \frac{y_4 A}{\alpha x_1^2} - \delta\left((1-\mu)\frac{x_5 + \beta x_3}{r_{14}^3} + \mu\frac{x_5 + \beta x_3}{r_{24}^3} + m_{sat}\frac{x_5 - (1-\beta)x_3}{r_{34}^3}\right),
\end{aligned}
\tag{4.7}
$$

where

$$
\begin{aligned}
r_{13}^2 &= (x_2 - \mu x_1)^2 + x_3^2, \\
r_{23}^2 &= (x_2 + (1-\mu)x_1)^2 + x_3^2, \\
r_{14}^2 &= (x_5 + \beta x_3)^2 + (x_4 + \beta x_2 - \mu x_1)^2, \\
r_{24}^2 &= (x_5 + \beta x_3)^2 + (x_4 + \beta x_2 + (1-\mu)x_1)^2, \\
r_{34}^2 &= (x_5 - (1-\beta)x_3)^2 + (x_4 - (1-\beta)x_2)^2,
\end{aligned}
$$

α and β are defined as before and A is now given by $A = \beta(x_2y_3-x_3y_2)+\gamma(x_4y_5-x_5y_4)+K$, with

$$\gamma = \alpha_3 = \frac{m_{ura}(1+m_{sat})}{1+m_{sat}+m_{ura}} = 4.36103844090970 \times 10^{-5},$$

$$\delta = \frac{1+m_{sat}+m_{ura}}{1+m_{sat}} = 1.00004359983741.$$

4.2 A method for computing invariant tori

In this section, we review (see [CJ00]) a method for computing 2-D invariant tori. We are interested in finding a quasi-periodic solution (with two basic frequencies) of a given vector field. We reduce this problem to the one of finding an invariant curve of a suitable Poincaré map. This invariant curve is seen as a truncated Fourier series and our aim is to compute its rotation number and a Fourier representation of it. We follow roughly the method developed by [CJ00], using some ideas of [GM01].

4.2.1 Numerical computation of invariant curves

Let be $\dot{x} = f(x)$ $(x, f \in \mathbb{R}^n)$ an autonomous vector field of dimension n (for example, the reduced field of the N-Planetary problem given at 4.1.2) and $\Phi(x,t) \equiv \Phi_t(x)$ its associated flow. Let us define the Poincaré map as the time T-flow $\Phi_T(\cdot)$, where T is a prefixed value.

Let ω be the rotation number of the invariant curve. Let, also, $\mathcal{C}(\mathbb{T}^1,\mathbb{R}^n)$ be the space of continuous functions from $\mathbb{T}^1$ in $\mathbb{R}^n$, and let us define the linear map $T_\omega : \mathcal{C}(\mathbb{T}^1,\mathbb{R}^n) \to \mathcal{C}(\mathbb{T}^1,\mathbb{R}^n)$ as the translation by ω, $(T_\omega\varphi)(\theta) = \varphi(\theta+\omega)$.

Let us define $F : \mathcal{C}(\mathbb{T}^1,\mathbb{R}^n) \to \mathcal{C}(\mathbb{T}^1,\mathbb{R}^n)$ as

$$F(\varphi)(\theta) = \Phi_T(\varphi(\theta)) - (T_\omega\varphi)(\theta) \qquad \forall\varphi \in \mathcal{C}(\mathbb{T}^1,\mathbb{R}^n). \tag{4.8}$$

It is clear that the zeros of F in $\mathcal{C}(\mathbb{T}^1,\mathbb{R}^n)$ correspond to invariant curves of rotation number ω. The equation satisfied is

$$\Phi_T(\varphi(\theta)) = \varphi(\theta+\omega) \quad \forall\theta \in \mathbb{T}. \tag{4.9}$$

The method we want to summarize in this section boils down to looking numerically for a zero of F. Hence, let us write $\varphi(\theta)$ as a real Fourier series,

$$\varphi(\theta) = A_0 + \sum_{k>0}(A_k\cos(k\theta) + B_k\sin(k\theta)), \quad A_k, B_k \in \mathbb{R}^n, \quad k \in \mathbb{N}.$$

Then, we will fix in advance a truncation value N_f for this series (the selection of the truncation value will be discussed later on), and let us try to determine (an approximation to) the $2N_f+1$ unknown coefficients A_0, A_k and B_k, $1 \le k \le N_f$. To this end, we will construct a discretized version of the map F as follows: first, we select the mesh of $2N_f+1$ points on $\mathbb{T}^1$,

$$\theta_j = \frac{2\pi j}{2N_f+1} \quad 0 \le j \le 2N_f, \tag{4.10}$$

and evaluate the function (4.8) on it. Let F_{N_f} be this discretization of F:

$$\Phi_T(\varphi(\theta_j)) - \varphi(\theta_j + \omega), \quad 0 \le j \le 2N_f. \tag{4.11}$$

So, given a (known) set of Fourier coefficients A_0, A_k and B_k ($1 \le k \le N_f$), we can compute the points $\varphi(\theta_j)$, then $\Phi_T(\varphi(\theta_j))$ and next the points $\Phi_T(\varphi(\theta_j)) - \varphi(\theta_j + \omega)$, $0 \le j \le N_f$. From these data, we can immediately obtain the Fourier coefficients of $\Phi_T(\varphi(\theta)) - \varphi(\theta + \omega)$.

To apply a Newton method to solve the equation $F_{N_f} = 0$, we also need to compute explicitly the differential of F_{N_f}. This can be done easily by applying the chain rule to the process used to compute F_{N_f}. Note that the number of equations to be solved is $(2N_f + 1)n$ and that the unknowns are $(A_0, A_1, B_1, \ldots, A_{N_f}, B_{N_f})$, ω and the time T for which we fix the Poincaré map associated to the flow ($\Phi_T(\cdot)$). That is, we deal with $(2N_f + 1)n + 2$ unknowns. We want to mention that the system that we deal with is degenerate unless we fix (keep constant during the computations) some of the unknowns. Thus, in each step of the Newton method, we solve a non-square linear system by means of a standard least-squares method.

Note that in the case of the reduced N-planetary problem, an integral of motion is still left: the energy. We can easily solve the problem of the degeneracy, induced by it, fixing a Poincaré section.

Three other unknowns have also to be fixed in order to solve other degeneracy problems: first, the rotation's magnitude has to be prefixed somehow (directly, by fixing the rotation number ω, or indirectly), second, we set the invariant curve on the 2-D torus; and third, we select one Fourier representation for the given invariant curve (this is the so-called problem of coefficient modulation, see [GM01]).

Thus, usually we will deal with non-square linear systems of dimension $(2N_f + 1)n \times ((2N_f + 1)n - 2)$.

4.2.2 Discretization error

Once we have solved equation (4.11) with a certain tolerance (error in the Newton method; we take typically 10^{-11}), we still do not have any information on the error of the approximated invariant curve. The reason, as explained in [CJ00], is that we have not estimated the discretization error; i.e., the error when passing from equation (4.8) to equation (4.11).

In order to do it, we compute

$$E(\varphi, \omega) = \max_{\theta \in \mathbb{T}} |\Phi_T(\varphi(\theta, z)) - \varphi(\theta + \omega, z)|$$

in a mesh of points, say, 100 times finer than the mesh (4.10) and consider it as an estimation of the error of the invariant curve.

If $||E||_\infty > 10^{-9}$, the solution obtained is not considered good enough and another one with the same initial approximation for the Newton method but with a greater discretization order N_f is computed. The process is repeated until the sub-infinity norm of the discretization error is smaller than 10^{-9}.

4.3 The Bianular solution of the SJS system

In this section, we apply the method explained in Section 4.2 for computing 2-D invariant tori to the planar Sun-Jupiter-Saturn case. Our main goal is to find a quasi-periodic solution (with two frequencies) of (4.6) such that the relative Sun-Jupiter motion simulates in the best possible way[1] the real one.

First, we give a good initial approximation needed in the Newton method for solving the invariant curve's equations. This initial approximation is based on the linear dynamics around the periodic orbit of the planar three body problem computed in Section 2.1.1.

Second, we compute two tori that come from two different normal linear directions of the periodic orbit. These tori belong to two different families that start at the same periodic orbit.

Finally, we continue these two families in order to find a torus in which Jupiter's motion is the desired one.

4.3.1 The initial approximation

In order to solve equations (4.11) for the reduced field (4.6), we need an initial approximation for the unknowns and to fix some of them during the computation.

4.3.1.1 The starting point: a periodic orbit

As the reduced equations (4.6) come from a Hamiltonian, the tori that we want to compute belong to a family of tori.

In order to compute the first torus of the family, it is useful to start from a known periodic orbit of the planar three body problem. We use the one computed in 2.1.1. This is a periodic orbit for the Hamiltonian (4.3) in the 2-planetary case. The rotating Jacobi coordinates of a point of this orbit (let's say, when $t = 0$) are shown in the following table:

$q_1(0)$	-0.999499455382433	$p_1(0)/\alpha$	0.0
$q_2(0)$	0.0	$p_2(0)/\alpha$	-1.00062422459750
$q_3(0)$	-1.83433334636804	$p_3(0)/\beta$	0.0
$q_4(0)$	0.0	$p_4(0)/\beta$	-0.738094038829119

We are interested in the linear normal behaviour of this periodic orbit. It is straightforward to compute the eigenvalues of the Monodromy matrix:

j	$\mathrm{Re}\,(\lambda_j)$	$\pm\mathrm{Im}\,(\lambda_j)$	$\lvert\lambda_j\rvert$	$\pm\mathrm{Arg}\,(\lambda_j)$
1	-0.4547032607925039	0.890642995046002	1.0	2.04283533844408
2	-0.4563371385719557	0.889806954322080	1.0	2.04467069171687
3	1.0	0.0	1.0	0.0
4	1.0	0.0	1.0	0.0

We can see that the norm of all of them is equal to one, so the linear dynamics is completely elliptic around it. On the other hand, the matrix has two Jordan boxes corresponding

[1] In this case, as we compute a 2-D torus, we have essentially two free parameters that will allow us to choose two osculating orbital elements of the relative Sun-Jupiter motion.

$\lambda = \cos(\nu) \pm i\sin(\nu)$	$\lvert\lambda\rvert$	$\pm\nu = \pm\mathrm{Arg}(\lambda)$	$\vec{v} = \vec{v_1} \pm i\vec{v_2}$
$-0.4563738 + 0.8897882$ i	1.0	2.04471185341918	$0.0 - 0.0701487$ i $0.0 - 0.3800818$ i $1.0 + 0.0$ i $-0.06941378 + 0.0$ i $0.0002378442 + 0.0$ i $0.0 - 0.1524362$ i
$-0.4546396 + 0.8906755$ i	1.0	2.04276384546609	$-0.5671793 + 0.0$ i $1.0 + 0.0$ i $0.0 - 0.04820275$ i $0.0 + 0.5683110$ i $0.0 - 0.0004070598$ i $0.4024776 + 0.0$ i

Table 4.1: Eigenvalues and eigenvectors of the Monodromy matrix for the periodic solution X_0 of the reduced TBP.

to the angular momentum and energy integrals of motion. This Jordan boxes in the Monodromy matrix could bring on troubles in the numerical computation of invariant curves; thus, we will use the reduction of one degree of freedom of the Hamiltonian explained in Section 4.1 in order one of these two Jordan boxes to be erased.

The initial condition $X_0 = (x_1(0), x_2(0), x_3(0), y_1(0), y_2(0), y_3(0))$ of this periodic orbit for the equations (4.6) is:

$x_1(0)$	`-0.999499455382433`	$y_1(0)$	`0.0`
$x_2(0)$	`-1.83433334636804`	$y_2(0)$	`0.0`
$x_3(0)$	`0.0`	$y_3(0)$	`0.73809403882911895`

and the angular momentum takes the value $K = 1.33953449145583 \times 10^{-3}$.

The eigenvalues (not contained in a Jordan box) of the Monodromy matrix and the corresponding eigenvectors are displayed in Table 4.1. With these two pairs of conjugated eigenvalues, we will be able to generate two different families of tori starting at the same periodic orbit.

4.3.1.2 On the two families of invariant curves

As we will see in the next sections, we can compute (numerically) an invariant curve starting from a periodic orbit. In this construction, the linear behaviour of this orbit is strongly used to obtain an approximation for the first step in the Newton method. Actually, what is used is one of the two eigenvalue-eigenvector pair of Table 4.1.

Each pair will give us a different family of tori. These are two different families that start at the same periodic orbit. They are known, in the literature, as Lyapunov families of invariant tori (for theoretical results on their existence, see [JV97a, JV01]). We want to continue these two families in order to try to set Jupiter's motion to a more realistic one (actually, by trying to fix some of its orbital elements).

From now on, we will call Family1 (or Torus1) to the one corresponding to the first eigenvalue-eigenvector pair in Table 4.1 and Family2 (or Torus2) to the one corresponding to the second one. The method we have followed in order to continue these families of invariant tori is explained in 4.3.3.

4.3.1.3 Fixing the unknowns

As stated in 4.2.1, in order to solve the degenerate linear system coming from the Newton method for (4.11), some of the unknowns must be fixed during the computation.

In this case, at every step, the prefixed unknowns are:

- $T = T_{sat} = \frac{2\pi}{\omega_{sat}}$; we fix Saturn's frequency.
- $A_0^{(3)} = X_0^{(3)} = 0$; we set the invariant curve on the torus[2].
- $A_1^{(l_1)} = \gamma(v_1^{(l_1)} \cos(\xi_0) + v_2^{(l_1)} \sin(\xi_0)) \neq 0$; we fix it in order not to go back to the periodic orbit and leave the rotation number ω to be self-adjusted.
- $A_1^{(l_2)} = \gamma(v_1^{(l_2)} \cos(\xi_0) + v_2^{(l_2)} \sin(\xi_0)) = 0$; in order to solve the problem of coefficient modulation (see [GM01]). This condition can be satisfied choosing $\xi_0 \in \mathbb{T}^1$ such that $\xi_0 = \arctan\left(-\frac{v_1^{(l_2)}}{v_2^{(l_2)}}\right)$.

The last two conditions can be explained from the initial approximation that we choose in the Newton method. The indexes l_1 and l_2 depend on the family we are interested in. For instance, $l_1 = 3$ and $l_2 = 2$ for one family (Family1) and $l_1 = 2$ and $l_2 = 3$ for the other (Family2).

Finally, the initial approximation of the unknowns in the Newton method is given by the linearization of the Poincaré map around the fixed point X_0:

$$\begin{aligned}
T &= T_{sat}, \\
\omega &= \nu, \\
A_0 &= X_0, \\
A_1 &= \gamma(v_1 \cos(\xi_0) + v_2 \sin(\xi_0)), \\
B_1 &= \gamma(v_1 \sin(\xi_0) + v_2 \cos(\xi_0)), \\
A_k &= 0\,,\ k \geq 2, \\
B_k &= 0\,,\ k \geq 2,
\end{aligned}$$

where $(\nu, \vec{v} = \vec{v_1} + i\vec{v_2})$ is one of the eigenvalue-eigenvector pair of Table 4.1, ξ_0 has been given before and γ is a sufficiently small parameter (for instance, $\gamma \sim 10^{-3}$) choosed in order the invariant curve not to be too far from the periodic orbit.

[2]The upper index indicates the component of the vector $A_k \in \mathbb{R}^6$

4.3.2 The first invariant torus for each family

With the method described in Section 4.2 and the initial approximation that has just been given, we have computed a first torus for each family. Here, we see how we can reconstruct the tori in the non-reduced coordinates and we compare some orbital elements of the two planets, Jupiter and Saturn, in this quasi-periodic orbit to the actual ones.

4.3.2.1 Going back to rotating Jacobi coordinates

We would like to display the invariant tori in the rotating Jacobi coordinates, $(q_1, \dots, q_4, p_1, \dots, p_4)$, in which the Hamiltonian (4.3) is written. Although we have computed them (seen as invariant curves of a Poincaré map) in the reduced coordinates $(x_1, \dots, x_6)$, if the rotating Jacobi coordinates of a point on the torus were known, we would be done because we can integrate the differential equations corresponding to Hamiltonian (4.3) taking this point as initial condition.

In order to obtain this 8-dimensional point from $x_1, \dots, x_6$ and K, in a unique way, we still have to select an extra condition. Note that when we make the reduction of the equations to pass from 4 to 3 degrees of freedom, we loose some information: the angle between the Sun-Jupiter's vector (P_0P_1 direction) and the "old" x-axis. Thus, if we want to invert this change we will have to fix the position of the "new" x-axis.

From now on, when we undo the reduction change, we will fix the x-axis in the following way: we find the angle θ for which $x_3(\theta) = 0$ (that is, when Sun, Jupiter and Saturn are in a particular collinear configuration) and set the rotating Jacobi coordinates as:

$q_1 = -x_1$	$p_1 = -\alpha x_4$
$q_2 = 0$	$p_2 = -\frac{A}{x_1}$
$q_3 = x_2$	$p_3 = \beta x_5$
$q_4 = -x_3$	$p_4 = -\beta x_6$

where, recall that, $A = \beta(x_2 x_6 - x_3 x_5) + K$, $\alpha = \mu(1-\mu)$ and $\beta = \frac{m_{sat}}{1+m_{sat}}$.

4.3.2.2 Some osculating orbital elements

Once the rotating Jacobi coordinates of a point for each torus is computed, we use them as initial conditions for integrating the Hamiltonian field (4.3) with $N = 2$ during a time span of 50 Jupiter sidereal revolutions.

The projection for Torus1 and Torus2 into the (q_1, q_2), (p_1, p_2) and (q_3, q_4) planes are shown in Figure 4.2. We can see (left and center plots) that the relative Sun-Jupiter motion is a libration around the point $(-1, 0, 0, -1)$; and that Saturn's orbit has "fattened" a little bit (right plots).

The evolution of Jupiter's and Saturn's osculating semi-major axis, eccentricity and perihelion argument for Torus1 and Torus2 are displayed in Figures 4.3 and 4.4. The integration time, in this case, is 52.6195485402068 adimensional units.

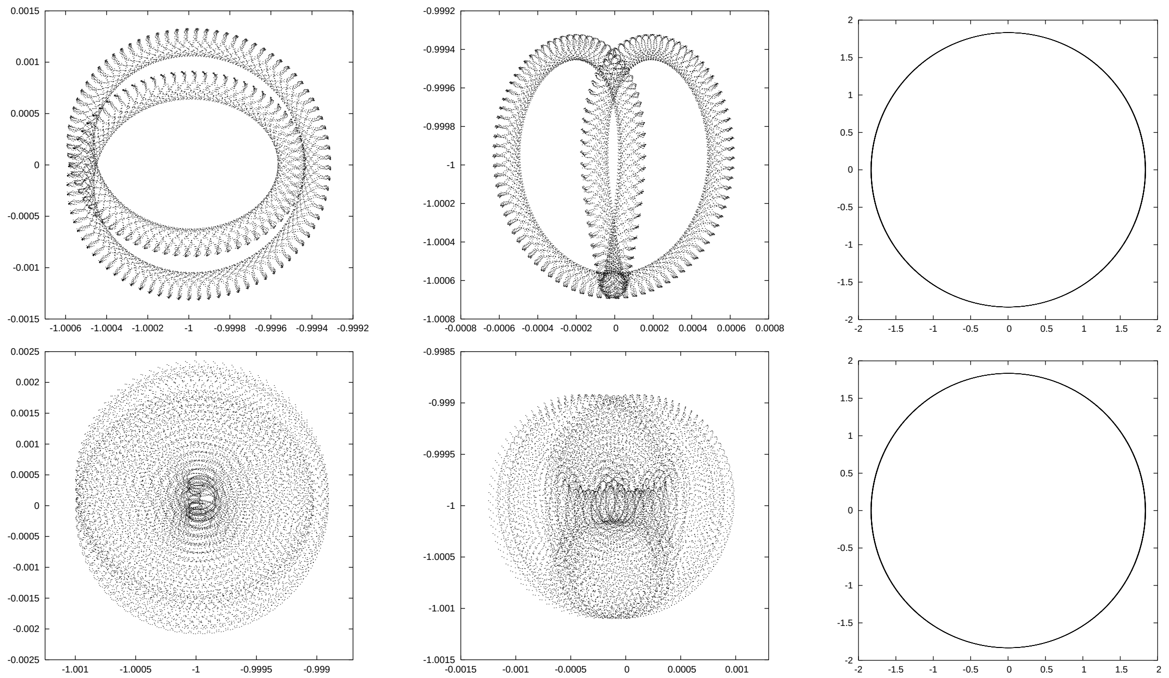

Figure 4.2: Left: Sun-Jupiter relative motion for Torus1 (top) and Torus2 (bottom). Center: Momenta for the Sun-Jupiter relative motion for Torus1 (top) and Torus2 (bottom). Right: Saturn's orbit around the Sun-Jupiter barycenter for Torus1 (top) and Torus2 (bottom).

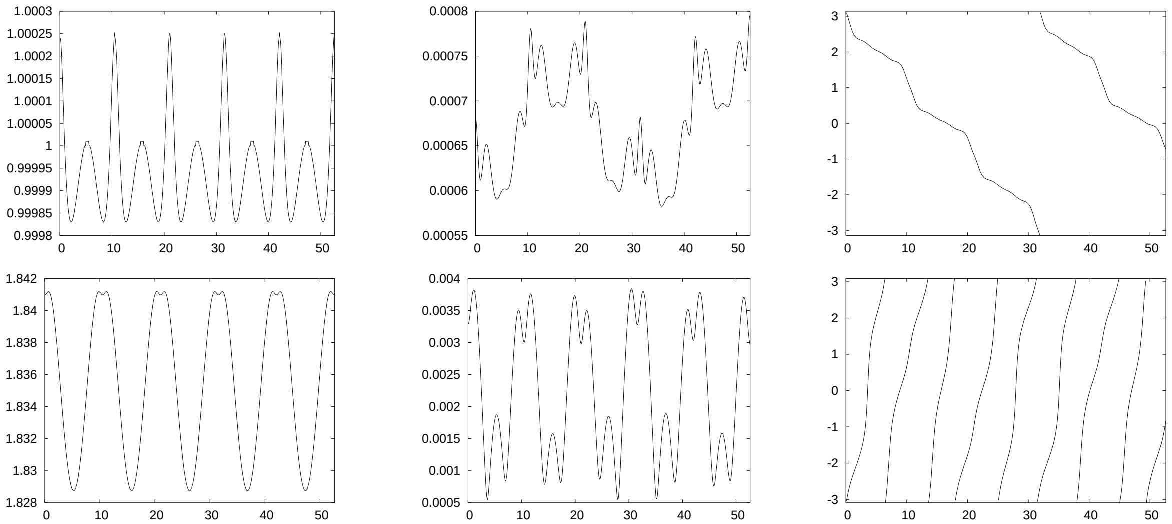

Figure 4.3: From left to right: Evolution in Torus1 of the osculating semi-major axis, eccentricity and argument of the perihelion of Jupiter's orbit (top) and Saturn's orbit (bottom) in a time span of 5 Jupiter's sidereal revolutions.

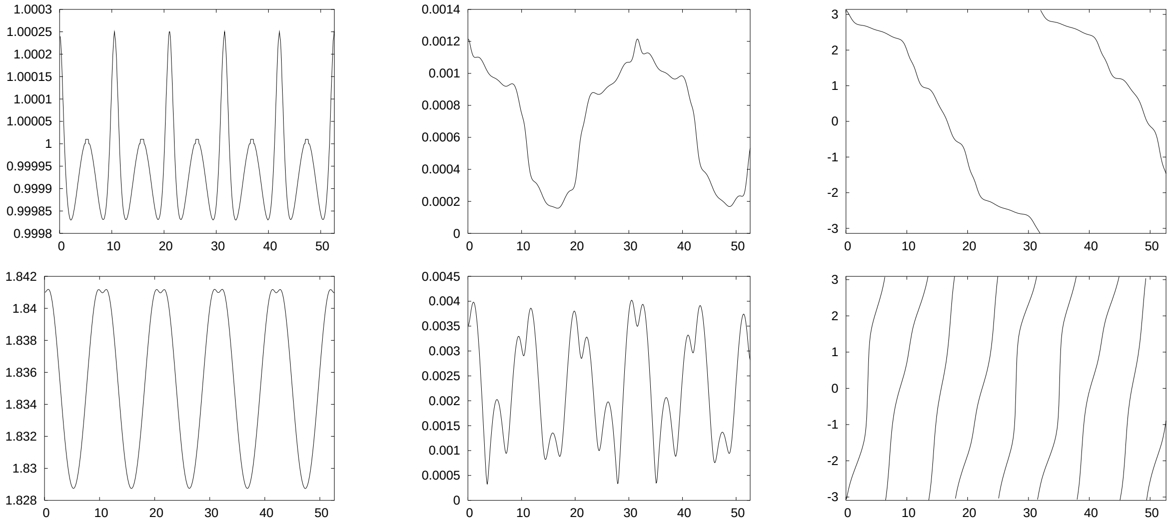

Figure 4.4: From left to right: Evolution in Torus2 of the osculating semi-major axis, eccentricity and argument of the perihelion of Jupiter's orbit (top) and Saturn's orbit (bottom) in a time span of 5 Jupiter's sidereal revolutions.

Note that the semi-major axis of Jupiter's and Saturn's orbits in either Torus1 or Torus2 are quite well adjusted (our unit of length is the Sun-Jupiter distance) and, in consequence, their period (that oscillate around 2π and $\frac{2\pi}{\omega_{sat}}$, respectively) are also closed to the actual ones. This was expected because, during the computations, the time T of the Poincaré map has been fixed equal to the period of Saturn relative to the Sun-Jupiter's one.

The osculating Jupiter's eccentricity in the two tori is still too small (10^{-3}, approximately) compared to the actual one ($e \sim 0.0484$). Something similar happens to the one of Saturn's orbit.

Recall that our main goal was to improve the simulation of Jupiter's motion. Thus, the next step is to find a torus, in Family1 or Family2, in which the eccentricity of Jupiter's orbit fits much better the actual one.

4.3.3 Continuation of the two families of invariant tori

As it is well known, the families of invariant tori are not continuous but Cantorian. However, it is quite common in many situations that the holes that conform the Cantor structure are too small to be detected by the standard double precision arithmetic of the computer (see [JV97a] for some analytical estimates, and [BHJ$^+$03] for a discussion on the effect of the different kind of resonances). Therefore, except by low order resonances, these families look continuous in the computer.

Once we have a first torus, we want to continue the family it belongs to. This family can be parameterized by the angular momentum K. It is easy to see (and also checked from the computations) that there is a strong relationship between the angular momentum, K, and the osculating orbital elements of Jupiter's and Saturn's orbits.

As we want to simulate in a more realistic way the Sun-Jupiter relative motion, we are more interested in adjusting Jupiter's orbital elements than Saturn's ones. As there is one degree of freedom (we are allowed to set K), we select the osculating eccentricity of Jupiter's orbit as the targeting value. Thus, by means of a continuation method, we try to find another torus inside Family1 or Family2 for which the osculating eccentricity of Jupiter is approximately 0.0484.

4.3.3.1 Method of Continuation

The continuation process starts with Torus1 or Torus2 computed in 4.3.2, depending on the family that we want to follow (Family1 or Family2, respectively).

To compute a torus belonging to a particular family, we use a small modification of the method explained in Section 4.2. We add to equations (4.11) a new one:

$$\mathrm{eccen}(x_1, x_2, x_3, x_4, x_5, x_6, K) = \sqrt{1 + \frac{A^4}{\alpha^4 x_1^2} + \frac{A^2 x_4^2}{\alpha^2} - 2\frac{A^2}{\alpha^2 x_1}} = e, \qquad (4.12)$$

where $\alpha = \mu(1-\mu)$, $A = \beta(x_2x_6 - x_3x_5) + K$, $\mathrm{eccen}(\cdot)$ is a function that gives us Jupiter's osculating eccentricity from the reduced coordinates in a given moment (we evaluate it when Sun, Jupiter and Saturn are in a particular collinear configuration; more concretely, when $x_3 = 0$) and e is a fixed constant that will be used as a control parameter.

Thus, at each step of the continuation scheme, we find an invariant curve (parameterized by $z = (A_0, A_1, B_1, A_2, B_2, \ldots, A_{N_f}, B_{N_f}))$ of the Poincaré map $\Phi_T(\cdot)$, a truncation number of the Fourier series (N_f), a rotation number (ω) and an angular momentum (K) that are solution of equations (4.11) and (4.12) for a fixed eccentricity (e). As explained in 4.2.1, every invariant curve is refined by means of a Newton method, and in each step of the Newton method we solve a non-square linear system using a least-squares method.

During the continuation process, the parameters that we keep constant are slightly different from those in 4.3.1.3:

- $T = T_{sat} = \frac{2\pi}{\omega_{sat}}$; we fix Saturn's frequency.
- $A_0^{(3)} = 0$; we fix the invariant curve on the torus.
- ω; we fix the rotation number.
- $A_1^{(l_2)} = 0$; in order to solve the problem of coefficient modulation.
- e; we fix the eccentricity and leave the angular momentum, K, to be self-adjusted.

where $l_2 = 2$ for Family1 and $l_2 = 3$ for Family2.

The continuation parameter is e and we want to increase it from the value that it initially has for Torus1 and Torus2 (10^{-3} approximately) to the value $e = 0.0484$.

4.3.3.2 Results: the Bianular solution

Now, we explain the results of these continuations, showing that the goal is not achieved in Family1 but, in Family2, we succeed in finding a torus for which Jupiter's osculating

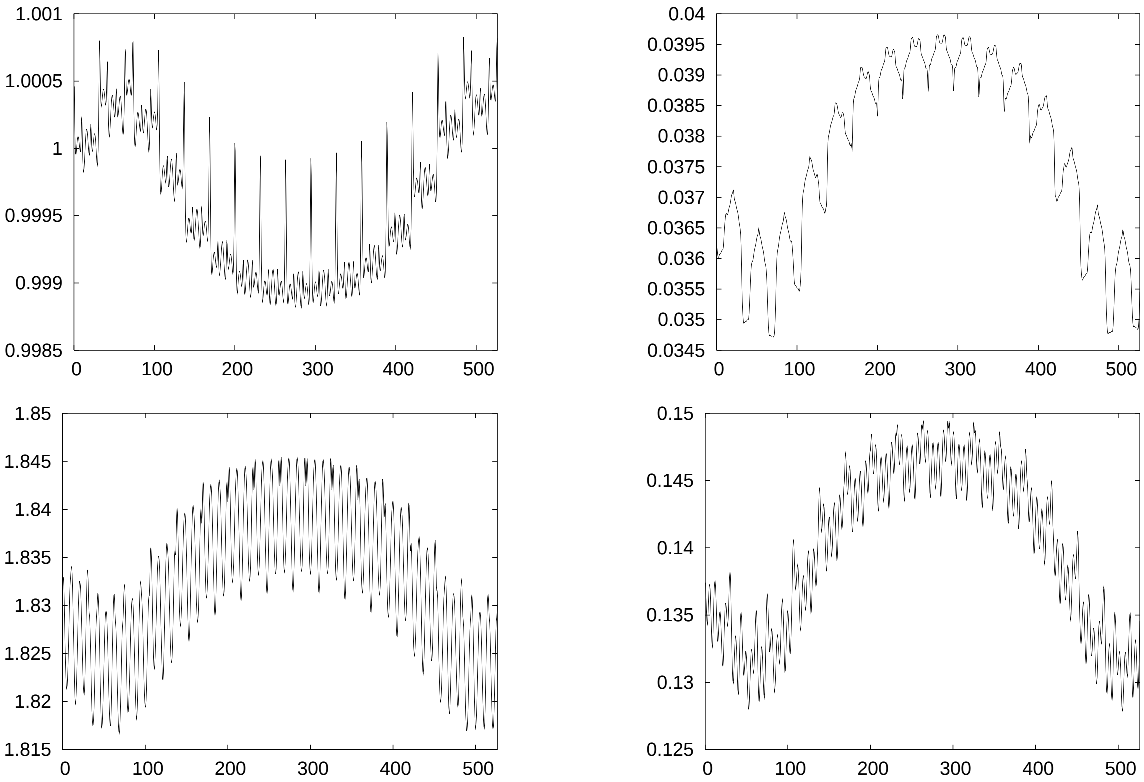

Figure 4.5: From left to right: Evolution of the osculating semi-major axis and eccentricity of Jupiter's orbit (top) and Saturn's orbit (bottom) in a time span of 50 Jupiter revolutions around the Sun, for the final torus in Family1.

eccentricity is (at a given moment) the actual one. We also have a look at some of the other orbital elements.

In Family1, we start from Torus1 increasing little by little the parameter e in order to have a good enough initial point for the Newton method in each step of the continuation process. What is observed is that, when e increases, the number of harmonics (N_f) has also to be increased if we want the discretization error of the invariant curve to be smaller than a certain tolerance (typically, we take 10^{-9}). We stop the continuation process when the number of harmonics is about 180. At this moment, the osculating eccentricity of Jupiter's orbit is approximately 0.036 and if we look at the other orbital elements of Jupiter's and Saturn's orbits, we see that they do not evolve in the desired direction, but they are getting farther from the real ones. The evolution of the eccentricity and semi-major axis of Jupiter and Saturn for this solution, during 50 Jupiter revolutions around the Sun, is shown in Figure 4.5. In Figure 4.6, the projection of this solution into the configuration space is shown. This solution is far from a planetary one because, for example, the big variation of the two semi-major axis. Thus, increasing Jupiter's eccentricity inside Family1 forces us to move away from the desired solution. In consequence, it is not possible to find an adequate torus in this family.

For Family2, we proceed in the same way as before but starting from Torus2. In this case, we are able to increase e up to the value 0.0484, because the number of harmonics

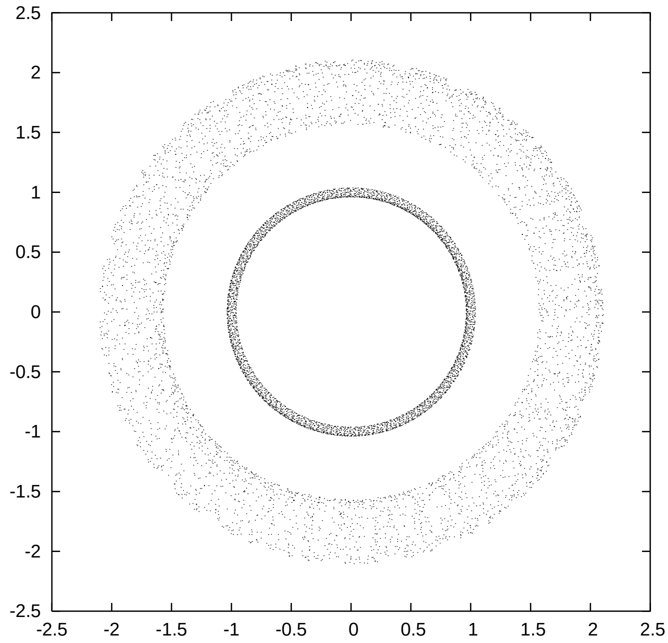

Figure 4.6: Projection into the configuration space of the torus belonging to Family1 when the continuation procedure is stopped. See the text for more details.

does not grow up very much (actually, if we ask the invariant curve to have an error smaller than 10^{-9}, N_f increases from 6 to 9) and the solution obtained is of the planetary type (see Figure 4.7). In Figure 4.8, we plot the variation of the angular momentum K of the planar SJS Three Body Problem when the parameter e is increased in the continuation process.

We can see the projection of the final torus on the rotating Jacobi configuration coordinates (q_1, q_2, q_3, q_4) in Figure 4.9. This solution of the planar Sun-Jupiter-Saturn TBP is what we call the Bianular solution of the TBP. This torus is parameterized with the angles $(\theta_1, \theta_2) = (\omega_1 t + \theta_1^0, \omega_2 t + \theta_2^0)$, where the frequencies are $\omega_1 = \omega_{sat} = 0.597039074021947$ and $\omega_2 = \frac{\omega_1 \bar{\omega}}{2\pi} = 0.194113943490717$, and $\theta_{1,2}^0$ are the initial phases.

We have also plotted the evolution of the osculating orbital elements of Jupiter and Saturn in a time span of $5T_{sat}$ adimensional units in Figure 4.10.

Let us comment this result: Recall that our main goal was to simulate in the most realistic way possible the relative Sun-Jupiter motion. We have obtained (numerically) a quasi-periodic solution of the TBP where the osculating eccentricity, the semi-major axis, the period and the mean motion of Jupiter's orbit are quite well adjusted. The argument of the perihelion still oscillates too much. We have tried to adjust it better by moving the rotation number ω, but what happens is that we loose the accuracy in the Jupiter's mean motion (it does not librate quasi-periodically around 1).

Concerning Saturn's motion on the torus, we have quite well fitted the semi-major axis and the period of its orbit; the obtained eccentricity is about the 80% of the actual one and the argument of the perihelion still oscillates too much. We have tried to adjust better the eccentricity of Saturn's orbit by changing the rotation number ω, but if we do so, we loose again accuracy on the Jupiter's mean motion.

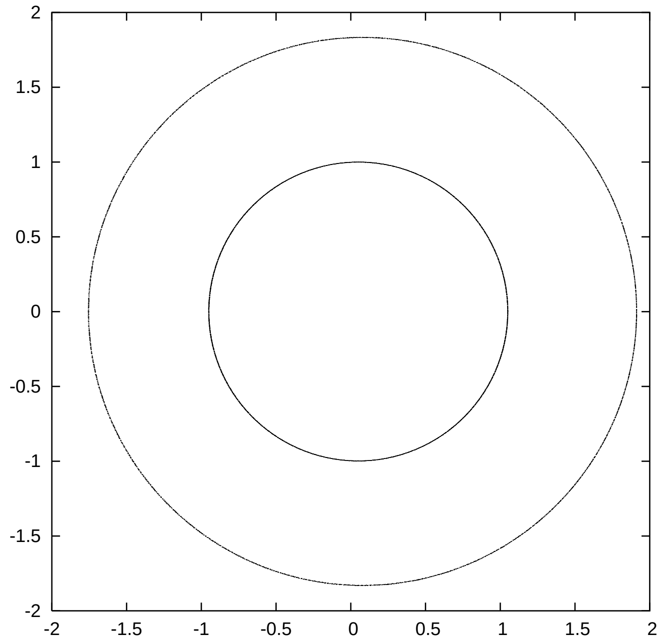

Figure 4.7: Projection into the configuration inertial space of the final torus of Family2.

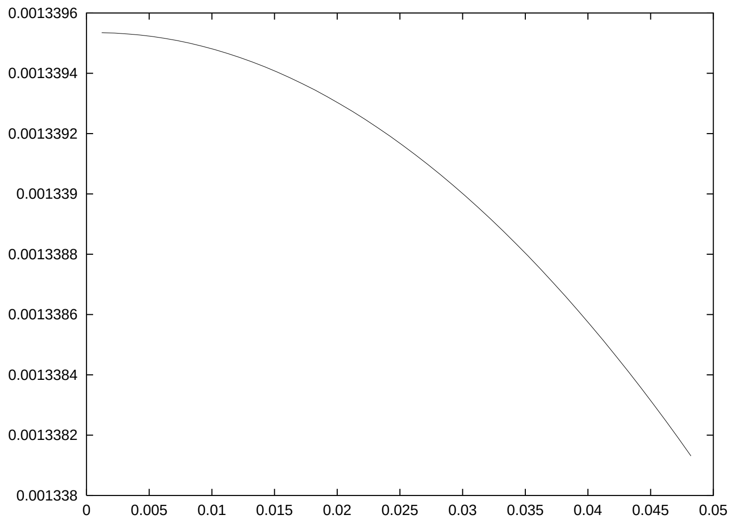

Figure 4.8: Plot of the evolution of the angular momentum K (vertical axis) when the parameter e (horizontal axis) is increased from 0.00121 (corresponding to Torus2) to 0.0484 (the desired value) in the continuation of Family2.

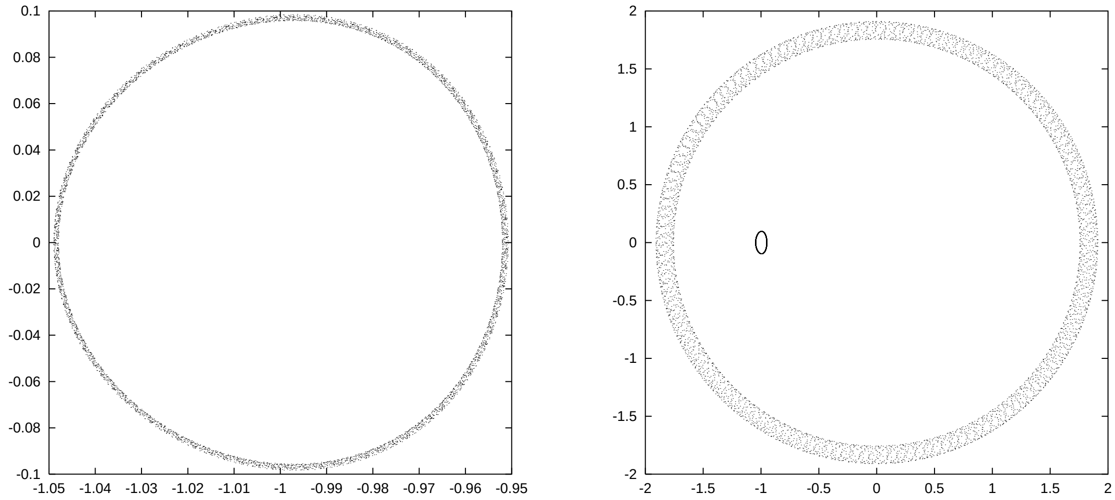

Figure 4.9: Left: (x_1, x_2)-projection of the Sun-Jupiter relative orbit on the torus. Right: Saturn's orbit around the Sun-Jupiter barycenter. Inside it, we can see the Sun-Jupiter relative orbit. This is what we call “Bianular solution” of the Sun-Jupiter-Saturn planar Three Body Problem.

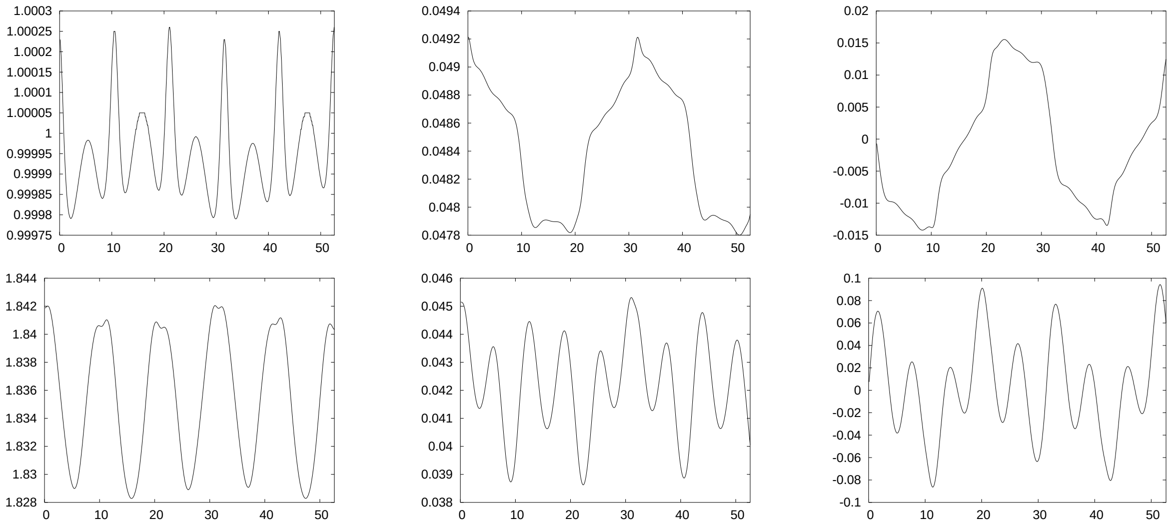

Figure 4.10: From left to right: Evolution of the osculating semi-major axis, eccentricity and argument of the perihelion of Jupiter's orbit (top) and Saturn's orbit (bottom) in a time span of 5 Jupiter revolutions around the Sun.

A possible way of overcoming these difficulties is to compute a resonant solution of the TBP (see [Had80]). In this case, the frequencies are not the actual ones but very close to them; for instance, if we consider the 5:2 resonance between the orbits of Jupiter and Saturn, we should take $\omega'_{sat} = 1 - \frac{2}{5} = 0.6$ instead of the true value $\omega_{sat} = 0.597039074$.

4.4 A quasi-periodic solution of the SJSU problem

In this section, we will explain how we compute quasi-periodic solutions with 2 frequencies of the planar four body problem SJSU (4.7). We will adapt the method described in Section 4.2 for computing invariant curves of maps to this case.

First, we will give an heuristic approximation of the initial point used in the Newton method for computing an invariant curve when $m_{ura} = 0$. Then, we compute a first torus for $m_{ura} = 0$. Finally, by means of a continuation method (taking m_{ura} as the parameter) we compute a quasi-periodic solution with 2 frequencies of the SJSU planar problem.

4.4.1 Heuristic first approximation

As a first approximation, we suppose that Uranus has mass equal to zero and that it is moving in a Keplerian orbit around the Sun. If we set that, at $t = 0$, Sun, Jupiter, Saturn and Uranus are in a particular collinear configuration (for instance, on the line $y = 0$), it is easy to obtain an approximate initial condition for Uranus in the rotating Jacobi coordinates (by imposing it to be a solution of the two body problem formed by the center of masses of the system and Uranus):

q_5	-3.6799515105016547	p_5/γ	0.0
q_6	0.0	p_6/γ	-0.521289469537814

On the other hand, we take the periodic orbit solution of the planar Sun-Jupiter-Saturn TBP computed in 2.1.1 (that has been used in 4.3.1.1 as the initial approximation for the Bianular solution). The period of this orbit, that is very close to a Bicircular one, is $T = T_{sat} = \frac{2\pi}{\omega_{sat}}$, where $\omega_{sat} = 0.597039074021947$ is the relative frequency of Saturn in the Sun-Jupiter rotating system. As in 4.3.1.1, we take the coordinates of the point of this orbit for which the three bodies are in the chosen collinear configuration:

q_1	-0.999499455382433	p_1/α	0.0
q_2	0.0	p_2/α	-1.00062422459750
q_3	-1.83433334636804	p_3/β	0.0
q_4	0.0	p_4/β	-0.738094038829119

If we integrate the flow corresponding to Hamiltonian (4.3), with $N = 3$, in the time interval $t \in [0, T_{sat}]$ taking as initial condition the point of the periodic orbit for the Sun-Jupiter-Saturn system and the Keplerian approximation for Uranus, we find that the orbit corresponding to Sun, Jupiter and Saturn obviously closes (it is a periodic orbit of period T_{sat}) and the one corresponding to Uranus does not close and turns one lap-odd (see Figure 4.11).

We are interested in measuring the angle that Uranus covers in its trajectory (actually, the angle between the two straight lines in Figure 4.11). We relate this angle with the

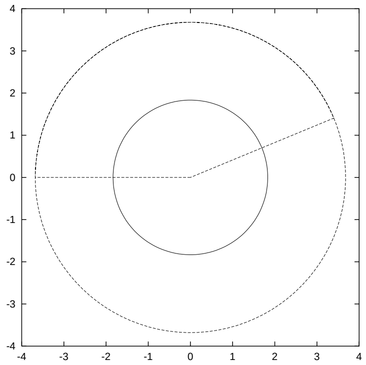

Figure 4.11: Heuristic first approximation of Uranus motion (exterior orbit) around the Sun. The inside orbit corresponds to a periodic orbit of Saturn. The straight lines show the starting and final points of Uranus orbit for an interval of time of T_{sat}.

rotation number of the invariant curve that we are looking for. It is possible, from the initial an final points of the integration, to compute the value of the angle: $\omega_0 = 2.749448441$.

Let us note that this angle is very close to the following number:

$$\tilde{\omega} = \frac{2\pi\omega_{ura}}{\omega_{sat}} \mod 2\pi = 2.750807556, \tag{4.13}$$

where $\omega_{ura} = 0.858425538978989$ is the relative frequency of Uranus in the Sun-Jupiter rotating system.

Thus, note that, if we keep constant (during the computations) the value T_{sat} and if we impose $\tilde{\omega}$ to be the rotation number of the invariant curve, the two frequencies of the 2-D invariant torus that we are computing will be ω_{sat} (Saturn's frequency) and ω_{ura} (Uranus's frequency).

4.4.2 A torus in the SJSU system with a massless Uranus

Now, using the method described in Section 4.2, we compute a 2-D invariant torus for the reduced planar SJSU problem (4.7) in the case that $m_{ura} = 0$.

4.4.2.1 Solving the invariant curve equations

As usual, in order to solve equations (4.11), we use a Newton method with a QR routine for the linear systems. As in the SJS case the system is degenerated. Thus, we fix some of the unknowns. In this case, the fixed unknowns are:

- $T = T_{sat}$ (Saturn's frequency).
- $\omega = \tilde{\omega}$ (the rotation number; which implies Uranus's frequency to be fixed).
- $A_0^{(3)} = 0$ (to set the invariant curve on the torus)[3].

[3] The upper-index indicates the component of the vector $A_k \in \mathbb{R}^{10}$

- $A_1^{(5)} = 0$ (to avoid coefficient modulation (in the sense of [GM01])).

4.4.2.2 First approximation

As initial approximation of the Newton method for solving the invariant curve equations (4.11) in the case $m_{ura} = 0$, we use the heuristic orbit that we have described in 4.4.1.

It is possible to write the initial point of that orbit in the reduced coordinates of the 3-Planetary problem (4.7) as:

x_1	0.999499455382433	x_6	0.0
x_2	-1.83433334636804	x_7	0.0
x_3	0.0	x_8	0.7380940388291189
x_4	-3.679951510501655	x_9	0.0
x_5	0.0	x_{10}	0.5212894695378142

If we denote this point as X_0 ($X_0 = (x_1, \ldots, x_{10})$), we have already shown in 4.4.1 (and can be graphically seen in Figure 4.11) that the following equation "almost" holds:

$$\Phi_T(X_0) = \begin{pmatrix} x_1 \\ x_2 \\ x_3 \\ \cos(\omega_0)x_4 - \sin(\omega_0)x_5 \\ \sin(\omega_0)x_4 + \cos(\omega_0)x_5 \\ x_6 \\ x_7 \\ x_8 \\ \cos(\omega_0)x_9 - \sin(\omega_0)x_{10} \\ \sin(\omega_0)x_9 + \cos(\omega_0)x_{10} \end{pmatrix}.$$

Thus, taking as initial approximation of the invariant curve for the first step in the Newton process the following values:

$$A_0 = \begin{pmatrix} x_1 \\ x_2 \\ x_3 \\ 0 \\ 0 \\ x_6 \\ x_7 \\ x_8 \\ 0 \\ 0 \end{pmatrix}, \quad A_1 = \begin{pmatrix} 0 \\ 0 \\ 0 \\ x_4 \\ x_5 \\ 0 \\ 0 \\ 0 \\ x_9 \\ x_{10} \end{pmatrix}, \quad B_1 = \begin{pmatrix} 0 \\ 0 \\ 0 \\ -x_5 \\ x_4 \\ 0 \\ 0 \\ 0 \\ -x_{10} \\ x_9 \end{pmatrix},$$

$A_k = B_k = 0$, $k \geq 2$, and $\omega = \tilde{\omega}$, we obtain an invariant curve of the map time T_{sat}-flow of the vector field (4.7) with $m_{ura} = 0$. For construction, the two frequencies of this quasi-periodic orbit are $\omega_1 = \omega_{sat}$ and $\omega_2 = \omega_{ura}$.

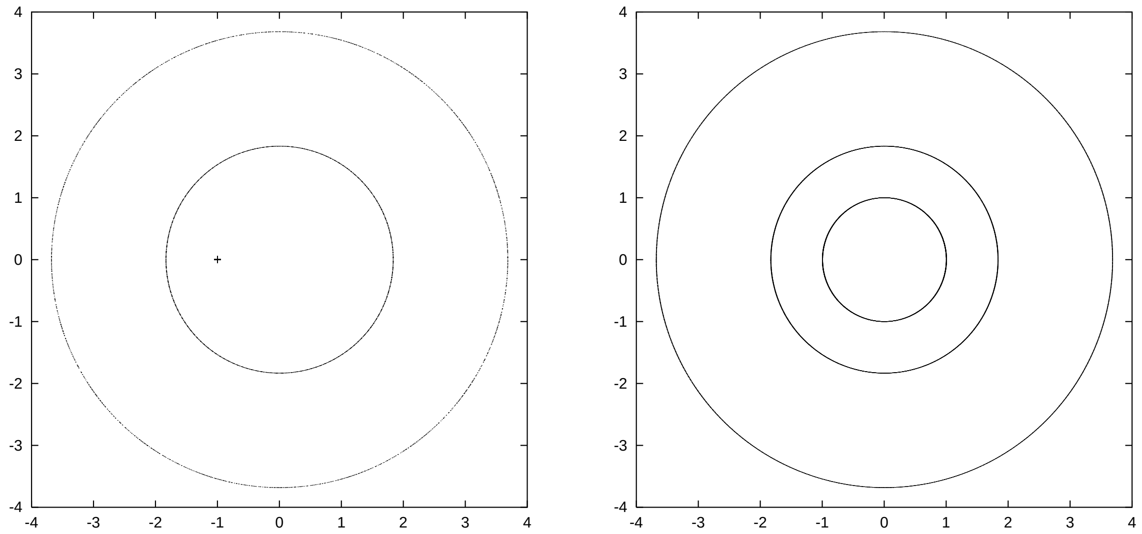

Figure 4.12: Quasi-periodic solution for the Four Body Sun-Jupiter-Saturn-Uranus Problem. The exterior orbit corresponds to Uranus, the one in the middle to Saturn and the interior one (seen as a small point that librates around the point $(-1, 0)$, in the left plot) is the relative Sun-Jupiter's orbit. The left plot corresponds to the rotating coordinates and the right one is represented in an inertial reference frame.

4.4.3 The Tricircular solution of the SJSU problem

Once we have computed an invariant torus for the case $m_{ura} = 0$, we proceed by a continuation method to increase the parameter m_{ura} up to its actual value. During the continuation, the two frequencies, $\omega_1 = \omega_{sat}$ and $\omega_2 = \omega_{ura}$ are kept constant. Thus, we obtain a quasi-periodic solution (that moves on a 2-D torus parameterized by the two angles $\theta_1 = \omega_1 t + \theta_1^0$ and $\theta_2 = \omega_2 t + \theta_2^0$) of the reduced four body field (4.7).

We want to display this torus in the non-reduced coordinates. To invert the reduction change, similarly as what happened in 4.3.2.1, we need to impose one external condition, because, when we do the direct change, the value of the angle between the P_0P_1 direction and the "old" x-axis is loosed. The condition imposed is the following one: the "new" x-axis is such that at $t = 0$ the bodies Sun, Jupiter and Saturn are in a particular collinear configuration (actually, on the line $y = 0$).

In Figure 4.12, we have plotted the projection into the configuration space of this torus in a rotating (left plot) and in an inertial (right plot) frame. As you can see, the shape of this plot is very close to three circles. This is the reason for calling this solution Tricircular solution of the SJSU four body problem.

4.5 The Hamiltonians of the BAP and TCCP models

In this section, we generalize the procedure used in 2.1.2 and 3.1 for constructing the BCCP and ESRTBP models from two particular solutions of the three and two body problems, respectively.

Thus, we construct the Hamiltonian of a massless particle that moves under the attraction of the main N+1 bodies in any solution of the N-planetary problem (4.1) and we write it as a perturbation of the RTBP, with P_0 and P_1 as primaries.

Afterwards, we compute the coefficients of the quasi-periodic functions appearing in the Hamiltonian for the Bianular and Tricircular solutions of the two and three planetary problems.

4.5.1 Hamiltonian of the Restricted N+2 Body Problem

Let us suppose that we know a solution of the planar N-planetary problem (4.1), and let be $(\vec{q}_1, \ldots, \vec{q}_N, \vec{p}_1, \ldots, \vec{p}_N)$ its representation in an inertial three dimensional reference frame (where the vertical components of $\vec{q}_i$ and $\vec{p}_i$ have been set to zero). Let also be $\vec{q}_{part}$ the position vector of the particle in the same inertial reference frame.

We are going to use the change of variables obtained from the composition of the following three transformations.

a) Translation of the origin from the global barycentre to the P_0-P_1 barycentre.

b) Rotation to fix P_0 and P_1 on the x-axis.

c) Scaling to force the distance between P_0 and P_1 to be one.

In this "rotating-pulsating" reference frame, the main bodies and the particle have the coordinates:

$$\begin{aligned}
P_0 &: \vec{Q}_0 = (\delta_1, 0, 0)^t \\
P_1 &: \vec{Q}_1 = (\delta_1 - 1, 0, 0)^t \\
P_k &: \vec{Q}_k = \frac{1}{||\vec{q}_1||} C^t (\vec{q}_k + \sum_{i=2}^{k-1} \delta_i \vec{q}_i) \qquad k = 2, \ldots, N \\
part &: \vec{r} = \frac{1}{||\vec{q}_1||} C^t (\vec{q}_{part} + \sum_{i=2}^{N} \delta_i \vec{q}_i)
\end{aligned}$$

where $\delta_i = \frac{m_i}{\eta_i}$ (recall that $\eta_i = \sum_{j=0}^{i} m_j$). The matrix C is defined as

$$C = \begin{pmatrix} -\frac{q_1^{(x)}}{||\vec{q}_1||} & \frac{q_1^{(y)}}{||\vec{q}_1||} & 0 \\ -\frac{q_1^{(y)}}{||\vec{q}_1||} & -\frac{q_1^{(x)}}{||\vec{q}_1||} & 0 \\ 0 & 0 & 1 \end{pmatrix}$$

where $\vec{q}_i = (q_i^{(x)}, q_i^{(y)}, 0)_{i=1,\ldots,N}$ is the solution of the N-planetary problem embedded in the three dimensional space. The inverse change is given by

$$\vec{q}_{part} = B\vec{r} - \sum_{i=2}^{N} \delta_i \vec{q}_i,$$

where $B = ||\vec{q}_1||C$. Defining the conjugate momentum as

$$\vec{p} = ||\vec{q}_1||^2 \dot{\vec{r}} + B^t \dot{B} \vec{r},$$

the equations for the particle become Hamiltonian, and the Hamiltonian is:

$$H = \frac{1}{2||\vec{q}_1||^2}\langle \vec{p}, \vec{p}\rangle - \frac{1}{||\vec{q}_1||^2}\vec{p}B^t\dot{B}\vec{r} - \sum_{i=2}^{N}\delta_i\,\ddot{\vec{q}}_i^{\,t}B\vec{r} + U,$$

where U, the potential energy, is given by

$$U = -\sum_{i=0}^{N} G\frac{m_i}{||\vec{q}_1||}\frac{1}{||\vec{Q}_i - \vec{r}||}.$$

To write the Hamiltonian in a more suitable way, we look at the vectors $\vec{q}_i$ as if they were in the complex plane

$$z_i \;=\; q_i^{(x)} + iq_1^{(y)},$$

for $i = 1, \ldots, N$ and we define the functions:

$$\begin{aligned}
\alpha_1 &= \frac{1}{||\vec{q}_1||^2}, & \alpha_2 &= \frac{-\mathrm{Re}\,(\dot{z}_1\bar{z}_1)}{||\vec{q}_1||^2},\\
\alpha_3 &= \frac{\mathrm{Im}\,(\dot{z}_1\bar{z}_1)}{||\vec{q}_1||^2}, & \alpha_4 &= \sum_{i=2}^{N}\delta_i\mathrm{Re}\,(\ddot{z}_i\bar{z}_1),\\
\alpha_5 &= \sum_{i=2}^{N}\delta_i\mathrm{Im}\,(\ddot{z}_i\bar{z}_1), & \alpha_6 &= \frac{1}{||\vec{q}_1||},\\
\alpha_{3+2k} &= \frac{-1}{||\vec{q}_1||^2}\mathrm{Re}\,(z_k\bar{z}_1 + \sum_{i=2}^{k-1}\delta_i z_i\bar{z}_1), & \alpha_{4+2k} &= \frac{-1}{||\vec{q}_1||^2}\mathrm{Im}\,(z_k\bar{z}_1 + \sum_{i=2}^{k-1}\delta_i z_i\bar{z}_1),
\end{aligned}$$

where $k = 2, \ldots, N$.

Note that these functions will be of the same type as the solution $(\vec{q}_i)_{i=1\div N}$ of the N-planetary problem. For instance, if we have a quasi-periodic solution with $m \geq N-1$ frequencies $\varpi = (\omega_1, \ldots, \omega_m)$, the α_i functions will also be quasi-periodic with the same m frequencies: $\alpha_i = \alpha_i(\theta)$ where $\theta = (\theta_1, \ldots, \theta_m)$, $\theta_j = \omega_j t + \theta_j^{(0)}$ and $\theta_j^{(0)}$ are the initial phases, for $j = 1, \ldots, m$ and $i = 1, \ldots, 2N+4$.

It is then possible to write the Hamiltonian of the restricted problem of $(N+2)$ bodies as:

$$\begin{aligned}
H \;=\;& \langle \varpi, p_\theta\rangle + \frac{1}{2}\alpha_1(\theta)(p_x^2 + p_y^2 + p_z^2) + \alpha_2(\theta)(xp_x + yp_y + zp_z)\\
&+\alpha_3(\theta)(yp_x - xp_y) + \alpha_4(\theta)x + \alpha_5(\theta)y - \alpha_6(\theta)\sum_{i=0}^{N} G\frac{m_i}{\rho_i},
\end{aligned}\qquad (4.14)$$

where $\rho_0^2 = (x-\delta_1)^2 + y^2 + z^2$, $\rho_1^2 = (x - \delta_1 + 1)^2 + y^2 + z^2$, $\rho_k^2 = (x - \alpha_{3+2k}(\theta))^2 + (y - \alpha_{4+2k}(\theta))^2 + z^2$ for $k = 2, \ldots, N$, and $p_\theta = (p_{\theta_1}, \ldots, p_{\theta_m})$ are the conjugate momenta of $\theta = (\theta_1, \ldots, \theta_m)$.

4.5.2 The Bianular Problem

Let

$$\varphi(\theta) = A_0 + \sum_{j=1}^{N_f} (A_j \cos j\theta + B_j \sin j\theta)$$

be a parameterization of the approximately invariant curve computed in Section 4.3. That is, $\varphi(\theta)$ is such that

$$\Phi_{T_{sat}}(\varphi(\theta)) = \varphi(\theta + \omega),$$

where $T_{sat} = \frac{2\pi}{\omega_{sat}}$ and ω is the rotation number of the invariant curve.

A parameterization of this 2-D torus, for the reduced three body vector field (4.6), can be computed from the following relation:

$$X(\theta_1, \theta_2) = \Phi_{\frac{\theta_1}{\omega_1}} \left(\varphi \left(\theta_2 - \frac{\omega\theta_1}{2\pi} \right) \right), \tag{4.15}$$

where $\omega_1 = \omega_{sat}$. It is very easy to check that $X(\theta_1, \theta_2)$ is 2π-periodic in each of its arguments:

$$X(\theta_1 + 2\pi, \theta_2 + 2\pi) = \Phi_{\frac{\theta_1+2\pi}{\omega_1}} \left(\varphi \left(\theta_2 + 2\pi - \frac{\omega\theta_1}{2\pi} - \omega \right) \right) =$$

$$= \Phi_{\frac{\theta_1}{\omega_1}} \left(\Phi_{T_{sat}} \left(\varphi \left(\theta_2 - \frac{\omega\theta_1}{2\pi} - \omega \right) \right) \right) = \Phi_{\frac{\theta_1}{\omega_1}} \left(\varphi \left(\theta_2 - \frac{\omega\theta_1}{2\pi} \right) \right) = X(\theta_1, \theta_2).$$

On the other hand, it is a straightforward computation to write the α_i functions of the Hamiltonian (4.14) for the 2-Planetary case in terms of the coordinates of the reduced three body vector field (4.6):

$$\begin{aligned}
\alpha_1 &= \frac{1}{x_1^2}, \quad \alpha_2 = -\frac{x_4}{x_1}, \quad \alpha_3 = \frac{A}{\alpha x_1^2}, \\
\alpha_4 &= m_{sat} x_1 \left[(1-\mu) \frac{x_2 - \mu x_1}{r_{13}^3} + \mu \frac{x_2 + (1-\mu) x_1}{r_{23}^3} \right], \\
\alpha_5 &= -m_{sat} x_1 x_3 \left[\frac{(1-\mu)}{r_{13}^3} + \frac{\mu}{r_{23}^3} \right], \\
\alpha_6 &= \frac{1}{x_1}, \quad \alpha_7 = \frac{x_2}{x_1}, \qquad \alpha_8 = -\frac{x_3}{x_1},
\end{aligned}$$

where, as usual, $\alpha = \mu(1-\mu)$, $\beta = m_{sat}/(1+m_{sat})$, $A = \beta(x_2 x_6 - x_3 x_5) + K$, $r_{13}^2 = (x_2 - \mu x_1)^2 + x_3^2$ and $r_{23}^2 = (x_2 + (1-\mu)x_1)^2 + x_3^2$ and K is the angular momentum of the system.

From an equally spaced tabulation of the 2-D torus (4.15) in the net

$$(\theta_1^{j_1}, \theta_2^{j_2})_{j_1, j_2 = 1 \div N_t} = \left(\frac{2\pi j_1}{N_t}, \frac{2\pi j_2}{N_t}\right),$$

it is directly obtained a tabulation of the $(\alpha_i)_{i=1\div 8}$ functions. Then, it is very easy, from this tabulation, to obtain the real Fourier coefficients of the 2-D series for the $(\alpha_i)_{i=1\div 8}$ functions.

For instance, let be the following generic quasi-periodic function with two frequencies:

$$f(\theta) = \sum_{k\in\mathbb{Z}^2} f_k e^{i\langle k,\theta\rangle},$$

where $\theta = (\theta_1, \theta_2)$ and $k = (k_1, k_2)$. If $f(\theta) \in \mathbb{R}$, it is possible to write its real Fourier expansion as:

$$f(\theta) = A_{00} + \sum_{\substack{k_1,k_2\geq 0\\ k_1+k_2>0}} \left(A_k \cos\langle k,\theta\rangle + B_k \sin\langle k,\theta\rangle\right) + \sum_{k_1,k_2\geq 1} \left(C_k \cos[k,\theta] + D_k \sin[k,\theta]\right),$$

where $\langle k,\theta\rangle = k_1\theta_1 + k_2\theta_2$ and $[k,\theta] = k_1\theta_1 - k_2\theta_2$. The Fourier coefficients are given by the following formulae:

$$A_{00} = \frac{1}{(2\pi)^2}\int_{\mathbb{T}^2} f(\theta)\, d\theta,$$

$$A_k = \frac{2}{(2\pi)^2}\int_{\mathbb{T}^2} f(\theta)\cos\langle k,\theta\rangle\; d\theta, \qquad B_k = \frac{2}{(2\pi)^2}\int_{\mathbb{T}^2} f(\theta)\sin\langle k,\theta\rangle\; d\theta,$$

$$C_k = \frac{2}{(2\pi)^2}\int_{\mathbb{T}^2} f(\theta)\cos[k,\theta]\; d\theta, \qquad D_k = \frac{2}{(2\pi)^2}\int_{\mathbb{T}^2} f(\theta)\sin[k,\theta]\; d\theta.$$

Thus, from this real Fourier expansion of a generic quasi-periodic function and due to the parity properties of the α_i functions, they can be written as:

$$\begin{aligned}
\alpha_i(\theta_1,\theta_2) &= \sum_{k\geq(0,0)} \alpha^+_{ik}\cos\langle k,\theta\rangle + \sum_{k\geq(1,1)} \alpha^-_{ik}\cos[k,\theta], \qquad i = 1,3,4,6,7\\
\alpha_i(\theta_1,\theta_2) &= \sum_{k>(0,0)} \alpha^+_{ik}\sin\langle k,\theta\rangle + \sum_{k\geq(1,1)} \alpha^-_{ik}\sin[k,\theta], \qquad i = 2,5,8
\end{aligned}$$

where, the angles $\theta_1(t)$ and $\theta_2(t)$ depend on the adimensional time as:

$$\begin{aligned}
\theta_1(t) &= \omega_1 t + \theta_1^{(0)},\\
\theta_2(t) &= \omega_2 t + \theta_2^{(0)},
\end{aligned}$$

and both phases ($\theta_1^{(0)}$ and $\theta_2^{(0)}$) are zero if we select the origin of time when Sun, Jupiter and Saturn are in a particular collinear configuration (that is, we choose $x_3 = 0$ when $t = 0$). In Figure 4.13, we plot the evolution of the $\alpha_i(t)$ functions in a time span of 3 relative periods of Saturn.

Finally, it is possible to write the Hamiltonian of the Bianular problem as:

$$\begin{aligned}
H_{BAP} &= \frac{1}{2}\alpha_1(t)(p_x^2 + p_y^2 + p_z^2) + \alpha_2(t)(xp_x + yp_y + zp_z) + \alpha_3(t)(yp_x - xp_y)\\
&\quad + \alpha_4(t)x + \alpha_5(t)y - \alpha_6(t)\left[\frac{1-\mu}{q_S} + \frac{\mu}{q_J} + \frac{m_{sat}}{q_{sat}}\right],
\end{aligned} \tag{4.16}$$

where $q_S^2 = (x-\mu)^2 + y^2 + z^2$, $q_J^2 = (x-\mu+1)^2 + y^2 + z^2$ and $q_{sat}^2 = (x-\alpha_7(t))^2 + (y-\alpha_8(t))^2 + z^2$. The concrete values for the coefficients of the quasi-periodic functions $(\alpha_i)_{i=1\div 8}$, are displayed in Tables A.3, A.4, A.5 and A.6 of Appendix A.3.

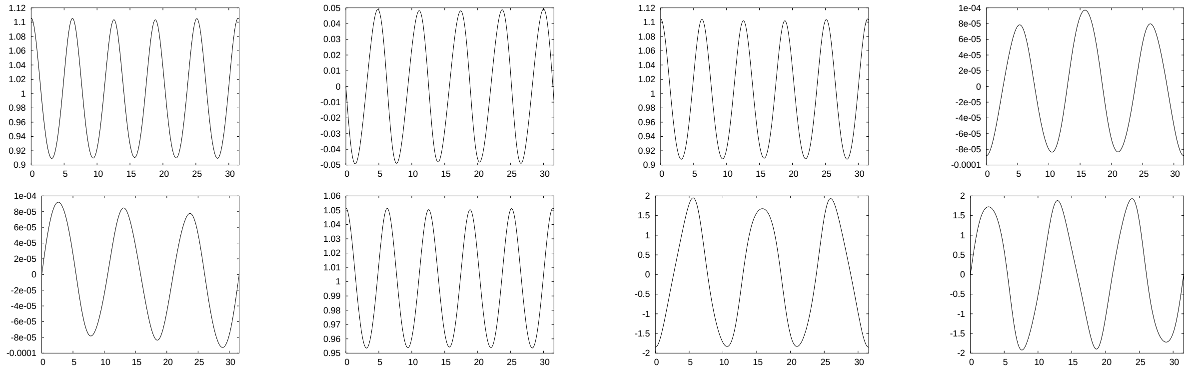

Figure 4.13: Plot of the α_i functions for the Bianular Problem. They are consecutively displayed from top-left (α_1) to bottom-right (α_8).

4.5.3 The Tricircular Coherent Problem

In the reduced SJSU four body problem (4.7), the $(\alpha_i)_{i=1\div 10}$ functions can be obtained from the following formulae:

$$\alpha_1 = \frac{1}{x_1^2}, \qquad \alpha_2 = -\frac{x_6}{x_1}, \qquad \alpha_3 = \frac{A}{\alpha x_1^2},$$

$$\begin{aligned}\alpha_4 &= m_{sat}x_1\left[(1-\mu)\frac{x_2-\mu x_1}{r_{13}^3}+\mu\frac{x_2+(1-\mu)x_1}{r_{23}^3}\right]+\\ &\quad m_{ura}x_1(1+\beta)\left((1-\mu)\frac{x_4+\beta x_2-\mu x_1}{r_{14}^3}+\mu\frac{x_4+\beta x_2+(1-\mu)x_1}{r_{24}^3}\right)+\\ &\quad m_{ura}\beta m_{sat}x_1\frac{x_4-(1-\beta)x_2}{r_{34}^3},\end{aligned}$$

$$\begin{aligned}\alpha_5 &= -m_{sat}x_1x_3\left[\frac{(1-\mu)}{r_{13}^3}+\frac{\mu}{r_{23}^3}\right]-\\ &\quad m_{ura}x_1\left[(1+\beta)(1-\mu)\frac{x_5+\beta x_3}{r_{14}^3}+(1+\beta)\mu\frac{x_5+\beta x_3}{r_{24}^3}+\beta m_{sat}\frac{x_5-(1-\beta)x_3}{r_{34}^3}\right],\end{aligned}$$

$$\alpha_6 = \frac{1}{x_1}, \qquad \alpha_7 = \frac{x_2}{x_1}, \qquad \alpha_8 = -\frac{x_3}{x_1},$$

$$\alpha_9 = \frac{x_4+\beta x_2}{x_1}, \quad \alpha_{10} = -\frac{x_5+\beta x_3}{x_1},$$

where, as usual, $\alpha = \mu(1-\mu)$, $\beta = m_{sat}/(1+m_{sat})$, $\gamma = (1+m_{sat})m_{ura}/(1+m_{sat}+m_{ura})$, $A = \beta(x_2x_6-x_3x_5)+\gamma(x_4x_{10}-x_5x_9)+K$, $r_{13}^2 = (x_2-\mu x_1)^2+x_3^2$, $r_{23}^2 = (x_2+(1-\mu)x_1)^2+x_3^2$, $r_{14}^2 = (x_5+\beta x_3)^2+(x_4+\beta x_2-\mu x_1)^2$, $r_{24}^2 = (x_5+\beta x_3)^2+(x_4+\beta x_2+(1-\mu)x_1)^2$, $r_{34}^2 = (x_5-(1-\beta)x_3)^2+(x_4-(1-\beta)x_2)^2$ and K is the angular momentum of the system.

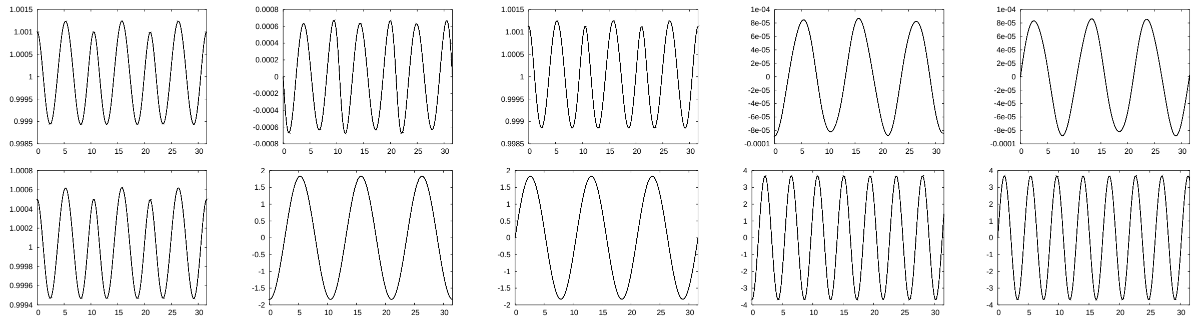

Figure 4.14: Plot of the α_i functions for the Tricircular Coherent Problem. They are consecutively displayed from top-left (α_1) to bottom-right (α_{10}).

In Figure 4.14, we have plotted the evolution of the $(\alpha_i)_{i=1\div10}$ functions during a time span of 31.57173 adimensional units.

In the same way as in the Bianular Problem, it is possible, from a numerical tabulation of these $(\alpha_i)_{i=1\div10}$ functions, to write them as real Fourier expansions in the following way:

$$\begin{aligned}
\alpha_i(\theta_1,\theta_2) &= \sum_{k\geq(0,0)} \alpha_{ik}^{+}\cos\langle k,\theta\rangle + \sum_{k\geq(1,1)} \alpha_{ik}^{-}\cos[k,\theta], \qquad i=1,3,4,6,7,9\\
\alpha_i(\theta_1,\theta_2) &= \sum_{k>(0,0)} \alpha_{ik}^{+}\sin\langle k,\theta\rangle + \sum_{k\geq(1,1)} \alpha_{ik}^{-}\sin[k,\theta], \qquad i=2,5,8,10
\end{aligned}$$

where recall that $\langle k,\theta\rangle = k_1\theta_1 + k_2\theta_2$, $[k,\theta] = k_1\theta_1 - k_2\theta_2$, $\theta_1 = \omega_{sat}t$, $\theta_2 = \omega_{ura}t$. The concrete values of the real Fourier coefficients up to order 5 are given in Tables A.7, A.8, A.9, A.10 and A.11 of Appendix A.4.

Finally, once the α_i functions are explicitly constructed, it is possible to write the Hamiltonian of the Tricircular Coherent Problem as:

$$\begin{aligned}
H_{TCCP} &= \frac{1}{2}\alpha_1(t)(p_x^2+p_y^2+p_z^2) + \alpha_2(t)(xp_x+yp_y+zp_z) + \alpha_3(t)(yp_x-xp_y)\\
&\quad +\alpha_4(t)x + \alpha_5(t)y - \alpha_6(t)\left[\frac{1-\mu}{q_S} + \frac{\mu}{q_J} + \frac{m_{sat}}{q_{sat}} + \frac{m_{ura}}{q_{ura}}\right], \qquad (4.17)
\end{aligned}$$

where $q_S^2 = (x-\mu)^2+y^2+z^2$, $q_J^2 = (x-\mu+1)^2+y^2+z^2$, $q_{sat}^2 = (x-\alpha_7(t))^2+(y-\alpha_8(t))^2+z^2$ and $q_{ura}^2 = (x-\alpha_9(t))^2+(y-\alpha_{10}(t))^2+z^2$.

4.5.4 Tests

In order to test the computations of the α_i functions of the BAP and TCCP Hamiltonians, as well as the changes of variables, we have integrated some different test particles (with initial conditions selected at random) in the fields coming from H_{BAP} and H_{TCCP}, in one hand, and the planar restricted four and five body problems, respectively, in the other. A good accuracy is obtained according to the order of truncation of the Fourier coefficients.

4.6 Semi-analytical study of the TCCP Hamiltonian

In this section, we make a local semi-analytical study of the TCCP Hamiltonian in a neighbourhood of the triangular points.

First, we focus on the construction of a suitable normal form of the TCCP Hamiltonian (4.17), up to high degree, in order to describe the non-linear dynamics around the L_4 and L_5 points. The procedure is a generalization, for two frequencies, of the computations done in Sections 2.3 and 2.4, and it is divided in the following steps: Transformation of the triangular point to a 2-D invariant torus, reduction of the linear part to constant coefficients around the triangular point, normal form of order higher than 2, and the change of variables that sends points from the initial phase space (the one in which the TCCP Hamiltonian is written) to the normal form space, and vice versa. Finally, we use this (high order) normal form of the Hamiltonian to give a description of the local non-linear dynamics around the invariant torus that replaces L_5.

Later on, we use the expanded Hamiltonian, written in normal form up to degree 2, to compute an approximate first integral of the system; which help us, on its turn, to find a region of effective stability around the invariant torus that replaces the triangular point.

4.6.1 The 2-D invariant torus that replaces L_5

In the TCCP system, the RTBP L_4 and L_5 points are replaced by quasi-periodic orbits with two internal frequencies and three normal ones. The two internal frequencies are ω_{sat} and ω_{ura}, the two proper frequencies of the TCCP system. The proof can be found in [JS96], where quasi-periodically perturbed elliptic equilibrium points are studied.

In order to compute this 2-D invariant torus (in the L_5 case, for instance), we use the method explained in Section 4.2 adapted to the non-autonomous case. Recall that the method consists in, basically, to compute an invariant curve of a map. In this case, we consider the time period-of-Saturn map associated to the flow of the TCCP (the Poincaré map obtained from a section of the first angle, $\theta_1 = 2\pi$). Note that this map can be easily evaluated by a numerical integration of the flow associated to (4.17), and its differential is also obtained integrating the variational flow.

Hence, it is possible to compute, in the Poincaré section, the invariant curve that corresponds, in the global phase space, to the 2-D invariant torus that replaces L_5 in the TCCP model. Due to the smallness of the perturbation, it is enough to use, as initial guess, the coordinates of the triangular point L_5. The (x, y) and (p_x, p_y) projections of the resulting invariant torus are shown in Figure 4.15. From now on, we will call this 2-D invariant torus T_5.

It is also possible, using the method explained in [Jor01], to compute the three normal modes of the invariant curve; that is, the frequencies of the three harmonic oscillators that govern the normal linear motion around T_5. They can be found as the solution of a generalized eigenvalue problem. In Table 4.2, the linear normal modes are shown. As all of them have modulus exactly 1, the 2-D invariant torus T_5 is linearly stable.

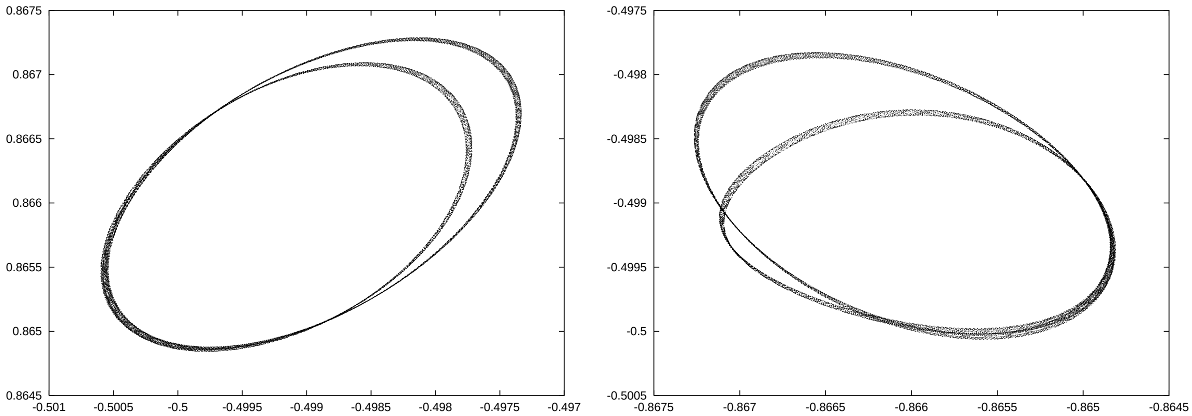

Figure 4.15: Planar projections of the 2-D invariant torus that replaces L_5: T_5. Left: (x, y)-projection. Right: (p_x, p_y)-projection.

j	$\mathrm{Re}\,(\lambda_j)$	$\pm\mathrm{Im}\,(\lambda_j)$	$\lvert\lambda_j\rvert$	$\pm\mathrm{Arg}\,(\lambda_j)$
1	0.662315481968626	0.749225067883254	1.0	0.846891268646165
2	-0.485204809265089	0.874400533546285	1.0	2.077393707458922
3	-0.453781923686027	0.891112768248671	1.0	2.041801148412721

Table 4.2: Linear normal modes around the 2-D invariant torus T_5 in the TCCP system.

4.6.2 Second order normal form

In the previous section we have derived a quasi-periodic time-dependent translation that cancels the first order terms in the Hamiltonian. Here we will derive a linear change of variables (that depends on time in a quasi-periodic way) that puts the second degree terms of the Hamiltonian into a more convenient form. This is, essentially, the quasi-periodic Floquet transformation for the variational flow along the quasi-periodic orbit, but taking into account the symplectic structure of the problem. To simplify further steps in the normalizing process, we also apply a complexifying change of variables that puts the second degree terms of the Hamiltonian in the so-called diagonal form.

4.6.2.1 The symplectic quasi-periodic Floquet change

The linear flow around the 2-D invariant torus T_5 is described by a linear system of differential equations, that depends quasi-periodically on time:

$$\begin{aligned} \dot{z} &= Q(\theta_1, \theta_2) z, \\ \dot{\theta}_1 &= \omega_{sat}, \\ \dot{\theta}_2 &= \omega_{ura}. \end{aligned} \tag{4.18}$$

Our goal is to find a real, symplectic and quasi-periodic change of variables, $z = P^r(\theta_1, \theta_2)x$, such that it reduces (4.18) to a linear system with real constant coefficients:

$$\dot{x} = Bx, \quad \frac{d}{dt}B \equiv 0. \tag{4.19}$$

First of all, we will see that such a change of variables exists in the complex domain. Then, we will build a real change from the complex one. All the process is constructive, so the implementation in a computer program will follow easily from the explanation.

We start by considering the $(\theta_1 = 2\pi)$-Poincaré section of the flow given by (4.18). Then, we have the following linear quasi-periodic skew product:

$$\begin{aligned} \bar{z} &= A(\theta)z, \\ \bar{\theta} &= \theta + \omega, \end{aligned}$$

where $\theta \equiv \theta_2$ and $\omega = 2\pi\left(\frac{\omega_{ura}}{\omega_{sat}} - 1\right) = 2.75080755611202$ is the rotation number of the invariant curve corresponding to (the slice in the Poincaré section of) the 2-D invariant torus T_5.

As it is shown in [Jor01], it is possible to reduce this quasi-periodic skew-product to

$$\bar{y} = \Lambda y, \tag{4.20}$$

by implementing a linear change of variables $z = C(\theta)y$. Λ is a diagonal complex 6×6 matrix with constant coefficients and satisfies, jointly with the matrix $C(\theta)$, the following equation:

$$A(\theta)C(\theta) = C(\theta + \omega)\Lambda. \tag{4.21}$$

If we define the operator $T_\omega : \Psi(\theta) \in \mathcal{C}(\mathbb{T}^1, \mathbb{C}^n) \to \Psi(\theta + \omega) \in \mathcal{C}(\mathbb{T}^1, \mathbb{C}^n)$ and if we call $\Psi_j(\theta)$ the j-th column of the matrix $C(\theta)$, we can write the system of equations (4.21) by columns as a generalized eigenvalue problem:

$$A(\theta)\Psi_j(\theta) = \lambda_j T_\omega \Psi(\theta). \tag{4.22}$$

Remarks:

- Note that $A(\theta)$ is a real matrix (it comes from $Q(\theta_1, \theta_2)$ that is also real). Thus, if $\Psi_j(\theta) \in \mathbb{C}^6$ is an eigenfunction of (4.22) with eigenvalue λ_j, then $\Psi_j^*(\theta)$ is also an eigenfunction of (4.22) with eigenvalue λ_j^* (λ_j^* and $\Psi_j^*(\theta)$ are the complex conjugates of λ_j and $\Psi_j(\theta)$, respectively).

  We construct the matrix $C(\theta)$ as $C(\theta) = (\Psi_1(\theta)\ \Psi_2(\theta)\ \Psi_3(\theta)\ \Psi_1^*(\theta)\ \Psi_2^*(\theta)\ \Psi_3^*(\theta))$, and, then, the matrix Λ takes the following form: $\Lambda = \mathrm{diag}(\lambda_1, \lambda_2, \lambda_3, \lambda_1^*, \lambda_2^*, \lambda_3^*)$.

- The eigenfunctions $\Psi_j(\theta)$ are scaled in such a way that $\|\Psi_j\|_2 = 1$.

Thus, it is possible to reduce equations (4.18) to complex constant coefficients in a Poincaré section of the flow (via the complex change of variables $C(\theta)$). Now, we want to extend the change of variables to the global phase space and to realify it.

Extension of the change of variables The goal is to compute a quasi-periodic change of variables $z = P^c(\theta_1, \theta_2)y$ that transforms the system (4.18) to

$$\dot{y} = D_B y, \tag{4.23}$$

where $D_B = \mathrm{diag}(i\omega_1, i\omega_2, i\omega_3, -i\omega_1, -i\omega_2, -i\omega_3)$ and ω_j is such that $\lambda_j = \exp(i\omega_j T_{sat})$, where as usual $T_{sat} = \frac{2\pi}{\omega_{sat}}$. Note that it is possible to add to ω_j any integer multiple of $\frac{2\pi}{T_{sat}}$ (if ω_j accomplishes the condition, then $\pm(\omega_j + \frac{2k_j\pi}{T_{sat}})$, $k_j \in \mathbb{Z}$, too). We have selected a special value of $k_j \in \mathbb{Z}$ for each $j = 1, 2, 3$ in order the values of ω_j to be the closest possible to the ones in the RTBP case. This is the right choice from a perturbative point of view and it is also a critical in order the change of variables to be symplectic.

Lemma 4.6.1 *The solution of the Initial Value Problem (IVP)*

$$\begin{aligned} \dot{P}^c(\theta_1, \theta_2) &= Q(\theta_1, \theta_2)P^c(\theta_1, \theta_2) - P^c(\theta_1, \theta_2)D_B \\ \dot{\theta}_1 &= \omega_{sat} \\ \dot{\theta}_2 &= \omega_{ura} \end{aligned}$$

with

$$\begin{aligned} P^c(0) &= C(\theta_2^{(0)}) \\ \theta_1(0) &= 0 \\ \theta_2(0) &= \theta_2^{(0)} \end{aligned}$$

is the linear change of variables with complex quasi-periodic coefficients that sends the system (4.18) to the system (4.23).

Proof If we insert the change $z = P^c(\theta_1, \theta_2)y$ to equation (4.18) and if we ask that (4.23) is satisfied, then P^c is such that:

$$\dot{P}^c(\theta_1, \theta_2) = Q(\theta_1, \theta_2)P^c(\theta_1, \theta_2) - P^c(\theta_1, \theta_2)D_B. \tag{4.24}$$

On the other hand, if we integrate equation (4.18) from $t = 0$ to $t = T_{sat}$ with the initial condition $\left[z(0) = \Psi_j(\theta_2^{(0)}), \theta_1(0) = 0, \theta_2(0) = \theta_2^{(0)}\right]$ (note that this is equivalent to apply $A(\theta_2^{(0)})$ to the vector $\Psi_j(\theta_2^{(0)})$), the solution (that we denote by $\bar{x}(t)$) accomplishes

$$\bar{x}(T_{sat}) = A(\theta_2^{(0)})\Psi_j(\theta_2^{(0)}) = \lambda_j \Psi_j(\theta_2^{(0)} + \omega),$$

where we have used equation (4.22).

An elementary result in the theory of ordinary differential equations states that if $\tilde{x}_1(t)$ is a solution of $\dot{x}_1 = Q(t)x_1$, then $\tilde{x}_2(t) = \exp(at)\tilde{x}_1(t)$ is a solution of $\dot{x}_1 = (Q(t) + aI)x_1$, being a any complex scalar number. Thus, $\hat{x}(t) = \exp(-i\omega_j t)\bar{x}(t)$ is a solution of [4]:

$$\dot{P}_j^c = (Q - i\omega_j I_6)P_j^c,$$

with the same initial condition ($\hat{x}(0) = \Psi_j(\theta_2^{(0)})$) and it satisfies the following relation:

$$\hat{x}(T_{sat}) = \exp(-i\omega_j T_{sat})\bar{x}(T_{sat}) = (\lambda_j)^{-1}\lambda_j\Psi_j(\theta_2^{(0)} + \omega) = \Psi_j(\theta_2^{(0)} + \omega).$$

■

[4]Note that it corresponds to the firsts three columns of equation (4.24)

Realification In order to actually implement the Floquet change, we are interested in computing the real change of variables. Thus, we will make use of the following Lemma:

Lemma 4.6.2 *Let us define the (real) matrix R by taking the real and imaginary parts of the columns of matrix C (recall that, due to the particular construction of C, its lasts three columns are the conjugate values of the firsts three ones):*

$$R(\theta) = \frac{1}{2}C(\theta)\left(\begin{array}{c|c} I_3 & -iI_3 \\ \hline I_3 & iI_3 \end{array}\right).$$

Then, the solution of the IVP

$$\begin{aligned} \dot{P}^r(\theta_1,\theta_2) &= Q(\theta_1,\theta_2)P^r(\theta_1,\theta_2) - P^r(\theta_1,\theta_2)B \qquad (4.25) \\ \dot{\theta}_1 &= \omega_{sat} \\ \dot{\theta}_2 &= \omega_{ura} \end{aligned}$$

with initial conditions

$$\begin{aligned} P^r(0) &= R(\theta_2^{(0)}) \\ \theta_1(0) &= 0 \\ \theta_2(0) &= \theta_2^{(0)} \end{aligned}$$

defines a (real) linear quasi-periodic change of variables ($z = P^r(\theta_1,\theta_2)x$) that transforms equation (4.18) to equation (4.19).

The (real) matrix B is defined by $B = R^{-1}CD_BC^{-1}R$ and takes the form

$$B = \left(\begin{array}{ccc|ccc} 0 & 0 & 0 & \omega_1 & 0 & 0 \\ 0 & 0 & 0 & 0 & \omega_2 & 0 \\ 0 & 0 & 0 & 0 & 0 & \omega_3 \\ \hline -\omega_1 & 0 & 0 & 0 & 0 & 0 \\ 0 & -\omega_2 & 0 & 0 & 0 & 0 \\ 0 & 0 & -\omega_3 & 0 & 0 & 0 \end{array}\right).$$

Proof Let us define the matrix P^r in the following manner:

$$P^r(\theta_1,\theta_2) = P^c(\theta_1,\theta_2)C^{-1}(\theta_1,\theta_2)R(\theta_1,\theta_2), \qquad (4.26)$$

where $R(\theta_1,\theta_2)$ and $C(\theta_1,\theta_2)$ are, respectively, the extensions of the matrices $R(\theta)$ and $C(\theta)$.

Then, we have:

- $P^r(0)$ is a real matrix: $P^r(0) = P^c(0)C^{-1}(\theta_2^{(0)})R(\theta_2^{(0)}) = C(\theta_2^{(0)})C^{-1}(\theta_2^{(0)})R(\theta_2^{(0)}) = R(\theta_2^{(0)})$.

- If we integrate $\dot{P}^r = QP^r - P^rB$ with $P^r(0) = R(\theta_2^{(0)})$ as i.c., then $P^r(\theta_1,\theta_2)$ is real $\forall(\theta_1,\theta_2) \in \mathbb{T}^2$.

- If we insert the relation (4.26) into the differential equation (4.25), we obtain

$$\dot{P^c}C^{-1}R + P^c(\dot{C^{-1}})R + P^cC^{-1}\dot{R} = QP^cC^{-1}R - P^cC^{-1}RB.$$

By multiplying this equation (in the right hand side) by the matrix $R^{-1}C$, we get

$$\dot{P^c} + P(\dot{C^{-1}})C + P^cC^{-1}\dot{R}R^{-1}C = QP^c - P^cD_B.$$

This equation holds (it corresponds to (4.24)) provided that

$$P^c(\dot{C^{-1}})C + P^cC^{-1}\dot{R}R^{-1}C = 0.$$

It is easy to see, by using the definition of R, that this equality is true:

$$\begin{aligned} P^c(\dot{C^{-1}})C + P^cC^{-1}\dot{R}R^{-1}C &= 0 \iff \\ (\dot{C^{-1}})R + C^{-1}\dot{R} &= 0 \iff \\ \frac{d}{dt}(C^{-1}R) &= 0 \end{aligned}$$

■

Finally, to ensure that the transformation is canonical, we only need to check that $P^r(\theta_1, \theta_2)$ is a symplectic matrix. This can be proved analytically (analogously at how it is done in [GJMS93]) by extending the matrix P^r to the phase space where it lives the autonomous Hamiltonian

$$H(x, y, z, \theta_1, \theta_2, p_x, p_y, p_z, p_{\theta_1}, p_{\theta_2}) = \omega_{sat}p_{\theta_1} + \omega_{ura}p_{\theta_2} + H_{TCCP}(x, y, z, \theta_1, \theta_2, p_x, p_y, p_z),$$

where H_{TCCP} is (4.17)) but here, to also check the correctness of the software, we have tested numerically this condition for a mesh of values of (θ_1, θ_2), with good agreement.

Implementing this quasi-periodic change of variables, the second degree terms of the Hamiltonian become:

$$H_2^r(x, y) = \frac{1}{2}\omega_1(x_1^2 + y_1^2) + \frac{1}{2}\omega_2(x_2^2 + y_2^2) + \frac{1}{2}\omega_3(x_3^2 + y_3^2), \tag{4.27}$$

where the frequencies take the following values: $\omega_1 = -0.080473064872369$, $\omega_2 = 0.996680625156409$ and $\omega_3 = 1.00006269133083$. In the same way as in the periodic case, we cannot use the Lagrange-Dirichlet theorem to derive the nonlinear stability of the 2-D invariant torus, due to the different signs for the values of the frequencies.

4.6.2.2 Complexification

As it is usual in these kind of computations, a complexifying change of variables is done in order to bring (4.27) into a diagonal form. The equations of this linear and symplectic transformation have already been given in equation (2.5).

Thus, after composing the three linear symplectic changes of variables (translation of the origin to the 2-D invariant torus, quasi-periodic symplectic transformation and complexification), the Hamiltonian of the TCCP in normal form up to order 2 takes the form:

$$H_2^c(q, p) = i\omega_1 q_1 p_1 + i\omega_2 q_2 p_2 + i\omega_3 q_3 p_3, \quad (q, p) \in \mathbb{C}^6. \tag{4.28}$$

4.6.3 Expansion of the Hamiltonian

Similarly to the periodic case (see Section 2.3.3), we need to produce a Fourier-Taylor power expansion of the Hamiltonian (4.17), in the complex coordinates described before,

$$H = \sum_{n=2}^{N} H_n(q,p,\theta) + R_{N+1}(q,p,\theta),$$

where H_n, $n \geq 2$, denotes an homogeneous polynomial of degree n in the variables q and p, $H_2 \neq H_2(\theta)$ is (4.28) and $\theta = (\theta_1, \theta_2) \in \mathbb{T}^2$.

In fact, if we are able to expand the terms of the TCCP Hamiltonian (4.17) that look like

$$\frac{1}{s_l} = \frac{1}{\sqrt{(x - x_l(\theta))^2 + (y - y_l(\theta))^2 + z^2}}, \tag{4.29}$$

where l stands for S (the Sun), J (Jupiter), sat (Saturn) or ura (Uranus), we are done.

It is possible to write them as the following power expansion

$$\frac{1}{s_l} = \sum_{n\geq 0} A_n^l(x,y,z,\theta),$$

where A_n^l denotes an homogeneous polynomial of degree n, whose coefficients are quasi-periodic functions of $\theta = (\theta_1, \theta_2) \in \mathbb{T}^2$, and can be recurrently computed using

$$A_{n+1}^l = \frac{1}{x_l^2(\theta) + y_l^2(\theta)} \left[\frac{2n+1}{n+1} (x_l(\theta)x + y_l(\theta)y) A_n^l - \frac{n}{n+1} (x^2 + y^2 + z^2) A_{n-1}^l \right],$$

for $n \geq 1$. The recurrence can be started using the values

$$A_0^l = \frac{1}{\sqrt{x_l^2(\theta) + y_l^2(\theta)}}, \qquad A_1^l = \frac{x_l(\theta)x + y_l(\theta)y}{(x_l^2(\theta) + y_l^2(\theta))^{3/2}},$$

and can be derived easily from the recurrence of the Legendre polynomials.

The practical implementation of the process to obtain the desired final expansion consists in, firstly, perform the quasi-periodic translation that fixes the 2-D invariant torus T_5 at the origin. Secondly (if we call again to the new coordinates x, y, and z), we substitute the values of the variables x, y and z in the A_n^l, $n \geq 0$, by their expressions in terms of the variables q and p used in (4.28). Finally, we apply the recurrence in order to expand the terms A_n^l up to a given degree $n = N$.

On the other hand, it is also convenient to autonomize the complete Hamiltonian by adding the fictitious momenta corresponding to the angular variables. Let us denote them $p_\theta = (p_{\theta_1}, p_{\theta_2}) \in \mathbb{C}^2$. In this way, it is possible to write the expanded Hamiltonian (in complex variables) as:

$$H(q,p,\theta,p_\theta) = \langle \varpi, p_\theta \rangle + H_2(q,p) + \sum_{n\geq 3} H_n(q,p,\theta), \quad (q,p) \in \mathbb{C}^6 \, , \; \theta \in \mathbb{T}^2, \tag{4.30}$$

where H_2 is given by (4.28), $\varpi = (\omega_{sat}, \omega_{ura})$ and $\langle \cdot, \cdot \rangle$ is the standard scalar product.

4.6.4 Normal form of order higher than 2

Here, we proceed, in the same way as we did for the BCCP Hamiltonian in 2.4.1, to compute a high order normal form for the expansion of the TCCP Hamiltonian, supposing that up to degree 2 is already in the normal form (4.28).

The goal of the normalizing transformation is to autonomize and to suppress the maximum number of terms of the Hamiltonian expansion. We use, basically, the Lie series method as described in [Jor99], but introducing the necessary modifications in order to deal with quasi-periodic coefficients.

For completeness, we rewrite how one step of the normalizing process works: Let us suppose that the Hamiltonian is already in normal form up to degree $r-1$:

$$H = \langle \varpi, p_\theta \rangle + H_2(q,p) + \sum_{j=3}^{r-1} H_j(q,p) + H_r(q,p,\theta) + H_{r+1}(q,p,\theta) + \cdots$$

where $H_r(q,p,\theta) = \sum_{|k|=r} h_r^k(\theta_1,\theta_2) q^{k^1} p^{k^2}$, $h_r^k(\theta_1,\theta_2) = \sum_{j=(j_1,j_2)} h_{r,j}^k e^{i(j_1\theta_1 + j_2\theta_2)}$ and $k = (k^1,k^2) \in \mathbb{Z}^3 \times \mathbb{Z}^3$ is a multi-index.

We will make a change of variables that suppress the maximum number of monomials and removes the dependence in θ_1 and in θ_2 in the terms of order r, H_r, of the Hamiltonian expansion. The canonical transformation that accomplishes this purpose is given by the following generating function:

$$G_r = G_r(q,p,\theta) = \sum_{|k|=r} g_r^k(\theta_1,\theta_2) q^{k^1} p^{k^2}, \qquad g_r^k(\theta_1,\theta_2) = \sum_{j=(j_1,j_2)\in\mathbb{Z}^2} g_{r,j}^k e^{i(j_1\theta_1+j_2\theta_2)}, \quad (4.31)$$

where the coefficients take the form

$$g_r^k(\theta_1,\theta_2) = \begin{cases} \displaystyle\sum_{j=(j_1,j_2)} \frac{h_{r,j}^k}{i(j_1\omega_{sat} + j_2\omega_{ura} - \langle \omega, k^2 - k^1 \rangle)} e^{i(j_1\theta_1+j_2\theta_2)} & \text{if} \quad k^1 \neq k^2, \\ \displaystyle\sum_{j=(j_1,j_2)\neq(0,0)} \frac{h_{r,j}^k}{i(j_1\omega_{sat} + j_2\omega_{ura})} e^{i(j_1\theta_1+j_2\theta_2)} & \text{if} \quad k^1 = k^2, \end{cases}$$

In this case, the frequencies of the normal linear oscillations around the 2-D invariant torus T_5, $\omega = (\omega_1,\omega_2,\omega_3)$, and the intrinsic frequencies of the system, ω_{sat} and ω_{ura}, are not in resonance up to a given order. That is, we check at every step of the process that $i(j_1\omega_{sat} + j_2\omega_{ura} - \langle \omega, k \rangle) \neq 0$, $j = (j_1,j_2) \in \mathbb{Z}^2$, $k \in \mathbb{Z}^3$, with $|j|$ and $|k|$ up to the orders we have worked with.

Now, the H' obtained with such a generating function does not depend on the variables θ_1 and θ_2 up to degree r and the expansion is recomputed using the following formulae

$$H' = H + \{H, G_r\} + \frac{1}{2!}\{\{H,G_r\},G_r\} + \cdots,$$

giving rise to

$$H' = \langle \varpi, p_\theta \rangle + H_2(q,p) + \sum_{j=3}^{r-1} H_j(q,p) + H_r'(q,p) + H_{r+1}'(q,p,\theta) + \cdots.$$

After performing all this changes up to a suitable degree $n = N$, the Hamiltonian takes the form

$$H = \langle \varpi, p_\theta \rangle + \mathcal{N}(q_1p_1, q_2p_2, q_3p_3) + \mathcal{R}(q_1, q_2, q_3, p_1, p_2, p_3, \theta_1, \theta_2), \tag{4.32}$$

where $\mathcal{N}$ denotes the normal form (that only depends on the products q_jp_j) and $\mathcal{R}$ is the remainder (of order greater than N).

Finally, we write the normal form $\mathcal{N}$ in real action-angle coordinates. This can be easily achieved by using the (canonical) transformation,

$$q_j = I_j^{1/2} \exp(i\varphi_j), \quad p_j = -iI_j^{1/2} \exp(-i\varphi_j), \quad j = 1, 2, 3. \tag{4.33}$$

It is not difficult to see that $\mathcal{N}$, in these coordinates, does not depend on the angles φ_j but only on the actions I_j,

$$\mathcal{N} = \sum_{|k|=1}^{[N/2]} h_k I_1^{k_1} I_2^{k_2} I_3^{k_3}, \qquad k \in \mathbb{Z}^3, \quad h_k \in \mathbb{R}. \tag{4.34}$$

Values for the coefficients h_k can be found in Table 4.3.

4.6.5 Changes of variables

We have also computed explicit expressions for the transformation from the initial variables of (4.28) to the final one. This change of variables is a Taylor truncated power series up to degree N with Fourier coefficients (with two angles) also truncated, in its turn, at orders (N_{f_1}, N_{f_2}). We will use this changes of variables to send information from the normal form coordinates to the initial ones, and vice versa.

4.6.6 Local non-linear dynamics

If we are close enough to the 2-D invariant torus T_5 and we obviate the rotators $\langle \varpi, p_\theta \rangle$, the (non-linear) dynamics can be described accurately by the truncated normal form of the TCCP Hamiltonian (4.34). As this is an integrable normal form, the dynamics is very simple: the phase space is completely foliated by a 3-parametric family of invariant tori (let be I_0 the parameter) and, on each torus, there is a linear flow with a given frequency (let us call it $\Omega(I_0)$). If the frequencies (i.e., the components of the vector $\Omega(I_0)$) are linearly independent over the rationals then the torus $I = I_0$ is filled densely by any trajectory starting on it. If the frequencies are linearly dependent over the rationals, then the orbits on this torus are not dense: if there are ℓ_i independent frequencies, the torus $I = I_0$ contains a $(3 - \ell_i)$-parametric family of ℓ_i dimensional tori, being each one densely filled by any trajectory starting on it. These tori of dimension ℓ_i are the lower dimensional tori, while the tori of dimension 3 are the maximal dimensional ones.

In the same way as in Section 2.4.3, we can easily compute lower and maximal invariant tori using the truncated normal form and send them, via the changes of variables, to the initial synodical coordinates of the TCCP system. This changes of variables add two

k_1	k_2	k_3	Re (h_k)	Im (h_k)
1	0	0	-8.0473064872368966e-02	0.0000000000000000e+00
0	1	0	9.9668062515640865e-01	0.0000000000000000e+00
0	0	1	1.0000626913308270e+00	0.0000000000000000e+00
2	0	0	5.6008074695424814e-01	9.9022635266146223e-14
1	1	0	-1.5539627415430354e-01	1.9737284347219547e-14
0	2	0	5.5093985824138381e-03	-3.4515403004164990e-16
1	0	1	5.4161903856716140e-02	2.6837558280952768e-15
0	1	1	6.6103538676104013e-03	-2.3704452239135327e-16
0	0	2	-3.4144388415478051e-04	1.3980906058550924e-20
3	0	0	1.7078141909448842e+01	7.0030369427282057e-09
2	1	0	2.5316327595194634e+00	5.6348897124143457e-09
1	2	0	1.2040309679987733e+00	2.4234795726771734e-10
0	3	0	-1.7159208395247699e-03	8.2745567480971449e-12
2	0	1	-2.0884357984263224e-01	2.7145888846396389e-10
1	1	1	1.3097591687221137e+00	8.5687025776165656e-11
0	2	1	-8.7878491487452266e-03	1.1230163355821964e-12
1	0	2	-3.8394291301547680e-02	4.9155879462758908e-12
0	1	2	-8.1852662066825860e-03	2.9493958070531223e-13
0	0	3	4.8084373364571027e-04	4.1626694220605631e-14

Table 4.3: Coefficients of the normal form, up to degree 3 in the actions for the TCCP case. The first three columns contain the exponents of the actions, and the fourth and fifth columns are the real and imaginary parts of the coefficients. Imaginary parts must be zero, but they are not due to the different accumulation errors (basically, the one that comes from the truncation of the Fourier series).

Figure 4.16: Projection on the (x, y) (left) and on the (z, p_z) (right) planes of an elliptic three-dimensional invariant torus of the vertical family near T_5. The intrinsic frequencies are ω_{sat}, ω_{ura} and $\omega_3 = 1.000062350$. The normal ones are $\omega_1 = -0.08044599352$ and $\omega_2 = 0.9966839283$.

additional frequencies (the system's intrinsic frequencies, ω_{sat} and ω_{ura}) to the invariant tori. Thus, in our case, the invariant tori are of dimensions three, four and five.

Figures 4.16, 4.17, 4.18, 4.19, 4.20 and 4.21 are examples of these computations. More concretely, Figure 4.16 and Figure 4.17 display different projections of a three dimensional torus of the vertical family –the family that "grows" in the (z, p_z) direction–. Figures 4.18 and 4.19 are different projections of two three-dimensional invariant tori contained in the $z = p_z = 0$ plane. Figure 4.20 displays two projections of a four-dimensional invariant torus of the vertical family near T_5. Finally, in Figure 4.21 two different projections of a five-dimensional invariant torus are shown. All these graphics have been obtained computing 10,000 points, with a time step of 0.1 units. See the captions for more details.

We also note that, in this way, it is possible to compute quasi-periodic orbits with a prescribed set of frequencies Ω_0, provided that Ω_0 belongs to the domain where the normal form is accurate.

4.6.7 Computing a quasi-integral

In a similar way as it is done in 2.5.1 for the periodic case, we compute an approximated first integral of the TCCP system in order to find (in 4.6.8) a region of effective stability around T_5.

We look for a function, $F(q, p, \theta_1, \theta_2)$ with $(q, p) \in \mathbb{C}^3 \times \mathbb{C}^3$, $(\theta_1, \theta_2) \in \mathbb{T}^2$, such that

$$\{H, F\} = 0, \tag{4.35}$$

where H is the Hamiltonian of the TCCP system as given in equation (4.30). That is, we suppose that H is already in normal form up to degree 2, that it is expanded in complex coordinates and that we have autonomize it by introducing the two fictitious momenta p_{θ_1} and p_{θ_2}.

It is also possible to write the function F as a truncated Fourier-Taylor expansion

$$F(q, p, \theta_1, \theta_2) = \sum_{n=2}^{N} F_n(q, p, \theta_1, \theta_2),$$

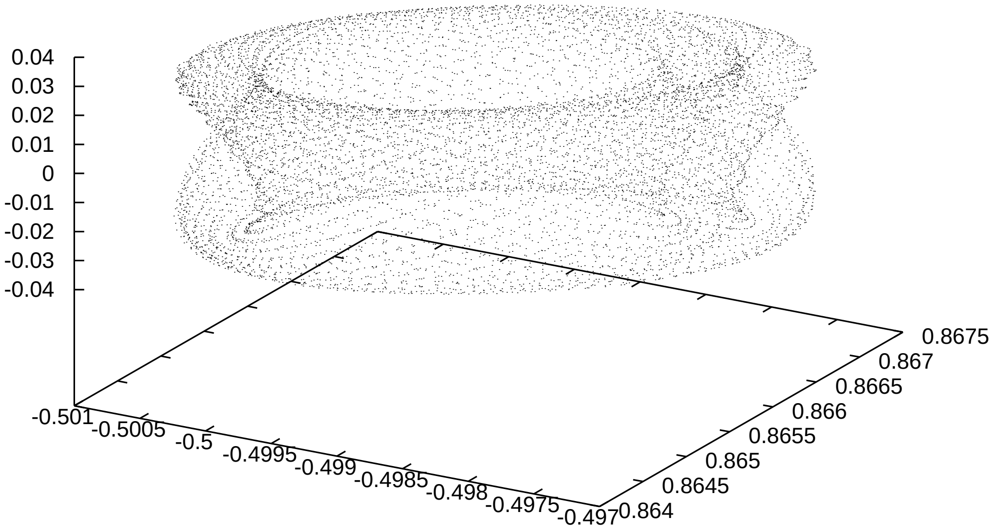

Figure 4.17: Projection on the configuration space of the same three-dimensional invariant torus of the vertical family shown in Figure 4.16.

Figure 4.18: Projections on two different planes of a planar invariant torus. The intrinsic frequencies are ω_{sat}, ω_{ura} and $\omega_1 = -0.08046185813$, and the normal ones are $\omega_2 = 0.9966790714$ and $\omega_3 = 1.000063233$.

Figure 4.19: Projections on the (x, y) (left) an (p_x, p_y) planes of a planar invariant torus. The intrinsic frequencies are ω_{sat}, ω_{ura} and $\omega_2 = 0.9966811761$, and the normal ones are $\omega_1 = -8.0480831675999259$ and $\omega_3 = 1.000063022$.

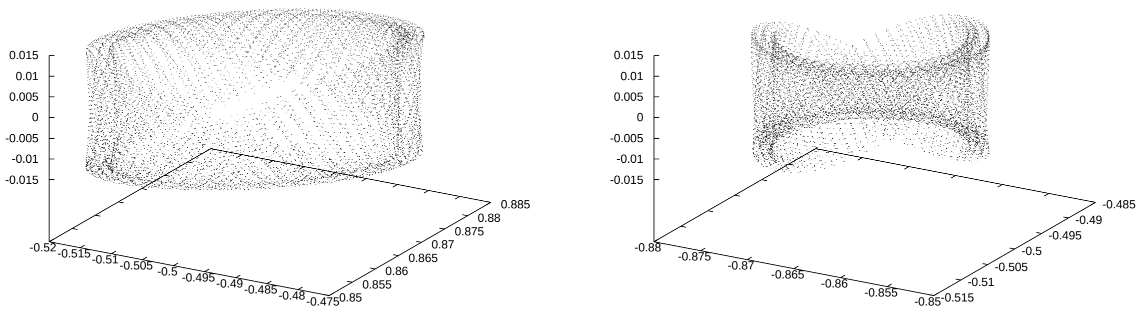

Figure 4.20: Projections on the (x, y, z) (left) an (p_x, p_y, p_z) spaces of a four-dimensional invariant torus of the vertical family near T_5. The intrinsic frequencies are ω_{sat}, ω_{ura}, $\omega_2 = 0.9966811761$ and $\omega_3 = 1.000063022$, and the normal one is $\omega_1 = -0.08048083168$.

Figure 4.21: Projections of an elliptic five-dimensional invariant torus of the vertical family near T_5. The proper frequencies are ω_{sat}, ω_{ura}, $\omega_1 = -0.08046420047$, $\omega_2 = 0.9966802858$ and $\omega_3 = 1.000063496$. Left plot: (x, y)-projection. Right plot: (z, p_z)-projection.

where, as usual, F_n stands for an homogeneous polynomial of degree n in the complex variables (q,p), with coefficients that are (truncated) Fourier series in the angles θ_1 and θ_2:

$$F_n(q,p,\theta_1,\theta_2) = \sum_{|k|=n} \sum_{j=(j_1,j_2)} \left(f_{n,j}^k e^{i(j_1\theta_1+j_2\theta_2)}\right) q^{k^1} p^{k^2}.$$

In order to compute the coefficients of this expansion, $f_{n,j}^k \in \mathbb{C}$, we solve equation (4.35) order by order. It is easy to see that there is some freedom while selecting the degree 2 of F, F_2. As our final goal is to bound the diffusion using this quasi-integral, a good choice (the reason is the same one given in 2.5.1) is:

$$F_2 = i \sum_{j=1}^{3} q_j p_j. \tag{4.36}$$

For what concerns to higher degrees, $n>2$, it is possible (following the same steps than in 2.5.1) to isolate $f_{n,j}^k$ in function of known things:

$$f_{n,j}^k = \frac{i c_{n,j}^k}{j_1\omega_{sat} + j_2\omega_{ura} - \langle k^2 - k^1, \omega\rangle}, \tag{4.37}$$

where $\omega = (\omega_1,\omega_2,\omega_3)$ and $c_{n,j}^k$ can be computed from the (known) expansion of the Hamiltonian and the (also known) coefficients up to degree $n-1$ of F.

We have used this recurrence for computing this approximate first integral truncated at order $N=14$. During the computations, two conditions must be verified at every step of the process. They appear easily looking at (4.37):

a) ω_{sat}, ω_{ura} and ω must satisfy that

$$j_1\omega_{sat} + j_2\omega_{ura} - \langle k,\omega\rangle \neq 0, \quad \forall\,(j_1,j_2)\in\mathbb{Z}^2, \quad \forall\, k\in\mathbb{Z}^3 \text{ such that } |j|+|k|\neq 0,$$

b) if $j_1=j_2=0$ and $k^1=k^2$, the value $c_{n,j}^k$ must vanish.

4.6.8 Bounding the diffusion

As F is not an exact first integral, the variation of the values of F on a given trajectory of the Hamiltonian is not constant. This time-dependence can be written (in terms of the Hamiltonian expanded in real coordinates $H(x,y,\theta,p_\theta)$ and in terms of the realified quasi-integral $F(x,y,\theta) = \frac{1}{2}\sum_{j=1}^{3}(x_j^2+y_j^2) + O(3)$) as

$$\dot{F} = \{F(x,y,\theta), H(x,y,\theta,p_\theta)\},$$

where $(x,y)\in\mathbb{R}^3\times\mathbb{R}^3$ and, as usual, $p_\theta = (p_{\theta_1}, p_{\theta_2})$ are the momenta corresponding to the angles $\theta=(\theta_1,\theta_2)\in\mathbb{T}^2$. Then, it is easy to see that the diffusion should be controlled by bounding the following expansion:

$$\dot{F} = \sum_{n>N}\sum_{l=3}^{N} \{F_l, H_{n-l+2}\} + \sum_{n>N} \{F_2, H_n\}. \tag{4.38}$$

The procedure to do this is the same one that we used in 2.5.2 for the BCCP model. Thus, we use Lemmas[5] in Section 2.3.4 to estimate the size of the terms of the Hamiltonian that have not been numerically computed (those homogeneous polynomials with degree greater than 14) and a bound of the drift of the formal first integral F is obtained by means of Lemma 2.5.1.

Then, in order to find a region of effective stability, we define the following compact domain of the phase space:

$$D_\rho = \{(x, y) \in \mathbb{R}^6 \,;\, (x_1^2 + y_1^2) + (x_2^2 + y_2^2) + (x_3^2 + y_3^2) \le \rho^2\}.$$

Assume, now, that we have an initial condition $(x(0), y(0))$ inside the domain D_{ρ_0}. We are interested in values $\rho > \rho_0$ such that the orbit $(x(t), y(t))$ is contained in D_ρ for all $t \in [0, T_S]$, where $T_S = 3\times 10^9$ is the age of the Solar System in adimensional coordinates. A sufficient condition to achieve this is that

$$|F_2(x(t), y(t)) - F_2(x(0), y(0))| \le \frac{1}{2}(\rho^2 - \rho_0^2), \quad 0 \le t \le T_S, \tag{4.39}$$

where $F_2(x, y) = \frac{1}{2}\sum_{j=1}^{3}(x_j^2 + y_j^2)$.

Let us now define

$$\Delta_N(\rho_0, \rho) = \frac{1}{2}(\rho^2 - \rho_0^2) - \sum_{j=3}^{N} \|F_j\|(\rho^j + \rho_0^j)$$

It is easy to see that, if $\Delta_N(\rho_0, \rho) \ge 0$ and

$$|F(x(t), y(t), \theta(t)) - F(x(0), y(0), \theta(0))| \le \Delta_N(\rho_0, \rho),$$

then, (4.39) holds. The function $\Delta_N(\rho_0, \rho)$ is used to bound the maximum variation of $F(x, y, \theta)$ on the interval of time $[0, T_S]$ because (4.39) is a sufficient condition for the trajectory to be inside the domain D_ρ. Note that, due to the particular form of Δ_N, the values ρ_0 and ρ have to be selected sufficiently small to achieve $\Delta_N(\rho_0, \rho) \ge 0$ but, on the other hand, we want Δ_N to be as large as possible, to allow a large variation of F with a controlled variation of ρ. Hence, we will carefully select the values ρ_0 and ρ to obtain the largest region of effective stability for time T_S.

So, if $\Delta_N(\rho_0, \rho) \ge 0$, we can bound the escaping time as a function of the initial radius,

$$T(\rho_0) = \sup_\rho \frac{\Delta_N(\rho_0, \rho)}{\mathcal{R}(\rho)}, \tag{4.40}$$

where $\mathcal{R}(\rho)$ is given in Lemma 2.5.1.

We solve equation (4.40) for different ρ_0's and plot T versus ρ_0. Afterwards, using inverse interpolation we find the initial radius ρ_0 for which an orbit does not leave the domain D_ρ in a time span of length $T_S = 3 \times 10^9$. The result obtained here is $\rho_0 = 1.7565 \times 10^{-4}$ and the maximal final radius is $\rho = 4.9666 \times 10^{-4}$. We want to mention

[5]The norms should be modified in the trivial way in order to deal with two angles, but the lemmas are still valid.

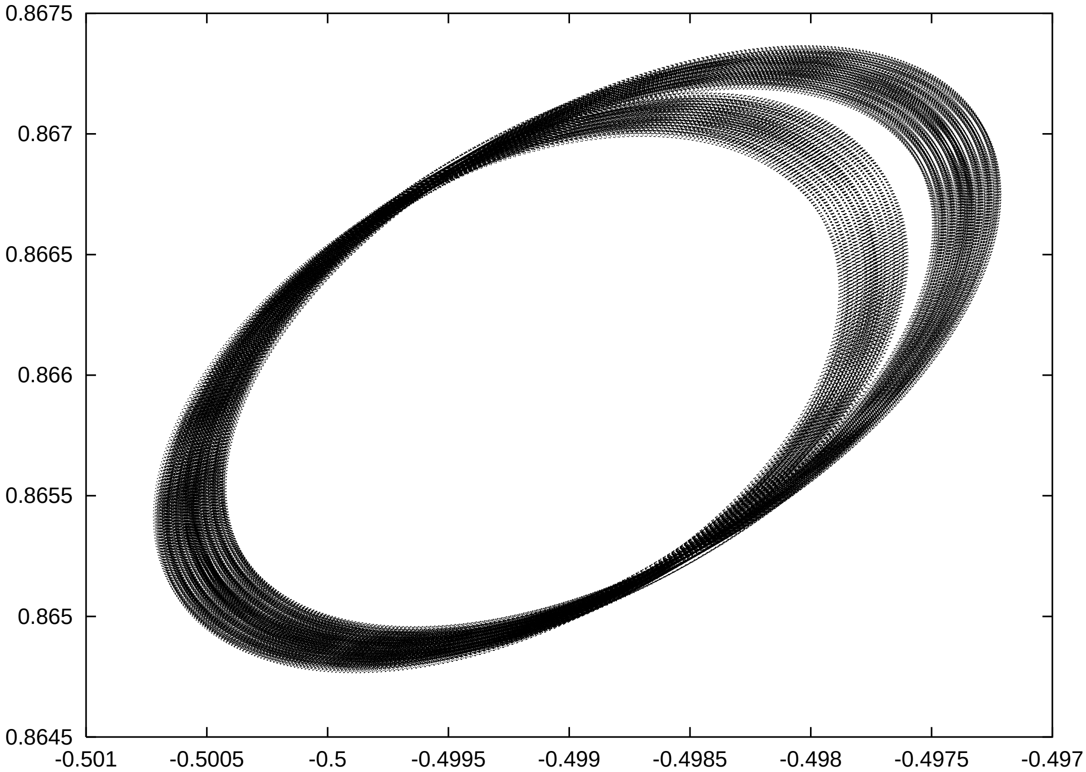

Figure 4.22: Projection on the Jupiter's plane of motion, (x, y), of the region of effective stability around the 2-D invariant torus T_5.

that this region D_{ρ_0} (seen in the physical space of the TCCP) is qualitatively different from (it is not contained neither contains) the effective stability zones obtained with other models, such as the RTBP one (for example, in [Sim89, CG91, SD00]), the BCCP in Section 2.5.3 and the ERTBP in Section 3.4.2. It can be seen as the subset of the phase space when a ball of radius ρ_0 "travels" around the invariant torus T_5. The projection of this region of effective stability into the Jupiter's plane of motion is shown in Figure 4.22.

Unfortunately, no Trojan asteroid lies inside the domain of effective stability D_{ρ_0}. This fact has been checked by taking the synodical coordinates of 432 Trojans in a given date (October 18th, 2001 – 2452200.5 Julian day), transporting them to the coordinates in which the approximate first integral is computed and finally checking if the value $r = \sqrt{(x_1^2 + y_1^2) + (x_2^2 + y_2^2) + (x_3^2 + y_3^2)}$ is smaller than ρ_0. The initial phases for the quasi-periodic functions involved in the computations have been obtained from the actual positions of Saturn and Uranus in the same Julian date.

Chapter 5

Frequency analysis of the motion of the Trojan asteroids

In this chapter, we make a systematic numerical study of the dynamics of the Trojan's actual orbits in different models. First, we describe the numerical integrator that we use during the simulations. In the realistic system, we choose a symplectic method in order the geometric properties of the system to be conserved. Then, we use the frequency analysis of some parameters of the orbits in order to describe the dynamics of "real" Trojan objects in the Outer Solar System. Finally, we compute the frequencies of the Trojan orbits supposing they move in different semi-analytical models, and we compare them with the ones obtained with the more realistic system (OSS).

5.1 Symplectic integrators

In this section, we describe a particular (high order) symplectic integrator that is used in the simulation of the true asteroidal orbits in a "realistic" model (for the Trojan case) of the Solar System. We adapt this, in principle, general integrator to the case of N planets and n particles revolving in quasi-Kepler orbits around the Sun. And, finally, we describe the parameters used in the symplectic integration of the "realistic" model, that is the Outer Solar System.

5.1.1 The general method

The symplectic integrator method of high order that we are going to use is due to J.Laskar and P.Robutel and it can be found in [LR01]. In this section, for completeness, we give a brief description of it.

Let be the Hamiltonian $H = A + \epsilon B$, where A and B are integrable and ϵ is a small parameter (the meaning of "small" will become clear later on). Let us suppose that we want to do one integration step of time τ. That is, we are interested in computing $e^{\tau L_H}$, where $L_\xi(\cdot)$ is the classical Lie operator, $L_\xi f = \{\xi, f\}$. The well known Baker-Campbell-Hausdorff formula (BCH) ensures that

$$e^{\tau L_H} = e^{\tau L_A} e^{\tau L_{\epsilon B}} + o(\tau).$$

Note that the operator $S_1 = e^{\tau L_A} e^{\tau L_{\epsilon B}}$ gives us the simplest integration method.

It is, then, straightforward to construct an integration scheme of n steps with the following operator:

$$S_n(\tau) = e^{c_1 \tau L_A} e^{d_1 \tau L_{\epsilon B}} \cdots e^{c_n \tau L_A} e^{d_n \tau L_{\epsilon B}},$$

where, of course, $\sum c_i = \sum d_i = 1$.

It is also easy (using the BCH Theorem and the linearity of the Lie operator) to see that there exists a formal operator K such that

$$S_n(\tau) = e^{\tau K}.$$

In general, a symplectic integrator for $H = A + \epsilon B$ of order p is obtained if $K = A + \epsilon B + O(\tau^p)$.

If we restrict to symmetric integrators, that is integrators such that $S_n(\tau)^{-1} = S_n(-\tau)$, we obtain four different symmetric symplectic integration schemes (see [LR01]):

$$\begin{array}{rl}
SABA_{2k} & : e^{c_1 \tau L_A} e^{d_1 \tau L_{\epsilon B}} \cdots e^{d_k \tau L_{\epsilon B}} e^{c_{k+1} \tau L_A} e^{d_k \tau L_{\epsilon B}} \cdots e^{d_1 \tau L_{\epsilon B}} e^{c_1 \tau L_A}, \\
SABA_{2k+1} & : e^{c_1 \tau L_A} e^{d_1 \tau L_{\epsilon B}} \cdots e^{c_{k+1} \tau L_A} e^{d_{k+1} \tau L_{\epsilon B}} e^{c_{k+1} \tau L_A} \cdots e^{d_1 \tau L_{\epsilon B}} e^{c_1 \tau L_A}, \\
SBAB_{2k-1} & : e^{d_1 \tau L_{\epsilon B}} e^{c_2 \tau L_A} e^{d_2 \tau L_{\epsilon B}} \cdots e^{d_k \tau L_{\epsilon B}} e^{c_{k+1} \tau L_A} e^{d_k \tau L_{\epsilon B}} \cdots e^{c_2 \tau L_A} e^{d_1 \tau L_{\epsilon B}}, \\
SBAB_{2k} & : e^{d_1 \tau L_{\epsilon B}} e^{c_2 \tau L_A} \cdots e^{c_{k+1} \tau L_A} e^{d_{k+1} \tau L_{\epsilon B}} e^{c_{k+1} \tau L_A} \cdots e^{c_2 \tau L_A} e^{d_1 \tau L_{\epsilon B}}.
\end{array} \tag{5.1}$$

Now, we take into account that the initial Hamiltonian H is a perturbation of an integrable one (ϵ is "small"). This will help us to obtain higher order symplectic integration schemes. Actually, we will be interested in finding integrators of the type $SABA_n$ and $SBAB_n$ for which the associated Hamiltonian K_{S_n} verifies

$$K_{S_n} = A + \epsilon B + O(\tau^{2n}\epsilon + \tau^2 \epsilon^2).$$

Let us remark that in order to construct the operator K_{S_n}, we just have to compute the constants (c_i, d_i) of any integration scheme in (5.1). The details on how to obtain them can be found in [LR01].

To end this general description of the method, we present three examples:

1. $\underline{n=1}$: Both cases $SABA_1 = e^{\frac{\tau}{2} L_A} e^{\tau L_{\epsilon B}} e^{\frac{\tau}{2} L_A}$ and $SBAB_1 = e^{\frac{\tau}{2} L_{\epsilon B}} e^{\tau L_A} e^{\frac{\tau}{2} L_{\epsilon B}}$ correspond to the classical leapfrog method (see, for example, [Rut83]). This is an integrator of order 2 and has been widely used in most computations by many astronomers.

2. $\underline{n=2}$: For the case $SABA_2$, the integrator corresponding to the operator K_{S_2} takes the form

   $$e^{\tau L_{K_{S_2}}} = e^{c_1 \tau L_A} e^{d_1 \tau L_{\epsilon B}} e^{c_2 \tau L_A} e^{d_1 \tau L_{\epsilon B}} e^{c_1 \tau L_A}$$

   where the values of the constants are:

   $$c_1 = \frac{1}{2}(1 - \frac{1}{\sqrt{3}}), \qquad c_2 = \frac{1}{\sqrt{3}}, \qquad d_1 = \frac{1}{2}.$$

3. $\underline{n=4}$: The integration scheme corresponding to $SABA_4$ is the one that we have used in the simulations of the following sections. The values of the constants involved are:

$$
\begin{aligned}
c_1 &= 1/2-\sqrt{525+70\sqrt{30}}/70, & d_1 &= 1/4-\sqrt{30}/72,\\
c_2 &= (\sqrt{525+70\sqrt{30}},-\sqrt{525-70\sqrt{30}})/70, & d_2 &= 1/4+\sqrt{30}/72,\\
c_3 &= \sqrt{525-70\sqrt{30}}/35,
\end{aligned}
$$

and the formal Hamiltonian K has the form

$$K = A+\epsilon B + O(\tau^8\epsilon+\tau^2\epsilon^2).$$

5.1.2 Application to the (N planets + n particles) problem

We turn now the sight into the question of the integration of the problem consisting in the mutual gravitational attraction of the Sun, N planets and n massless particles (asteroids, for instance). We will assume that the planets and the particles move in slightly perturbed Kepler orbits around the Sun. This is what we shall call the (N planets + n particles) problem, or NPnPP, for short.

In this section, we are going to see several expressions for the Hamiltonian of the problem. We will start from the barycentric coordinates, go through the heliocentric coordinates and finally write the Hamiltonian of the problem in the Jacobi coordinates, which is essentially the addition of an integrable Keplerian Hamiltonian, A, and a perturbation, ϵB, consisting in the attraction of the pairs planet-planet and planet-particle.

5.1.2.1 Barycentric coordinates

We denote U_0, U_1, $\ldots$, U_N the barycentric vector positions of the Sun and the N planets, respectively, and $u_1,\ldots,u_n$ the barycentric positions of the n massless particles. The corresponding momenta will be given by $\tilde{U}_0,\ldots,\tilde{U}_N$ and $\tilde{u}_1,\ldots,\tilde{u}_n$, where $\tilde{U}_i = m_i\dot{U}_i$, $i=0,\ldots,N$, and m_i represent the masses of the Sun (m_0) and the planets.

The Hamiltonian of the NPnPP in barycentric coordinates can be written as:

$$
\begin{aligned}
H &= \sum_{i=0}^{N}\frac{||\tilde{U}_i||^2}{2m_i} - G\sum_{0\le i<j\le N}\frac{m_i m_j}{\Delta_{ij}}\\
&+ \sum_{i=1}^{n}\frac{||\tilde{u}_i||^2}{2} - G\sum_{i=1}^{n}\sum_{j=0}^{N}\frac{m_j}{\bar{\Delta}_{ij}},
\end{aligned}
$$

where $\Delta_{ij}=||U_i-U_j||$, $\bar{\Delta}_{ij}=||u_i-U_j||$ and G is the universal constant of gravitation.

5.1.2.2 Heliocentric coordinates

The canonical heliocentric coordinates (see [Las89]), $(R_i,\tilde{R}_i)_{i=0,\ldots,N}$ and $(r_i,\tilde{r}_i)_{i=1,\ldots,n}$, are obtained from the barycentric ones by the following linear change of variables:

$$
\begin{aligned}
R_0 &= U_0, & \tilde{R}_0 &= \textstyle\sum_{i=0}^{N}\tilde{U}_i,\\
R_i &= U_i-U_0, & \tilde{R}_i &= \tilde{U}_i,\\
r_i &= r_i-U_0, & \tilde{r}_i &= \tilde{u}_i.
\end{aligned}
$$

It is easy to see that the Hamiltonian of the NPnPP in the heliocentric coordinates can be written as:

$$
\begin{aligned}
H &= \sum_{i=1}^{N}\left(\frac{||\tilde{R}_i||^2}{2\beta_i} - G\frac{m_0 m_i}{||R_i||}\right) + \sum_{0<i<j\leq N}\left(\frac{\tilde{R}_i\tilde{R}_j}{m_0} - G\frac{m_i m_j}{\Delta_{ij}}\right) \\
&+ \sum_{i=1}^{n}\left(\frac{||\tilde{r}_i||^2}{2} - G\frac{m_0}{||r_i||}\right) + \sum_{i=1}^{n}\sum_{j=1}^{N}\left(\frac{\tilde{r}_i\tilde{R}_j}{m_0} - G\frac{m_j}{\bar{\Delta}_{ij}}\right),
\end{aligned}
$$

where $\beta_i = \frac{m_0 m_i}{m_0+m_i}$, $\Delta_{ij} = ||R_i - R_j||$ and $\bar{\Delta}_{ij} = ||r_i - R_j||$.

5.1.2.3 Jacobi coordinates

We use a second change of variables that will give us the Hamiltonian in the desired way. The canonical Jacobi coordinates, $(V_i, \tilde{V}_i)_{i=0,\ldots,N}$ and $(v_i, \tilde{v}_i)_{i=1,\ldots,n}$, can be deduced from the barycentric ones with the following change of coordinates:

$$
\begin{aligned}
V_0 &= \textstyle\sum_{j=0}^{N} \frac{m_j}{\eta_N} U_j, & \tilde{V}_0 &= \textstyle\sum_{j=0}^{N} \tilde{U}_j, \\
V_i &= U_i - \textstyle\sum_{j=0}^{i-1} \frac{m_j}{\eta_{i-1}} U_j, & \tilde{V}_i &= \frac{\eta_{i-1}}{\eta_i}\tilde{U}_i - \frac{m_i}{\eta_i}\textstyle\sum_{j=0}^{i-1}\tilde{U}_j, \\
v_i &= u_i - \textstyle\sum_{j=0}^{N} \frac{m_j}{\eta_N} U_j, & \tilde{v}_i &= \tilde{u}_i,
\end{aligned}
$$

where $\eta_i = \sum_{j=0}^{i} m_j$.

Finally, it is easy to obtain the Hamiltonian of the NPnPP written in the Jacobi coordinates:

$$
\begin{aligned}
H &= \sum_{i=1}^{N}\left(\frac{\eta_i}{\eta_{i-1}}\frac{||\tilde{V}_i||^2}{2m_i} - G\frac{m_i\eta_{i-1}}{||v_i||}\right) + G\sum_{i=2}^{N} m_i\left(\frac{\eta_{i-1}}{||V_i||} - \frac{m_0}{||R_i||}\right) \\
&- G\sum_{0<i<j\leq N}\frac{m_i m_j}{\Delta_{ij}} + \sum_{i=1}^{n}\left(\frac{||\tilde{v}_i||^2}{2} - G\frac{\eta_N}{||v_i||}\right) + G\sum_{i=1}^{n}\left(\frac{\eta_N}{||v_i||} - \sum_{j=0}^{N}\frac{m_j}{||r_i - R_j||}\right).
\end{aligned}
$$

This Hamiltonian can be splited in two ($H = H_0 + H_1$): an integrable Keplerian Hamiltonian (H_0) and a perturbative part (H_1). This will be very useful in order to use the symplectic integrator described in 5.1.1.

The non-perturbative part of the Hamiltonian is the addition of N Kepler problems corresponding, respectively, to a body of mass m_i attracted by the center of masses of the i preceding bodies, and n Kepler problems corresponding to a massless body attracted by the center of masses of the system:

$$
H_0 = \sum_{i=1}^{N}\left(\frac{\eta_i}{\eta_{i-1}}\frac{||\tilde{V}_i||^2}{2m_i} - G\frac{m_i\eta_{i-1}}{||V_i||}\right) + \sum_{i=1}^{n}\left(\frac{||\tilde{v}_i||^2}{2} - G\frac{\eta_N}{||v_i||}\right).
$$

Due to the relative smallness of the masses of the planets with respect to the mass of the Sun, there is a perturbative part in the Hamiltonian of the NPnPP. This perturbative part can be written as:

$$H_1 = G\sum_{i=2}^{N} m_i\left(\frac{\eta_{i-1}}{||V_i||} - \frac{m_0}{||R_i||}\right) - G\sum_{0<i<j\leq N}\frac{m_i m_j}{\Delta_{ij}} + G\sum_{i=1}^{n}\left(\frac{\eta_N}{||v_i||} - \sum_{j=0}^{N}\frac{m_j}{||r_i - R_j||}\right).$$

5.1.2.4 Implementation of the symplectic integrator

The Hamiltonian $H = H_0 + H_1$ has been integrated using the symplectic scheme $SABA_4$ described in Section 5.1.1. Recall that, if we denote $A \equiv H_0$ and $\epsilon B \equiv H_1$, what is done is to integrate exactly a Hamiltonian "very close" to H; the order of the error is $(\tau^8\epsilon + \tau^2\epsilon^2)$, where τ is the step of the integration and, in our case, $\epsilon = \frac{m_1}{m_0}$.

The operators L_A and L_B, corresponding respectively to the implementation of one step of integration of Hamiltonians A and B, act in the following manner:

Action of the operator L_A: As has already been mentioned before, the Hamiltonian A is the addition of several Kepler problems. The value of $x(t) = e^{\tau L_A}x(t_0)$, where $\tau = t - t_0$, is easily obtained using the elliptical coordinates of the orbits. One step of integration for each Kepler problem is performed using the classical f and g functions (see [Dan62], page 162):

If $r_0 = r(t_0)$ and $v_0 = v(t_0)$ are the position and velocity vectors at time t_0 of a body following a Keplerian orbit, it is possible to obtain its value at any time t, $r = r(t)$ and $v = v(t)$, in the following manner:

$$\begin{aligned} r(t) &= f(t,t_0)r(t_0) + g(t,t_0)v(t_0), \\ v(t) &= \frac{\partial f(t,t_0)}{\partial t}r(t_0) + \frac{\partial g(t,t_0)}{\partial t}v(t_0). \end{aligned}$$

The functions f, g, $\dot{f} = \frac{\partial f(t,t_0)}{\partial t}$ and $\dot{g} = \frac{\partial g(t,t_0)}{\partial t}$ can be written in terms of the elliptical coordinates of the Keplerian orbit:

$$\begin{aligned} f &= \frac{a}{r_0}(\cos(E - E_0) - 1) + 1, \\ g &= \frac{1}{n}(\sin(E - E_0) - e\sin E + e\sin E), \\ \dot{f} &= -\frac{a}{r_0}\frac{a}{r}n\sin(E - E_0), \\ \dot{g} &= \frac{a}{r}(\cos(E - E_0) - 1) + 1, \end{aligned}$$

where E, a and n stand for the eccentric anomaly, the semi-major axis and the mean motion of the elliptic orbit, respectively.

Action of the operator L_B: The perturbative part of the Hamiltonian, $H_1 = \epsilon B$, written in the Jacobi coordinates, only depends on the position vectors. Thus, it is trivially integrable: The operator $L_{\epsilon B}$ is the map that associates the positions and momenta of the N planets and the n particles at any time t, $(V_i(t), v_i(t), \tilde{V}_i(t), \tilde{v}_i(t))$, with their known values at a time $t_0 < t$, $(V_i(t_0), v_i(t_0), \tilde{V}_i(t_0), \tilde{v}_i(t_0))$, in the following way:

$$\begin{array}{rclcl}
V_i(t) & = & V_i(t_0) + \tau\{V_i(t_0), H_1\} & = & V_i(t_0), \\
\tilde{V}_i(t) & = & \tilde{V}_i(t_0) + \tau\{\tilde{V}_i(t_0), H_1\} & = & \tilde{V}_i(t_0) - \tau\frac{\partial H_1}{\partial V_i(t_0)}, \\
v_i(t) & = & v_i(t_0) + \tau\{v_i(t_0), H_1\} & = & v_i(t_0), \\
\tilde{v}_i(t) & = & \tilde{v}_i(t_0) + \tau\{\tilde{v}_i(t_0), H_1\} & = & \tilde{v}_i(t_0) - \tau\frac{\partial H_1}{\partial v_i(t_0)} ,
\end{array}$$

where $\{\cdot,\cdot\}$ stands for the Poisson bracket and $\tau = t - t_0$. Thus, the positions are not modified by the perturbation.

By the way, we would eventually prefer to compute the change in velocities than in momenta. The corresponding equations are:

$$\begin{array}{rcl}
\dot{V}_i(t) & = & \dot{V}_i(t_0) - \dfrac{\eta_i}{\eta_{i-1}}\dfrac{\tau}{m_i}\dfrac{\partial H_1}{\partial V_i(t_0)}, \\
\dot{v}_i(t) & = & \dot{v}_i(t_0) - \dfrac{\eta_i}{\eta_{i-1}}\dfrac{\tau}{m_i}\dfrac{\partial H_1}{\partial v_i(t_0)}.
\end{array}$$

We can, thus, define the accelerations of the planets and the particles due to the perturbation as $A_i = \frac{\eta_i}{\eta_{i-1}m_i}\frac{\partial H_1}{\partial V_i}$ and $a_i = \frac{\eta_i}{\eta_{i-1}m_i}\frac{\partial H_1}{\partial v_i}$. It is not very difficult to see that they can be expressed in terms of the heliocentric and Jacobi positions of the N planets and the n particles in the following way:

$$\begin{array}{rcl}
A_1 & = & G\displaystyle\sum_{i=2}^{N} m_i\left(\frac{R_i}{||R_i||^3} + \frac{R_1 - R_i}{||R_1 - R_i||^3}\right), \\
A_k & = & G\dfrac{\eta_k}{\eta_{k-1}}\left(m_0\dfrac{R_k}{||R_k||^3} - \eta_{k-1}\dfrac{V_k}{||V_k||^3} + \dfrac{m_0}{\eta_k}\displaystyle\sum_{i=k+1}^{N} m_i\frac{R_k}{||R_k||^3} - \sum_{i=1}^{k-1} m_i\frac{R_i - R_k}{||R_i - R_k||^3}\right. \\
 & + & \left.\dfrac{\eta_{k-1}}{\eta_k}\displaystyle\sum_{i=k+1}^{N} m_i\frac{R_k - R_i}{||R_k - R_i||^3} + \frac{1}{\eta_k}\sum_{i=k+1}^{N}\sum_{j=1}^{k-1} m_i m_j\frac{R_i - R_j}{||R_i - R_j||^3}\right), \quad k = 2, \ldots, N , \\
a_k & = & G\left(m_0\dfrac{r_k}{||r_k||^3} - \eta_N\dfrac{v_k}{||v_k||^3} + \displaystyle\sum_{i=1}^{N} m_i\frac{r_k - R_i}{||r_k - R_i||^3}\right), \quad k = 1, \ldots, n.
\end{array}$$

5.1.3 The Outer Solar System model

We focus now on the integration of the five body problem consisting in the Sun and the four main outer planets of the Solar System (Jupiter, Saturn, Uranus and Neptune). This model is known in the literature as the Outer Solar System (OSS, for short). In the frequency analysis that is performed in Section 5.2, we use the OSS as the basis model for the Trojan motion.

The initial conditions for the planets are taken from the JPL Ephemerides DE405 at the Julian date 2452200.5 (October 10th, 2001). In order to take into account the (small) effect of the inner planets, their masses are added to Sun's one. In Table 5.1, we show the numerical values of the masses of the bodies that are used in the integration of the OSS. The unit of mass is such that Sun's mass is equal to one. The units of time and length used in the computations are years and A.U., respectively. The chosen integration

Body	Mass
Sun + inner planets	$0.1000005976999797 \times 10^{+1}$
Jupiter $(p = 5)$	$0.9547919384243266 \times 10^{-3}$
Saturn $(p = 6)$	$0.2858859806661309 \times 10^{-3}$
Uranus $(p = 7)$	$0.4366244043351564 \times 10^{-4}$
Neptune $(p = 8)$	$0.5151389020466116 \times 10^{-4}$
G	39.476926421373

Table 5.1: Masses of the bodies used in the Outer Solar System computations. The mass unit is Sun's mass. In the last row, the value of the constant of gravitation is given.

method for this problem is the symplectic integrator $SABA_4$ with a fixed time step of 1/2 year.

We also study the performance of the integrator $SABA_4$ in this problem by computing the variation of the energy in a long integration. In Figure 5.1, we have plotted the logarithm of the variation of the system's energy for a time span of 5 Million years for the integrators $SABA_4$. We can see that we have a random error around a constant variation of the energy (which is approximately 10^{-11}). That is, we integrate exactly a Hamiltonian "close" to the one we want to integrate.

5.2 Frequency analysis

In this section, Laskar's Frequency Map Analysis (FMA) (see [Las90], [Las99], [RL01]) is used in order to study the dynamics of the Trojan swarms. First, the FMA is briefly described. Then, we obtain the basic frequencies of the planets in the OSS and the proper frequencies of the Trojan asteroids also in the OSS (obviously, we suppose that the motion of the particles does not disturb the motion of the planets). Finally, the FMA is also used in order to estimate the diffusion rate of the frequencies.

5.2.1 Frequency Map Analysis

Let

$$f(t) = e^{i\nu_1 t} + \sum_{k\in\mathbb{Z}^d} a_k e^{i<k,\nu>t}, \quad a_k \in \mathbb{C},$$

be a quasi-periodic function that can be numerically determined in the time span $[-T, T]$. The frequency analysis algorithm given by Laskar will provide the values of the frequencies ω_k and the amplitudes $\tilde{a}_k$ of a function $\tilde{f}(t) = \sum \tilde{a}_k e^{i\omega_k t}$ that approximates $f(t)$ in $[-T, T]$. The iterative scheme goes as follows: First, the frequency ω_1 is found by looking for the maximum amplitude of

$$\Phi(\sigma) =< f(t), e^{i\sigma t} >:= \frac{1}{2T}\int_{-T}^{T} f(t)e^{-i\sigma t}\chi(t)dt,$$

where $\chi(t) = 1 + \cos(\pi t/T)$ is a Hanning window filter (see [Las99] or [GMS02]). Second, the corresponding amplitude itself, $\tilde{a}_1$, is computed by orthogonal projection of $f(t)$ on

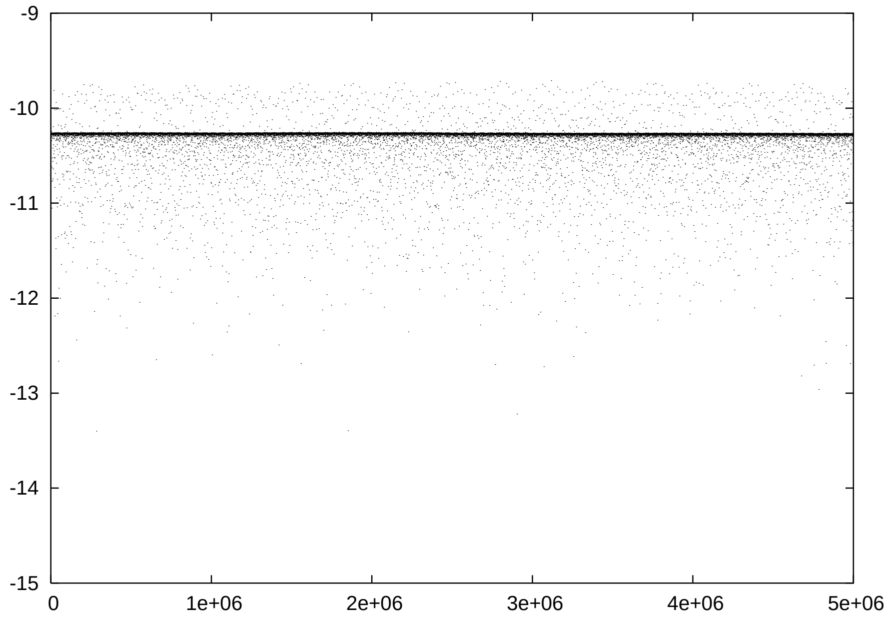

Figure 5.1: Logarithm of the relative variation of the energy during the integration of the OSS with the $SABA_4$ method. We can see that there is a random variation of the relative error around a fixed energy.

$e^{i\omega_1 t}$. Then, the process is restarted again with the function $f_1(t) = f(t) - \tilde{a}_1 e^{i\omega_1 t}$ in order to obtain the pairs $(\omega_k, \tilde{a}_k)_{k>1}$. In every step, the set $(e^{i\omega_k t})_k$ should be orthogonalized when projecting the functions f_i. See [Las99], for details.

Another method for approximating the frequencies is the one given by [GMS02]. Their procedure consists, basically, in equating the discrete Fourier transforms of the sampled initial data and of the quasi-periodic approximation. This alternative method is used in further computations in order to check the results.

5.2.2 Basic frequencies of the OSS

As it has been mentioned before, the chosen model for the Trojan motion is the Outer Solar System. It is known that the basic frequencies of the planets play an important role when studying the proper elements and proper frequencies of any group of asteroids in the Solar System (there is an endless list of references on this topic; see for example [MK90], [KMF$^+$91], [MK92] and references therein).

For the motion of a planet, we basically have to deal with three basic frequencies: one related with the mean motion (the fast one) and two secular ones, related with perihelion and node precessions. They appear as basic frequencies (in most cases with the biggest amplitude) when we apply the frequency analysis to the following three complex functions:

$$\begin{aligned}
\alpha_p(t) &= a_p(t)\,\exp(i\lambda_p(t)),\\
\beta_p(t) &= e_p(t)\,\exp(i\varpi_p(t)),\\
\gamma_p(t) &= \sin\left(\frac{i_p(t)}{2}\right)\exp(i\Omega_p(t)),
\end{aligned} \tag{5.2}$$

Planet	ν_p (*deg*)	g_p (*sec*)	s_p (*sec*)	Sidereal Orbit Period (yr)
Jupiter ($p = 5$)	5.2968048×10^{-1}	4.24512464	0.0	11.862
Saturn ($p = 6$)	2.1329183×10^{-1}	28.2468157	−26.3382192	29.458
Uranus ($p = 7$)	7.4782874×10^{-2}	3.08791946	−2.99175127	84.019
Neptune ($p = 8$)	3.8134035×10^{-2}	0.67409606	−0.70379108	164.766

Table 5.2: Basic frequencies of the planetary orbits in the Outer Solar System.

where the symbols denoting the osculating elliptic elements at time t for a planet p are: a_p the semi-major axis, e_p the eccentricity, i_p the inclination, λ_p the mean longitude ($\lambda_p = \varpi_p + M_p$, with M_p the mean anomaly), ϖ_p the longitude of the perihelion ($\varpi_p = \Omega_p + \omega_p$, with ω_p the argument of the perihelion) and Ω_p the longitude of the ascending node.

Thus, we integrate the OSS with the symplectic integrator $SABA_4$ (see Section 5.1) for a time span of 5 Million years with a time step of 1/2 year. We tabulate the elliptic elements of the orbits of the planets in a mesh of 99,996 points and use them to make the frequency analysis of the functions (5.2). Finally, we obtain the basic frequencies of the planets: ν_p (mean motion frequency), g_p (perihelion frequency) and s_p (node frequency). Their values for Jupiter, Saturn, Uranus and Neptune can be seen in Table 5.2. In order to check this computation, we can compare this basic set of frequencies with others obtained in prior works (such as [Las90] or [NMC89]) or we can repeat the computations by halving the integration step. We also have tested it by using the method of the running box. The agreement, in all the cases, is good enough for our purposes.

5.2.3 Basic frequencies of the Trojan orbits

The computation of asteroid proper elements and basic frequencies for the Trojan case is a topic of research that has already been considered by many authors. See, for example, the works of Bien and Schubart ([SB86], [BJ87] and [SB87]), or the papers by Milani ([Mil93] and [Mil94]). See [BR01] for a more recent work.

In this section, we are interested in finding the basic frequencies that arise from the analysis of the orbits of the Trojan asteroids when we integrate them in the OSS with the same conditions as in 5.2.2. That is, we integrate the OSS together with 420 Trojans with the symplectic integrator $SABA_4$ for a time span of 5 Million years. We tabulate the osculating elliptic elements of the Trojan orbits in a mesh of 99,996 equidistant points. We evaluate the functions

$$\begin{aligned} \alpha_k(t) &= a_k(t)\,\exp(i(\lambda_k(t) - \lambda_5(t))), \\ \beta_k(t) &= e_k(t)\,\exp(i\varpi_k(t)), \\ \gamma_k(t) &= \sin\left(\frac{i_k(t)}{2}\right)\exp(i\Omega_k(t)), \end{aligned} \tag{5.3}$$

in this mesh of points for every asteroid (where $(a_k, e_k, i_k, \lambda_k, \varpi_k, \Omega_k)$ are the osculating orbital elements at time t of the Trojan asteroid with catalog number k and λ_5 is the mean longitude of Jupiter) and we apply Laskar's algorithm to obtain the firsts 10 frequencies

C.N.	Name	$\nu\,(deg)$	$g\,(sec)$	$s\,(sec)$
588	Achilles	2.434	344.40	-11.02
617	Patroclus	2.350	310.62	-6.76
624	Hektor	2.316	335.74	-12.99
659	Nestor	2.467	355.01	-16.48
884	Priamus	2.424	353.41	-12.24
911	Agamemnon	2.290	317.35	-8.69
1143	Odysseus	2.439	365.38	-10.91
1172	Aneas	2.366	331.54	-7.92
1173	Anchises	2.371	378.19	-23.67
1208	Troilus	2.199	258.54	-0.45
1404	Ajax	2.310	334.43	-15.15
1437	Diomedes	2.213	331.25	-20.05
1583	Antilochus	2.181	282.18	-10.79
1647	Menelaus	2.438	359.34	-9.96
1749	Telamon	2.421	366.33	-13.79
1867	Deiphobus	2.233	286.24	-5.76
1868	Thersites	2.316	345.09	-20.48
1869	Philoctetes	2.382	388.78	-20.44
1870	Glaukos	2.429	363.50	-9.48
1871	Astyanax	2.311	401.29	-25.28

Table 5.3: Basic frequencies of the Trojan asteroids in the Outer Solar System model. In the first column we display the catalog number of the asteroid and in the second one the asteroid's name. The frequency of libration can be seen in the third column, while in the fourth and fifth columns the two secular frequencies are shown.

that have maximum amplitude. From them, after removing the resonances with planets basic frequencies, we obtain the Trojans proper frequencies. The results for the 20 firsts numbered Trojan asteroids can be seen in Table 5.3, where the first column is the catalog number (C.N.) of the asteroid and the second contains its name. The third, fourth and fifth columns are the three basic frequencies (ν, g and s, respectively). For a complete list of the 420 Trojans studied, see Appendix B.1.

ν is the frequency of libration. It appears (usually when the frequencies of the planets are removed) as the basic frequency of the function $\alpha_k(t)$ and its related period is about 150 years. g and s are known as the secular frequencies and they correspond, respectively, to the secular motion of the asteroid's perihelion and node.

In Figure 5.2, the Trojan swarm is plotted in the frequency space. The projection into the ν-g plane is given in the first plot and into the g-s plane in the second one.

As a first test of this computation, we have repeated the integration with a time step of 0.25 years. The agreement of the frequencies computed in this case and in the prior one is good for the precision required. As a second checking, we have compared the values in Table 5.3 with the ones obtained by Milani [Mil93]. The differences are quite small and can come from using, possibly, different values for the mass parameters and/or from

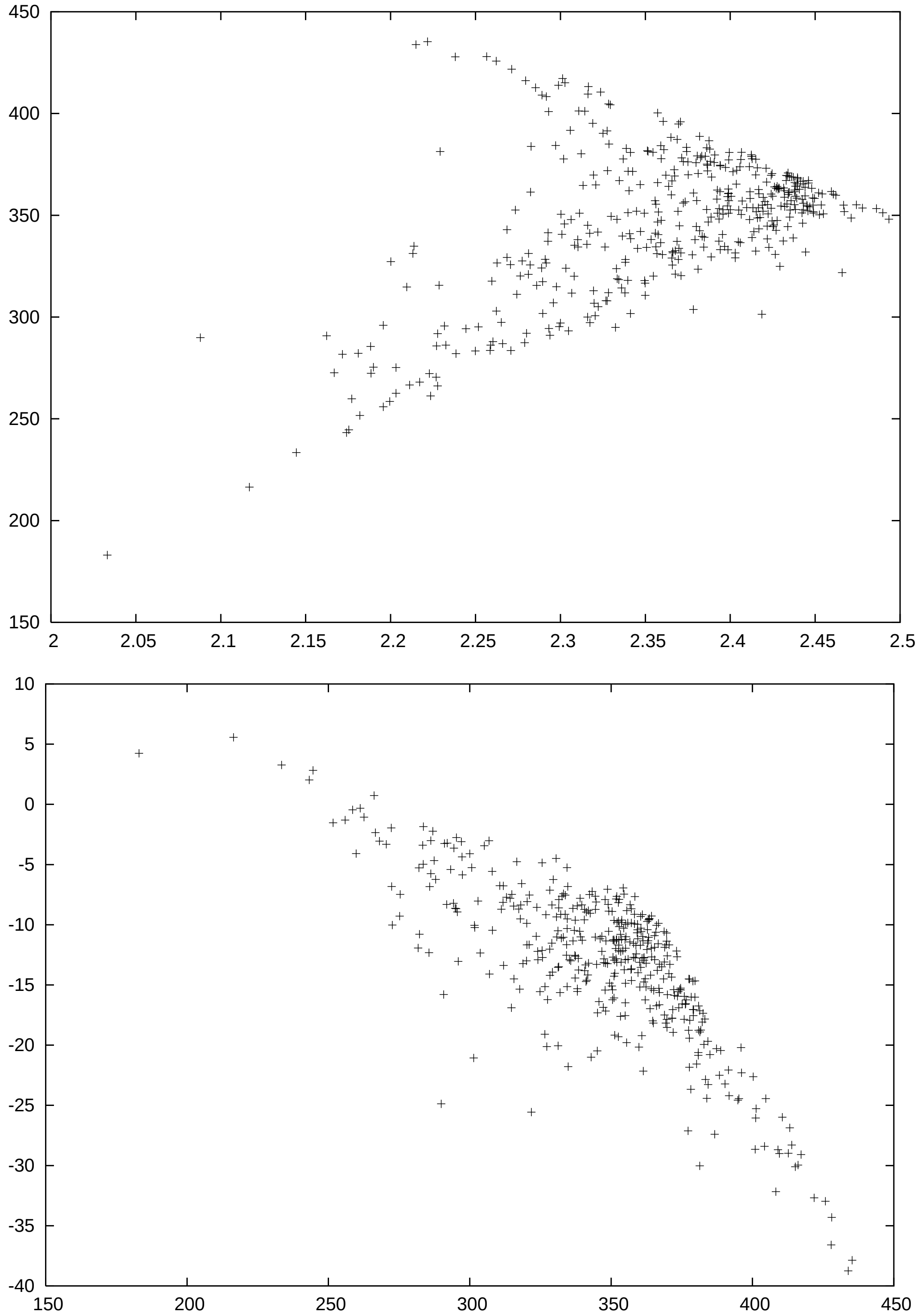

Figure 5.2: Distribution of the Trojan asteroids in the frequency space. Top: g in sec/yr versus ν in deg/yr. Bottom: s versus g, both in sec/yr.

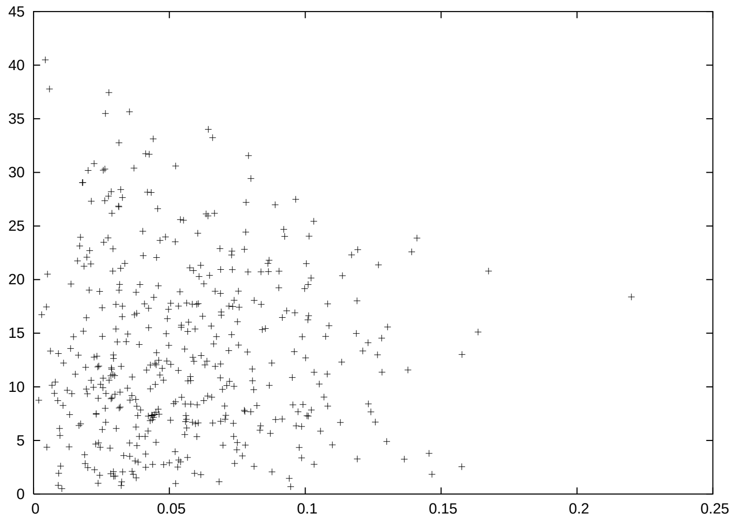

Figure 5.3: Distribution of the Trojan asteroids in the secular proper elements plane. In the x-axis, the proper eccentricity is plotted, and in the y-axis the proper inclination (in degrees).

the fact that Milani translates the origin of the initial conditions to the inner planets barycenter and we don't. Anyway, the results obtained are sufficiently accurate for our purposes.

The secular proper elements for the asteroids, e^* and i^*, are also computed just by taking the amplitudes corresponding to the secular frequencies, g and s, respectively. In Figure 5.3, we show the distribution of the proper eccentricity and inclination of the 420 Trojans studied.

We are also interested in looking at the distribution of the basic frequencies depending on the elliptic elements of the asteroids. In Figure 5.4, we display the different distribution of the three basic frequencies with respect the initial semi-major axis. We can clearly see that there is a symmetry around the semi-major axis of Jupiter ($a \simeq 5.2$). In Figure 5.5, we display the three basic frequencies with respect to the proper inclination. It seems that there is some dependence (the points distribute themselves more or less around a line) between the values of the frequencies (ν, g and s) and the proper inclination (i^*) of the asteroids.

5.2.4 Diffusion in frequencies of the Trojan orbits

The Frequency Map Analysis allows us also to estimate the diffusion rate of the Trojan orbits by computing the time behaviour of their basic frequencies (see [Las93]).

In order to do this, we integrate the orbit of 420 Trojans in the OSS in the interval of time $[0, T]$, where $T = 5$ Myrs. We evaluate the three basic frequencies of the Trojan orbits and we call them $\nu^{(1)}$, $g^{(1)}$ and $s^{(1)}$ (up to here, it corresponds to what we did in 5.2.3). Afterwards, we repeat the integration in the interval of time $[T, 2T]$ and we recompute the frequencies. In this case, we call them $\nu^{(2)}$, $g^{(2)}$ and $s^{(2)}$. Finally, we consider the values $\sigma_\nu = \log(1 - \nu^{(2)}/\nu^{(1)})$, $\sigma_g = \log(1 - g^{(2)}/g^{(1)})$ and $\sigma_s = \log(1 - s^{(2)}/s^{(1)})$ as an

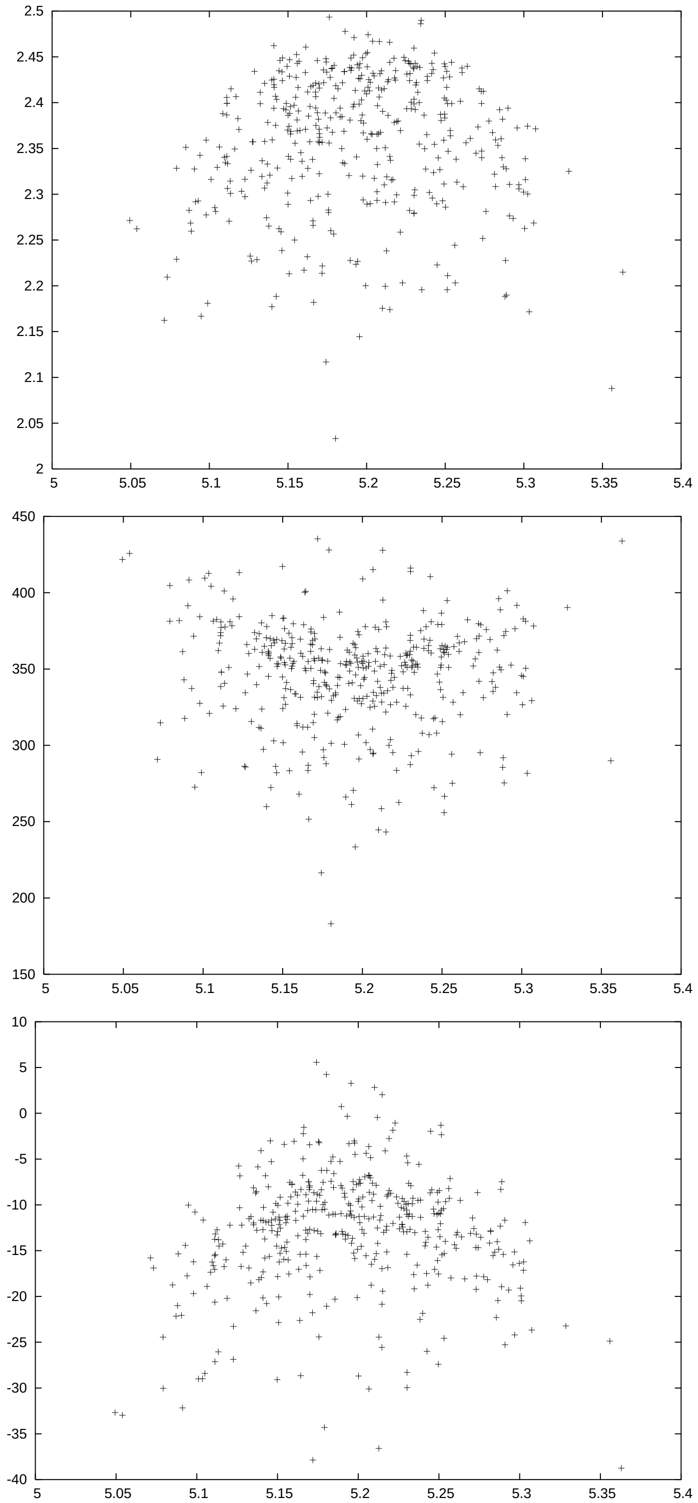

Figure 5.4: Distribution of the three basic frequencies (ν for the top picture, g for the middle one and s for the bottom one) depending on the initial osculating semi-major axis of the asteroids. Note the a symmetry around $a \simeq 5.2$ (Jupiter's semi-major axis).

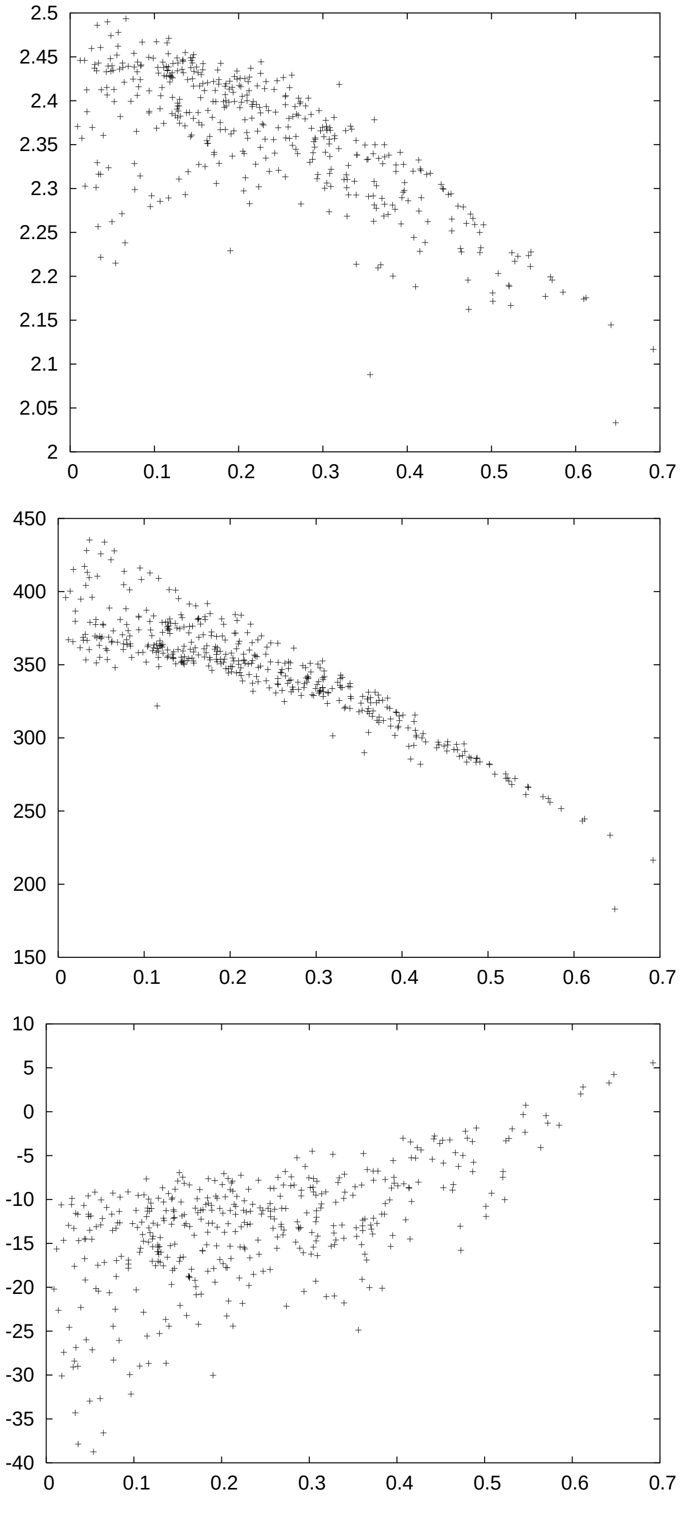

Figure 5.5: Distribution of the three basic frequencies (ν for the top picture, g for the middle one and s for the bottom one) depending on the proper inclination of the asteroids.

estimation of the diffusion rate. Figure 5.6 shows the representation of σ_ν versus ν, of σ_g versus g and of σ_s versus s.

5.3 Frequency analysis in semi-analytical models

In this section, we describe the results of a Fourier analysis of the Trojan orbits in some (semi-analytical) models. These models are the RTBP and some of the (time-dependent) perturbations that have been studied in this work: the BCCP, the ERTBP and the TCCP. The goal of these computations is to search for differences between these models when any study of the Trojans dynamics is focused. That is, to compare the performance of these semi-analytical models with the reality.

In order to achieve this, we can compute the three basic frequencies ν, g and s for every Trojan orbit in the different models by making a Fourier analysis of the functions (5.3). Afterwards, we compare the results of these computations with the ones obtained with the OSS model (that will be considered as the closest to the reality).

5.3.1 The Restricted Three Body Problem

First, the initial conditions for the 420 Trojan asteroids are taken from the Bowell Catalog [Bow] at the Julian date 2452200.5 (October 10th, 2001), in the same way as in 5.2.3. Second, we recompute these initial conditions in the RTBP frame of coordinates. Afterwards, we integrate the orbit of each Trojan in the circular RTBP for a time span of 1 Myr. and tabulate the functions (5.3) in a net of 99,996 equidistant points. Finally, in order to obtain the basic frequencies ν, g and s, a Fourier analysis is performed.

In this case, some asteroids escape from the Solar system (they reach a distance to the Sun that is greater than 100 times the Sun-Jupiter distance) before ending a 2 Myrs. trajectory. For some other asteroids, the frequency analysis of the orbits does not give a precise enough result; thus they are skipped over. The asteroids Catalog Numbers (C.N.) for the first case are 3801, 7815, 15440, 15539, 16956, 24449 and 24471, and for the last one are 1868, 2146, 2895, 4060, 5264, 7641, 12444, 12916, 12929, 18046, 19844, 23694 and 24531. Note that none of them appear in the Tables of results.

Thus, in Table 5.4, the three proper frequencies of the 20 firsts asteroids, for which we are able to compute them, are shown. For the complete frequency catalog, see Appendix B.2.

Let us make a side comment: It is usual in the literature to study the dynamics near the triangular points of the Sun-Jupiter RTBP by using some normal form of the Hamiltonian. This normal form can be written as

$$H(I,\theta) = \omega_1 I_1 + \omega_2 I_2 + \omega_3 I_3 + \mathcal{R}(I,\theta),$$

where $I = (I_1, I_2, I_3)$ and $\theta \in \mathbb{T}^3$ are the usual action-angle variables, $\mathcal{R}(I,\theta) = O(||I||^2)$ and $I_1 = I_2 = I_3 = 0$ corresponds to the triangular point L_4 or L_5. Thus, the "frequencies" ω_1, ω_2 and ω_3 can be taken as the frequencies of the fixed point L_4 or L_5 and their concrete

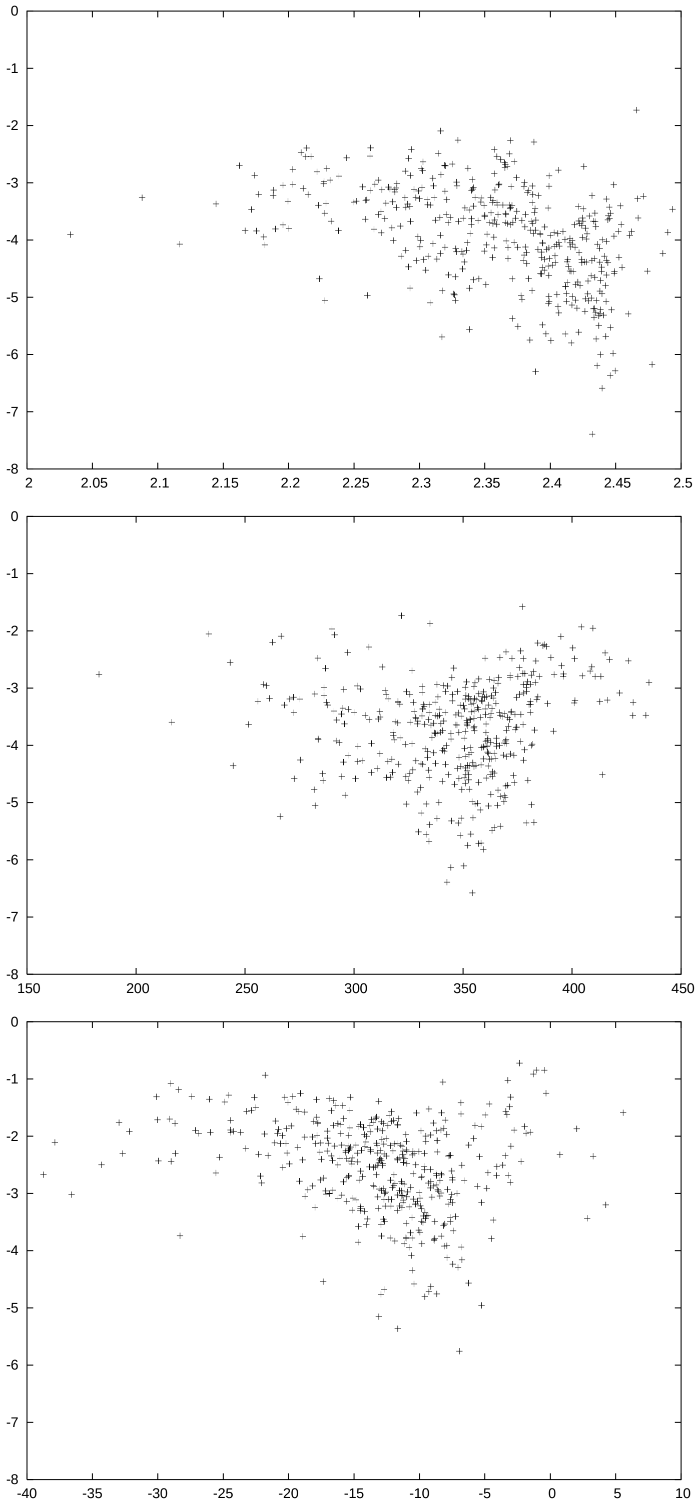

Figure 5.6: Distribution of the diffusion rates in the three basic frequencies of the Trojan asteroids. From top to bottom: σ_ν versus ν in deg/yr, σ_g versus g in sec/yr and σ_s versus s in sec/yr.

C.N.	Name	$\nu\,(deg)$	$g\,(sec)$	$s\,(sec)$
588	Achilles	2.370	320.95	-2.97
617	Patroclus	2.394	327.13	-4.53
624	Hektor	2.349	375.03	-12.79
659	Nestor	2.369	312.65	-5.72
884	Priamus	2.294	318.32	-10.13
911	Agamemnon	2.378	361.83	-7.02
1143	Odysseus	2.238	294.05	-4.61
1172	Aneas	2.169	246.16	2.39
1173	Anchises	2.264	306.65	-7.64
1208	Troilus	2.308	303.50	1.04
1404	Ajax	2.397	345.87	-7.24
1437	Diomedes	2.252	352.93	-14.89
1583	Antilochus	1.978	152.22	10.90
1647	Menelaus	2.200	289.80	-7.75
1749	Telamon	2.354	326.43	-3.65
1867	Deiphobus	2.202	263.21	3.47
1869	Philoctetes	2.269	326.03	-9.94
1870	Glaukos	2.208	272.46	0.84
1871	Astyanax	2.061	250.42	-15.12
1872	Helenos	2.039	202.41	-4.38

Table 5.4: Basic frequencies of the Trojan asteroids in the circular Restricted Three Body Problem. In the first column we display the catalog number of the asteroid and in the second one the asteroid's name. The frequency of libration can be seen in the third column, while in the fourth and fifth columns the two secular frequencies are shown.

numerical values for the RTBP are:

$$\begin{aligned}\omega_1 &= -0.080463875837,\\ \omega_2 &= 0.99675752552,\\ \omega_3 &= 1.0.\end{aligned}$$

If a Trojan asteroid move quasi-periodically (or almost quasi-periodically) "near" one of the triangular points, it is natural to think that the basic frequencies of the motion of the Trojan should be related, in some way, with a perturbation of these ω_1, ω_2 and ω_3. Let be $\tilde{\omega}_1$, $\tilde{\omega}_2$ and $\tilde{\omega}_3$ these perturbations (they normally appear when a Fourier analysis of the functions $f_x = \frac{x^2+p_x^2}{2}$, $f_y = \frac{y^2+p_y^2}{2}$ and $f_z = \frac{z^2+p_z^2}{2}$ is performed). Then, it is easy to see that this three basic frequencies are related with the three proper frequencies ν, g and s in the following manner:

$$\begin{aligned}\nu &= \tilde{\omega}_1 \frac{2\pi}{T_5}\frac{180}{\pi}, \\ g &= (1-\tilde{\omega}_2)\frac{2\pi}{T_5}\frac{180}{\pi}3600, \\ s &= (1-\tilde{\omega}_3)\frac{2\pi}{T_5}\frac{180}{\pi}3600,\end{aligned} \tag{5.4}$$

where $T_5 = 11.862$ is the sidereal period (in years) of Jupiter's orbit.

In Table 5.5, we show the values of $\tilde{\omega}_1$ for the several studied models. The difference between these values and ω_1 gives us an idea of "how far", in the RTBP, is the asteroid from the librating point. For the other semi-analytical models, we should compare them with the frequency of the corresponding invariant object.

5.3.2 The Bicircular Coherent Problem

In this section, we perform a similar frequency analysis of the orbits than in 5.3.1, but using the BCCP (2.2) as the model for the Trojan motion. In this case, the actual position of Saturn in the Julian date 2452200.5 is used in order to fix the phase of the (periodic time-dependent) perturbation.

In this case, the Catalog Numbers of the escaped particles are 1868, 2146, 2895, 3801, 4060, 5264, 7641, 7815, 12444, 12916, 12929, 15440, 15527, 15539, 15977, 16956, 18046, 19844, 22180, 24449, 24471 and 24531. Thus, we have been able to determine the three proper frequencies for 398 Trojans. Their numerical values are shown in Appendix B.3.

5.3.3 The Elliptic Restricted Three Body Problem

We integrate the ERTBP (3.6) with the same conditions as in the former sections. The phase of the time-dependent perturbation is obtained by computing the actual perihelion argument of Jupiter's orbit in the Julian date 2452200.5 and solving equation (3.2).

In this case, the Catalog Numbers of the escaped particles are 1868, 1873, 3801, 4946, 15440, 15539, 24471 and 24531. There are some cases for which the proper frequencies

$\tilde{\omega}_1$						
C.N.	Name	OSS	RTBP	BCCP	ERTBP	TCCP
588	Achilles	0.080195	0.078084	0.078097	0.078524	0.078099
617	Patroclus	0.077431	0.078879	0.078898	0.079341	0.078901
624	Hektor	0.076299	0.077394	0.077354	0.077441	0.077364
659	Nestor	0.081280	0.078065	0.078073	0.077198	0.078087
884	Priamus	0.079874	0.075595	0.075557	0.077358	0.075599
911	Agamemnon	0.075440	0.078353	0.078347	0.078122	0.078338
1143	Odysseus	0.080375	0.073745	0.073731	0.074371	0.073763
1172	Aneas	0.077967	0.071468	0.071465	0.071942	0.071481
1173	Anchises	0.078138	0.074612	0.074652	0.075012	0.074625
1208	Troilus	0.072473	0.076044	0.076052	0.076437	0.076046
1404	Ajax	0.076125	0.078972	0.078943	0.077430	0.078925
1437	Diomedes	0.072922	0.074216	0.074217	0.074698	0.074266
1583	Antilochus	0.071864	0.065181	0.065193	0.065448	0.065198
1647	Menelaus	0.080348	0.072482	0.072460	0.072651	0.072495
1749	Telamon	0.079785	0.077557	0.077562	0.077767	0.077545

Table 5.5: $\tilde{\omega}_1$ values for the OSS and the semi-analytic models. They are computed from equation (5.4).

cannot be well determined. The corresponding C.N. are 2146, 2363, 7641, 7815, 11395, 12444, 12916, 12929, 15527, 15977, 16956, 18046, 19844, 24449 and 24587.

The concrete values of the proper frequencies of the rest 397 Trojan asteroids can be found in Table B.4 of Appendix B.4.

5.3.4 The Tricircular Coherent Problem

With the same conditions as before, the equations corresponding to the TCCP model (4.17) are integrated. The initial phases for the quasi-periodic angles θ_1 and θ_2 are obtained from the actual positions of Saturn and Uranus in the Julian date 2452200.5.

In this simulation, 20 asteroids do not survive to the integration (they escape from the Solar system). Their catalog numbers are 1868, 2146, 2895, 3801, 4060, 5264, 7641, 12444, 12916, 12929, 15440, 15527, 15539, 15977, 16956, 19844, 22180, 24449, 24471 and 24531. On the other hand, for the asteroids 7815 and 18046, the proper frequencies are not well determined.

The basic frequencies of the rest 377 asteroids can be found in Table B.5 of Appendix B.5.

5.3.5 Comparison between the OSS and the semi-analytical models

We are interested in the performance of the semi-analytical models when describing the dynamics of the Trojan asteroids. In order to achieve this, we show a brief comparison

Frequency of libration (ν)						
C.N.	Name	OSS	RTBP	BCCP	ERTBP	TCCP
588	Achilles	2.434	0.026	0.026	0.021	0.026
617	Patroclus	2.350	0.019	0.019	0.025	0.019
624	Hektor	2.316	0.014	0.014	0.015	0.014
659	Nestor	2.467	0.040	0.039	0.050	0.039
884	Priamus	2.424	0.054	0.054	0.031	0.054
911	Agamemnon	2.290	0.039	0.039	0.036	0.038
1143	Odysseus	2.439	0.082	0.083	0.075	0.082
1172	Aneas	2.366	0.083	0.083	0.077	0.083
1173	Anchises	2.371	0.045	0.045	0.040	0.045
1208	Troilus	2.199	0.049	0.049	0.055	0.049
1404	Ajax	2.310	0.037	0.037	0.017	0.037
1437	Diomedes	2.213	0.018	0.018	0.024	0.018
1583	Antilochus	2.181	0.093	0.093	0.089	0.093
1647	Menelaus	2.438	0.098	0.098	0.096	0.098
1749	Telamon	2.421	0.028	0.028	0.025	0.028

Table 5.6: Relative differences between the frequencies of libration of the 15 firsts numbered Trojan asteroids computed in the different models. In the first and second columns we display the catalog number and the name of the asteroid. The frequency of libration in the "realistic" model can be seen in the third column. From columns four to seven, the relative differences $\left|\frac{\nu^{OSS}-\nu^{model}}{\nu^{OSS}}\right|$ are shown.

between the values of the proper Trojan frequencies obtained in the "realistic" model (OSS) and the RTBP, BCCP, ERTBP and TCCP.

In Table 5.6, the relative differences between the frequencies of libration around the (corresponding) triangular point obtained with the several models are shown. We see that all these models simulate in an acceptable way the librational motion, since the relative differences between the frequency corresponding to this motion in the OSS and in the models is less than 10%. But, we do not see any significant difference between the models themselves.

Finally, let us mention that, for what concerns the secular motion, the semi-analytical models simulate it in a worse way (for instance, see Table 5.7 for a comparison between the Perihelion frequencies). This was expected, since the Trojan secular frequencies mainly come from the indirect action of the perturbative planets (Saturn, Uranus and Neptune) to Jupiter's motion and their motion is not simulated accurately enough in these semi-analytical models.

Perihelion's frequency (g)						
C.N.	Name	OSS	RTBP	BCCP	ERTBP	TCCP
588	Achilles	344.40	0.07	0.05	0.07	0.05
617	Patroclus	310.62	0.05	0.07	0.05	0.07
624	Hektor	335.74	0.12	0.14	0.12	0.14
659	Nestor	355.01	0.12	0.11	0.10	0.11
884	Priamus	353.41	0.10	0.09	0.12	0.09
911	Agamemnon	317.35	0.14	0.16	0.16	0.16
1143	Odysseus	365.38	0.20	0.19	0.20	0.19
1172	Aneas	331.54	0.26	0.25	0.26	0.25
1173	Anchises	378.19	0.19	0.18	0.19	0.18
1208	Troilus	258.54	0.17	0.19	0.17	0.19
1404	Ajax	334.43	0.03	0.05	0.08	0.06
1437	Diomedes	331.25	0.07	0.08	0.06	0.08
1583	Antilochus	282.18	0.46	0.45	0.46	0.45
1647	Menelaus	359.34	0.19	0.18	0.19	0.18
1749	Telamon	366.33	0.11	0.10	0.11	0.09

Table 5.7: Relative differences between the frequencies of the perihelion argument of the 15 firsts numbered Trojan asteroids computed in the different models. In the firsts two columns we display the catalog number and the name of the asteroid. The perihelion's frequency in the "realistic" model can be seen in the third column. From columns four to seven, the relative differences are shown.

Chapter 6

Final remarks and conclusions

The usual studies on the dynamics of the Trojan asteroids can be roughly divided in several categories, according to the models used. Some of the works use the classical RTBP. The closed (and simple) form of this model allows to apply analytical ([GDF+89]) and semi-analytical ([Sim89, CG91]) tools to it, to conclude results that are either a mathematical proof, or quite close to it.

Some other works use the OSS model. Due to its complexity, this model has been only used for numerical studies, based on long term numerical integrations of the motion of the asteroids. Note that, generically speaking, to derive –analytically– stability results for an asteroid in the OSS requires an analytical stability result for the Outer Solar System itself, which seems a harder problem.

In this scenario, there are two kinds of improvements needed to study the dynamics of the Trojan asteroids for realistic models:

a) Theoretical advances: we need a stability theory for the neighbourhood of a nearly quasi-periodic solution, ready to be used in practical examples.

b) Computational advances: we need numerical procedures to approximate the motion of Trojan asteroids, with a quite high degree of accuracy.

Recently, there have been advances in both directions that, apparently, make this goal feasible. For one side, there are results on KAM theory that do not require the use of action-angle variables and can be applied far from equilibrium points.[1] They only require to compute an approximate quasi-periodic orbit (plus some technical conditions, see [Gon02] for details). On the other side, recent advances on computational techniques allow for the computation of accurate quasi-periodic trajectories of Hamiltonian systems (see, for instance, [RL01] and the previous chapters of this memoir).

The present work can be seen as the start of a long term project that aims to fill the gap between the theoretical developments on the stability of Hamiltonian systems and the numerical computation of regular orbits. The ultimate goal is to compute an approximate quasi-periodic solution for a Trojan asteroid[2] and to use a result of the type contained in [Gon02] to conclude its practical stability for the estimated life time of the Solar system.

[1] This has been done in [JV98], but still using action-angle variables that makes the computations extremely cumbersome.

[2] Of course, Trojans whose dynamics is not quasi-periodic are not considered.

In this work we have tried to develop some basic steps in this direction. First, we have built some models that can be seen as corrections to the RTBP towards the OSS model. Then, we have designed numerical methods and software to compute quasi-periodic solutions, its –symplectic– Floquet theory, normal forms (and approximate first integrals) up to a high order, and the procedures to bound the remainders so that we can derive regions of effective stability around these orbits. We have proceeded gradually, starting from simple models (BCCP) to more complex ones (BAP and TCCP).

6.1 On the periodic models

In Chapter 2, we have developed a model for the motion of an asteroid under the gravitational attraction of Sun, Jupiter and Saturn. This model is based on computing, in suitable coordinates, a periodic orbit for these three bodies. This model is the natural extension of the RTBP to include three primaries, in the sense that they move in the simplest solution that resembles the planetary system. Then, assuming that Sun, Jupiter and Saturn move on this orbit, it is not difficult to write the equations of motion for the asteroid; this is what we refer as BCCP. In suitable coordinates, the BCCP is a periodic time-dependent perturbation of the well known RTBP.

In the BCCP, the Lagrangian points $L_{4,5}$ are replaced by periodic orbits. Thus, we have performed a study of the dynamics around this periodic orbit. By means of a high order normal form calculation, it is possible to compute approximations to invariant tori (of dimensions 2, 3 and 4) nearby. Moreover, using suitable estimates on the remainder of this normal form, we have also derived a region such that the time needed to go away from it is bigger that the age of the Solar system. We have also used a second approach for the computation of these regions of effective stability: the computation of a suitable first integral. We have seen that the first integral produces a slightly larger region of stability but, on the other hand, it does not provide with a complete description of the dynamics inside this region as the normal form does. As we have used the same estimates for both approaches, it seems that first integrals are more suitable than normal forms for estimating practical stability regions, but normal forms give a complete description of the dynamics inside the region.

Chapter 3 can be seen as an application of the tools developed in the previous chapter. The results obtained are not completely new (see [JS94]); although the process to produce them is slightly different (we have used the physical time as independent variable while [JS94] uses the true anomaly) and we have also computed an approximate first integral. One of the main interests of this model is that it includes a 1:1 (exact) resonance between the vertical mode of the periodic orbit that replaces L_5 and the frequency of the perturbation.

6.2 On the quasi-periodic models

Chapter 4 contains, in our opinion, the most interesting results of this memoir. We have first considered the development of better models than the BCCP, in two different ways. First, we have computed a quasi-periodic solution of the general planar three body problem (BAP) to better simulate Jupiter's motion (compared to the BCCP), and then we have added a fourth massive body (Uranus) to the model (TCCP). Again, the solution that we have computed for the Sun-Jupiter-Saturn-Uranus system is the simplest planetary one. In this sense, the TCCP is the natural extension of the RTBP that includes four primaries.[3]

Next, we focus on a preliminary study of the TCCP model. Although the BAP has not been studied in the memoir, it contain many interesting features that make it worth to consider. For instance, the perturbation with respect to the RTBP is quite strong, such that it seems to produce bifurcations near the triangular points. This is actually work in progress.

The study of the TCCP is based on computing the quasi-periodic orbit that replaces the equilibrium point, the symplectic Floquet change for it and on constructing a high order normal form to describe the local non-linear dynamics in a zone near the L_5 point. On the other hand, an approximate first integral of the system is used to find a region of effective stability. We believe that the tools developed in this chapter will be very useful in future studies of this problem.

An important point is that the regions of effective stability for the different models considered are not contained one each other. This is due to the fact that, when the perturbation is changed, the solution that replaces the Lagrangian point changes so that the region of stability move to a different place. In particular this implies, for instance, that the stability regions for the BCCP and TCCP are not contained in the stability region of the RTBP.

6.3 On the OSS model

To discuss the quality of the previous models (as well as of any other model) we need to compare with the dynamics in the real Solar system. To this end, in Chapter 5, we have done long term numerical integrations of the OSS model. More concretely, we have computed the proper frequencies of 420 Trojan asteroids. For every asteroid, 14 frequencies appear as to play some role: we have 3 proper frequencies (one fast and two secular ones) for every planet (except Jupiter, for which 2 are enough) and the asteroid proper ones. These asteroid proper frequencies are the frequency of libration (around the corresponding triangular point) and two secular ones (corresponding to node and perihelion precessions). A similar analysis has been done for the RTBP, ERTBP, BCCP and TCCP models.

A general conclusion is that all these models simulate in an acceptable way the librational motion but, on the other hand, the secular motion is not well simulated by any of them mainly due to the fact that the motion of Jupiter in the models is too far from reality.

An important conclusion of these calculations is that the RTBP is not an accurate model to describe the Trojan motion. In fact, as the BCCP, ERTBP and TCCP are still too close to the RTBP, it turns out that none of them is an accurate model for the Trojan

[3] A different methodology for constructing semi-analytical models is given in [GMM02].

family. However, we also want to note that the level of accuracy of these models is not uniform but it depends on the asteroid considered.

Although it may seem that the developed models are not close enough to reality to be considered interesting, we believe that we need to design methods, tools and numerical algorithms to deal with them as a prior step to deal with realistic models. In this sense, we also think that some of the techniques developed here (mainly, the computation of the dynamics around quasi-periodic solutions) can play a relevant role in the future.

Appendix A

Fourier coefficients of the semi-analytical models

In this appendix, we give the tables that contain the Fourier coefficients of the truncated series used in the construction of the semi-analytical models BCCP, ERTBP, BAP and TCCP.

A.1 Fourier coefficients of the BCCP Hamiltonian

Table A.1: Fourier coefficients of the α_j functions for the BCCP Hamiltonian.

k	α_{1k}	α_{2k}
0	1.0000229103367e+00	
1	-2.4625442466082e-04	7.3489010270281e-05
2	1.0692997833207e-03	-6.3838867444849e-04
3	1.1072514120538e-04	-9.9274907586755e-05
4	2.9395638118780e-05	-3.4773894741059e-05
5	9.6357689500536e-06	-1.4298396775494e-05
6	3.5898146133472e-06	-6.3979830253489e-06
7	1.4410862906317e-06	-2.9979375918958e-06
8	6.0824013631496e-07	-1.4465316666017e-06
9	2.6614065300065e-07	-7.1220154567716e-07
10	1.1966249108316e-07	-3.5585209038792e-07
11	5.4958783422932e-08	-1.7979955710516e-07
12	2.5676210989306e-08	-9.1644956539906e-08
13	1.2164925220641e-08	-4.7041404009398e-08
14	5.8313526149925e-09	-2.4285784691065e-08
15	2.8231508669084e-09	-1.2598151894953e-08
16	1.3784483145000e-09	-6.5617762784026e-09
17	6.7801911497764e-10	-3.4295814921550e-09
18	3.3564142722057e-10	-1.7978841280872e-09

Table A.1: Coef. of the BCCP Hamiltonian (continued).

19	1.6708562404220e-10	-9.4496759384261e-10
20	8.3581273137913e-11	-4.9781719277559e-10
21	4.1980189546065e-11	-2.6278872316222e-10
22	2.1153800361327e-11	-1.3897319248812e-10
23	1.0679961410137e-11	-7.3614276754566e-11
24	5.3913470680877e-12	-3.9050764190409e-11
25	2.7113331748446e-12	-2.0743116521916e-11
26	1.3484095106391e-12	-1.1031719256898e-11
27	6.5357191716947e-13	-5.8734235014882e-12
28	2.9841178255536e-13	-3.1302409488675e-12
29	1.1686197120064e-13	-1.6698014620367e-12
30		-8.9152275313946e-13
31		-4.7633548461561e-13
32		-2.5468448292376e-13
33		-1.3627804460175e-13
34		
35		
36		
37		
38		
39		
k	α_{3k}	α_{4k}
0	9.9999999999996e-01	1.8683998336181e-08
1	-2.2690009041484e-04	-8.4902019367202e-05
2	1.1363399491921e-03	6.1119009876598e-09
3	1.4136168493846e-04	-6.7719183997133e-08
4	4.4107455176617e-05	-3.5059978301804e-08
5	1.6876958861351e-05	-2.1449287908083e-08
6	7.2162964157201e-06	-1.2865543976738e-08
7	3.2797951707916e-06	-7.5942597889570e-09
8	1.5491190393914e-06	-4.4309481776779e-09
9	7.5103465539173e-07	-2.5631437413467e-09
10	3.7098142180483e-07	-1.4729218230818e-09
11	1.8582126179188e-07	-8.4199627253305e-10
12	9.4079610762909e-08	-4.7927857076890e-10
13	4.8036708770421e-08	-2.7184824645694e-10
14	2.4695509277314e-08	-1.5373202008873e-10
15	1.2767319353483e-08	-8.6713668070536e-11
16	6.6315320635797e-09	-4.8802764491092e-11
17	3.4581591802673e-09	-2.7412900395289e-11
18	1.8094310379346e-09	-1.5371559456188e-11
19	9.4951415926778e-10	-8.6062784716560e-12
20	4.9952036015783e-10	-4.8118990780187e-12

Table A.1: Coef. of the BCCP Hamiltonian (continued).

21	2.6335950126803e-10	-2.6870763063189e-12
22	1.3910823012993e-10	-1.4988429844728e-12
23	7.3590899572993e-11	-8.3519567146204e-13
24	3.8975472003626e-11	-4.6495795153670e-13
25	2.0654834223060e-11	-2.5862161911170e-13
26	1.0942941344773e-11	-1.4373717430659e-13
27	5.7876067508202e-12	
28	3.0474789497484e-12	
29	1.5895632089763e-12	
30	8.1281103126901e-13	
31	3.9864454704904e-13	
32	1.7762737864127e-13	
33		
34		
35		
36		
37		
38		
39		
k	α_{5k}	α_{6k}
0		1.0000113790275e+00
1	8.5038739285915e-05	-1.2310815571124e-04
2	9.0042160544415e-10	5.3463936985746e-04
3	6.6847162817034e-08	5.5394410077412e-05
4	3.3789429836980e-08	1.4629397040756e-05
5	2.0586042700103e-08	4.8038307284955e-06
6	1.2356399258993e-08	1.7904636579843e-06
7	7.3089050441129e-09	7.1893707037605e-07
8	4.2746562023276e-09	3.0348698554719e-07
9	2.4785285257152e-09	1.3280647828267e-07
10	1.4273953770014e-09	5.9716865285170e-08
11	8.1758426458481e-10	2.7428323421911e-08
12	4.6621243388905e-10	1.2814770897150e-08
13	2.6486124514575e-10	6.0715948627968e-09
14	1.4999717545588e-10	2.9105292390507e-09
15	8.4717310296649e-11	1.4090973320662e-09
16	4.7735483982614e-11	6.8800862121621e-10
17	2.6842146941483e-11	3.3839839892254e-10
18	1.5066221391336e-11	1.6750153628245e-10
19	8.4428628978439e-12	8.3365861135690e-11
20	4.7244021728395e-12	4.1683410110021e-11
21	2.6402083422443e-12	2.0917395828236e-11
22	1.4737281057965e-12	1.0521182329644e-11

Table A.1: Coef. of the BCCP Hamiltonian (continued).

23	8.2173293911073e-13	5.2927613953424e-12
24	4.5773965813371e-13	2.6528033362031e-12
25	2.5475121389577e-13	1.3149319394888e-12
26	1.4166254541944e-13	6.3454154644198e-13
27		2.8771322535924e-13
28		1.1043509119259e-13
29		
30		
31		
32		
33		
34		
35		
36		
37		
38		
39		
k	α_{7k}	α_{8k}
0	-9.5119006464056e-05	
1	-1.8329661864760e+00	1.8337450514950e+00
2	-2.9367433444226e-04	3.3361070260376e-04
3	-1.6370880944081e-03	1.6425448004752e-03
4	-1.8365505787890e-04	1.8457416665148e-04
5	-4.9450725079203e-05	4.9606585602030e-05
6	-1.6325554708267e-05	1.6342581026461e-05
7	-6.1142165432777e-06	6.1092374518341e-06
8	-2.4658502950480e-06	2.4602100818054e-06
9	-1.0451201414901e-06	1.0415553346148e-06
10	-4.5903435562686e-07	4.5708275431929e-07
11	-2.0709877586864e-07	2.0608977144147e-07
12	-9.5411188282379e-08	9.4903232393163e-08
13	-4.4700023198492e-08	4.4447630075285e-08
14	-2.1231804110912e-08	2.1107192827594e-08
15	-1.0201087693978e-08	1.0139747346973e-08
16	-4.9490508198564e-09	4.9189012476368e-09
17	-2.4210825496966e-09	2.4062890435151e-09
18	-1.1929493142679e-09	1.1857176667276e-09
19	-5.9149946233812e-10	5.8799582702008e-10
20	-2.9488924238224e-10	2.9322802022019e-10
21	-1.4771221716195e-10	1.4696227465797e-10
22	-7.4284775195241e-11	7.3986884270086e-11
23	-3.7473052275067e-11	3.7400716963246e-11
24	-1.8937759895552e-11	1.8977153763911e-11

Table A.1: Coef. of the BCCP Hamiltonian (continued).

25	-9.5677917478410e-12	9.6633362047704e-12
26	-4.8143498721907e-12	4.9377717872101e-12
27	-2.3952732098106e-12	2.5321037487699e-12
28	-1.1606207988323e-12	1.3038289746771e-12
29	-5.2829803293851e-13	6.7502087180315e-13
30	-2.0505915863890e-13	3.5239655881542e-13
31		1.8582020700132e-13
32		1.0010092665032e-13
33		
34		
35		
36		
37		
38		
39		

A.2 Fourier coefficients of the ERTBP Hamiltonian

k	α_{1k}	α_{2k}
0	1.00117298538995e+00	
1	-9.68704963045320e-02	4.83501577213403e-02
2	5.85646038583858e-03	-3.50774827835306e-03
3	-3.68213874846975e-04	2.40344008577281e-04
4	2.35159378617304e-05	-1.61828837052564e-05
5	-1.51412317299167e-06	1.08101809263866e-06
6	9.79675371792316e-08	-7.18971983402371e-08
7	-6.35911769791538e-09	4.76888974059318e-09
8	4.13700140846200e-10	-3.15745541403711e-10
9	-2.69583380515066e-11	2.08792297472776e-11
10	1.75855300912059e-12	-1.37887710954116e-12
11	-1.15124602563699e-13	9.14522763175808e-14
12	7.31121489901978e-15	-5.64852202751241e-15
k	α_{3k}	α_{4k}
0	1.00000000000000e+00	1.00000000000000e+00
1	-9.67570017550984e-02	-4.83784953411305e-02
2	5.84959889180137e-03	2.34002199050274e-03
3	-3.67782471381216e-04	-1.27326511096275e-04
4	2.34883863276647e-05	7.29865686034066e-06
5	-1.51234920953979e-06	-4.30910078921953e-07
6	9.78527574166718e-08	2.59294977719740e-08
7	-6.35166730699347e-09	-1.58115578371107e-09
8	4.13215469417840e-10	9.73680162773051e-11
9	-2.69266417505108e-11	-6.04157458963682e-12
10	1.75655609728757e-12	3.76858985004082e-13
11	-1.14995198367677e-13	-2.38707368961630e-14
12	7.31314904406652e-15	1.34010530426405e-15

Table A.2: Real Fourier coefficients of the α_j functions for the ERTBP Hamiltonian.

A.3 Fourier coefficients of the BAP Hamiltonian

k_1	k_2	α^+_{1k}	α^-_{1k}	α^+_{2k}	α^-_{2k}
0	0	1.0012005708e+00			
1	0	-2.4815098142e-04		7.3672422723e-05	
0	1	1.4029937539e-04		-8.5639486462e-06	
2	0	1.0960862810e-03		-6.4890366115e-04	
1	1	-6.9015522178e-05	-1.7613232873e-06	2.9159795163e-05	-2.0823826150e-06
0	2	-8.1796687544e-07		3.7365269957e-07	
3	0	1.0139637739e-04		-9.3726011699e-05	
2	1	2.2645717633e-05	9.7074096718e-02	-1.4685465534e-05	-4.8448545618e-02
1	2	-3.7513125445e-05	-9.4041573332e-06	1.8541850579e-05	6.3099860119e-07
0	3	-4.9135929446e-08		2.3959571832e-08	
4	0	3.1920890353e-05		-3.6373210600e-05	
3	1	4.7465358994e-07	-4.2502882354e-05	-1.8465965247e-06	2.4285825409e-05
2	2	6.6876937521e-07	-1.3940506628e-05	-4.5339192162e-07	8.5955542933e-06
1	3	4.3128955834e-08	-5.8373958936e-07	-2.1231004810e-08	-8.7460026101e-09
0	4	7.0718574586e-10		1.0155648952e-10	
5	0	9.7386391057e-06		-1.4418442978e-05	
4	1	1.9167397951e-06	1.2867775283e-04	-2.1910580096e-06	-8.2630254064e-05
3	2	1.6861771321e-07	2.8877650057e-07	-1.6379213242e-07	-3.6872151075e-07
2	3	1.6002365878e-08	-1.7004323856e-07	-8.9425210224e-09	4.3578694010e-08
1	4	2.0398947613e-11	-7.4167379510e-09	2.0629614167e-10	-9.5523176292e-10
0	5	1.2093928682e-09		-5.7088450266e-10	
5	1	7.7065385647e-07	1.1937696969e-05	-1.0983523731e-06	-9.8752246512e-06
4	2	9.0110148112e-08	5.8810285673e-03	-1.0297894823e-07	-3.5222752368e-03
3	3	4.8293854780e-09	-1.8628276108e-06	-3.6230538255e-09	8.2454316931e-07
2	4	1.1169205322e-09	-1.7632874441e-10	-5.3531542846e-10	-3.8543406200e-10
1	5	-3.3175914248e-11	4.4658537860e-11	3.1061625880e-11	5.1763455906e-12
5	2	4.3162391111e-08	-4.3543858261e-06	-6.0134495088e-08	2.7839511123e-06
4	3	3.0952705500e-09	-2.1256076177e-06	-2.9286653655e-09	1.3950477752e-06
3	4	5.1394428021e-11	8.7452132174e-07	3.2080376814e-11	-4.6809066397e-07
2	5	-1.2340069490e-11	6.1064846224e-10	1.6786083891e-11	-6.3629160212e-11
5	3	1.6616129617e-09	4.5610568748e-08	-2.0060349396e-09	-4.4404825737e-08
4	4	5.5196248223e-11	-2.1010412559e-08	-1.1480477809e-11	1.0069292977e-08
3	5	-4.4599955239e-12	1.1139536837e-09	9.2360679825e-12	-5.5324078529e-10
5	4	4.0487134828e-11	-1.9634168365e-07	-2.4268100564e-11	1.1029582233e-07
4	5	-1.4175629460e-12	2.2865648103e-10	5.0538686305e-12	-1.7735861776e-10
5	5	-3.3051586196e-13	1.0835436773e-07	2.7039633938e-12	-6.7187777538e-08

Table A.3: Fourier coefficients of the α_i functions for the BAP (I).

k_1	k_2	α^+_{3k}	α^-_{3k}	α^+_{4k}	α^-_{4k}
0	0	9.9999980195e-01		3.4996492977e-08	
1	0	-2.2785938970e-04		-8.4734308679e-05	
0	1	8.8178754301e-05		-7.1378744476e-06	
2	0	1.1590376222e-03		-1.6692621009e-07	
1	1	-6.7385510206e-05	3.0327819854e-06	-4.3034852128e-08	6.3025396506e-06
0	2	-1.1869933265e-06		-1.7152722239e-08	
3	0	1.3190268132e-04		-6.8888070333e-08	
2	1	2.4389410250e-05	9.6958043271e-02	-1.3358171529e-10	3.7949585198e-09
1	2	-3.7417763500e-05	-5.6729831736e-06	4.1793025862e-10	-5.1619790534e-07
0	3	-5.9922033170e-08		2.4510971060e-09	
4	0	4.6640553426e-05		-3.4893083547e-08	
3	1	1.7866942055e-06	-4.2573111867e-05	-2.0783307660e-09	-2.0538050743e-06
2	2	7.1761583131e-07	-1.6807057883e-05	8.6263859326e-10	5.2252265638e-07
1	3	4.0089678517e-08	2.2579924283e-07	8.7611781947e-11	-1.7856731590e-09
0	4	1.1685862826e-10		1.0586796980e-11	
5	0	1.7023165025e-05		-2.1422819214e-08	
4	1	2.7636488101e-06	1.3212916031e-04	-1.6891619838e-09	-2.9017320861e-09
3	2	2.1622271252e-07	5.3877681890e-07	-5.0218202167e-11	-4.0511075563e-08
2	3	1.4819029484e-08	-1.1885819398e-07	6.2305720476e-12	-3.4984151514e-08
1	4	-2.3206898629e-10	-7.0745904960e-09	4.9431175437e-13	3.4663904124e-10
0	5	1.1752728740e-09		1.2728517799e-14	
5	1	1.2931388260e-06	1.3923045171e-05	-1.3799612993e-09	-2.5272153516e-09
4	2	1.2779167664e-07	5.8739923454e-03	-6.4765348143e-11	-4.3070334121e-11
3	3	4.9978383184e-09	-1.7047108288e-06	2.7828227601e-12	3.6702267420e-08
2	4	9.6815343215e-10	6.0409458075e-10	3.8693259806e-13	-3.0043876042e-10
1	5	-4.5267613172e-11	2.8487030260e-11	-3.2896768700e-14	2.1512563748e-12
5	2	7.0303183233e-08	-4.3684781119e-06	-6.3097455865e-11	-7.4671556315e-08
4	3	3.7283368243e-09	-2.2895229868e-06	7.5162208218e-13	-3.0958174619e-09
3	4	-2.2694060291e-11	9.1491639243e-07	2.8413049014e-13	-2.0526787231e-09
2	5	-2.1351122923e-11	4.2610846313e-10	1.7460937749e-14	3.4315212273e-11
5	3	2.3704941667e-09	6.2362914326e-08	-4.8458176958e-13	-7.3223096343e-10
4	4	2.3606812245e-11	-2.0220900959e-08	2.0473935095e-13	2.3851478437e-09
3	5	-1.0666787540e-11	1.1424502065e-09	1.7733389955e-14	-3.4981008201e-11
5	4	3.2350665045e-11	-1.8619495084e-07	1.2380438564e-13	-2.1674830872e-10
4	5	-5.4458581813e-12	3.5184188246e-10	1.5138638160e-14	-1.2483270662e-10
5	5	-2.7778283633e-12	1.1063147589e-07	1.1828382098e-14	1.5755677408e-10

Table A.4: Fourier coefficients of the α_i functions for the BAP (II).

k_1	k_2	α^+_{5k}	α^-_{5k}	α^+_{6k}	α^-_{6k}
0	0			1.0000112577e+00	
1	0	8.4855949601e-05		-1.2366230991e-04	
0	1	7.1313784026e-06		5.7081478962e-05	
2	0	1.7398209274e-07		5.4541880211e-04	
1	1	4.7016879164e-08	6.0617192289e-06	-3.5662185550e-05	2.1493146185e-06
0	2	1.2828958205e-08		-6.9045365284e-07	
3	0	6.8009951805e-08		5.1484451242e-05	
2	1	5.0564411559e-10	2.2598849399e-09	1.0942140621e-05	4.8479363216e-02
1	2	-3.1894554330e-10	-4.9453292256e-07	-1.8778160106e-05	-3.8745319015e-06
0	3	-2.4319476723e-09		-3.3179423089e-08	
4	0	3.3637170791e-08		1.5585838972e-05	
3	1	2.0465225682e-09	2.0530664414e-06	5.8304342239e-07	-1.8217730450e-05
2	2	-8.4667459996e-10	5.1807564108e-07	3.0965801399e-07	-8.9750182480e-06
1	3	-8.4842370629e-11	-1.8724734474e-09	1.9771712342e-08	1.5141911514e-07
0	4	-1.0982179146e-11		8.7566263714e-11	
5	0	2.0567358089e-08		4.8524816036e-06	
4	1	1.6062979051e-09	3.0822237108e-09	9.0268436980e-07	5.0949201898e-05
3	2	4.9203583591e-11	-9.5286076789e-09	7.9469293199e-08	2.4061212122e-07
2	3	-5.5443886771e-12	-3.0759281783e-08	6.4671464225e-09	-8.1628920950e-08
1	4	-4.3483858052e-13	3.4877608828e-10	-7.5086431834e-11	-4.5326296391e-09
0	5	-9.0270821824e-15		5.9342236814e-10	
5	1	1.3097514776e-09	2.5982220765e-09	3.6523635031e-07	4.7616987888e-06
4	2	6.0378101484e-11	-1.3711412284e-10	4.0937284767e-08	2.3498112735e-03
3	3	-2.6914112278e-12	3.7231263696e-08	1.9466705609e-09	-7.9678986108e-07
2	4	-3.5931546296e-13	-2.8544868987e-10	4.1127324244e-10	3.0605408554e-10
1	5	3.4205902437e-14	2.0892816305e-12	-1.8464113722e-11	1.6777347227e-11
5	2	5.8838121933e-11	7.4645368317e-08	1.9649558579e-08	-1.5872153696e-06
4	3	-8.5393206326e-13	-1.1403796145e-09	1.2521529518e-09	-9.4555069081e-07
3	4	-2.7345279412e-13	-2.0547422198e-09	4.8410193968e-12	4.5452982426e-07
2	5	-1.6389711925e-14	3.4881375505e-11	-7.1374592780e-12	2.9070296621e-10
5	3	3.3411294136e-13	-9.2953030416e-11	6.9051973789e-10	2.2726803321e-08
4	4	-2.0254876684e-13	2.5298517770e-09	1.4638244679e-11	-8.4157941309e-09
3	5	-1.6989589792e-14	-3.4691938076e-11	-2.8828198646e-12	6.0231279890e-10
5	4	-1.2584651146e-13	-8.5582899017e-11	1.2839006146e-11	-7.2165972990e-08
4	5	-1.4720448808e-14	-1.2497913607e-10	-1.1630689192e-12	1.2190330594e-10
5	5	-1.1687857824e-14	1.5784876822e-10	-4.5558132225e-13	4.4089937074e-08

Table A.5: Fourier coefficients of the α_i functions for the BAP (III).

k_1	k_2	α^+_{7k}	α^-_{7k}	α^+_{8k}	α^-_{8k}
0	0	-2.8459268275e-03			
1	0	-1.8270553227e+00		1.8277890138e+00	
0	1	-3.8501026560e-02		3.8370220485e-02	
2	0	-3.0602227381e-03		3.0969960529e-03	
1	1	-2.1821830440e-03	4.5825941388e-02	2.1951665051e-03	4.3081038842e-02
0	2	-1.6057028306e-04		1.2737537751e-04	
3	0	-1.8208574783e-03		1.8266621544e-03	
2	1	7.6406451615e-06	1.1544531158e-01	-7.2880304314e-06	-1.1551271638e-01
1	2	1.6981218199e-04	-1.2289878559e-03	-1.6950758638e-04	-1.1118957705e-03
0	3	4.8575123196e-05		-4.8509944316e-05	
4	0	-1.7494084598e-04		1.7587713612e-04	
3	1	-3.1028587431e-05	-1.3288001326e-01	3.1268120015e-05	1.3290222785e-01
2	2	5.3284539527e-05	1.0470698817e-03	-5.3254093006e-05	8.2465822386e-04
1	3	9.9999163045e-07	-9.1665389796e-06	-9.9504034637e-07	-1.1600478176e-05
0	4	2.8673999166e-07		-2.8769353764e-07	
5	0	-5.3362784953e-05		5.3537293248e-05	
4	1	-1.7364255715e-06	-7.9082504148e-05	1.7848664693e-06	8.0884667952e-05
3	2	-9.2264787284e-07	2.6161812176e-04	9.3053859326e-07	8.1641626937e-04
2	3	2.3858164946e-08	-9.1838858596e-05	-2.3258586417e-08	6.0784637895e-06
1	4	1.7270900171e-09	1.7971766485e-06	-1.5206757529e-09	1.8036308861e-06
0	5	-3.5249599253e-09		3.5095124604e-09	
5	1	-3.3067938021e-06	-2.1377522106e-04	3.3159005891e-06	2.1420748650e-04
4	2	-2.8183643163e-07	8.3953516638e-03	2.8356843425e-07	-8.3976941538e-03
3	3	-1.9116425594e-08	2.3129594598e-05	1.9306690120e-08	3.6830753670e-05
2	4	-3.9852111503e-09	-1.1975273499e-06	3.9883449812e-09	-1.0392141184e-06
1	5	-2.8679787901e-09	1.7661144797e-08	2.8661551211e-09	1.7311838586e-08
5	2	-1.5141040543e-07	-9.1271263119e-03	1.5167238630e-07	9.1282267327e-03
4	3	-7.0419756095e-09	1.3781006795e-05	7.0800108013e-09	8.9029810970e-06
3	4	-1.5479757262e-09	-8.0837179242e-07	1.5497341393e-09	-2.7817268774e-06
2	5	6.8118220198e-11	7.4641224140e-08	-6.8502013138e-11	7.7978742207e-08
5	3	-4.5036742509e-09	-1.2532544145e-06	4.5045619941e-09	3.6104569977e-05
4	4	4.3785441626e-11	-3.7071287698e-06	-4.3577186780e-11	5.9629437402e-06
3	5	3.3254776819e-11	-5.5382693134e-08	-3.3336429751e-11	-4.6248584818e-08
5	4	-2.6642355939e-11	-3.4718148270e-07	2.6325695691e-11	1.0821995157e-06
4	5	1.4832227061e-11	-8.1754955059e-08	-1.4860670128e-11	-7.9115787460e-08
5	5	6.3181411455e-12	1.9423553229e-07	-6.3393352014e-12	-1.0401726086e-07

Table A.6: Fourier coefficients of the α_i functions for the BAP (IV).

A.4 Fourier coefficients of the TCCP Hamiltonian

k_1	k_2	α_{1k}^+	α_{1k}^-	α_{2k}^+	α_{2k}^-
0	0	1.0000158873e+00		0.0000000000e+00	
1	0	-2.4624881589e-04		7.3487853447e-05	
0	1	4.2411792250e-09		-4.7619170164e-10	
2	0	1.0692291079e-03		-6.3835096328e-04	
1	1	-3.8369689615e-06	7.4423915653e-09	1.6468543833e-06	-1.5995931990e-09
0	2	1.7932859434e-09		-5.9756596136e-11	
3	0	1.1072011409e-04		-9.9271093796e-05	
2	1	5.9467795464e-09	2.3261609310e-07	-3.9792437263e-09	-1.0857655202e-07
1	2	3.7444946122e-08	-7.0083103975e-08	-2.1200966443e-08	2.6116219682e-09
0	3	4.2173965468e-09		-1.6409637280e-09	
4	0	2.9394219320e-05		-3.4772486702e-05	
3	1	-3.5473772637e-09	-1.6194218643e-08	1.5362478497e-09	1.2325143753e-08
2	2	3.0537941259e-06	-1.4292050552e-07	-2.6214181409e-06	4.7988676917e-08
1	3	-4.6089498145e-09	3.9834540041e-09	3.2959650090e-09	3.5127753245e-10
0	4	3.7064115378e-09		-1.9396602396e-09	
5	0	9.6352859680e-06		-1.4297784700e-05	
4	1	2.4210819333e-10	-3.9328229531e-09	-5.9682230337e-10	4.2971131220e-09
3	2	-1.6262163711e-09	7.8963636881e-08	1.4677588402e-09	-5.0078237437e-08
2	3	-5.0468202014e-10	-1.4874154914e-08	4.6811890873e-10	3.0387387615e-09
1	4	7.8242710179e-11	2.8393553740e-11	-6.3100183497e-11	6.6783972554e-12
0	5	1.5715645967e-10		-1.0183196104e-10	
5	1	2.1159379498e-10	-1.5519784484e-09	-4.3562549200e-10	2.1116795837e-09
4	2	3.6085222215e-09	1.2461656664e-08	-2.8733987503e-09	-1.1701788820e-08
3	3	2.9328866752e-07	4.2162262822e-07	-3.7765313362e-07	-2.1227233527e-07
2	4	-2.5768698450e-10	-7.4738318682e-09	3.1647728974e-10	5.5522916720e-10
1	5	2.8345574069e-11	-1.5797429191e-11	-2.6827143153e-11	-5.5876936673e-12
5	2	1.9745926569e-10	4.1320816815e-09	-5.0782585805e-11	-5.0453133400e-09
4	3	-2.0983110545e-10	2.2359382568e-09	2.7527085823e-10	-1.8407943276e-09
3	4	-4.2820334845e-11	-4.3083443079e-09	5.3605997369e-11	1.6064889285e-09
2	5	4.8758553064e-12	2.4804583603e-09	-5.4293691581e-12	1.3989844958e-10
5	3	3.7913354306e-10	1.2060138285e-09	-4.1891366920e-10	-1.0801744738e-09
4	4	4.3155143999e-08	1.2680181466e-09	-7.4086896064e-08	-8.5348271016e-10
3	5	-4.6473834903e-11	-9.6037100053e-10	7.8287156598e-11	2.3238214853e-10
5	4	-2.7851460457e-11	2.1696483384e-10	4.5366371974e-11	-2.1313412002e-10
4	5	-1.0074986775e-11	1.6934080754e-09	1.6931995667e-11	-9.1468633269e-10
5	5	7.5526564532e-09	8.2543049256e-11	-1.6207484896e-08	-6.9776292564e-11

Table A.7: Fourier coefficients of the α_i functions for the TCCP (I).

k_1	k_2	α_{3k}^+	α_{3k}^-	α_{4k}^+	α_{4k}^-
0	0	9.9999449512e-01		1.8636712759e-08	
1	0	-2.2689546647e-04		-8.4900572188e-05	
0	1	3.9364921287e-09		-1.0599905523e-09	
2	0	1.1362691701e-03		6.1112015479e-09	
1	1	-3.7286112371e-06	7.6295778062e-09	-3.2185308880e-06	5.2677469534e-09
0	2	-9.1074879464e-10		-1.3037125674e-10	
3	0	1.4135592308e-04		-6.7716934089e-08	
2	1	6.5937168311e-09	2.2792832860e-07	5.1608000733e-10	2.1492326660e-10
1	2	3.8731886012e-08	-5.4929582269e-08	4.3335135345e-10	-5.5390142446e-09
0	3	3.7440118730e-09		-2.6797903021e-12	
4	0	4.4105581926e-05		-3.5059024969e-08	
3	1	-2.9912109863e-09	-1.9022950076e-08	-6.7251976806e-10	5.1102637808e-11
2	2	3.8417342110e-06	-1.2905373802e-07	-7.6006922949e-11	1.0022343091e-10
1	3	-5.3895568282e-09	2.7683615692e-09	-7.9366267285e-11	-4.5660807115e-10
0	4	3.7191579784e-09		-7.0838615960e-15	
5	0	1.6876213446e-05		-2.1448619658e-08	
4	1	6.4804271317e-10	-5.6225455966e-09	-3.8873554406e-11	2.0228569713e-11
3	2	-2.1058336758e-09	8.5907722446e-08	-2.9325295307e-11	-1.2752867812e-12
2	3	-6.6849234604e-10	-1.2326312187e-08	1.4021083848e-11	3.8547740799e-11
1	4	8.0490390198e-11	-4.6193763283e-11	-2.6784575892e-11	-1.5301345944e-10
0	5	1.6014477523e-10		-2.7037686460e-14	
5	1	4.8348078231e-10	-2.5540551710e-09	-7.3096366166e-12	8.7633361236e-12
4	2	4.0803107834e-09	1.6322922589e-08	7.8455592834e-13	-8.1053630149e-12
3	3	4.7149336910e-07	4.2256476269e-07	-4.4677887722e-10	8.7673851106e-13
2	4	-4.1122074847e-10	-5.8055422544e-09	4.2080739827e-13	-7.5138588123e-12
1	5	3.3240954422e-11	-3.3004985391e-11	-9.4265951356e-12	-4.7105768053e-11
5	2	1.1297393986e-10	6.3288588420e-09	6.0800058754e-13	-5.3261404617e-12
4	3	-3.3907658174e-10	2.7480637033e-09	-1.2041210646e-12	-9.5369121756e-12
3	4	-6.8263636423e-11	-3.9748573397e-09	2.0364440689e-12	2.5158781169e-12
2	5	5.4787638809e-12	1.8228527871e-09	1.1750475923e-14	5.5731366066e-14
5	3	5.2838004985e-10	1.5139581216e-09	-1.5264756851e-13	-6.2319778113e-13
4	4	8.5523511149e-08	1.4154764830e-09	-1.4097994573e-10	-5.9313956891e-15
3	5	-9.2039819633e-11	-8.1550929975e-10	1.5395050355e-13	5.5239973306e-12
5	4	-5.2823754356e-11	2.9215992948e-10	-6.3093673550e-14	-1.5196437367e-13
4	5	-1.9681186857e-11	1.7375894768e-09	3.6829745779e-13	3.8197583994e-14
5	5	1.7905545730e-08	1.0269633662e-10	-4.2959623226e-11	-5.9943562457e-14

Table A.8: Fourier coefficients of the α_i functions for the TCCP (II).

k_1	k_2	α^+_{5k}	α^-_{5k}	α^+_{6k}	α^-_{6k}
0	0	0.0000000000e+00		1.0000078675e+00	
1	0	8.5037280783e-05		-1.2310578472e-04	
0	1	5.2442198630e-10		1.9711717645e-09	
2	0	9.0046433985e-10		5.3460591020e-04	
1	1	3.2183628872e-06	-4.5805077375e-10	-1.9184716984e-06	4.2434179547e-09
0	2	1.4168964590e-10		5.0546857360e-10	
3	0	6.6844823755e-08		5.5392088628e-05	
2	1	-5.1640324146e-10	2.1667216406e-10	2.8536740919e-09	1.1636000931e-07
1	2	-1.0269375364e-10	5.5516501572e-09	1.8827553160e-08	-3.5103606736e-08
0	3	2.8399586421e-12		2.1006749225e-09	
4	0	3.3788483405e-08		1.4628747876e-05	
3	1	6.7247199261e-10	5.3322037401e-11	-1.2610740363e-09	-8.0770210935e-09
2	2	3.6967484563e-11	-8.8819112669e-11	1.5268862524e-06	-7.1472988163e-08
1	3	8.0544076250e-11	7.6948298439e-10	-2.3453988278e-09	1.9344981314e-09
0	4	2.1081953994e-13		1.8541843682e-09	
5	0	2.0585389627e-08		4.8036076218e-06	
4	1	3.8820126183e-11	1.3155334887e-11	1.7312343267e-10	-1.9934366809e-09
3	2	2.9456434772e-11	2.4309096257e-12	-7.2370072467e-10	3.9482473188e-08
2	3	1.4125942132e-11	1.5857813522e-11	-2.4448762774e-10	-7.4250507144e-09
1	4	2.7060082998e-11	1.3533789056e-10	3.8768651172e-11	1.4543361244e-11
0	5	8.5525189888e-14		7.8247340786e-11	
5	1	7.2720476244e-12	3.4788382499e-12	1.2005387464e-10	-7.7562215387e-10
4	2	-7.4145595876e-13	8.1368021075e-12	1.3956778671e-09	6.2519743175e-09
3	3	4.3709025565e-10	-8.4421268255e-13	1.4664498431e-07	2.1080843391e-07
2	4	-3.9190605419e-13	9.4556485682e-12	-1.3507587403e-10	-3.7375096184e-09
1	5	9.5108007502e-12	3.9297355477e-11	1.4131327552e-11	-7.8848786086e-12
5	2	-5.9054321034e-13	5.1855996975e-12	5.6627039711e-11	2.0574803421e-09
4	3	1.2131260798e-12	9.5544604774e-12	-9.5843145943e-11	1.1328012081e-09
3	4	1.9190702064e-12	-2.3066539046e-12	-2.0153488171e-11	-2.1544401992e-09
2	5	-7.4786298127e-15	1.0599427628e-12	2.3043833627e-12	1.2399341886e-09
5	3	1.5483850143e-13	6.1741571467e-13	1.5035149832e-10	5.4688091976e-10
4	4	1.3858041221e-10	3.1438734806e-14	2.1576979159e-08	6.3484884098e-10
3	5	-1.5143935494e-13	-5.2795790335e-12	-2.4253395406e-11	-4.8006534838e-10
5	4	6.4217250183e-14	1.5461294475e-13	-1.2590236500e-11	1.0918258746e-10
4	5	3.0779486087e-13	-2.6795134141e-14	-4.8098242287e-12	8.4633848535e-10
5	5	4.2358300192e-11	6.1837472874e-14	3.7762115832e-09	4.1423948599e-11

Table A.9: Fourier coefficients of the α_i functions for the TCCP (III).

k_1	k_2	α^+_{7k}	α^-_{7k}	α^+_{8k}	α^-_{8k}
0	0	-9.5129726990e-05		0.0000000000e+00	
1	0	-1.8329742082e+00		1.8337530237e+00	
0	1	-2.1091048002e-06		-2.3421318647e-06	
2	0	-2.9362155529e-04		3.3355605800e-04	
1	1	-4.7413700938e-05	2.3041391838e-05	4.7405992216e-05	-2.2795097190e-05
0	2	-2.2045153804e-06		2.2411164381e-06	
3	0	-1.6369993303e-03		1.6424557532e-03	
2	1	5.7509451908e-06	-2.9114374608e-07	-5.7519506955e-06	2.8397792187e-07
1	2	8.8227730005e-05	-2.2624987512e-05	-8.6913295542e-05	2.2471010692e-05
0	3	-2.0423944661e-07		2.0222275157e-07	
4	0	-1.8364814001e-04		1.8456719541e-04	
3	1	-4.5454213673e-08	-2.6841657844e-07	4.5419405945e-08	2.6751862137e-07
2	2	-7.4978538343e-08	2.7402933461e-06	7.5166541927e-08	-2.6868770043e-06
1	3	9.4021138143e-06	-6.6284184746e-07	-9.4014947797e-06	2.2985488310e-06
0	4	1.3574354137e-07		-1.3556075704e-07	
5	0	-4.9448707847e-05		4.9604557325e-05	
4	1	2.3822359789e-09	2.9401217244e-08	-2.3818434582e-09	-2.9583290517e-08
3	2	-3.3843058023e-06	-5.9615162742e-08	3.3848730783e-06	6.3831531774e-08
2	3	3.7065112775e-08	3.0961547957e-07	2.9792674330e-08	7.4146241539e-08
1	4	2.1717526179e-06	-3.3766237478e-07	-2.1716828601e-06	1.1417819059e-07
0	5	7.6709210234e-09		-7.6288147967e-09	
5	1	-1.3370318397e-09	7.4732289308e-09	1.3375656226e-09	-7.5110465689e-09
4	2	7.3314526531e-09	-1.2797113928e-07	-7.2968636650e-09	1.2870305546e-07
3	3	7.4655919508e-09	-2.5265947469e-06	-7.4921773413e-09	2.5272782107e-06
2	4	-7.1607030772e-10	-4.3253201869e-08	7.1368357387e-10	3.8916711119e-08
1	5	6.4607756972e-07	-1.5142553557e-07	-6.4605008680e-07	-5.7408200618e-08
5	2	-3.4651533554e-09	-2.2338591382e-08	3.4688515765e-09	2.2488076982e-08
4	3	-3.0148712217e-07	-5.8362382494e-07	3.0152766553e-07	5.8386293834e-07
3	4	5.1268266738e-09	1.6579865923e-07	9.7966307332e-10	-1.6492803385e-07
2	5	-2.7423607379e-10	4.8672281612e-10	2.6873967096e-10	3.3337635170e-09
5	3	3.3599860590e-10	-6.0351564966e-09	-3.3337932842e-10	6.0748825546e-09
4	4	1.4486020739e-10	2.3108205747e-09	-1.4824535526e-10	-2.2312057156e-09
3	5	4.8470279706e-10	7.5662069994e-08	-4.8599972279e-10	-7.4164954278e-08
5	4	-4.2574791415e-08	-1.9533410169e-09	4.2579783868e-08	1.9676755161e-09
4	5	4.6926042969e-10	-8.6091027491e-09	2.5595530306e-10	8.6518639130e-09
5	5	1.3028751531e-11	-2.4135628070e-09	-1.3562576667e-11	2.4204927046e-09

Table A.10: Fourier coefficients of the α_i functions for the TCCP (IV).

k_1	k_2	α_{9k}^{+}	α_{9k}^{-}	α_{10k}^{+}	α_{10k}^{-}
0	0	-5.2595925237e-06		0.0000000000e+00	
1	0	-5.0924122949e-04		5.0946331689e-04	
0	1	-4.7318431596e-04		4.7323944549e-04	
2	0	-1.5103056986e-07		1.6178605785e-07	
1	1	-3.6820560192e+00	7.6644104361e-04	3.6820574726e+00	7.6886875816e-04
0	2	7.0859694160e-09		-1.2125233762e-08	
3	0	-1.1219718073e-06		1.1236722746e-06	
2	1	9.2595311705e-04	4.3051412246e-05	-9.2595371217e-04	4.3659830504e-05
1	2	-1.4516760734e-04	-5.4597607157e-07	1.4516811853e-04	1.0760715739e-06
0	3	-5.4850011058e-07		5.4851299937e-07	
4	0	-1.3768541431e-08		1.4094286810e-08	
3	1	-2.7362405386e-03	7.6023784226e-06	2.7362416024e-03	6.6382912470e-06
2	2	8.9215374161e-06	4.8175067544e-07	-8.9143111416e-06	-4.9455778418e-07
1	3	-7.4222230000e-05	-4.7851572651e-07	7.4222310976e-05	5.5034275947e-08
0	4	-1.9051751252e-06		1.9052002969e-06	
5	0	-5.8254394966e-09		5.8950708721e-09	
4	1	-2.4664781316e-04	1.3840573930e-06	2.4664785635e-04	1.7800463611e-06
3	2	-1.2353913761e-07	6.3368334621e-08	1.2350883499e-07	-6.5231380134e-08
2	3	-8.4746662342e-08	5.5299043253e-08	8.4784537027e-08	5.0009443444e-08
1	4	-1.5750029767e-05	-1.3795111878e-07	1.5750074145e-05	4.0917938100e-08
0	5	-6.3133666255e-08		6.3138845979e-08	
5	1	-6.1762513106e-05	3.9168627154e-07	6.1762512012e-05	4.4629061838e-07
4	2	1.1569789697e-09	-1.1608166171e-06	-1.0863857536e-09	1.1603336409e-06
3	3	-1.1062041338e-05	9.3183824035e-07	1.1056659480e-05	-9.2241358060e-07
2	4	2.0010630326e-08	3.8424648186e-07	-2.0003605121e-08	3.8483273769e-07
1	5	-4.5058440647e-06	-3.9132454717e-07	4.5058582216e-06	-3.2927653751e-07
5	2	-2.7083424177e-09	-5.0102319213e-09	2.7127208102e-09	4.8652964326e-09
4	3	1.1593575564e-09	1.4186181896e-08	-1.1588075649e-09	-1.2238056138e-08
3	4	-1.0410330777e-08	-4.7554213557e-07	1.0415825292e-08	4.7771260043e-07
2	5	1.4756578092e-09	-6.8365733291e-09	-1.4744527166e-09	-6.0726006076e-09
5	3	-1.4337274439e-08	-2.1883762549e-09	1.4343622874e-08	2.7031759720e-09
4	4	-1.1495123614e-06	4.2298894516e-09	1.1481453040e-06	-3.6689040337e-09
3	5	-2.1768189728e-09	2.9095026150e-09	2.1785901183e-09	-1.3421469870e-09
5	4	5.2303870390e-10	-4.8316466115e-09	-5.2254011900e-10	4.9392525029e-09
4	5	-1.2643932886e-10	6.0719331622e-09	1.2743057462e-10	-5.9322596903e-09
5	5	-1.7602234876e-07	8.7823087655e-10	1.7572901878e-07	-8.5038557598e-10

Table A.11: Fourier coefficients of the α_i functions for the TCCP (V).

Appendix B

Frequencies of the Trojan asteroids

In this appendix, we give the tables that contain the basic frequencies of the Trojan motion in the different models.

B.1 Basic frequencies in the OSS

We show the three basic frequencies of the 420 Trojan asteroids studied in the Outer Solar System model. See captions for more details.

Table B.1: Basic frequencies of the Trojan asteroids in the Outer Solar System model. In the first column we display the catalog number of the asteroid and in the second one the asteroid's name. The frequency of libration can be seen in the third column, while in the fourth and fifth columns we show the two secular frequencies.

C.N.	Name	$\nu\,(deg)$	$g\,(sec)$	$s\,(sec)$
588	Achilles	2.434	344.40	-11.02
617	Patroclus	2.350	310.62	-6.76
624	Hektor	2.316	335.74	-12.99
659	Nestor	2.467	355.01	-16.48
884	Priamus	2.424	353.41	-12.24
911	Agamemnon	2.290	317.35	-8.69
1143	Odysseus	2.439	365.38	-10.91
1172	Aneas	2.366	331.54	-7.92
1173	Anchises	2.371	378.19	-23.67
1208	Troilus	2.199	258.54	-0.45
1404	Ajax	2.310	334.43	-15.15
1437	Diomedes	2.213	331.25	-20.05
1583	Antilochus	2.181	282.18	-10.79
1647	Menelaus	2.438	359.34	-9.96
1749	Telamon	2.421	366.33	-13.79
1867	Deiphobus	2.233	286.24	-5.76

Table B.1: Basic frequencies of the Trojan asteroids in the OSS model (continued).

C.N.	Name	$\nu\,(deg)$	$g\,(sec)$	$s\,(sec)$
1868	Thersites	2.316	345.09	-20.48
1869	Philoctetes	2.382	388.78	-20.44
1870	Glaukos	2.429	363.50	-9.48
1871	Astyanax	2.311	401.29	-25.28
1872	Helenos	2.313	364.71	-17.98
1873	Agenor	2.327	308.03	-10.46
2146	Stentor	2.145	233.44	3.27
2148	Epeios	2.430	354.54	-7.46
2207	Antenor	2.406	373.80	-15.55
2223	Sarpedon	2.358	340.50	-9.59
2241	Alcathous	2.366	329.00	-11.52
2260	Neoptolemus	2.384	334.39	-5.25
2357	Phereclos	2.448	363.27	-9.59
2363	Cebriones	2.177	259.80	-4.09
2456	Palamedes	2.358	351.62	-11.97
2594	Acamas	2.292	408.29	-32.17
2674	Pandarus	2.461	360.36	-11.70
2759	Idomeneus	2.336	314.28	-7.81
2797	Teucer	2.277	327.55	-16.22
2893	Peiroos	2.372	356.01	-12.87
2895	Memnon	2.293	294.38	-3.63
2920	Automedon	2.271	325.72	-12.72
3063	Makhaon	2.389	349.12	-10.54
3240	Laocoon	2.443	365.39	-12.90
3317	Paris	2.294	291.06	-3.25
3391	Sinon	2.340	351.30	-14.04
3451	Mentor	2.210	314.75	-16.90
3540	Protesilaos	2.296	306.96	-14.09
3548	Eurybates	2.388	376.51	-16.24
3564	Talthybius	2.393	337.32	-9.62
3596	Meriones	2.274	311.15	-8.70
3708	1974FV1	2.426	330.76	-11.01
3709	Polypoites	2.338	328.31	-7.13
3793	Leonteus	2.334	318.38	-6.59
3794	Sthenelos	2.471	348.70	-13.24
3801	Thrasymedes	2.172	281.73	-11.93
4007	Euryalos	2.399	357.14	-9.85
4035	1986WD	2.373	356.64	-11.43
4057	Demophon	2.440	367.91	-13.50
4060	Deipylos	2.403	331.48	-13.48
4063	Euforbo	2.371	331.46	-8.60

Table B.1: Basic frequencies of the Trojan asteroids in the OSS model (continued).

C.N.	Name	$\nu\,(deg)$	$g\,(sec)$	$s\,(sec)$
4068	Menestheus	2.341	340.96	-13.34
4086	Podalirius	2.292	326.59	-15.14
4138	Kalchas	2.434	369.43	-11.67
4348	Poulydamas	2.443	352.64	-12.14
4489	1988AK	2.281	331.22	-13.54
4501	Eurypylos	2.389	368.82	-13.09
4543	Phoinix	2.282	361.38	-22.16
4707	Khryses	2.449	351.71	-12.82
4708	Polydoros	2.380	375.83	-17.85
4709	Ennomos	2.232	295.59	-8.93
4715	1989TS1	2.301	340.63	-13.82
4722	Agelaos	2.455	350.69	-11.27
4754	Panthoos	2.366	366.89	-15.29
4791	Iphidamas	2.260	287.94	-6.24
4792	Lykaon	2.417	362.68	-12.06
4805	Asteropaios	2.393	348.15	-11.35
4827	Dares	2.387	371.81	-17.05
4828	Misenus	2.385	339.23	-11.00
4829	Sergestus	2.351	381.73	-18.74
4832	Palinurus	2.369	328.29	-12.03
4833	Meges	2.196	255.93	-1.30
4834	Thoas	2.279	287.39	-4.67
4835	1989BQ	2.419	301.40	-21.07
4836	Medon	2.357	331.18	-10.50
4867	Polites	2.259	286.24	-3.01
4902	Thessandrus	2.432	354.26	-6.95
4946	Askalaphus	2.263	326.58	-19.10
5012	Eurymedon	2.433	367.09	-13.28
5023	Agapenor	2.386	352.86	-10.15
5025	1986TS6	2.416	348.70	-7.06
5027	Androgeos	2.190	275.38	-7.48
5028	Halaesus	2.340	318.01	-8.36
5041	Theotes	2.375	369.92	-15.81
5119	1988RA1	2.389	329.54	-6.24
5120	Bitias	2.252	295.16	-8.66
5123	1989BL	2.443	355.90	-9.85
5126	Achaemenides	2.259	283.59	-1.85
5130	Ilioneus	2.311	351.03	-16.07
5144	Achates	2.466	321.80	-25.56
5209	1989CW1	2.329	384.97	-20.78
5233	1988RL10	2.440	368.55	-14.50

Table B.1: Basic frequencies of the Trojan asteroids in the OSS model (continued).

C.N.	Name	$\nu\,(deg)$	$g\,(sec)$	$s\,(sec)$
5244	Amphilochos	2.429	363.08	-11.33
5254	Ulysses	2.327	307.95	-5.57
5257	1988RS10	2.434	370.79	-13.29
5258	1989AU1	2.404	372.16	-15.39
5259	Epeigeus	2.415	332.39	-11.11
5264	Telephus	2.224	261.25	-0.32
5283	Pyrrhus	2.403	329.05	-8.35
5284	Orsilocus	2.366	325.58	-4.85
5285	Krethon	2.229	315.63	-14.50
5436	Eumelos	2.438	352.85	-7.89
5476	1989TO11	2.340	362.04	-16.24
5511	Cloanthus	2.413	353.70	-11.22
5637	Gyas	2.260	317.66	-15.35
5638	Deikoon	2.399	360.85	-19.22
5648	1990VU1	2.328	311.98	-13.37
5652	Amphimachus	2.452	361.04	-9.16
5907	1989TU5	2.446	367.09	-15.63
6002	1988RO	2.394	333.14	-7.42
6090	1989DJ	2.269	329.24	-13.93
6443	1988RH12	2.442	351.13	-12.94
6545	1986TR6	2.335	367.03	-16.65
6997	Laomedon	2.368	321.09	-7.53
6998	Tithonus	2.441	366.77	-9.88
7119	Hiera	2.291	328.38	-14.21
7152	Euneus	2.433	369.61	-10.69
7214	Antielus	2.319	369.76	-18.53
7352	1994CO	2.385	378.98	-17.04
7543	Prylis	2.369	351.94	-11.23
7641	1986TT6	2.175	244.58	2.82
7815	Dolon	2.308	335.29	-12.91
8060	Anius	2.397	373.47	-15.94
8125	Tyndareus	2.321	364.92	-18.17
8241	Agrius	2.399	380.85	-20.62
8317	Eurysaces	2.370	394.85	-24.57
9023	Mnesthus	2.286	315.52	-8.44
9030	1989UX5	2.316	409.54	-29.01
9142	Rhesus	2.398	354.64	-13.74
9430	1996HU10	2.412	378.93	-14.69
9431	1996PS1	2.289	324.08	-12.91
9590	1991DK1	2.374	383.39	-22.85
9694	Lycomedes	2.279	416.14	-29.96

Table B.1: Basic frequencies of the Trojan asteroids in the OSS model (continued).

C.N.	Name	$\nu\,(deg)$	$g\,(sec)$	$s\,(sec)$
9712	Nauplius	2.446	352.11	-9.82
9713	Oceax	2.438	366.05	-10.05
9790	1995OK8	2.428	362.84	-10.41
9799	1996RJ	2.228	266.14	0.74
9807	1997SJ4	2.467	351.84	-11.25
9817	Thersander	2.372	376.40	-16.55
9818	Eurymachos	2.402	371.40	-14.34
9828	Antimachos	2.443	366.67	-11.58
9857	1991EN	2.303	323.99	-12.21
9907	Oileus	2.374	381.36	-17.14
10247	Amphiaraos	2.238	427.87	-36.59
10664	Phemios	2.359	377.82	-17.94
10989	Dolios	2.417	353.69	-9.82
11089	1994CS8	2.365	388.29	-22.50
11251	Icarion	2.435	368.92	-11.88
11252	Laertes	2.416	373.33	-12.66
11273	1988RN11	2.388	386.63	-27.40
11275	1988SL3	2.322	305.12	-3.44
11351	1997TS25	2.302	377.71	-21.84
11395	1998XN77	2.317	297.27	-4.36
11396	1998XZ77	2.417	343.29	-7.24
11397	1998XX93	2.200	327.23	-20.12
11428	Alcinoos	2.274	352.58	-19.30
11429	Demodokus	2.300	350.47	-16.23
11487	1988RG10	2.425	370.49	-11.67
11488	1988RM11	2.415	377.52	-14.50
11509	1990VL6	2.371	320.32	-8.07
11552	1993BD4	2.356	355.48	-19.79
11554	1993BZ12	2.380	357.21	-13.66
11663	1997GO24	2.370	344.85	-13.29
11668	Balios	2.444	363.77	-16.97
11869	1989TS2	2.399	360.62	-10.57
11887	Echemmon	2.300	297.05	-3.10
12052	1997JB16	2.340	371.58	-17.78
12054	1997TT9	2.352	381.41	-18.91
12126	1999RM11	2.490	351.25	-19.17
12238	1987YU1	2.338	311.87	-6.77
12242	Koon	2.167	272.59	-10.02
12444	1996GE19	2.211	266.61	-2.34
12649	Ascanios	2.434	360.15	-15.18
12658	Peiraios	2.371	395.93	-20.20

Table B.1: Basic frequencies of the Trojan asteroids in the OSS model (continued).

C.N.	Name	$\nu\,(deg)$	$g\,(sec)$	$s\,(sec)$
12714	Alkimos	2.398	359.17	-10.67
12916	1998TL15	2.196	295.93	-13.04
12917	1998TG16	2.364	364.22	-15.32
12921	1998WZ5	2.411	347.89	-7.91
12929	1999TZ1	2.033	183.03	4.24
12972	Eumaios	2.445	354.99	-17.55
12973	Melanthios	2.391	379.63	-16.01
12974	Halitherses	2.436	357.17	-8.67
13060	1991EJ	2.290	301.78	-10.23
13062	Podarkes	2.314	401.16	-26.06
13181	Peneleos	2.474	355.12	-11.95
13182	1996SO8	2.444	359.50	-13.99
13183	1996TW	2.381	323.51	-10.96
13184	1996TS49	2.411	373.91	-16.90
13185	1996TH52	2.420	356.72	-8.34
13229	Echion	2.406	377.42	-18.77
13230	1997VG1	2.271	421.79	-32.68
13323	1998SQ	2.303	415.13	-30.10
13331	1998SU52	2.329	404.26	-28.41
13353	1998TU12	2.406	336.51	-11.34
13362	1998UQ16	2.425	359.40	-11.17
13366	1998US24	2.450	358.26	-9.13
13372	1998VU6	2.431	363.45	-9.53
13379	1998WX9	2.421	373.13	-12.18
13383	1998XS31	2.383	378.33	-16.01
13385	1998XO79	2.414	341.95	-8.83
13387	1998YW6	2.445	354.45	-10.28
13402	1999RV165	2.426	363.95	-14.19
13463	Antiphos	2.392	357.93	-11.55
13475	Orestes	2.433	355.52	-8.83
13650	1996TN49	2.362	369.70	-17.87
13694	1997WW7	2.289	409.05	-28.69
13780	1998UZ8	2.386	375.14	-16.58
13782	1998UM18	2.271	283.52	-4.98
13790	1998UF31	2.432	362.08	-14.49
13862	1999XT160	2.394	374.63	-15.42
14235	1999XA187	2.359	384.24	-19.68
14268	2000AK156	2.330	349.44	-14.85
14518	1996RZ30	2.438	361.58	-14.75
14690	2000AR25	2.441	362.75	-9.73
14707	2000CC20	2.283	383.85	-24.42

Table B.1: Basic frequencies of the Trojan asteroids in the OSS model (continued).

C.N.	Name	$\nu\,(deg)$	$g\,(sec)$	$s\,(sec)$
14791	Atreus	2.462	359.86	-20.16
14792	Thyestes	2.394	361.64	-12.71
15033	1998VY29	2.444	331.92	-15.63
15094	1999WB2	2.357	366.05	-16.73
15398	1997UZ23	2.227	285.83	-6.83
15436	1998VU30	2.378	330.56	-4.50
15440	1998WX4	2.228	291.82	-8.31
15442	1998WN11	2.478	353.55	-13.11
15502	1999NV27	2.317	341.13	-14.72
15521	1999XH133	2.422	350.67	-12.70
15527	1999YY2	2.378	303.72	-12.35
15529	2000AA80	2.440	364.34	-12.66
15535	2000AT177	2.393	353.30	-10.79
15536	2000AG191	2.405	336.98	-10.48
15539	2000CN3	2.088	289.88	-24.88
15651	Tlepolemos	2.324	410.55	-25.99
15663	Periphas	2.182	251.64	-1.53
15913	Telemachus	2.439	358.41	-7.66
15977	1998MA11	2.351	334.21	-12.53
16070	1999RB101	2.341	338.46	-13.76
16099	1999VQ24	2.422	344.70	-8.11
16152	1999YN12	2.407	380.94	-16.74
16428	1988RD12	2.424	369.67	-11.37
16560	1991VZ5	2.229	381.35	-30.03
16667	1993XM1	2.429	324.87	-15.56
16956	1998MQ11	2.203	275.19	-9.28
16974	1998WR21	2.379	338.02	-8.43
17171	1999NB38	2.265	297.41	-5.85
17172	1999NZ41	2.266	286.91	-2.23
17314	Aisakos	2.428	347.42	-13.15
17351	Pheidippos	2.383	339.63	-8.35
17365	1978VF11	2.392	351.00	-11.24
17414	1988RN10	2.357	346.73	-12.22
17415	1988RO10	2.298	314.90	-7.48
17416	1988RR10	2.333	348.03	-13.18
17417	1988RY10	2.446	365.82	-10.62
17418	1988RT12	2.454	355.05	-14.86
17419	1988RH13	2.349	351.04	-14.27
17420	1988RL13	2.380	344.46	-8.73
17421	1988SW1	2.369	337.16	-12.54
17423	1988SK2	2.460	361.66	-12.94

Table B.1: Basic frequencies of the Trojan asteroids in the OSS model (continued).

C.N.	Name	$\nu\,(deg)$	$g\,(sec)$	$s\,(sec)$
17424	1988SP2	2.437	338.90	-10.55
17442	1989UO5	2.345	352.02	-13.11
17492	Hippasos	2.162	290.79	-15.79
17874	1998YM3	2.222	435.28	-37.87
18037	1999NA38	2.387	346.72	-10.96
18046	1999RN116	2.203	262.59	-1.06
18054	1999SW7	2.345	333.73	-9.13
18058	1999XY129	2.375	376.23	-16.62
18060	1999XJ156	2.394	374.28	-15.38
18062	1999XY187	2.356	341.21	-8.95
18063	1999XW211	2.326	334.44	-10.31
18071	2000BA27	2.299	413.90	-28.30
18137	2000OU30	2.293	400.95	-28.66
18228	Hyperenor	2.436	368.86	-17.49
18263	Anchialos	2.312	380.26	-21.57
18268	Dardanos	2.370	333.77	-7.54
18278	Drymas	2.366	332.15	-9.14
18281	Tros	2.419	358.77	-11.72
18282	Ilos	2.438	355.17	-9.97
18493	1996HV9	2.302	345.72	-16.38
18940	2000QV49	2.361	396.12	-22.30
18971	2000QY177	2.423	334.24	-11.66
19018	2000RL100	2.238	282.01	-5.28
19020	2000SC6	2.397	334.68	-6.82
19725	1999WT4	2.354	380.95	-18.77
19844	2000ST317	2.117	216.42	5.57
19913	Aigyptios	2.369	387.28	-20.29
20144	1996RA33	2.435	352.58	-8.16
20424	1998VF30	2.316	299.99	-4.10
20428	1998WG20	2.350	317.89	-9.52
20716	1999XG91	2.305	293.23	-5.41
20720	1999XP101	2.353	338.08	-15.55
20729	1999XS143	2.320	306.83	-3.02
20738	1999XG191	2.406	350.35	-8.89
20739	1999XM193	2.422	338.39	-12.79
20947	Polyneikes	2.301	417.19	-29.09
20952	Tydeus	2.410	353.77	-9.62
20961	Arkesilaos	2.404	365.35	-11.87
20995	1985VY	2.269	342.91	-20.99
21271	1996RF33	2.388	382.52	-17.35
21284	1996TC51	2.442	357.89	-12.70

Table B.1: Basic frequencies of the Trojan asteroids in the OSS model (continued).

C.N.	Name	$\nu\,(deg)$	$g\,(sec)$	$s\,(sec)$
21370	1997TB28	2.428	364.24	-11.96
21371	1997TD28	2.427	363.27	-11.04
21372	1997TM28	2.415	351.76	-7.86
21593	1998VL27	2.328	404.70	-24.44
21595	1998WJ5	2.320	300.68	-5.25
21599	1998WA15	2.425	344.42	-7.63
21601	1998XO89	2.214	334.83	-21.79
21602	Ialmenus	2.412	361.54	-12.75
21900	1999VQ10	2.381	370.47	-14.06
22008	1999XM71	2.413	377.74	-14.53
22009	1999XK77	2.438	364.27	-9.28
22010	1999XM78	2.357	400.28	-22.62
22012	1999XO82	2.449	358.51	-12.76
22014	1999XQ96	2.217	268.07	-3.06
22035	1999XR170	2.322	341.78	-14.17
22041	1999XK192	2.399	362.93	-11.51
22042	1999XP194	2.435	361.26	-11.33
22049	1999XW257	2.215	433.86	-38.75
22052	2000AQ14	2.400	359.31	-10.42
22054	2000AP21	2.319	312.97	-7.71
22055	2000AS25	2.422	355.26	-10.99
22056	2000AU31	2.399	377.21	-27.12
22059	2000AD75	2.452	350.24	-15.08
22149	2000WD49	2.307	311.79	-8.14
22180	2000YZ	2.227	270.49	-3.32
22199	Klonios	2.325	390.27	-23.22
22203	Prothoenor	2.486	353.31	-17.61
22222	Hodios	2.316	413.21	-26.87
22227	Polyxenos	2.427	342.62	-9.05
22404	1995ME4	2.392	362.36	-15.16
22503	Thalpius	2.419	352.02	-7.64
22808	1999RU12	2.426	345.21	-17.32
23075	1999XV83	2.431	337.37	-12.61
23114	2000AL16	2.437	368.72	-10.57
23118	2000AU27	2.493	348.08	-17.17
23119	2000AP33	2.355	320.15	-9.88
23123	2000AU57	2.306	391.76	-24.21
23126	2000AK95	2.257	428.01	-34.30
23135	2000AN146	2.310	338.05	-15.31
23144	2000AY182	2.367	372.42	-15.86
23152	2000CS8	2.443	346.13	-11.17

Table B.1: Basic frequencies of the Trojan asteroids in the OSS model (continued).

C.N.	Name	$\nu\,(deg)$	$g\,(sec)$	$s\,(sec)$
23269	2000YH62	2.435	349.16	-8.87
23285	2000YH119	2.306	347.86	-15.43
23355	Elephenor	2.415	369.87	-12.58
23382	Epistrophos	2.395	340.58	-8.73
23383	Schedios	2.400	352.74	-11.26
23463	1989TX11	2.417	348.94	-8.31
23480	1991EL	2.332	294.87	-8.63
23549	1994ES6	2.432	358.87	-12.42
23622	1996RW29	2.343	371.56	-17.75
23624	1996UX3	2.333	318.84	-13.22
23694	1997KZ3	2.361	382.25	-18.08
23706	1997SY32	2.434	361.18	-10.98
23709	1997TA28	2.419	354.92	-11.23
23710	1997UJ	2.297	384.30	-23.27
23939	1998TV33	2.327	391.49	-22.07
23947	1998UH16	2.454	360.49	-13.54
23958	1998VD30	2.299	295.27	-2.77
23963	1998WY8	2.386	383.17	-17.83
23968	1998XA13	2.425	347.22	-16.86
23970	1998YP6	2.223	272.23	-1.96
23987	1999NB63	2.341	301.68	-10.04
24018	1999RU134	2.382	342.37	-7.49
24022	1999RA144	2.341	380.86	-20.85
24212	1999XW59	2.285	412.70	-28.98
24225	1999XV80	2.412	358.26	-9.93
24233	1999XD94	2.347	365.08	-15.46
24244	1999XY101	2.189	272.39	-6.82
24275	1999XW167	2.356	357.20	-14.63
24279	1999XR171	2.378	360.95	-12.76
24312	1999YO22	2.399	333.08	-11.03
24313	1999YR27	2.356	334.46	-9.52
24340	2000AP84	2.449	355.01	-12.90
24341	2000AJ87	2.365	360.06	-13.12
24357	2000AC115	2.339	382.81	-19.95
24380	2000AA160	2.391	375.90	-15.95
24390	2000AD177	2.405	352.60	-9.69
24403	2000AX193	2.282	325.59	-12.14
24420	2000BU22	2.383	379.09	-17.55
24426	2000CR12	2.381	379.18	-17.05
24444	2000OP32	2.319	395.20	-24.44
24446	2000PR25	2.244	294.25	-8.22

Table B.1: Basic frequencies of the Trojan asteroids in the OSS model (continued).

C.N.	Name	$\nu\,(deg)$	$g\,(sec)$	$s\,(sec)$
24448	2000QE42	2.387	374.57	-15.26
24449	2000QL63	2.174	243.20	2.03
24451	2000QS104	2.308	320.06	-13.00
24452	2000QU167	2.447	354.16	-12.13
24453	2000QG173	2.337	377.67	-19.42
24454	2000QF198	2.262	425.78	-32.96
24456	2000RO25	2.417	360.53	-10.29
24458	2000RP100	2.338	326.94	-9.16
24459	2000RF103	2.347	342.02	-13.20
24467	2000SS165	2.368	332.63	-7.63
24470	2000SJ310	2.262	302.92	-8.03
24471	2000SH313	2.188	285.56	-12.32
24472	2000SY317	2.281	320.99	-11.66
24479	2000WU157	2.333	323.75	-8.56
24485	2000YL102	2.396	352.71	-11.69
24486	2000YR102	2.449	351.06	-11.36
24498	2001AC25	2.399	351.04	-9.65
24501	2001AN37	2.350	316.66	-4.77
24505	2001BZ	2.360	330.71	-9.35
24506	2001BS15	2.328	371.96	-18.94
24508	2001BL26	2.412	379.69	-14.66
24519	2001CH	2.413	339.04	-7.80
24528	2001CP11	2.359	347.47	-12.83
24530	2001CP18	2.407	357.00	-13.73
24531	2001CE21	2.276	320.19	-11.67
24534	2001CX27	2.396	350.48	-15.40
24536	2001CN33	2.280	292.02	-3.22
24537	2001CB35	2.337	339.79	-11.28
24539	2001DP5	2.367	369.33	-18.17
24587	4613T-2	2.250	283.37	-3.40
24603	1973SQ	2.438	362.40	-13.19
24882	1996RK30	2.424	360.44	-9.32
25344	1999RN72	2.293	341.41	-14.61
25347	1999RQ116	2.359	336.49	-8.64
25883	2000RD88	2.293	337.26	-14.43

B.2 Basic frequencies in the RTBP

We give the three basic frequencies, in the Restricted Three Body Problem, of the 400 Trojan asteroids for which they are well determined. See captions for more details.

Table B.2: Basic frequencies of the Trojan asteroids in the circular Restricted Three Body Problem. In the first column we display the catalog number of the asteroid and in the second one the asteroid's name. The frequency of libration can be seen in the third column, while in the fourth and fifth columns we show the two secular frequencies. The asteroids whose frequencies are not well determined are omitted.

C.N.	Name	$\nu\,(deg)$	$g\,(sec)$	$s\,(sec)$
588	Achilles	2.370	320.95	-2.97
617	Patroclus	2.394	327.13	-4.53
624	Hektor	2.349	375.03	-12.79
659	Nestor	2.369	312.65	-5.72
884	Priamus	2.294	318.32	-10.13
911	Agamemnon	2.378	361.83	-7.02
1143	Odysseus	2.238	294.05	-4.61
1172	Aneas	2.169	246.16	2.39
1173	Anchises	2.264	306.65	-7.64
1208	Troilus	2.308	303.50	1.04
1404	Ajax	2.397	345.87	-7.24
1437	Diomedes	2.252	352.93	-14.89
1583	Antilochus	1.978	152.22	10.90
1647	Menelaus	2.200	289.80	-7.75
1749	Telamon	2.354	326.43	-3.65
1867	Deiphobus	2.202	263.21	3.47
1869	Philoctetes	2.269	326.03	-9.94
1870	Glaukos	2.208	272.46	0.84
1871	Astyanax	2.061	250.42	-15.12
1872	Helenos	2.039	202.41	-4.38
1873	Agenor	1.943	128.73	0.08
2148	Epeios	2.195	257.87	4.37
2207	Antenor	2.236	271.93	3.11
2223	Sarpedon	2.120	226.66	4.32
2241	Alcathous	2.221	268.95	0.39
2260	Neoptolemus	2.264	284.42	3.96
2357	Phereclos	2.283	290.26	2.90
2363	Cebriones	1.893	95.08	11.75
2456	Palamedes	2.370	342.68	-2.86
2594	Acamas	2.141	357.21	-27.59
2674	Pandarus	2.292	291.27	0.93
2759	Idomeneus	1.951	134.45	0.33
2797	Teucer	2.269	297.63	-3.33
2893	Peiroos	2.179	268.46	-2.75
2920	Automedon	2.105	214.79	8.43

Table B.2: Basic frequencies of the Trojan asteroids in the RTBP (continued).

C.N.	Name	$\nu\,(deg)$	$g\,(sec)$	$s\,(sec)$
3063	Makhaon	2.286	307.65	-2.67
3240	Laocoon	2.320	304.29	0.20
3317	Paris	2.008	168.72	8.94
3391	Sinon	2.357	363.37	-8.84
3451	Mentor	1.984	155.42	9.63
3540	Protesilaos	2.362	366.46	-16.41
3548	Eurybates	2.320	334.47	-6.13
3564	Talthybius	2.360	362.66	-13.63
3596	Meriones	2.406	369.77	-6.50
3708	1974FV1	2.325	297.41	-1.49
3709	Polypoites	1.958	145.15	-3.20
3793	Leonteus	2.008	169.82	3.39
3794	Sthenelos	2.374	317.25	-6.60
4007	Euryalos	2.397	342.19	-0.30
4035	1986WD	2.115	250.51	-6.17
4057	Demophon	2.319	315.60	-3.26
4063	Euforbo	2.175	243.80	4.55
4068	Menestheus	1.924	121.96	-13.39
4086	Podalirius	2.319	323.49	-8.87
4138	Kalchas	2.292	294.16	2.68
4348	Poulydamas	2.160	259.48	-9.41
4489	1988AK	2.054	253.22	-17.15
4501	Eurypylos	2.222	282.31	-0.79
4543	Phoinix	2.275	363.87	-18.15
4707	Khryses	2.361	309.92	-2.13
4708	Polydoros	2.188	307.83	-17.01
4709	Ennomos	2.050	198.21	0.64
4715	1989TS1	2.389	373.39	-8.73
4722	Agelaos	2.320	313.11	-8.57
4754	Panthoos	2.161	245.32	3.69
4791	Iphidamas	2.088	211.46	-1.07
4792	Lykaon	2.320	321.71	-3.43
4805	Asteropaios	2.237	294.99	-7.58
4827	Dares	2.253	278.11	0.72
4828	Misenus	2.422	347.64	-5.36
4829	Sergestus	2.205	269.51	1.02
4832	Palinurus	2.100	214.39	1.97
4833	Meges	1.991	161.24	2.95
4834	Thoas	2.207	264.23	-2.16
4835	1989BQ	2.094	178.17	-21.77
4836	Medon	2.266	284.86	0.90

Table B.2: Basic frequencies of the Trojan asteroids in the RTBP (continued).

C.N.	Name	$\nu\,(deg)$	$g\,(sec)$	$s\,(sec)$
4867	Polites	2.398	342.33	-1.48
4902	Thessandrus	2.185	258.88	2.50
4946	Askalaphus	2.104	316.82	-34.28
5012	Eurymedon	2.335	319.98	-4.46
5023	Agapenor	2.336	326.24	-1.47
5025	1986TS6	2.398	339.14	0.07
5027	Androgeos	2.103	242.98	-6.23
5028	Halaesus	2.397	327.27	-1.92
5041	Theotes	2.367	340.98	-3.11
5119	1988RA1	2.378	325.72	0.05
5120	Bitias	2.251	289.44	-2.01
5123	1989BL	2.285	308.58	-5.34
5126	Achaemenides	1.956	140.11	-0.69
5130	Ilioneus	2.078	229.38	-8.14
5144	Achates	2.340	299.91	-34.32
5209	1989CW1	2.289	345.47	-10.30
5233	1988RL10	2.267	289.71	-0.43
5244	Amphilochos	2.250	276.71	3.26
5254	Ulysses	2.257	280.48	0.80
5257	1988RS10	2.267	296.96	-1.36
5258	1989AU1	2.175	289.34	-14.03
5259	Epeigeus	2.323	304.77	-6.50
5283	Pyrrhus	2.320	299.41	-1.79
5284	Orsilocus	2.184	253.52	3.62
5285	Krethon	1.997	163.22	7.07
5436	Eumelos	2.262	288.26	-0.07
5476	1989TO11	2.110	227.30	1.57
5511	Cloanthus	2.175	245.06	3.11
5637	Gyas	2.349	391.50	-18.77
5638	Deikoon	2.153	242.52	-2.59
5648	1990VU1	2.264	287.66	-11.03
5652	Amphimachus	2.313	302.75	1.51
5907	1989TU5	2.265	302.22	-6.87
6002	1988RO	2.103	217.17	1.87
6090	1989DJ	2.320	364.12	-12.18
6443	1988RH12	2.127	239.08	-9.40
6545	1986TR6	2.258	300.99	-2.04
6997	Laomedon	2.061	193.35	6.61
6998	Tithonus	2.313	311.51	0.38
7119	Hiera	2.253	292.43	-1.74
7152	Euneus	2.290	297.55	2.53

Table B.2: Basic frequencies of the Trojan asteroids in the RTBP (continued).

C.N.	Name	$\nu\,(deg)$	$g\,(sec)$	$s\,(sec)$
7214	Antielus	2.104	225.96	0.75
7352	1994CO	2.189	277.33	-3.78
7543	Prylis	2.122	227.25	4.50
8060	Anius	2.334	339.62	-8.13
8125	Tyndareus	2.322	348.19	-10.05
8241	Agrius	2.350	317.52	-2.35
8317	Eurysaces	2.139	295.90	-23.30
9023	Mnesthus	1.907	97.18	-2.12
9030	1989UX5	2.264	315.32	-7.65
9142	Rhesus	2.147	243.97	-0.73
9430	1996HU10	2.289	310.89	-2.29
9431	1996PS1	2.043	186.41	8.36
9590	1991DK1	2.317	334.93	-10.14
9694	Lycomedes	2.204	351.21	-19.06
9712	Nauplius	2.198	256.97	0.64
9713	Oceax	2.238	287.72	-1.65
9790	1995OK8	2.226	284.65	-2.20
9799	1996RJ	2.066	199.12	6.25
9807	1997SJ4	2.276	281.89	0.81
9817	Thersander	2.259	364.37	-17.13
9818	Eurymachos	2.286	351.84	-13.30
9828	Antimachos	2.309	299.46	1.43
9857	1991EN	2.281	294.22	0.48
9907	Oileus	2.118	259.71	-8.70
10247	Amphiaraos	2.037	269.95	-23.98
10664	Phemios	2.208	278.73	-1.57
10989	Dolios	2.185	249.51	5.48
11089	1994CS8	2.159	282.65	-12.27
11251	Icarion	2.304	297.51	2.76
11252	Laertes	2.297	310.89	-0.83
11273	1988RN11	2.227	297.05	-9.59
11275	1988SL3	2.079	203.14	6.74
11351	1997TS25	2.103	262.32	-13.53
11395	1998XN77	1.934	127.50	-1.47
11396	1998XZ77	2.149	236.46	4.04
11397	1998XX93	2.030	216.20	-13.26
11428	Alcinoos	2.296	400.41	-20.89
11429	Demodokus	2.293	400.59	-20.59
11487	1988RG10	2.333	318.27	-0.18
11488	1988RM11	2.282	291.77	2.17
11509	1990VL6	2.084	204.82	5.36

Table B.2: Basic frequencies of the Trojan asteroids in the RTBP (continued).

C.N.	Name	$\nu\,(deg)$	$g\,(sec)$	$s\,(sec)$
11552	1993BD4	2.143	237.10	0.32
11554	1993BZ12	2.185	253.38	1.83
11663	1997GO24	2.140	235.72	1.48
11668	Balios	2.343	319.51	-5.26
11869	1989TS2	2.144	249.41	-0.82
11887	Echemmon	2.069	200.05	5.57
12052	1997JB16	2.106	242.43	-5.36
12054	1997TT9	2.332	338.02	-4.67
12126	1999RM11	2.343	298.49	-9.53
12238	1987YU1	2.090	206.75	7.67
12242	Koon	1.962	143.47	11.93
12649	Ascanios	2.321	332.67	-10.84
12658	Peiraios	2.255	307.49	-4.14
12714	Alkimos	2.299	321.02	-3.35
12917	1998TG16	2.100	233.64	-4.83
12921	1998WZ5	2.138	236.23	2.78
12972	Eumaios	2.328	328.34	-13.28
12973	Melanthios	2.330	335.36	-4.23
12974	Halitherses	2.382	328.77	0.73
13060	1991EJ	2.236	268.84	0.04
13062	Podarkes	2.249	303.69	-5.33
13181	Peneleos	2.340	308.85	-3.80
13182	1996SO8	2.338	307.28	-2.55
13183	1996TW	2.459	345.11	-6.39
13184	1996TS49	2.266	285.63	-0.44
13185	1996TH52	2.388	336.01	0.45
13229	Echion	2.268	330.13	-11.68
13230	1997VG1	2.269	326.77	-8.37
13323	1998SQ	2.178	307.09	-15.82
13331	1998SU52	2.246	313.01	-10.13
13353	1998TU12	2.406	327.27	-3.37
13362	1998UQ16	2.288	329.35	-9.35
13366	1998US24	2.287	297.07	-0.28
13372	1998VU6	2.278	297.86	0.59
13379	1998WX9	2.303	303.54	1.93
13383	1998XS31	2.252	293.37	-0.78
13385	1998XO79	2.101	220.74	-1.77
13387	1998YW6	2.386	326.04	-1.04
13402	1999RV165	2.219	265.86	-0.56
13463	Antiphos	2.365	331.51	-1.06
13475	Orestes	2.381	331.85	-1.30

Table B.2: Basic frequencies of the Trojan asteroids in the RTBP (continued).

C.N.	Name	$\nu\,(deg)$	$g\,(sec)$	$s\,(sec)$
13650	1996TN49	2.134	245.07	-2.64
13694	1997WW7	2.129	289.91	-17.04
13780	1998UZ8	2.318	346.22	-9.69
13782	1998UM18	1.956	142.23	11.71
13790	1998UF31	2.287	317.61	-8.50
13862	1999XT160	2.180	272.69	-4.19
14235	1999XA187	2.311	340.84	-8.02
14268	2000AK156	2.244	302.99	-5.33
14518	1996RZ30	2.219	266.80	-0.39
14690	2000AR25	2.351	320.84	0.14
14707	2000CC20	2.055	216.35	-5.88
14791	Atreus	2.228	281.02	-10.80
14792	Thyestes	2.174	248.95	3.86
15033	1998VY29	2.214	265.58	-7.17
15094	1999WB2	2.316	339.36	-8.72
15398	1997UZ23	1.915	111.85	9.44
15436	1998VU30	2.190	259.64	3.04
15442	1998WN11	2.294	288.66	-2.47
15502	1999NV27	2.324	326.33	-5.26
15521	1999XH133	2.351	352.98	-12.84
15527	1999YY2	1.534	90.03	-16.97
15529	2000AA80	2.161	274.33	-10.70
15535	2000AT177	2.162	239.82	5.67
15536	2000AG191	2.118	219.03	3.03
15651	Tlepolemos	2.192	330.04	-16.54
15663	Periphas	2.398	346.21	-5.51
15913	Telemachus	2.349	320.99	1.27
15977	1998MA11	1.960	147.54	-12.94
16070	1999RB101	2.247	321.72	-14.41
16099	1999VQ24	2.267	281.62	3.03
16152	1999YN12	2.290	315.43	-4.18
16428	1988RD12	2.324	322.24	-1.54
16560	1991VZ5	2.084	267.34	-15.59
16667	1993XM1	2.233	263.46	-6.19
16974	1998WR21	2.178	251.75	2.83
17171	1999NB38	2.335	329.61	-2.99
17172	1999NZ41	1.984	155.60	8.67
17314	Aisakos	2.405	336.37	-7.47
17351	Pheidippos	2.412	354.95	-4.06
17365	1978VF11	2.180	270.33	-5.22
17414	1988RN10	2.107	219.26	5.32

Table B.2: Basic frequencies of the Trojan asteroids in the RTBP (continued).

C.N.	Name	$\nu\,(deg)$	$g\,(sec)$	$s\,(sec)$
17415	1988RO10	1.989	158.58	6.83
17416	1988RR10	2.082	208.82	5.15
17417	1988RY10	2.295	299.56	0.27
17418	1988RT12	2.218	266.16	-1.89
17419	1988RH13	2.372	335.23	-2.56
17420	1988RL13	2.330	325.03	-2.16
17421	1988SW1	2.353	359.75	-13.56
17423	1988SK2	2.296	292.25	-0.10
17424	1988SP2	2.160	235.91	4.50
17442	1989UO5	2.347	361.92	-9.70
17492	Hippasos	2.120	238.30	-1.08
17874	1998YM3	2.131	330.44	-22.53
18037	1999NA38	2.116	244.97	-10.43
18054	1999SW7	2.141	231.41	6.65
18058	1999XY129	2.327	348.51	-8.55
18060	1999XJ156	2.237	280.71	1.20
18062	1999XY187	2.358	350.80	-5.30
18063	1999XW211	2.376	345.18	-3.56
18071	2000BA27	2.195	337.51	-18.85
18137	2000OU30	2.118	260.64	-12.92
18228	Hyperenor	2.313	318.77	-7.32
18263	Anchialos	2.278	340.24	-9.77
18268	Dardanos	2.125	224.07	6.70
18278	Drymas	2.397	348.65	-5.09
18281	Tros	2.202	256.74	4.54
18282	Ilos	2.201	259.54	1.04
18493	1996HV9	2.028	191.20	-3.67
18940	2000QV49	2.138	290.01	-17.46
18971	2000QY177	2.123	220.12	2.43
19018	2000RL100	1.996	162.07	8.52
19020	2000SC6	2.252	278.88	2.68
19725	1999WT4	2.268	351.14	-14.16
19913	Aigyptios	2.153	272.08	-10.12
20144	1996RA33	2.372	334.38	-2.12
20424	1998VF30	2.285	291.72	-0.71
20428	1998WG20	2.377	330.08	-5.80
20716	1999XG91	2.094	209.62	5.72
20720	1999XP101	2.168	253.97	-6.78
20729	1999XS143	2.331	314.90	0.50
20738	1999XG191	2.388	337.73	-1.05
20739	1999XM193	2.365	318.62	-7.60

Table B.2: Basic frequencies of the Trojan asteroids in the RTBP (continued).

C.N.	Name	$\nu\,(deg)$	$g\,(sec)$	$s\,(sec)$
20947	Polyneikes	2.226	324.68	-12.31
20952	Tydeus	2.356	324.92	-0.13
20961	Arkesilaos	2.374	334.68	-0.73
20995	1985VY	2.228	300.45	-10.00
21271	1996RF33	2.276	289.59	2.75
21284	1996TC51	2.213	264.12	-0.56
21370	1997TB28	2.318	306.07	0.89
21371	1997TD28	2.268	327.44	-10.31
21372	1997TM28	2.130	241.91	-0.85
21593	1998VL27	2.276	316.04	-4.19
21595	1998WJ5	2.019	173.54	9.91
21599	1998WA15	2.196	253.56	4.83
21601	1998XO89	2.065	240.64	-11.62
21602	Ialmenus	2.325	322.43	-3.48
21900	1999VQ10	2.260	291.52	0.85
22008	1999XM71	2.246	302.25	-4.61
22009	1999XK77	2.234	296.09	-3.71
22010	1999XM78	2.255	316.15	-7.09
22012	1999XO82	2.209	292.44	-13.54
22014	1999XQ96	2.066	198.13	2.59
22035	1999XR170	2.252	301.72	-4.44
22041	1999XK192	2.387	335.73	0.13
22042	1999XP194	2.362	327.81	-1.72
22049	1999XW257	1.870	255.54	-37.08
22052	2000AQ14	2.253	305.07	-3.91
22054	2000AP21	2.248	287.77	-2.61
22055	2000AS25	2.249	303.01	-7.65
22056	2000AU31	2.277	331.74	-20.92
22059	2000AD75	2.159	254.50	-10.23
22149	2000WD49	2.288	293.12	0.78
22180	2000YZ	1.761	63.22	-12.73
22199	Klonios	2.297	359.24	-13.10
22203	Prothoenor	2.241	287.90	-14.82
22222	Hodios	2.251	323.94	-9.14
22227	Polyxenos	2.322	303.40	-0.22
22404	1995ME4	2.221	284.06	-3.94
22503	Thalpius	2.191	261.53	2.27
22808	1999RU12	2.244	320.44	-29.68
23075	1999XV83	2.239	265.19	-0.78
23114	2000AL16	2.304	313.55	-1.05
23118	2000AU27	2.340	309.07	-11.91

Table B.2: Basic frequencies of the Trojan asteroids in the RTBP (continued).

C.N.	Name	$\nu\,(deg)$	$g\,(sec)$	$s\,(sec)$
23119	2000AP33	2.384	323.79	-7.10
23123	2000AU57	2.211	350.14	-18.26
23126	2000AK95	2.149	320.29	-22.21
23135	2000AN146	2.069	237.60	-11.80
23144	2000AY182	2.164	266.46	-3.86
23152	2000CS8	2.211	257.87	1.54
23269	2000YH62	2.270	310.08	-6.12
23285	2000YH119	2.381	346.48	-3.78
23355	Elephenor	2.186	273.54	-3.63
23382	Epistrophos	2.104	216.51	3.22
23383	Schedios	2.323	318.31	-2.65
23463	1989TX11	2.231	272.12	1.71
23480	1991EL	2.100	247.10	-19.06
23549	1994ES6	2.216	274.22	-2.04
23622	1996RW29	2.176	246.49	6.20
23624	1996UX3	2.018	175.28	-0.10
23706	1997SY32	2.368	326.06	-1.32
23709	1997TA28	2.369	333.67	-3.20
23710	1997UJ	2.126	251.26	-4.91
23939	1998TV33	2.286	324.78	-5.46
23947	1998UH16	2.106	278.88	-20.90
23958	1998VD30	1.941	129.38	-2.83
23963	1998WY8	2.252	308.81	-6.36
23968	1998XA13	2.291	291.92	-5.52
23970	1998YP6	2.148	251.46	-1.12
23987	1999NB63	2.241	266.18	0.07
24018	1999RU134	2.122	223.45	7.27
24022	1999RA144	2.144	249.64	-3.00
24212	1999XW59	2.233	324.77	-11.02
24225	1999XV80	2.288	302.01	0.00
24233	1999XD94	2.257	334.28	-11.68
24244	1999XY101	2.193	272.90	-1.53
24275	1999XW167	2.262	295.65	-2.81
24279	1999XR171	2.338	329.69	-2.27
24312	1999YO22	2.350	310.76	-3.65
24313	1999YR27	2.401	343.01	-2.97
24340	2000AP84	2.287	296.39	-3.01
24341	2000AJ87	2.162	256.01	-0.30
24357	2000AC115	2.108	273.60	-13.75
24380	2000AA160	2.333	340.34	-7.64
24390	2000AD177	2.071	229.59	-8.44

Table B.2: Basic frequencies of the Trojan asteroids in the RTBP (continued).

C.N.	Name	$\nu\,(deg)$	$g\,(sec)$	$s\,(sec)$
24403	2000AX193	1.921	116.47	-5.51
24420	2000BU22	2.157	284.67	-10.48
24426	2000CR12	2.154	262.37	-4.89
24444	2000OP32	2.217	323.02	-12.03
24446	2000PR25	2.159	269.44	-7.42
24448	2000QE42	2.146	255.67	-5.73
24451	2000QS104	2.403	352.32	-8.04
24452	2000QU167	2.247	271.70	-0.35
24453	2000QG173	2.252	319.41	-7.52
24454	2000QF198	2.199	311.06	-13.10
24456	2000RO25	2.235	270.39	4.42
24458	2000RP100	2.195	264.78	-1.25
24459	2000RF103	2.344	319.56	-1.69
24467	2000SS165	2.164	244.87	3.76
24470	2000SJ310	2.113	228.17	1.69
24472	2000SY317	2.105	214.81	6.50
24479	2000WU157	2.209	258.72	4.22
24485	2000YL102	2.164	240.78	5.04
24486	2000YR102	2.208	258.16	0.66
24498	2001AC25	2.017	203.48	-10.41
24501	2001AN37	2.438	349.68	-1.38
24505	2001BZ	2.415	354.83	-6.26
24506	2001BS15	2.263	376.06	-18.50
24508	2001BL26	2.259	310.22	-4.95
24519	2001CH	2.408	349.26	-5.42
24528	2001CP11	2.104	234.50	-5.88
24530	2001CP18	2.173	249.09	2.36
24534	2001CX27	2.404	337.34	-6.75
24536	2001CN33	2.436	353.53	-1.91
24537	2001CB35	2.374	351.74	-5.75
24539	2001DP5	2.303	362.95	-14.15
24587	4613T-2	1.886	81.66	7.90
24603	1973SQ	2.346	321.06	-4.27
24882	1996RK30	2.335	334.47	-4.21
25344	1999RN72	2.008	176.02	-0.02
25347	1999RQ116	2.000	172.26	-3.52
25883	2000RD88	2.115	221.69	6.25

B.3 Basic frequencies in the BCCP

We give the three basic frequencies, in the Bicircular Coherent Problem, of the 398 Trojan asteroids for which we are able to compute them. See captions for more details.

Table B.3: Basic frequencies of the Trojan asteroids in the Bicircular Coherent Problem. In the first, column we display the catalog number of the asteroid and in the second one the asteroid's name. The frequency of libration can be seen in the third column, while in the fourth and fifth columns we show the two secular frequencies. The asteroids whose frequencies are not well determined are omitted.

C.N.	Name	$\nu\,(deg)$	$g\,(sec)$	$s\,(sec)$
588	Achilles	2.370	325.56	-9.12
617	Patroclus	2.394	332.14	-11.17
624	Hektor	2.348	382.31	-20.08
659	Nestor	2.369	317.04	-11.86
884	Priamus	2.293	322.48	-16.10
911	Agamemnon	2.378	368.62	-14.01
1143	Odysseus	2.238	297.12	-9.63
1172	Aneas	2.169	248.10	-1.51
1173	Anchises	2.266	309.95	-12.89
1208	Troilus	2.308	306.86	-4.22
1404	Ajax	2.396	352.43	-14.43
1437	Diomedes	2.252	357.88	-20.92
1583	Antilochus	1.979	155.26	8.58
1647	Menelaus	2.199	293.01	-12.66
1749	Telamon	2.354	331.05	-9.82
1867	Deiphobus	2.202	265.41	-0.61
1869	Philoctetes	2.268	330.36	-15.67
1870	Glaukos	2.208	274.95	-3.47
1871	Astyanax	2.061	254.43	-19.32
1872	Helenos	2.039	206.31	-7.72
1873	Agenor	1.942	133.31	-2.78
2148	Epeios	2.194	259.91	0.33
2207	Antenor	2.236	274.28	-1.21
2223	Sarpedon	2.120	228.82	0.95
2241	Alcathous	2.221	271.27	-4.00
2260	Neoptolemus	2.264	287.01	-0.69
2357	Phereclos	2.283	293.02	-1.97
2363	Cebriones	1.893	101.82	9.84
2456	Palamedes	2.371	347.99	-9.18
2594	Acamas	2.141	362.09	-33.54
2674	Pandarus	2.293	294.14	-4.13

Table B.3: Basic frequencies of the Trojan asteroids in the BCCP (continued).

C.N.	Name	$\nu\,(deg)$	$g\,(sec)$	$s\,(sec)$
2759	Idomeneus	1.950	139.22	-2.48
2797	Teucer	2.269	300.53	-8.52
2893	Peiroos	2.179	271.16	-6.97
2920	Automedon	2.105	216.48	5.26
3063	Makhaon	2.286	311.24	-8.05
3240	Laocoon	2.320	307.61	-5.19
3317	Paris	2.010	171.00	6.57
3391	Sinon	2.356	369.95	-15.77
3451	Mentor	1.984	158.26	7.16
3540	Protesilaos	2.363	373.06	-23.85
3548	Eurybates	2.320	339.03	-12.07
3564	Talthybius	2.361	369.19	-20.82
3596	Meriones	2.407	377.22	-13.79
3708	1974FV1	2.326	300.71	-7.02
3709	Polypoites	1.960	151.86	-5.92
3793	Leonteus	2.012	174.03	0.88
3794	Sthenelos	2.375	321.55	-12.96
4007	Euryalos	2.398	348.06	-6.90
4035	1986WD	2.115	253.61	-10.24
4057	Demophon	2.319	319.52	-9.00
4063	Euforbo	2.176	245.51	0.82
4068	Menestheus	1.948	143.82	-14.20
4086	Podalirius	2.319	327.84	-14.76
4138	Kalchas	2.292	297.13	-2.24
4348	Poulydamas	2.159	262.32	-13.91
4489	1988AK	2.052	256.90	-21.62
4501	Eurypylos	2.222	285.05	-5.35
4543	Phoinix	2.277	369.12	-24.40
4707	Khryses	2.361	314.19	-8.07
4708	Polydoros	2.186	311.82	-22.47
4709	Ennomos	2.050	201.47	-2.49
4715	1989TS1	2.390	380.59	-15.95
4722	Agelaos	2.320	317.05	-14.57
4754	Panthoos	2.161	247.41	-0.06
4791	Iphidamas	2.088	213.65	-4.56
4792	Lykaon	2.321	325.73	-9.18
4805	Asteropaios	2.237	298.35	-12.69
4827	Dares	2.254	280.71	-3.81
4828	Misenus	2.422	354.53	-12.62
4829	Sergestus	2.205	271.96	-3.23
4832	Palinurus	2.101	216.08	-1.47

Table B.3: Basic frequencies of the Trojan asteroids in the BCCP (continued).

C.N.	Name	$\nu\,(deg)$	$g\,(sec)$	$s\,(sec)$
4833	Meges	1.992	165.45	0.26
4834	Thoas	2.207	266.68	-6.46
4835	1989BQ	2.113	181.00	-24.99
4836	Medon	2.267	287.28	-3.98
4867	Polites	2.398	348.27	-8.10
4902	Thessandrus	2.185	261.08	-1.58
4946	Askalaphus	2.098	320.81	-40.52
5012	Eurymedon	2.334	324.48	-10.45
5023	Agapenor	2.335	330.72	-7.33
5025	1986TS6	2.398	345.01	-6.52
5027	Androgeos	2.102	246.00	-10.25
5028	Halaesus	2.397	332.59	-8.40
5041	Theotes	2.368	346.43	-9.52
5119	1988RA1	2.378	330.59	-6.18
5120	Bitias	2.251	292.38	-6.76
5123	1989BL	2.285	311.94	-10.84
5126	Achaemenides	1.955	145.34	-3.50
5130	Ilioneus	2.077	232.88	-11.94
5144	Achates	2.339	303.74	-42.69
5209	1989CW1	2.289	350.30	-16.29
5233	1988RL10	2.267	292.63	-5.26
5244	Amphilochos	2.250	279.16	-1.22
5254	Ulysses	2.257	283.11	-3.85
5257	1988RS10	2.267	300.11	-6.31
5258	1989AU1	2.174	292.68	-19.07
5259	Epeigeus	2.322	308.59	-12.29
5283	Pyrrhus	2.320	302.79	-7.12
5284	Orsilocus	2.184	255.45	-0.35
5285	Krethon	1.998	166.59	4.52
5436	Eumelos	2.262	291.09	-4.97
5476	1989TO11	2.113	230.41	-1.48
5511	Cloanthus	2.175	246.80	-0.73
5637	Gyas	2.348	399.62	-26.74
5638	Deikoon	2.154	244.68	-6.55
5648	1990VU1	2.265	290.32	-16.51
5652	Amphimachus	2.314	306.10	-3.76
5907	1989TU5	2.265	305.54	-12.15
6002	1988RO	2.104	219.40	-1.50
6090	1989DJ	2.319	370.56	-18.99
6443	1988RH12	2.128	241.74	-13.48
6545	1986TR6	2.258	304.16	-6.95

Table B.3: Basic frequencies of the Trojan asteroids in the BCCP (continued).

C.N.	Name	$\nu\,(deg)$	$g\,(sec)$	$s\,(sec)$
6997	Laomedon	2.061	194.94	3.65
6998	Tithonus	2.314	315.12	-5.02
7119	Hiera	2.253	295.45	-6.61
7152	Euneus	2.290	300.56	-2.45
7214	Antielus	2.104	228.64	-2.71
7352	1994CO	2.190	280.22	-8.16
7543	Prylis	2.122	229.25	1.03
8060	Anius	2.335	344.55	-14.35
8125	Tyndareus	2.323	353.46	-16.30
8241	Agrius	2.351	321.78	-8.21
8317	Eurysaces	2.138	300.07	-28.35
9023	Mnesthus	1.909	108.80	-4.44
9030	1989UX5	2.264	319.13	-12.99
9142	Rhesus	2.147	246.07	-4.63
9430	1996HU10	2.289	314.41	-7.60
9431	1996PS1	2.044	188.52	5.57
9590	1991DK1	2.318	339.54	-16.18
9694	Lycomedes	2.204	355.92	-24.93
9712	Nauplius	2.199	259.01	-3.50
9713	Oceax	2.238	290.51	-6.44
9790	1995OK8	2.225	287.52	-6.94
9799	1996RJ	2.065	201.17	3.17
9807	1997SJ4	2.277	284.44	-3.98
9817	Thersander	2.258	369.91	-23.61
9818	Eurymachos	2.285	357.07	-19.60
9828	Antimachos	2.309	302.60	-3.85
9857	1991EN	2.282	297.15	-4.53
9907	Oileus	2.116	262.58	-13.23
10247	Amphiaraos	2.035	273.96	-28.81
10664	Phemios	2.208	281.49	-6.08
10989	Dolios	2.186	251.29	1.65
11089	1994CS8	2.158	286.09	-17.05
11251	Icarion	2.304	300.67	-2.32
11252	Laertes	2.297	314.44	-6.12
11273	1988RN11	2.227	300.36	-14.74
11275	1988SL3	2.080	204.88	3.69
11351	1997TS25	2.103	265.95	-17.86
11395	1998XN77	1.942	134.24	-3.53
11396	1998XZ77	2.149	238.35	0.39
11397	1998XX93	2.028	220.35	-17.20
11428	Alcinoos	2.294	408.47	-28.42

Table B.3: Basic frequencies of the Trojan asteroids in the BCCP (continued).

C.N.	Name	$\nu\,(deg)$	$g\,(sec)$	$s\,(sec)$
11429	Demodokus	2.292	408.20	-28.02
11487	1988RG10	2.334	322.30	-5.80
11488	1988RM11	2.282	294.66	-2.67
11509	1990VL6	2.085	206.63	2.20
11552	1993BD4	2.143	238.84	-3.59
11554	1993BZ12	2.185	255.47	-2.13
11663	1997GO24	2.140	237.78	-2.20
11668	Balios	2.344	323.63	-11.24
11869	1989TS2	2.143	251.94	-4.74
11887	Echemmon	2.070	202.18	2.48
12052	1997JB16	2.109	246.09	-8.85
12054	1997TT9	2.332	342.71	-10.66
12126	1999RM11	2.342	302.29	-15.49
12238	1987YU1	2.090	208.30	4.56
12242	Koon	1.962	146.55	9.69
12649	Ascanios	2.321	337.32	-17.22
12658	Peiraios	2.256	310.88	-9.21
12714	Alkimos	2.299	325.12	-8.97
12917	1998TG16	2.101	236.80	-8.51
12921	1998WZ5	2.138	238.28	-0.87
12972	Eumaios	2.330	332.61	-19.40
12973	Melanthios	2.331	339.95	-10.12
12974	Halitherses	2.382	333.82	-5.46
13060	1991EJ	2.237	271.16	-4.31
13062	Podarkes	2.250	307.12	-10.33
13181	Peneleos	2.341	312.53	-9.71
13182	1996SO8	2.337	311.17	-8.31
13183	1996TW	2.458	353.05	-14.19
13184	1996TS49	2.266	288.47	-5.17
13185	1996TH52	2.389	341.47	-5.93
13229	Echion	2.267	334.58	-17.62
13230	1997VG1	2.270	330.69	-13.86
13323	1998SQ	2.180	310.84	-20.87
13331	1998SU52	2.247	316.65	-15.40
13353	1998TU12	2.407	332.34	-10.29
13362	1998UQ16	2.288	333.65	-15.15
13366	1998US24	2.287	300.09	-5.42
13372	1998VU6	2.278	301.02	-4.43
13379	1998WX9	2.303	306.77	-3.21
13383	1998XS31	2.253	296.29	-5.53
13385	1998XO79	2.101	223.28	-5.29

Table B.3: Basic frequencies of the Trojan asteroids in the BCCP (continued).

C.N.	Name	$\nu\,(deg)$	$g\,(sec)$	$s\,(sec)$
13387	1998YW6	2.386	331.12	-7.37
13402	1999RV165	2.218	268.05	-4.95
13463	Antiphos	2.365	336.50	-7.23
13475	Orestes	2.381	337.02	-7.73
13650	1996TN49	2.134	247.65	-6.59
13694	1997WW7	2.117	292.49	-23.05
13780	1998UZ8	2.318	351.45	-16.05
13782	1998UM18	1.957	144.77	9.46
13790	1998UF31	2.287	321.29	-14.24
13862	1999XT160	2.179	275.44	-8.66
14235	1999XA187	2.312	345.42	-13.93
14268	2000AK156	2.243	306.47	-10.56
14518	1996RZ30	2.219	269.05	-4.77
14690	2000AR25	2.351	325.29	-5.72
14707	2000CC20	2.055	220.13	-9.42
14791	Atreus	2.230	283.78	-15.69
14792	Thyestes	2.174	250.93	0.04
15033	1998VY29	2.217	268.15	-11.65
15094	1999WB2	2.317	344.06	-14.74
15398	1997UZ23	1.916	117.22	7.32
15436	1998VU30	2.189	261.84	-1.09
15442	1998WN11	2.294	291.55	-7.49
15502	1999NV27	2.325	330.68	-11.07
15521	1999XH133	2.350	359.24	-19.86
15529	2000AA80	2.160	277.64	-15.25
15535	2000AT177	2.163	241.47	1.98
15536	2000AG191	2.119	220.73	-0.32
15651	Tlepolemos	2.192	334.32	-22.10
15663	Periphas	2.399	352.21	-12.35
15913	Telemachus	2.349	325.31	-4.53
16070	1999RB101	2.246	325.93	-20.14
16099	1999VQ24	2.267	284.19	-1.62
16152	1999YN12	2.291	319.01	-9.49
16428	1988RD12	2.324	326.36	-7.24
16560	1991VZ5	2.086	271.50	-19.83
16667	1993XM1	2.235	265.05	-11.16
16974	1998WR21	2.177	253.79	-1.15
17171	1999NB38	2.335	334.10	-8.89
17172	1999NZ41	1.985	158.50	6.24
17314	Aisakos	2.405	342.41	-14.61
17351	Pheidippos	2.413	361.67	-11.10

Table B.3: Basic frequencies of the Trojan asteroids in the BCCP (continued).

C.N.	Name	$\nu\,(deg)$	$g\,(sec)$	$s\,(sec)$
17365	1978VF11	2.180	273.27	-9.61
17414	1988RN10	2.107	221.29	2.02
17415	1988RO10	1.989	162.08	4.27
17416	1988RR10	2.082	211.06	2.00
17417	1988RY10	2.296	302.68	-4.86
17418	1988RT12	2.219	268.20	-6.38
17419	1988RH13	2.372	340.42	-8.89
17420	1988RL13	2.330	329.25	-7.99
17421	1988SW1	2.354	365.91	-20.49
17423	1988SK2	2.296	295.13	-5.27
17424	1988SP2	2.161	237.26	0.73
17442	1989UO5	2.347	368.31	-16.56
17492	Hippasos	2.114	239.97	-5.48
17874	1998YM3	2.130	334.79	-28.06
18037	1999NA38	2.116	247.96	-14.52
18054	1999SW7	2.141	233.16	3.18
18058	1999XY129	2.328	353.73	-14.87
18060	1999XJ156	2.237	283.29	-3.31
18062	1999XY187	2.358	356.43	-11.79
18063	1999XW211	2.376	350.74	-9.99
18071	2000BA27	2.195	341.93	-24.55
18137	2000OU30	2.122	264.67	-16.80
18228	Hyperenor	2.314	322.88	-13.22
18263	Anchialos	2.279	344.81	-15.61
18268	Dardanos	2.125	225.79	3.35
18278	Drymas	2.397	354.97	-11.96
18281	Tros	2.202	258.57	0.47
18282	Ilos	2.201	261.77	-3.09
18493	1996HV9	2.029	195.37	-6.79
18940	2000QV49	2.136	293.47	-22.57
18971	2000QY177	2.124	221.49	-1.15
19018	2000RL100	1.997	164.87	5.97
19020	2000SC6	2.253	281.15	-1.93
19725	1999WT4	2.267	356.13	-20.35
19913	Aigyptios	2.153	275.07	-14.71
20144	1996RA33	2.372	339.65	-8.47
20424	1998VF30	2.285	294.75	-5.72
20428	1998WG20	2.377	335.30	-12.24
20716	1999XG91	2.095	211.39	2.47
20720	1999XP101	2.169	256.37	-10.97
20729	1999XS143	2.331	318.89	-5.09

Table B.3: Basic frequencies of the Trojan asteroids in the BCCP (continued).

C.N.	Name	$\nu\,(deg)$	$g\,(sec)$	$s\,(sec)$
20738	1999XG191	2.388	343.26	-7.50
20739	1999XM193	2.365	323.15	-14.03
20947	Polyneikes	2.227	328.60	-17.68
20952	Tydeus	2.356	329.45	-6.07
20961	Arkesilaos	2.374	339.80	-6.96
20995	1985VY	2.229	303.75	-15.08
21271	1996RF33	2.276	292.38	-2.02
21284	1996TC51	2.213	266.38	-4.94
21370	1997TB28	2.319	309.51	-4.56
21371	1997TD28	2.268	331.50	-16.09
21372	1997TM28	2.130	244.38	-4.73
21593	1998VL27	2.277	319.62	-9.41
21595	1998WJ5	2.020	175.48	7.32
21599	1998WA15	2.196	255.39	0.85
21601	1998XO89	2.065	244.49	-15.65
21602	Ialmenus	2.325	326.80	-9.38
21900	1999VQ10	2.260	294.39	-3.95
22008	1999XM71	2.246	305.57	-9.62
22009	1999XK77	2.234	299.24	-8.63
22010	1999XM78	2.256	319.84	-12.34
22012	1999XO82	2.209	295.40	-18.81
22014	1999XQ96	2.067	200.44	-0.48
22035	1999XR170	2.251	305.16	-9.66
22041	1999XK192	2.388	341.07	-6.26
22042	1999XP194	2.362	332.55	-7.81
22049	1999XW257	1.918	268.51	-39.96
22052	2000AQ14	2.252	308.45	-8.99
22054	2000AP21	2.248	290.67	-7.54
22055	2000AS25	2.248	306.64	-12.89
22056	2000AU31	2.280	336.01	-26.95
22059	2000AD75	2.159	257.10	-14.85
22149	2000WD49	2.288	296.10	-4.30
22199	Klonios	2.295	365.07	-19.69
22203	Prothoenor	2.243	291.47	-19.70
22222	Hodios	2.252	327.80	-14.53
22227	Polyxenos	2.322	306.92	-5.66
22404	1995ME4	2.221	286.95	-8.72
22503	Thalpius	2.190	263.75	-1.90
22808	1999RU12	2.240	325.35	-36.26
23075	1999XV83	2.239	267.36	-5.19
23114	2000AL16	2.303	317.35	-6.50

Table B.3: Basic frequencies of the Trojan asteroids in the BCCP (continued).

C.N.	Name	$\nu\,(deg)$	$g\,(sec)$	$s\,(sec)$
23118	2000AU27	2.341	313.12	-17.88
23119	2000AP33	2.384	328.75	-13.71
23123	2000AU57	2.211	355.00	-24.24
23126	2000AK95	2.149	324.56	-27.59
23135	2000AN146	2.068	241.22	-15.92
23144	2000AY182	2.163	269.24	-8.17
23152	2000CS8	2.211	259.83	-2.58
23269	2000YH62	2.270	313.81	-11.63
23285	2000YH119	2.381	352.21	-10.38
23355	Elephenor	2.185	276.33	-8.11
23382	Epistrophos	2.104	218.47	-0.12
23383	Schedios	2.323	322.49	-8.43
23463	1989TX11	2.231	274.48	-2.65
23480	1991EL	2.100	250.19	-23.62
23549	1994ES6	2.217	276.88	-6.53
23622	1996RW29	2.177	248.25	2.44
23624	1996UX3	2.020	178.20	-2.91
23694	1997KZ3	2.223	318.00	-14.80
23706	1997SY32	2.368	330.98	-7.54
23709	1997TA28	2.370	338.67	-9.39
23710	1997UJ	2.127	254.37	-8.81
23939	1998TV33	2.287	328.67	-10.92
23947	1998UH16	2.107	282.71	-25.74
23958	1998VD30	1.950	138.96	-4.74
23963	1998WY8	2.253	312.29	-11.54
23968	1998XA13	2.291	294.65	-10.93
23970	1998YP6	2.147	253.92	-5.12
23987	1999NB63	2.242	268.43	-4.46
24018	1999RU134	2.122	225.19	3.97
24022	1999RA144	2.144	252.16	-6.99
24212	1999XW59	2.234	328.63	-16.35
24225	1999XV80	2.288	305.18	-5.14
24233	1999XD94	2.256	338.81	-17.50
24244	1999XY101	2.193	275.54	-5.90
24275	1999XW167	2.262	298.77	-7.85
24279	1999XR171	2.339	334.18	-8.16
24312	1999YO22	2.350	315.17	-9.57
24313	1999YR27	2.401	349.42	-9.86
24340	2000AP84	2.288	299.54	-8.16
24341	2000AJ87	2.162	258.41	-4.36
24357	2000AC115	2.104	276.89	-18.58

Table B.3: Basic frequencies of the Trojan asteroids in the BCCP (continued).

C.N.	Name	$\nu\,(deg)$	$g\,(sec)$	$s\,(sec)$
24380	2000AA160	2.333	345.34	-13.87
24390	2000AD177	2.070	232.88	-12.43
24403	2000AX193	1.921	125.33	-8.26
24420	2000BU22	2.157	287.97	-15.19
24426	2000CR12	2.153	265.13	-9.16
24444	2000OP32	2.218	326.94	-17.37
24446	2000PR25	2.158	272.39	-12.02
24448	2000QE42	2.146	258.56	-9.78
24451	2000QS104	2.403	358.87	-15.31
24452	2000QU167	2.247	274.22	-4.88
24453	2000QG173	2.252	323.20	-12.87
24454	2000QF198	2.200	314.80	-18.15
24456	2000RO25	2.235	272.63	0.13
24458	2000RP100	2.195	267.08	-5.66
24459	2000RF103	2.345	323.71	-7.49
24467	2000SS165	2.164	246.88	0.00
24470	2000SJ310	2.113	230.63	-1.84
24472	2000SY317	2.106	216.68	3.33
24479	2000WU157	2.209	260.45	0.05
24485	2000YL102	2.164	242.67	1.43
24486	2000YR102	2.208	260.36	-3.46
24498	2001AC25	2.016	207.54	-14.13
24501	2001AN37	2.438	356.92	-8.67
24505	2001BZ	2.415	362.22	-13.60
24506	2001BS15	2.261	382.27	-25.25
24508	2001BL26	2.258	313.81	-10.27
24519	2001CH	2.408	355.82	-12.63
24528	2001CP11	2.103	237.07	-9.86
24530	2001CP18	2.174	251.11	-1.49
24534	2001CX27	2.404	343.47	-13.58
24536	2001CN33	2.436	361.06	-9.35
24537	2001CB35	2.375	357.60	-12.35
24539	2001DP5	2.303	368.58	-20.79
24587	4613T-2	1.887	91.66	5.96
24603	1973SQ	2.346	325.44	-10.29
24882	1996RK30	2.334	339.33	-10.34
25344	1999RN72	2.008	180.12	-2.96
25347	1999RQ116	1.999	176.23	-6.66
25883	2000RD88	2.116	223.65	3.00

B.4 Basic frequencies in the ESRTBP

We write the three basic frequencies, in the Elliptic Restricted Three Body Problem, of the 397 Trojan asteroids for which we are able to compute them. See captions for more details.

Table B.4: Basic frequencies of the Trojan asteroids in the Elliptic RTBP. In the first, column we display the catalog number of the asteroid and in the second one the asteroid's name. The frequency of libration can be seen in the third column, while in the fourth and fifth columns the two secular frequencies are shown. The asteroids whose frequencies are not well determined are omitted.

C.N.	Name	$\nu\,(deg)$	$g\,(sec)$	$s\,(sec)$
588	Achilles	2.383	319.13	-3.56
617	Patroclus	2.408	325.94	-3.26
624	Hektor	2.350	377.17	-12.40
659	Nestor	2.343	318.66	-11.17
884	Priamus	2.348	311.28	-3.06
911	Agamemnon	2.371	366.62	-10.05
1143	Odysseus	2.257	292.64	-3.06
1172	Aneas	2.183	246.06	3.02
1173	Anchises	2.277	306.22	-6.80
1208	Troilus	2.320	302.54	1.22
1404	Ajax	2.350	360.17	-16.54
1437	Diomedes	2.267	350.09	-14.48
1583	Antilochus	1.986	152.98	11.12
1647	Menelaus	2.205	289.47	-7.75
1749	Telamon	2.360	326.98	-3.68
1867	Deiphobus	2.218	263.07	4.64
1869	Philoctetes	2.212	331.36	-17.78
1870	Glaukos	2.203	271.84	-0.88
1871	Astyanax	2.049	243.80	-17.57
1872	Helenos	2.010	189.89	-7.82
2148	Epeios	2.191	257.28	2.69
2207	Antenor	2.248	271.34	3.35
2223	Sarpedon	2.120	225.17	3.37
2241	Alcathous	2.204	266.77	-4.02
2260	Neoptolemus	2.266	284.80	2.98
2357	Phereclos	2.290	290.70	2.61
2456	Palamedes	2.383	340.95	-2.10
2594	Acamas	2.183	356.04	-23.03
2674	Pandarus	2.304	291.17	1.46
2759	Idomeneus	1.991	156.74	4.32
2797	Teucer	2.261	299.47	-5.18

Table B.4: Basic frequencies of the Trojan asteroids in the ESRTBP (continued).

C.N.	Name	$\nu\,(deg)$	$g\,(sec)$	$s\,(sec)$
2893	Peiroos	2.186	267.51	-2.21
2895	Memnon	1.952	114.82	-2.11
2920	Automedon	2.113	214.44	8.36
3063	Makhaon	2.298	306.62	-1.78
3240	Laocoon	2.323	304.23	-0.26
3317	Paris	1.997	159.50	6.65
3391	Sinon	2.356	365.32	-10.98
3451	Mentor	1.997	158.71	10.47
3540	Protesilaos	2.411	354.46	-9.49
3548	Eurybates	2.346	329.41	-4.53
3564	Talthybius	2.356	365.28	-15.86
3596	Meriones	2.433	362.02	-4.12
3708	1974FV1	2.335	296.95	-1.40
3709	Polypoites	1.954	140.19	-4.37
3793	Leonteus	2.022	173.00	3.97
3794	Sthenelos	2.394	315.36	-4.18
4007	Euryalos	2.409	340.73	0.03
4035	1986WD	2.098	245.38	-8.77
4057	Demophon	2.328	314.85	-3.88
4060	Deipylos	2.028	180.47	-8.68
4063	Euforbo	2.186	243.30	4.65
4068	Menestheus	2.007	171.24	-4.49
4086	Podalirius	2.327	321.69	-10.71
4138	Kalchas	2.302	294.01	3.03
4348	Poulydamas	2.216	264.31	-2.38
4489	1988AK	2.078	257.42	-15.02
4501	Eurypylos	2.222	280.09	-1.02
4543	Phoinix	2.342	349.81	-11.01
4707	Khryses	2.363	311.74	-2.89
4708	Polydoros	2.228	306.28	-13.46
4709	Ennomos	2.056	198.76	0.65
4715	1989TS1	2.393	374.82	-9.71
4722	Agelaos	2.358	308.66	-3.39
4754	Panthoos	2.168	245.47	3.43
4791	Iphidamas	2.100	211.38	-1.54
4792	Lykaon	2.339	319.11	-1.77
4805	Asteropaios	2.277	293.20	-3.15
4827	Dares	2.264	278.78	-0.16
4828	Misenus	2.433	347.01	-7.04
4829	Sergestus	2.216	270.18	0.79
4832	Palinurus	2.120	217.18	3.62

Table B.4: Basic frequencies of the Trojan asteroids in the ESRTBP (continued).

C.N.	Name	$\nu\,(deg)$	$g\,(sec)$	$s\,(sec)$
4833	Meges	1.916	102.04	-6.12
4834	Thoas	2.208	264.16	-3.21
4835	1989BQ	2.131	185.91	-18.55
4836	Medon	2.277	283.92	1.03
4867	Polites	2.415	339.22	-0.12
4902	Thessandrus	2.191	258.85	2.02
5012	Eurymedon	2.286	329.18	-12.36
5023	Agapenor	2.331	328.96	-3.37
5025	1986TS6	2.403	340.55	-0.62
5027	Androgeos	2.071	233.79	-10.87
5028	Halaesus	2.397	329.74	-4.21
5041	Theotes	2.375	341.43	-2.97
5119	1988RA1	2.386	325.88	-0.41
5120	Bitias	2.253	289.48	-3.24
5123	1989BL	2.314	305.56	-2.04
5126	Achaemenides	1.960	142.02	-0.33
5130	Ilioneus	2.067	220.94	-11.54
5144	Achates	2.395	298.95	-24.62
5209	1989CW1	2.308	341.99	-9.09
5233	1988RL10	2.273	285.84	-0.18
5244	Amphilochos	2.253	277.27	2.53
5254	Ulysses	2.253	281.26	-1.35
5257	1988RS10	2.268	295.92	-2.69
5258	1989AU1	2.221	290.64	-8.49
5259	Epeigeus	2.305	307.57	-10.51
5264	Telephus	1.921	113.87	4.38
5283	Pyrrhus	2.331	298.64	-1.63
5284	Orsilocus	2.191	252.85	3.42
5285	Krethon	1.999	161.15	6.68
5436	Eumelos	2.282	287.40	1.58
5476	1989TO11	2.128	229.58	2.87
5511	Cloanthus	2.182	244.55	2.90
5637	Gyas	2.348	393.50	-19.59
5638	Deikoon	2.091	227.80	-10.68
5648	1990VU1	2.245	290.93	-13.13
5652	Amphimachus	2.318	305.13	0.38
5907	1989TU5	2.304	299.19	-1.63
6002	1988RO	2.131	222.26	4.91
6090	1989DJ	2.276	374.83	-19.04
6443	1988RH12	2.190	248.68	-1.05
6545	1986TR6	2.268	295.67	-0.42

Table B.4: Basic frequencies of the Trojan asteroids in the ESRTBP (continued).

C.N.	Name	$\nu\,(deg)$	$g\,(sec)$	$s\,(sec)$
6997	Laomedon	2.057	189.54	5.29
6998	Tithonus	2.326	312.85	0.37
7119	Hiera	2.250	292.63	-2.83
7152	Euneus	2.299	297.51	2.52
7214	Antielus	2.109	226.88	0.71
7352	1994CO	2.197	275.48	-3.77
7543	Prylis	2.126	226.49	3.99
8060	Anius	2.366	333.20	-4.91
8125	Tyndareus	2.342	345.06	-8.01
8241	Agrius	2.362	316.97	-1.39
8317	Eurysaces	2.071	292.14	-28.46
9023	Mnesthus	1.912	98.40	-3.23
9030	1989UX5	2.270	315.61	-7.39
9142	Rhesus	2.128	233.20	0.30
9430	1996HU10	2.265	314.68	-6.68
9431	1996PS1	2.045	184.24	7.61
9590	1991DK1	2.323	333.52	-11.42
9694	Lycomedes	2.193	351.73	-20.79
9712	Nauplius	2.213	256.66	1.00
9713	Oceax	2.229	277.73	0.29
9790	1995OK8	2.193	284.04	-7.27
9799	1996RJ	2.051	191.65	3.31
9807	1997SJ4	2.287	280.35	0.63
9817	Thersander	2.267	363.84	-16.62
9818	Eurymachos	2.275	354.45	-15.58
9828	Antimachos	2.319	299.12	1.57
9857	1991EN	2.290	294.98	0.77
9907	Oileus	2.082	251.83	-13.41
10247	Amphiaraos	2.020	269.40	-24.36
10664	Phemios	2.211	277.42	-1.34
10989	Dolios	2.195	249.58	5.76
11089	1994CS8	2.136	273.94	-17.47
11251	Icarion	2.311	297.61	2.49
11252	Laertes	2.302	311.02	-1.48
11273	1988RN11	2.194	295.65	-14.41
11275	1988SL3	2.091	204.37	7.35
11351	1997TS25	2.062	251.83	-18.12
11396	1998XZ77	2.160	247.08	-0.38
11397	1998XX93	2.005	204.19	-15.81
11428	Alcinoos	2.264	409.99	-24.44
11429	Demodokus	2.289	402.68	-21.48

Table B.4: Basic frequencies of the Trojan asteroids in the ESRTBP (continued).

C.N.	Name	$\nu\,(deg)$	$g\,(sec)$	$s\,(sec)$
11487	1988RG10	2.339	317.84	-0.55
11488	1988RM11	2.289	291.94	1.82
11509	1990VL6	2.098	206.85	6.37
11552	1993BD4	2.160	237.75	1.35
11554	1993BZ12	2.158	245.01	-0.51
11663	1997GO24	2.146	235.94	1.26
11668	Balios	2.349	320.24	-5.30
11869	1989TS2	2.136	245.96	-2.44
11887	Echemmon	2.092	204.50	7.63
12052	1997JB16	2.104	241.06	-6.13
12054	1997TT9	2.349	335.45	-3.72
12126	1999RM11	2.365	297.00	-7.20
12238	1987YU1	2.097	206.12	7.52
12242	Koon	1.968	142.95	11.85
12649	Ascanios	2.329	332.67	-10.61
12658	Peiraios	2.273	305.38	-2.97
12714	Alkimos	2.304	321.13	-3.62
12917	1998TG16	2.107	233.42	-4.51
12921	1998WZ5	2.141	234.36	1.11
12972	Eumaios	2.381	320.39	-5.49
12973	Melanthios	2.341	334.38	-3.80
12974	Halitherses	2.390	329.30	0.60
13060	1991EJ	2.231	268.59	-1.51
13062	Podarkes	2.261	304.04	-4.03
13181	Peneleos	2.362	306.33	-1.84
13182	1996SO8	2.296	314.28	-9.86
13183	1996TW	2.439	355.42	-10.38
13184	1996TS49	2.260	281.56	0.11
13185	1996TH52	2.400	335.29	0.72
13229	Echion	2.292	328.15	-8.92
13230	1997VG1	2.269	327.53	-9.22
13323	1998SQ	2.189	307.72	-14.76
13331	1998SU52	2.241	314.05	-11.38
13353	1998TU12	2.409	329.31	-4.15
13362	1998UQ16	2.297	328.42	-9.43
13366	1998US24	2.299	295.95	0.24
13372	1998VU6	2.270	299.47	-1.51
13379	1998WX9	2.317	302.51	2.63
13383	1998XS31	2.277	292.28	1.12
13385	1998XO79	2.064	208.45	-6.64
13387	1998YW6	2.373	332.25	-4.25

Table B.4: Basic frequencies of the Trojan asteroids in the ESRTBP (continued).

C.N.	Name	$\nu\,(deg)$	$g\,(sec)$	$s\,(sec)$
13402	1999RV165	2.225	263.79	-0.07
13463	Antiphos	2.372	331.59	-0.89
13475	Orestes	2.395	330.00	-0.39
13650	1996TN49	2.140	241.56	-3.47
13694	1997WW7	2.115	284.17	-19.65
13780	1998UZ8	2.326	346.28	-9.44
13782	1998UM18	1.945	129.82	9.42
13790	1998UF31	2.321	313.31	-5.10
13862	1999XT160	2.142	267.94	-9.85
14235	1999XA187	2.342	335.02	-5.22
14268	2000AK156	2.219	303.68	-9.47
14518	1996RZ30	2.212	263.60	-3.44
14690	2000AR25	2.351	322.89	-0.93
14707	2000CC20	2.052	212.54	-7.09
14791	Atreus	2.294	281.16	-2.05
14792	Thyestes	2.190	249.40	4.97
15033	1998VY29	2.252	265.07	-3.77
15094	1999WB2	2.358	330.94	-4.47
15398	1997UZ23	1.929	118.76	10.46
15436	1998VU30	2.192	259.79	2.17
15442	1998WN11	2.310	287.12	-1.86
15502	1999NV27	2.341	323.29	-5.62
15521	1999XH133	2.380	347.87	-8.50
15529	2000AA80	2.145	273.79	-12.39
15535	2000AT177	2.171	239.33	5.55
15536	2000AG191	2.124	217.39	2.41
15651	Tlepolemos	2.174	329.07	-19.65
15663	Periphas	2.428	339.02	-2.08
15913	Telemachus	2.354	322.66	0.41
16070	1999RB101	2.296	317.55	-8.36
16099	1999VQ24	2.266	282.41	1.72
16152	1999YN12	2.318	311.55	-1.22
16428	1988RD12	2.332	322.10	-1.57
16560	1991VZ5	2.119	268.75	-12.77
16667	1993XM1	2.238	264.40	-6.04
16974	1998WR21	2.155	246.76	-0.75
17171	1999NB38	2.346	329.34	-2.58
17172	1999NZ41	1.997	158.80	9.43
17314	Aisakos	2.424	332.98	-7.84
17351	Pheidippos	2.426	352.92	-3.09
17365	1978VF11	2.210	271.77	-1.98

Table B.4: Basic frequencies of the Trojan asteroids in the ESRTBP (continued).

C.N.	Name	$\nu\,(deg)$	$g\,(sec)$	$s\,(sec)$
17414	1988RN10	2.117	219.44	5.60
17415	1988RO10	1.988	154.72	5.92
17416	1988RR10	2.097	211.07	6.25
17417	1988RY10	2.311	302.94	-0.06
17418	1988RT12	2.227	266.72	-1.19
17419	1988RH13	2.371	338.23	-4.03
17420	1988RL13	2.336	325.28	-2.16
17421	1988SW1	2.401	348.06	-6.87
17423	1988SK2	2.278	294.71	-3.70
17424	1988SP2	2.165	235.15	4.15
17442	1989UO5	2.361	359.53	-9.19
17492	Hippasos	2.145	242.18	1.40
17874	1998YM3	2.142	326.08	-23.61
18037	1999NA38	2.163	251.87	-4.73
18054	1999SW7	2.143	230.46	5.82
18058	1999XY129	2.332	349.36	-8.72
18060	1999XJ156	2.255	287.53	0.01
18062	1999XY187	2.365	351.22	-5.60
18063	1999XW211	2.402	339.09	-0.73
18071	2000BA27	2.176	334.96	-22.57
18137	2000OU30	2.120	252.33	-16.49
18228	Hyperenor	2.347	313.97	-3.32
18263	Anchialos	2.290	338.64	-9.21
18268	Dardanos	2.133	224.04	6.75
18278	Drymas	2.406	348.43	-5.17
18281	Tros	2.207	256.28	4.02
18282	Ilos	2.221	260.26	3.03
18493	1996HV9	1.998	176.73	-7.22
18940	2000QV49	2.183	291.66	-13.22
18971	2000QY177	2.089	209.02	-2.41
19018	2000RL100	2.009	165.07	9.49
19020	2000SC6	2.260	279.05	2.55
19725	1999WT4	2.276	350.88	-13.72
19913	Aigyptios	2.178	273.60	-7.56
20144	1996RA33	2.377	335.33	-2.97
20424	1998VF30	2.290	292.31	-1.35
20428	1998WG20	2.376	332.50	-7.20
20716	1999XG91	2.063	194.25	-0.93
20720	1999XP101	2.180	252.64	-7.07
20729	1999XS143	2.332	316.31	-0.76
20738	1999XG191	2.395	338.45	-1.79

Table B.4: Basic frequencies of the Trojan asteroids in the ESRTBP (continued).

C.N.	Name	$\nu\,(deg)$	$g\,(sec)$	$s\,(sec)$
20739	1999XM193	2.388	316.03	-4.66
20947	Polyneikes	2.230	323.91	-12.72
20952	Tydeus	2.359	325.92	-0.78
20961	Arkesilaos	2.384	333.96	-0.75
20995	1985VY	2.215	301.37	-12.32
21271	1996RF33	2.287	289.29	3.14
21284	1996TC51	2.161	258.76	-8.29
21370	1997TB28	2.329	305.67	1.16
21371	1997TD28	2.300	323.79	-6.73
21372	1997TM28	2.100	222.47	0.48
21593	1998VL27	2.294	313.77	-2.61
21595	1998WJ5	2.008	164.97	7.47
21599	1998WA15	2.201	252.62	4.04
21601	1998XO89	2.066	239.07	-11.91
21602	Ialmenus	2.337	321.49	-2.50
21900	1999VQ10	2.274	292.62	0.57
22008	1999XM71	2.243	302.14	-6.18
22009	1999XK77	2.235	296.13	-4.50
22010	1999XM78	2.258	315.59	-8.00
22012	1999XO82	2.272	292.32	-5.28
22014	1999XQ96	2.094	205.02	5.56
22035	1999XR170	2.233	302.43	-7.94
22041	1999XK192	2.394	335.20	-0.00
22042	1999XP194	2.361	330.42	-2.98
22049	1999XW257	1.896	260.43	-35.88
22052	2000AQ14	2.245	306.17	-6.06
22054	2000AP21	2.261	287.30	-0.96
22055	2000AS25	2.225	305.34	-11.14
22056	2000AU31	2.375	319.23	-7.03
22059	2000AD75	2.220	260.81	-2.56
22149	2000WD49	2.300	293.02	1.32
22180	2000YZ	1.962	141.99	-2.68
22199	Klonios	2.261	365.90	-19.12
22203	Prothoenor	2.155	280.13	-27.73
22222	Hodios	2.256	323.72	-9.34
22227	Polyxenos	2.334	302.09	-0.53
22404	1995ME4	2.214	281.85	-6.43
22503	Thalpius	2.185	259.55	-0.02
22808	1999RU12	2.345	314.00	-15.37
23075	1999XV83	2.242	264.29	-1.98
23114	2000AL16	2.294	316.34	-3.65

Table B.4: Basic frequencies of the Trojan asteroids in the ESRTBP (continued).

C.N.	Name	$\nu\,(deg)$	$g\,(sec)$	$s\,(sec)$
23118	2000AU27	2.367	304.99	-10.30
23119	2000AP33	2.366	329.06	-11.72
23123	2000AU57	2.183	349.96	-22.87
23126	2000AK95	2.139	320.86	-22.62
23135	2000AN146	2.091	241.91	-9.77
23144	2000AY182	2.163	263.48	-5.17
23152	2000CS8	2.223	256.79	1.54
23269	2000YH62	2.262	311.37	-7.99
23285	2000YH119	2.384	348.09	-4.61
23355	Elephenor	2.146	269.85	-9.12
23382	Epistrophos	2.115	216.63	3.39
23383	Schedios	2.333	317.63	-2.41
23463	1989TX11	2.244	271.71	2.07
23480	1991EL	2.112	249.64	-17.93
23549	1994ES6	2.185	271.80	-6.99
23622	1996RW29	2.184	246.23	6.08
23624	1996UX3	2.007	167.13	-1.93
23694	1997KZ3	2.217	313.35	-11.42
23706	1997SY32	2.346	333.81	-6.05
23709	1997TA28	2.386	331.30	-1.63
23710	1997UJ	2.141	250.45	-3.86
23939	1998TV33	2.300	323.54	-4.67
23947	1998UH16	2.160	285.53	-14.91
23958	1998VD30	2.028	177.85	-0.52
23963	1998WY8	2.277	305.20	-4.66
23968	1998XA13	2.309	289.17	-5.52
23970	1998YP6	2.153	252.27	-1.69
23987	1999NB63	2.231	265.16	-3.07
24018	1999RU134	2.129	223.19	7.19
24022	1999RA144	2.136	246.14	-4.86
24212	1999XW59	2.239	324.52	-11.10
24225	1999XV80	2.292	299.74	0.30
24233	1999XD94	2.230	337.15	-15.67
24244	1999XY101	2.202	272.16	-1.40
24275	1999XW167	2.275	294.13	-2.02
24279	1999XR171	2.352	327.60	-1.83
24312	1999YO22	2.306	319.54	-11.14
24313	1999YR27	2.375	354.50	-8.52
24340	2000AP84	2.306	293.23	-2.64
24341	2000AJ87	2.161	254.13	-1.81
24357	2000AC115	2.081	267.24	-17.27

Table B.4: Basic frequencies of the Trojan asteroids in the ESRTBP (continued).

C.N.	Name	$\nu\,(deg)$	$g\,(sec)$	$s\,(sec)$
24380	2000AA160	2.334	341.06	-9.39
24390	2000AD177	2.102	235.59	-5.55
24403	2000AX193	1.920	113.86	-5.88
24420	2000BU22	2.171	284.56	-9.80
24426	2000CR12	2.128	255.64	-9.31
24444	2000OP32	2.221	322.28	-12.73
24446	2000PR25	2.199	272.18	-3.37
24448	2000QE42	2.160	254.77	-5.32
24451	2000QS104	2.430	345.70	-5.34
24452	2000QU167	2.258	269.93	0.15
24453	2000QG173	2.256	319.31	-8.25
24454	2000QF198	2.202	309.13	-14.22
24456	2000RO25	2.243	270.31	4.43
24458	2000RP100	2.216	264.71	0.95
24459	2000RF103	2.346	320.96	-3.22
24467	2000SS165	2.169	243.61	3.19
24470	2000SJ310	2.122	226.59	1.80
24472	2000SY317	2.111	214.46	6.43
24479	2000WU157	2.218	258.72	4.39
24485	2000YL102	2.162	239.25	3.63
24486	2000YR102	2.176	254.03	-4.81
24498	2001AC25	2.040	210.20	-8.37
24501	2001AN37	2.448	349.45	-1.47
24505	2001BZ	2.400	363.29	-9.11
24506	2001BS15	2.252	379.13	-20.03
24508	2001BL26	2.249	311.41	-7.37
24519	2001CH	2.433	343.25	-2.52
24528	2001CP11	2.106	232.57	-6.92
24530	2001CP18	2.196	250.40	4.44
24534	2001CX27	2.402	340.92	-7.46
24536	2001CN33	2.448	352.36	-1.43
24537	2001CB35	2.407	343.54	-2.28
24539	2001DP5	2.326	358.47	-12.64
24603	1973SQ	2.352	321.72	-4.49
24882	1996RK30	2.348	332.92	-3.46
25344	1999RN72	1.990	165.44	-2.15
25347	1999RQ116	2.005	168.34	0.29
25883	2000RD88	2.131	223.08	7.34

B.5 Basic frequencies in the TCCP

We write the three basic frequencies, in the Tricircular Coherent Problem, of the 377 Trojan asteroids for which we are able to compute them. See captions for more details.

Table B.5: Basic frequencies of the Trojan asteroids in the TCCP. In the first, column we display the catalog number of the asteroid and in the second one the asteroid's name. The frequency of libration can be seen in the third column, while in the fourth and fifth columns the two secular frequencies are shown. The asteroids whose frequencies are not well determined are omitted.

C.N.	Name	$\nu\,(deg)$	$g\,(sec)$	$s\,(sec)$
588	Achilles	2.370	326.09	-8.56
617	Patroclus	2.395	332.88	-10.78
624	Hektor	2.348	382.91	-19.53
659	Nestor	2.370	317.60	-11.30
884	Priamus	2.294	323.04	-15.38
911	Agamemnon	2.377	369.38	-13.50
1143	Odysseus	2.239	297.70	-8.93
1172	Aneas	2.169	248.79	-0.89
1173	Anchises	2.265	310.65	-12.41
1208	Troilus	2.308	307.55	-3.74
1404	Ajax	2.395	353.29	-13.80
1437	Diomedes	2.254	358.33	-20.21
1583	Antilochus	1.979	156.00	9.17
1647	Menelaus	2.200	293.49	-12.00
1749	Telamon	2.353	331.80	-9.29
1867	Deiphobus	2.202	266.04	-0.06
1869	Philoctetes	2.269	330.87	-14.98
1870	Glaukos	2.208	275.58	-2.99
1871	Astyanax	2.060	254.69	-18.97
1872	Helenos	2.039	206.99	-7.19
1873	Agenor	1.943	134.64	-2.16
2148	Epeios	2.194	260.59	0.90
2207	Antenor	2.237	274.80	-0.69
2223	Sarpedon	2.119	229.35	1.39
2241	Alcathous	2.222	272.10	-3.41
2260	Neoptolemus	2.264	287.63	-0.16
2357	Phereclos	2.283	293.77	-1.40
2363	Cebriones	1.893	102.55	10.40
2456	Palamedes	2.371	348.69	-8.67
2594	Acamas	2.140	362.93	-33.06
2674	Pandarus	2.293	294.94	-3.50
2759	Idomeneus	1.950	139.73	-1.88

Table B.5: Basic frequencies of the Trojan asteroids in the TCCP (continued).

C.N.	Name	$\nu\,(deg)$	$g\,(sec)$	$s\,(sec)$
2797	Teucer	2.269	301.44	-7.98
2893	Peiroos	2.179	271.92	-6.42
2920	Automedon	2.105	217.01	5.79
3063	Makhaon	2.286	311.72	-7.53
3240	Laocoon	2.320	308.40	-4.67
3317	Paris	2.011	171.91	7.17
3391	Sinon	2.356	370.74	-15.29
3451	Mentor	1.984	159.02	7.74
3540	Protesilaos	2.363	373.50	-23.50
3548	Eurybates	2.320	339.74	-11.49
3564	Talthybius	2.361	369.64	-20.14
3596	Meriones	2.407	377.88	-13.24
3708	1974FV1	2.325	301.01	-6.60
3709	Polypoites	1.959	152.07	-5.45
3793	Leonteus	2.012	174.63	1.46
3794	Sthenelos	2.375	322.74	-12.32
4007	Euryalos	2.398	348.71	-6.37
4035	1986WD	2.115	254.19	-9.69
4057	Demophon	2.319	320.37	-8.46
4063	Euforbo	2.176	246.34	1.42
4068	Menestheus	1.948	144.31	-13.85
4086	Podalirius	2.319	328.65	-14.19
4138	Kalchas	2.292	297.80	-1.73
4348	Poulydamas	2.160	262.47	-13.45
4489	1988AK	2.052	257.69	-21.08
4501	Eurypylos	2.222	285.71	-4.77
4543	Phoinix	2.277	369.89	-23.89
4707	Khryses	2.362	314.37	-7.74
4708	Polydoros	2.187	312.13	-21.91
4709	Ennomos	2.051	202.20	-1.91
4715	1989TS1	2.390	381.15	-15.44
4722	Agelaos	2.319	317.99	-13.77
4754	Panthoos	2.161	247.95	0.42
4791	Iphidamas	2.090	214.70	-3.81
4792	Lykaon	2.320	326.44	-8.75
4805	Asteropaios	2.237	298.55	-12.26
4827	Dares	2.254	281.19	-3.27
4828	Misenus	2.422	355.11	-12.11
4829	Sergestus	2.205	272.50	-2.68
4832	Palinurus	2.101	216.67	-1.02
4833	Meges	1.992	165.99	0.80

Table B.5: Basic frequencies of the Trojan asteroids in the TCCP (continued).

C.N.	Name	$\nu\,(deg)$	$g\,(sec)$	$s\,(sec)$
4834	Thoas	2.207	267.42	-5.92
4835	1989BQ	1.763	179.45	-24.54
4836	Medon	2.267	288.13	-3.37
4867	Polites	2.398	348.82	-7.53
4902	Thessandrus	2.185	261.67	-1.03
4946	Askalaphus	2.144	324.85	-35.08
5012	Eurymedon	2.334	325.20	-9.87
5023	Agapenor	2.336	331.35	-6.77
5025	1986TS6	2.398	345.69	-5.99
5027	Androgeos	2.103	246.96	-9.56
5028	Halaesus	2.397	333.31	-7.88
5041	Theotes	2.368	346.98	-9.00
5119	1988RA1	2.378	331.12	-5.65
5120	Bitias	2.250	292.93	-6.36
5123	1989BL	2.284	312.79	-10.35
5126	Achaemenides	1.956	146.63	-2.84
5130	Ilioneus	2.078	233.57	-11.33
5144	Achates	2.333	307.74	-39.41
5209	1989CW1	2.290	350.93	-15.71
5233	1988RL10	2.267	293.22	-4.72
5244	Amphilochos	2.250	279.78	-0.67
5254	Ulysses	2.257	283.83	-3.29
5257	1988RS10	2.267	300.71	-5.77
5258	1989AU1	2.174	293.18	-18.55
5259	Epeigeus	2.323	309.06	-11.65
5283	Pyrrhus	2.321	303.51	-6.55
5284	Orsilocus	2.184	256.22	0.20
5285	Krethon	1.998	167.04	5.02
5436	Eumelos	2.262	291.56	-4.45
5476	1989TO11	2.113	231.09	-0.94
5511	Cloanthus	2.175	247.69	-0.08
5637	Gyas	2.349	399.97	-25.93
5638	Deikoon	2.153	245.63	-5.95
5648	1990VU1	2.265	291.38	-15.99
5652	Amphimachus	2.314	306.86	-3.20
5907	1989TU5	2.265	306.44	-11.49
6002	1988RO	2.103	219.47	-1.14
6090	1989DJ	2.319	371.21	-18.45
6443	1988RH12	2.127	241.96	-13.05
6545	1986TR6	2.258	304.82	-6.43
6997	Laomedon	2.062	195.96	4.30

Table B.5: Basic frequencies of the Trojan asteroids in the TCCP (continued).

C.N.	Name	$\nu\,(deg)$	$g\,(sec)$	$s\,(sec)$
6998	Tithonus	2.313	315.85	-4.47
7119	Hiera	2.253	296.02	-6.11
7152	Euneus	2.290	301.24	-1.92
7214	Antielus	2.103	229.11	-2.26
7352	1994CO	2.190	280.87	-7.63
7543	Prylis	2.123	230.05	1.66
8060	Anius	2.335	345.39	-13.75
8125	Tyndareus	2.323	354.11	-15.73
8241	Agrius	2.350	322.45	-7.70
8317	Eurysaces	2.136	300.40	-28.24
9023	Mnesthus	1.906	107.34	-4.17
9030	1989UX5	2.264	319.65	-12.47
9142	Rhesus	2.147	246.82	-4.16
9430	1996HU10	2.288	315.27	-7.12
9431	1996PS1	2.044	189.24	6.14
9590	1991DK1	2.318	340.15	-15.74
9694	Lycomedes	nan	356.56	-24.42
9712	Nauplius	2.198	259.67	-2.97
9713	Oceax	2.238	291.07	-5.93
9790	1995OK8	2.226	288.23	-6.32
9799	1996RJ	2.066	201.97	3.78
9807	1997SJ4	2.277	285.08	-3.45
9817	Thersander	2.258	370.41	-23.05
9818	Eurymachos	2.286	357.49	-18.99
9828	Antimachos	2.309	303.18	-3.30
9857	1991EN	2.282	297.93	-3.97
9907	Oileus	2.121	263.95	-12.11
10247	Amphiaraos	2.034	274.61	-28.28
10664	Phemios	2.208	282.05	-5.53
10989	Dolios	2.186	252.04	2.20
11089	1994CS8	2.159	286.58	-16.45
11251	Icarion	2.304	301.21	-1.80
11252	Laertes	2.297	315.07	-5.60
11273	1988RN11	2.227	301.26	-14.03
11275	1988SL3	2.079	205.48	4.17
11351	1997TS25	2.106	267.19	-16.96
11395	1998XN77	1.944	136.34	-2.71
11396	1998XZ77	2.149	239.11	0.98
11397	1998XX93	2.028	221.31	-16.59
11428	Alcinoos	2.294	408.97	-27.88
11429	Demodokus	2.292	408.69	-27.46

Table B.5: Basic frequencies of the Trojan asteroids in the TCCP (continued).

C.N.	Name	$\nu\,(deg)$	$g\,(sec)$	$s\,(sec)$
11487	1988RG10	2.334	322.85	-5.30
11488	1988RM11	2.282	295.17	-2.16
11509	1990VL6	2.084	206.82	2.65
11552	1993BD4	2.144	239.87	-2.90
11554	1993BZ12	2.185	256.23	-1.58
11663	1997GO24	2.140	238.39	-1.62
11668	Balios	2.344	324.54	-10.62
11869	1989TS2	2.143	252.56	-4.22
11887	Echemmon	2.069	202.50	2.99
12052	1997JB16	2.107	246.34	-8.57
12054	1997TT9	2.332	343.36	-10.11
12126	1999RM11	2.343	302.94	-14.92
12238	1987YU1	2.090	209.05	5.15
12242	Koon	1.962	147.08	10.24
12649	Ascanios	2.322	338.01	-16.47
12658	Peiraios	2.255	311.58	-8.73
12714	Alkimos	2.299	325.70	-8.43
12917	1998TG16	2.100	237.15	-8.11
12921	1998WZ5	2.138	238.97	-0.34
12972	Eumaios	2.329	333.82	-18.83
12973	Melanthios	2.331	340.69	-9.63
12974	Halitherses	2.382	334.51	-4.95
13060	1991EJ	2.237	271.85	-3.77
13062	Podarkes	2.250	307.67	-9.82
13181	Peneleos	2.340	313.30	-9.14
13182	1996SO8	2.338	311.96	-7.68
13183	1996TW	2.459	353.33	-13.93
13184	1996TS49	2.266	289.13	-4.66
13185	1996TH52	2.389	342.15	-5.40
13229	Echion	2.268	334.84	-17.08
13230	1997VG1	2.270	331.34	-13.35
13323	1998SQ	2.175	311.46	-20.63
13331	1998SU52	2.247	317.34	-14.84
13353	1998TU12	2.406	333.42	-9.66
13362	1998UQ16	2.288	334.13	-14.65
13366	1998US24	2.287	300.87	-4.89
13372	1998VU6	2.278	301.66	-3.89
13379	1998WX9	2.303	307.46	-2.68
13383	1998XS31	2.253	296.85	-4.79
13385	1998XO79	2.102	224.15	-4.60
13387	1998YW6	2.386	331.86	-6.79

Table B.5: Basic frequencies of the Trojan asteroids in the TCCP (continued).

C.N.	Name	$\nu\,(deg)$	$g\,(sec)$	$s\,(sec)$
13402	1999RV165	2.219	268.94	-4.25
13463	Antiphos	2.365	337.16	-6.70
13475	Orestes	2.381	337.66	-7.24
13650	1996TN49	2.135	248.44	-5.89
13694	1997WW7	2.130	294.48	-21.21
13780	1998UZ8	2.318	352.23	-15.52
13782	1998UM18	1.957	145.44	9.99
13790	1998UF31	2.287	322.00	-13.74
13862	1999XT160	2.179	276.23	-8.09
14235	1999XA187	2.312	346.15	-13.39
14268	2000AK156	2.243	307.07	-10.00
14518	1996RZ30	2.219	269.77	-4.23
14690	2000AR25	2.351	325.92	-5.19
14707	2000CC20	2.055	220.67	-8.91
14791	Atreus	2.229	284.90	-15.20
14792	Thyestes	2.174	251.66	0.58
15033	1998VY29	2.216	268.53	-11.20
15094	1999WB2	2.316	344.86	-14.18
15398	1997UZ23	1.916	117.65	7.87
15436	1998VU30	2.189	262.44	-0.51
15442	1998WN11	2.294	292.25	-6.94
15502	1999NV27	2.325	331.40	-10.55
15521	1999XH133	2.351	359.41	-19.30
15529	2000AA80	2.161	278.26	-14.58
15535	2000AT177	2.163	242.13	2.56
15536	2000AG191	2.120	221.44	0.29
15651	Tlepolemos	2.192	335.03	-21.58
15663	Periphas	2.399	353.09	-11.77
15913	Telemachus	2.349	325.99	-4.00
16070	1999RB101	2.247	326.40	-19.50
16099	1999VQ24	2.267	284.79	-1.10
16152	1999YN12	2.291	319.77	-9.00
16428	1988RD12	2.324	327.04	-6.77
16560	1991VZ5	2.085	272.01	-19.41
16667	1993XM1	2.235	266.18	-10.68
16974	1998WR21	2.178	254.56	-0.52
17171	1999NB38	2.336	334.65	-8.32
17172	1999NZ41	1.984	158.79	6.68
17314	Aisakos	2.405	343.10	-13.90
17351	Pheidippos	2.412	362.40	-10.57
17365	1978VF11	2.179	273.58	-9.20

Table B.5: Basic frequencies of the Trojan asteroids in the TCCP (continued).

C.N.	Name	$\nu\,(deg)$	$g\,(sec)$	$s\,(sec)$
17414	1988RN10	2.107	221.88	2.54
17415	1988RO10	1.989	162.79	4.83
17416	1988RR10	2.082	211.80	2.57
17417	1988RY10	2.296	303.21	-4.43
17418	1988RT12	2.218	268.76	-5.97
17419	1988RH13	2.373	340.96	-8.35
17420	1988RL13	2.330	330.09	-7.50
17421	1988SW1	2.354	366.65	-19.78
17423	1988SK2	2.296	296.08	-4.63
17424	1988SP2	2.160	237.89	1.26
17442	1989UO5	2.347	368.95	-16.08
17492	Hippasos	2.117	241.26	-4.53
17874	1998YM3	2.134	335.54	-27.18
18037	1999NA38	2.116	248.42	-14.08
18054	1999SW7	2.141	233.71	3.69
18058	1999XY129	2.327	354.49	-14.35
18060	1999XJ156	2.238	283.97	-2.70
18062	1999XY187	2.358	357.19	-11.29
18063	1999XW211	2.376	351.47	-9.48
18071	2000BA27	2.195	342.72	-23.96
18137	2000OU30	2.116	264.26	-16.94
18228	Hyperenor	2.314	323.21	-12.83
18263	Anchialos	2.279	345.42	-15.06
18268	Dardanos	2.125	226.22	3.85
18278	Drymas	2.397	355.70	-11.39
18281	Tros	2.202	259.12	0.99
18282	Ilos	2.201	262.12	-2.68
18493	1996HV9	2.028	195.87	-6.29
18940	2000QV49	2.139	294.03	-21.89
18971	2000QY177	2.125	222.64	-0.45
19018	2000RL100	1.996	165.17	6.49
19020	2000SC6	2.253	282.01	-1.41
19725	1999WT4	2.267	356.88	-19.81
19913	Aigyptios	2.152	275.57	-14.21
20144	1996RA33	2.372	340.17	-7.93
20424	1998VF30	2.285	295.46	-5.19
20428	1998WG20	2.377	335.90	-11.68
20716	1999XG91	2.095	212.04	3.07
20720	1999XP101	2.169	257.36	-10.38
20729	1999XS143	2.331	319.55	-4.55
20738	1999XG191	2.388	343.91	-7.00

Table B.5: Basic frequencies of the Trojan asteroids in the TCCP (continued).

C.N.	Name	$\nu\,(deg)$	$g\,(sec)$	$s\,(sec)$
20739	1999XM193	2.366	323.45	-13.66
20947	Polyneikes	2.226	329.24	-17.27
20952	Tydeus	2.356	330.15	-5.54
20961	Arkesilaos	2.374	340.48	-6.48
20995	1985VY	2.230	304.62	-14.40
21271	1996RF33	2.276	292.93	-1.53
21284	1996TC51	2.214	267.22	-4.30
21370	1997TB28	2.319	310.07	-4.03
21371	1997TD28	2.267	332.17	-15.64
21372	1997TM28	2.131	245.02	-4.09
21593	1998VL27	2.276	320.32	-8.94
21595	1998WJ5	2.020	176.33	7.91
21599	1998WA15	2.196	256.03	1.40
21601	1998XO89	2.065	245.20	-15.11
21602	Ialmenus	2.325	327.21	-8.86
21900	1999VQ10	2.260	294.96	-3.44
22008	1999XM71	2.246	306.11	-9.08
22009	1999XK77	2.234	299.78	-8.07
22010	1999XM78	2.256	320.45	-11.85
22012	1999XO82	2.208	296.04	-18.38
22014	1999XQ96	2.067	200.85	0.03
22035	1999XR170	2.250	305.74	-9.14
22041	1999XK192	2.388	341.74	-5.74
22042	1999XP194	2.363	333.28	-7.24
22049	1999XW257	1.917	267.49	-38.77
22052	2000AQ14	2.252	309.07	-8.48
22054	2000AP21	2.248	291.29	-7.04
22055	2000AS25	2.249	307.06	-12.35
22056	2000AU31	2.278	337.43	-26.55
22059	2000AD75	2.159	257.04	-14.42
22149	2000WD49	2.289	296.74	-3.78
22199	Klonios	2.295	365.82	-19.14
22203	Prothoenor	2.243	291.95	-19.25
22222	Hodios	2.251	328.50	-14.09
22227	Polyxenos	2.322	307.49	-5.14
22404	1995ME4	2.221	287.52	-8.22
22503	Thalpius	2.191	264.43	-1.32
22808	1999RU12	2.250	325.66	-34.84
23075	1999XV83	2.240	268.21	-4.59
23114	2000AL16	2.304	317.96	-5.92
23118	2000AU27	2.341	313.84	-17.10

Table B.5: Basic frequencies of the Trojan asteroids in the TCCP (continued).

C.N.	Name	$\nu\,(deg)$	$g\,(sec)$	$s\,(sec)$
23119	2000AP33	2.384	329.74	-12.97
23123	2000AU57	2.210	355.71	-23.75
23126	2000AK95	2.150	325.37	-26.96
23135	2000AN146	2.070	241.87	-15.30
23144	2000AY182	2.164	269.90	-7.57
23152	2000CS8	2.212	260.67	-1.99
23269	2000YH62	2.271	314.31	-10.91
23285	2000YH119	2.381	352.93	-9.90
23355	Elephenor	2.186	277.05	-7.49
23382	Epistrophos	2.104	219.18	0.49
23383	Schedios	2.323	323.11	-7.94
23463	1989TX11	2.231	275.00	-2.21
23480	1991EL	2.099	250.83	-23.26
23549	1994ES6	2.216	277.46	-6.12
23622	1996RW29	2.176	248.79	2.96
23694	1997KZ3	2.222	318.64	-14.30
23706	1997SY32	2.368	331.75	-6.96
23709	1997TA28	2.369	339.41	-8.91
23710	1997UJ	2.127	255.13	-8.18
23939	1998TV33	2.286	329.40	-10.46
23958	1998VD30	1.950	139.71	-4.17
23968	1998XA13	2.291	295.68	-10.19
23970	1998YP6	2.147	254.58	-4.70
23987	1999NB63	2.242	268.72	-3.98
24018	1999RU134	2.122	225.72	4.47
24022	1999RA144	2.144	253.00	-6.36
24225	1999XV80	2.288	305.81	-4.65
24233	1999XD94	2.256	339.54	-16.95
24275	1999XW167	2.262	299.26	-7.35
24279	1999XR171	2.339	334.78	-7.61
24313	1999YR27	2.400	350.11	-9.30
24340	2000AP84	2.288	300.10	-7.61
24341	2000AJ87	2.163	259.16	-3.74
24357	2000AC115	2.104	277.48	-18.06
24390	2000AD177	2.070	233.35	-11.88
24420	2000BU22	2.156	288.47	-14.70
24426	2000CR12	2.153	265.89	-8.61
24446	2000PR25	2.158	272.86	-11.49
24448	2000QE42	2.145	258.84	-9.45
24451	2000QS104	2.404	359.26	-14.62
24452	2000QU167	2.247	274.71	-4.39

Table B.5: Basic frequencies of the Trojan asteroids in the TCCP (continued).

C.N.	Name	$\nu\,(deg)$	$g\,(sec)$	$s\,(sec)$
24453	2000QG173	2.252	323.85	-12.32
24454	2000QF198	2.200	315.32	-17.63
24456	2000RO25	2.235	273.15	0.63
24458	2000RP100	2.196	267.83	-4.97
24459	2000RF103	2.345	324.41	-7.02
24467	2000SS165	2.164	247.40	0.55
24470	2000SJ310	2.113	231.15	-1.31
24505	2001BZ	2.415	362.83	-13.16
24506	2001BS15	2.262	382.82	-24.68
24508	2001BL26	2.259	314.49	-9.68
24519	2001CH	2.408	356.37	-12.18
24528	2001CP11	2.103	237.83	-9.34
24530	2001CP18	2.174	251.91	-0.95
24534	2001CX27	2.404	343.93	-13.27
24536	2001CN33	2.437	361.66	-8.85
24537	2001CB35	2.375	358.34	-11.81
24539	2001DP5	2.303	369.30	-20.31

Appendix C

Resum

És conegut que prop dels punts triangulars (també anomenats punts de Lagrange) del sistema Sol-Júpiter hi ha un grup d'asteroids, els anomenats asteroids Troians. L'objectiu d'aquesta tesi doctoral és aprofondir en les propietats dinàmiques del seu moviment.

Una part dels resultats coneguts per aquest problema utilitzen, com a model per la dinàmica, el ben conegut problema restringit de tres cossos. Aquest model presuposa que tant Júpiter com el Sol són masses puntuals que es mouen en una òrbita circular al voltant del seu centre de masses (seguint les lleis de Kepler), i que el moviment de l'asteroid queda determinat per les atraccions gravitatòries d'aquests dos cossos.

Un dels propòsits d'aquest treball és el desenvolupament i estudi d'altres models més complexos. En aquests models es vol recollir l'efecte de les principals pertorbacions respecte el problema restringit, tals com l'efecte d'altres planetes (i.e. Saturn o/i Urà) d'una banda i l'excentricitat de l'òrbita de Júpiter per l'altra. Els models que es presenten es basen en el càlcul de solucions (periòdiques i quasi-periòdiques) dels problemes de 2, 3 i 4 cossos i s'escriuen com a pertorbacions no autònomes del problema restringit Sol-Júpiter.

En particular, els models desenvolupats són:

- **Model Bicircular coherent**: basat en una solució periòdica del problema pla de tres cossos Sol-Júpiter-Saturn. S'escriu com a pertorbació dependent del temps periòdicament del restringit Sol-Júpiter i es tracta del model restringit (coherent) de quatre cossos més senzill.

- **Model Restringit El.líptic**: basat en una òrbita excèntrica Kepleriana del problema de 2 cossos Sol-Júpiter. Aquest és un model ja clàssic, però es presenta escrit de manera diferent a l'habitual. La raó de la seva inclusió en el treball és que es tracta també d'un model periòdic però que conté una ressonància, cosa que afegeix aspectes nous a la dinàmica.

- **Model Bianular**: basat en una solució quasi-periòdica (amb dues freqüències) del problema de tres cossos Sol-Jupiter-Saturn, on s'intenta simular de forma més realista el moviment de Júpiter.

- **Model Tricircular coherent**: basat en una solució quasi-periòdica (amb dues freqüències) del problema de quatre cossos Sol-Jupiter-Saturn-Urà. D'alguna manera, aquest model pot ser vist com el model restringit (coherent) de cinc cossos més senzill i una continuació natural del Bicircular coherent a l'afegir al sistema un cos massiu més.

Un altre dels propòsits del treball comprèn l'estudi de la dinàmica d'aquests models mitjantçant eines semi-analítiques, tals com el càlcul de formes normals truncades i d'integrals primeres aproximades. L'aspecte més novedós de l'aplicació d'aquestes tècniques és l'implementació de canvis simplèctics que redueixen la part lineal d'aquests sistemes dependents del temps (periòdica o quasi-periòdicament) a coeficients constants. Una altre aplicació important d'aquestes tècniques és el càlcul de zones d'estabilitat efectiva, és a dir, de zones on una partícula es manté, com a mínim un temps igual a l'edat del sistema solar.

L'últim, però no el menys important, dels propòsits és realitzar un estudi numèric de les propietats dinàmiques de les òrbites dels asteroids Troians en un model "realista". Nosaltres, com la majoria d'astrònoms quan estudien aquest problema, usarem el OSS (sistema solar extern, en anglès). Això és, el problema de N-cossos format pel Sol, Júpiter, Saturn, Urà, Neptú i l'asteroid. Aquest estudi està basat en l'anàlisi de freqüències de les òrbites dels Troians produïdes en llargues (al voltant de 5 mil.lions d'anys) integracions. Per tal de realitzar de forma acurada aquestes integracions sobre intervals de temps tan grans, s'usa un integrador simplèctic.

La tesi s'ha organitzat de la següent manera: en el primer capítol, es dóna una extensa introducció al problema. En el capítol dos, es dedueix el model Bicircular coherent i s'estudia en detall. En el tercer capítol, es reescriu el model restringit el.líptic i se'n fa un estudi semi-analític, tenint present la ressonància que afegirà nous aspectes a la dinàmica. En el capítol quart, es dedueixen els dos models quasi-periòdics i se'n fa l'estudi semi-analític d'un d'ells. En el cinquè capítol, mostrem els resultats de l'anàlisi de freqüències de les òrbites generades per l'integrador simplèctic de les posicions i velocitats (extretes de dades reals) de 420 asteroids Troians en el model OSS. També es calculen les freqüències pròpies dels asteroids en els models semi-analítics i es comparen els resultats amb el model realista.

C.1 Introducció i perspectiva històrica

Comencem pel ben conegut problema restingit de tres cossos (a partir d'ara, RTBP). El RTBP modelitza el moviment d'una partícula sota l'atracció gravitatòria de Júpiter i el Sol (també anomenats primaris), sota les següents suposicions: I) la partícula es considera prou petita com perquè no afecti els moviments de Júpiter i el Sol; i II) Jupiter i el Sol són masses puntuals que giren en òrbites circulars al voltant del centre de masses del sistema. És usual prendre un sistema de referència rotatori amb origen en el centre de masses, i tal que el Sol i Júpiter quedin fixats en l'eix x, el pla (x, y) sigui el pla de moviment dels primaris, i l'eix z sigui ortogonal al pla (x, y). Aquestes coordenades s'anomenen, normalment, coordenades sinòdiques. Les unitats adimensionals que s'acostumen a prendre són tals que: la unitat de distància és la distància Sol-Júpiter, la unitat de massa és la massa total del sistema Sol-Júpiter, i la unitat de temps és tal que el periode de Júpiter al voltant del Sol és igual a 2π. És molt fàcil veure que, amb aquesta el.lecció d'unitats, la constant de gravitació és igual a 1. Si es defineixen els moments com: $p_x = \dot{x} - y$, $p_y = \dot{y} + x$

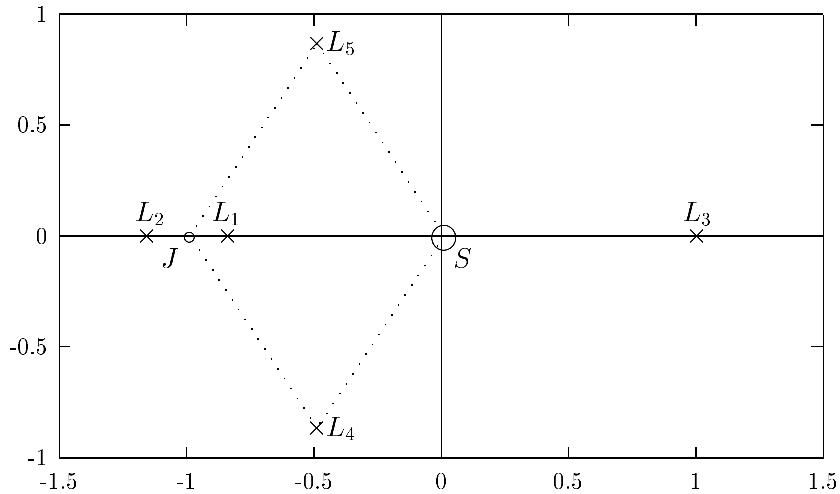

Figure C.1: Els cinc punts d'equilibri del problema restringit de tres cossos.

i $p_z = \dot{z}$, les equacions de moviment per la partícula poden ser escrites com un sistema Hamiltonià autònom amb tres graus de llibertat. La corresponent funció Hamiltoniana és:

$$H_{RTBP} = \frac{1}{2}(p_x^2 + p_y^2 + p_z^2) + yp_x - xp_y - \frac{1-\mu}{r_{PS}} - \frac{\mu}{r_{PJ}},$$

on μ és la massa de Júpiter (en unitats adimensionals), $r_{PS}^2 = (x-\mu)^2 + y^2 + z^2$ és la distància que hi ha des de la partícula al Sol, i $r_{PJ}^2 = (x-\mu+1)^2 + y^2 + z^2$ és la distància des de la partícula a Júpiter. Els detalls de tots aquests càlculs es poden trobar en pràcticament qualsevol llibre de text sobre Mecànica Celest (veieu, per exemple, [MH92, Sze67]).

És també força conegut que en aquestes coordenades rotatòries, el RTBP té cinc punts d'equilibri (veieu la figura C.1): tres d'aquests punts estan sobre l'eix x (s'anomenen punts colineals, punts d'Euler, o simplement $L_{1,2,3}$) i els altres dos formen un triangle equilàter (dins el pla (x, y)) amb el Sol i Júpiter (s'anomenen punts triangulars, punts de Lagrange, o simplement $L_{4,5}$).

No és difícil estudiar l'estabilitat lineal d'aquests cinc punts. Els punts colineals són del tipus centre$\times$centre$\times$sella (per tota μ), mentre que l'estabilitat dels punts triangulars depenen del valor de μ. Si μ és més petita que $\mu_R = \frac{1}{2}(1 - \sqrt{23/27})$ (aquest valor es coneix com la massa de Routh, o el valor crític de Routh), aquests punts són linealment estables. Pel contrari, per $\mu_R < \mu < \frac{1}{2}$, aquests punts són inestables. Els casos típics del sistema solar (com el Sol-Júpiter o el Terra-Lluna) tenen un paràmetre de masses més petit que μ_R, i, per tant, són linealment estables ([Sze67]).

L'estabilitat no lineal de punts el.líptics de sistemes conservatius és un problema difícil. El cas de dos graus de llibertat es resol mitjantçant el cèlebre teorema KAM ([Kol54, Arn63, Mos62], veieu [AKN88] i [dlL01] com a "survey", o [BHS96] per una presentació en un context més general), mentre que en el cas general es tracta, encara, d'un problema obert. D'un costat, un teorema degut a Lagrange i Dirichlet (see [AKN88], p. 271) mostra que, si la Hessiana del Hamiltonià al punt d'equilibri és definida positiva, llavors el punt el.líptic és estable, en el sentit clàssic de Lyapunov. D'altra banda, tenim l'exemple (veieu

[Dou88]) d'un sistema C^∞ –i no analític– amb un punt d'equilibri linealment estable i inestable pel sistema complet (veieu també [FM01] pel cas analític).

Sota condicions molt generals, el teorema KAM pot ser aplicat en un entorn del punts Lagrangians del RTBP [Leo62, DDB67, Mar71, Mar73, MS86] per assegurar l'existència de moviments quasi-periòdics. Cada trajectoria quasi-periòdica omple densament una varietat compacte difeomòrfica a un tor. La unió d'aquests tors invariants és un conjunt de mesura de Lebesgue positiva i interior buït. En el cas pla (el moviment d'una partícula es restringeix al pla $z = p_z = 0$, de tal manera que el sistema té dos graus de llibertat), cada tor és una varietat dos dimensional que separa les hipersuperfícies equienergètiques de tres dimensions; així doncs, actuen com barreres pel moviment, el confinen en una regió de l'espai –aquest és el punt clau en la prova d'estabilitat en sistemes Hamiltonians de dos graus de llibertat–. En el cas espaial, els tors són ara tridimensionals i l'hipersuperfície de l'energia és 5-D, així doncs els tors, ara, no poden actuar de barreres pel moviment. En aquest cas, és possible tenir trajectòries que errin entre aquests tors i escapin de qualsevol entorn del punt el.líptic. Hom creu en l'existència d'aquests tipus de trajectòries de forma genèrica en sistemes Hamiltonians no-integrables. Aquest fenòmen és conegut com a difusió d'Arnold, ja que va ser conjecturada per V.I. Arnold a [Arn64].

Un altre punt de vista de l'estabilitat dels sistemes Hamiltonians va ser introduït per en N.N. Nekhoroshev a [Nek77]. La idea consisteix en derivar una cota superior per la velocitat de difusió en un conjunt obert de l'espai de fases, i veure que la (possible) inestabilitat és tan lenta que no es mostra en aplicacions pràctiques. Això porta al concepte d'estabilitat efectiva d'un sistema físic: Un sistema es considera efectivament estable si el temps que es necessita per "observar" canvis significatius és més gran que el propi temps de vida del sistema. Per exemple, [GDF$^+$89] demostra, a part d'altres coses, l'estabilitat efectiva d'un entorn dels punts triangulars del RTBP en el cas Sol-Júpiter, per un interval de temps de l'ordre de l'edat estimada del sistema solar. Treballs remarcables, també, en aquesta direcció són [Sim89, CG91, BFG98]. Per una aplicació a una situació més general, veieu [Nie96].

Podem resumir ambdos visions dient que la teoria KAM assegura estabilitat (per tot temps) en un conjunt de condicions inicials de mesura de Lebesgue positiva però interior buït –aquest conjunt és completament foliat per tors invariants–, mentre que la teoria de Nekhoroshev assegura l'estabilitat efectiva (és a dir, per temps finits, però molt llargs) d'un conjunt obert de condicions inicials. Una presentació formal d'aquestes idees en un context més general pot ser trobat a [JV97a].

Una pregunta natural és la persistència d'aquestes zones d'estabilitat en el sistema solar real. En relació a aquesta qüestió, cal esmentar que, a l'any, 1906, Max Wolf va descobrir (fotogràficament) un asteroid (més tard anomenat, 588 Aquil.les) movent-se prop del punt de Lagrange L_4 del sistema Sol-Júpiter. En un any, August Kopff n'havia descobert dos més: 617 Patrocle, situat prop del punt L_5, i 624 Hector prop de L_4. Va ser més tard que es decidí de posar, a aquests asteroids, els noms dels participants en la guerra de Troia, tal i com està escrit a *La Ilíada* i, a més a més, de donar noms de guerrers grecs als que són propers del punt L_4 i de guerrers troians als que són propers a L_5 (veieu Figura C.2). Amb la única excepció dels dos espies (Hector, l'únic troià en el campament dels grecs, i Patroclus, l'únic grec en el campament dels troians), aquesta tradició ha sigut mantinguda. Fins al moment, s'han donat noms permanents seguint

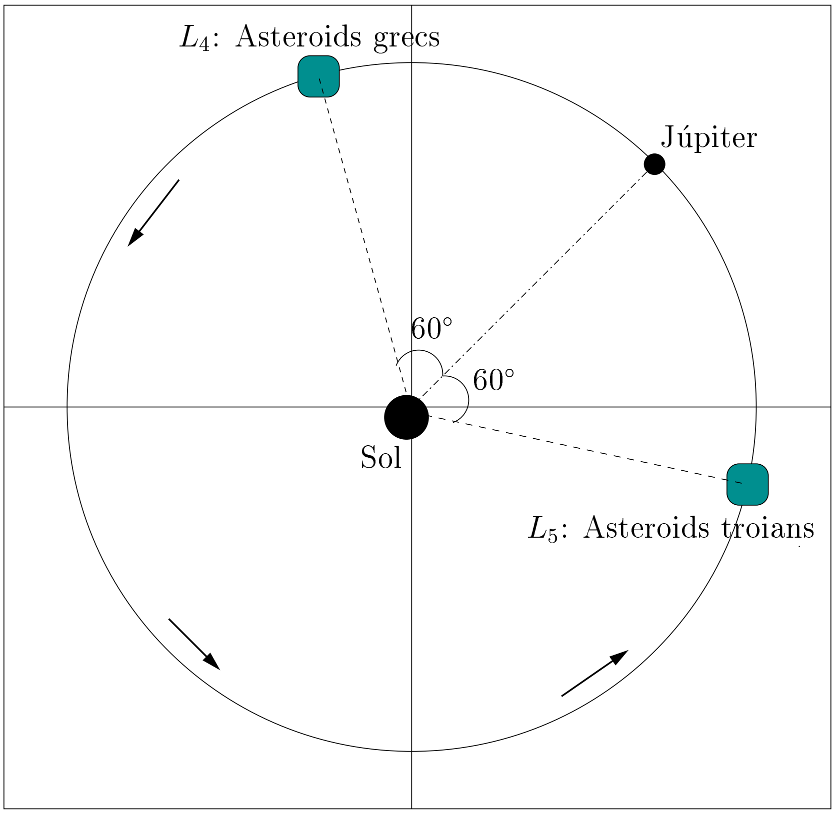

Figure C.2: Projecció en el pla de moviment orbital de Júpiter dels dos grups d'asteroids Troians. Els grecs (grup proper al punt L_4) segueixen l'òrbita de Júpiter precedint-lo en uns 60° i els troians (grup proper al punt L_5) es troben darrera l'òrbita de Júpiter en, també, uns 60°.

aquest conveni a 180 asteroids (una dada que demostra l'esforç dels que busquen dins les pàgines de *La Ilíada* i d'altres llibres de mitología grega per tal de trobar noms adequats). A 15 de febrer de 2003, s'han observat 962 asteroids Troians prop del punt L_4 i 602 prop de L_5; s'ha donat un nombre permanent a 667 d'ells (d'ambdos punts de Lagrange). Veieu una llista completa (i actualitzada diàriament) dels asteroids Troians a la URL: `http://cfa-www.harvard.edu/iau/lists/JupiterTrojans.html`.

El terme Troià ha sigut també usat per qualsevol objecte que es trobi prop dels punts Lagrangians d'altres sistemes de parelles de cossos. Se n'han realitzat búsquedes en el cas de la Terra, Mart, Saturn i Neptú, així com del sistema Terra-Lluna; però, la búsqueda ha resultat infructuosa excepte en els casos de Mart i Neptú. L'existència d'aquests tipus d'objectes es va considerar, durant molt de temps, força dubtosa en aquests sistemes, bàsicament degut a les pertorbacions dels planetes més grans. Tot i així, l'any 1990, els astrònoms americans David H.Levy i Henry E. Holt (veieu [BLH90]) van descobrir un asteroid librant al voltant del punt de Lagrange L_5 del sistema Sol-Mart, reobrint aquesta qüestió. Avui en dia, s'han descobert 6 Troians de Mart i 1 de Neptú (veieu [PMW$^+$03]).

Sembla que els asteroids Troians de Júpiter (o, com a mínim, alguns d'ells) es mouen en una zona estable propera als punts d'equilibri. Hi ha hagut certs intents de provar rigurosament l'estabilitat del moviment d'alguns d'aquests Troians en el RTBP, amb no massa fortuna. Voldriem notar que, inclús amb una prova d'estabilitat efectiva en el RTBP, l'estabilitat efectiva dels Troians en el sistema real continuaria essent un problema obert, ja que el RTBP no és un model acurat per la dinàmica d'un asteroid en el sistema solar real.

Un dels models més acurats per la dinàmica del sistema solar és el que ve donat per les efemèrides JPL (veieu [JPL]). Essencialment, aquest model consisteix en un arxiu d'ordinador on es guarden una seqüència de polinomis que interpolen les posicions de tots els planetes; aquests polinomis s'han obtingut d'unes integracions numèriques d'un model molt sofisticat –conté, per exemple, correccions relativistes–. Així doncs, aquest és un model numèric, només definit en un interval de temps finit –la versió més llarga és valida únicament durant 6.000 anys–. Per tant, no és difícil integrar numèricament el moviment d'una partícula en el model JPL, però sembla extraordinàriament difícil deduir resultats teòrics d'un model tan complexe.

D'altra banda, la majoria d'estudis numèrics de les propietats dinàmiques dels asteroids Troians s'han fet simulant el seu moviment en l'anomenat sistema solar Extern (OSS, a partir d'ara). Aquest model s'ocupa del moviment d'una partícula sense massa (per exemple, un asteroid) en el camp gravitatori generat pel Sol i pels quatre grans planetes del sistema solar (Júpiter, Saturn, Urà i Neptú). Tot i que és molt fàcil d'escriure les equacions de moviment per aquest model, no sembla tan senzill l'extreure'n resultats semi-analítics (teòrics). Veieu [BJ87, SB87, Mil93, LSS97, PLDB99, TDPL00] per alguns resultats numèrics sobre la dinàmica dels Troians en el model OSS.

Sembla, doncs, natural buscar una escala de models incrementalment més acurats (i més complexes), començant pel RTBP i apropant-nos al model OSS. En cadascun d'aquests models, ens podem centrar en alguna estructura dinàmica i estudiar-la en detall. Aquest estudi detallat d'alguns aspectes d'un determinat model pot portar al punt de partida d'un altre estudi en el següent model en la nostra jerarquia de models. En cada estadi, apareixen nous fenòmens. Al final, es cobreixen alguns aspectes presents en el model més realístic, però que no ho eren (ni de forma qualitativa) en el model més simple.

C.2 El model Bicircular coherent

El primer model intermig que es presenta és una pertorbació periòdica del RTBP on s'intenta incloure l'efecte de Saturn al sistema. Aquest model està basat en el càlcul numèric d'una òrbita periòdica pel problema pla de tres cossos Sol-Júpiter-Saturn, "propera" a l'òrbita (no-periòdica) d'aquests cossos en el sistema solar real. Usant aquesta òrbita, és fàcil escriure les equacions de moviment d'una partícula que es mou sota l'atracció gravitatòria dels primaris. En coordenades adequades, aquestes equacions s'escriuen com una pertorbació dependent del temps periòdicament del RTBP, on la dependència temporal conté l'efecte de Saturn. Aquest model és un problema restringit de quatre cossos i l'anomenem Problema Bicircular Coherent (BCCP). Posteriorment, es realitza l'estudi d'aquest model mitjantçant eines semi-analítiques, tals com els càlculs d'una forma normal truncada a ordre alt i d'una integral primera aproximada amb l'objectiu d'acotar la difusió en una zona propera als punts de Lagrange. També s'hi han inclòs algunes comparacions d'òrbites amb el sistema solar real, mitjantçant les efemèrides del

JPL [JPL].

C.2.1 Construcció del model

És possible trobar, en un sistema de coordenades rotatòries, solucions periòdiques del problema de tres cossos Sol-Júpiter-Saturn mitjantçant, per exemple, un mètode de continuació usant les masses dels planetes com a paràmetres. El període relatiu de Saturn respecte el sistema Sol-Júpiter (T_{sat}) pot ser escollit com el real, i la seva corresponent freqüència és $\omega_{sat} = \frac{2\pi}{T} = 0.597039074021947$. Suposant que els tres planetes es mouen en aquesta òrbita periòdica, és possible (situant-nos en un sistema de referència polsant i rotant) escriure el Hamiltonià pel moviment d'una quarta partícula (sense massa) com:

$$\begin{aligned} H &= \omega_{sat}p_\theta + \frac{1}{2}\alpha_1(\theta)(p_x^2+p_y^2+p_z^2) + \alpha_2(\theta)(xp_x+yp_y+zp_z) \\ &\quad +\alpha_3(\theta)(yp_x-xp_y) + \alpha_4(\theta)x + \alpha_5(\theta)y - \alpha_6(\theta)\left[\frac{1-\mu}{q_S}+\frac{\mu}{q_J}+\frac{m_{sat}}{q_{sat}}\right], \quad \text{(C.1)} \end{aligned}$$

on $q_S^2 = (x-\mu)^2+y^2+z^2$, $q_J^2 = (x-\mu+1)^2+y^2+z^2$ i $q_{sat}^2 = (x-\alpha_7(\theta))^2+(y-\alpha_8(\theta))^2+z^2$. Les funcions $\alpha_i(\theta)$ són funcions periòdiques en $\theta = \omega_{sat}t+\theta^{(0)}$, on $\theta^{(0)}$ és la fase, i poden ser calculades mitjantçant un anàlisi de Fourier de la solució periòdica del problema de tres cossos.

En aquest moment, voldriem mencionar que un model Bicircular Coherent (el problema Quasi-Bicircular) va ser desenvolupat per primera vegada per M.A. Andreu a [And98] per estudiar la dinàmica prop dels punts d'Euler del sistema Terra-Lluna-Sol.

Per comparar els models RTBP i BCCP respecte el JPL, hem integrat numèricament el moviment del Troià 588 Aquiles (proper a L_4) en aquests tres models. La figura C.3 mostra el resultat d'aquesta integració, on les condicions inicials han estat preses de la base de dades [Bow] el dia 22 de desembre de 2000 (corresponent al dia Julià 2451900.5) i el temps d'integració ha sigut de 20 anys (suficient pel que es pretén). La posició real de Saturn el mateix dia ens dóna la fase ($\theta_{(0)}$) que cal agafar en la variable angular de la pertorbació.

C.2.2 Difusió prop dels punts triangulars

Com ja s'ha dit anteriorment, és molt interessant determinar zones d'estabilitat efectiva al voltant dels punts triangulars. Usarem el model BCCP i diferents tècniques per estimar diverses d'aquestes regions d'estabilitat. Les eines que s'usen són: simulació numèrica directa, càlcul de formes normals i d'integrals primeres aproximades. Degut a una simetria del Hamiltonià (C.1), és suficient centrar-se en l'estudi d'un únic punt triangular (per exemple, L_5). En la figura C.4 (part superior esquerra), es pot veure la projecció al pla (x, y) d'una regió d'estabilitat al voltant de L_5, calculada amb una simple integració numèrica del BCCP. El temps d'escapament d'aquesta regió és superior a 1 milió d'anys.

En el model BCCP, els punts d'equilibri del RTBP (per exemple, l'L_5) són reemplaçats per una òrbita periòdica. És fàcil veure que la dinàmica lineal d'aquestes òrbites és totalment el.líptica.

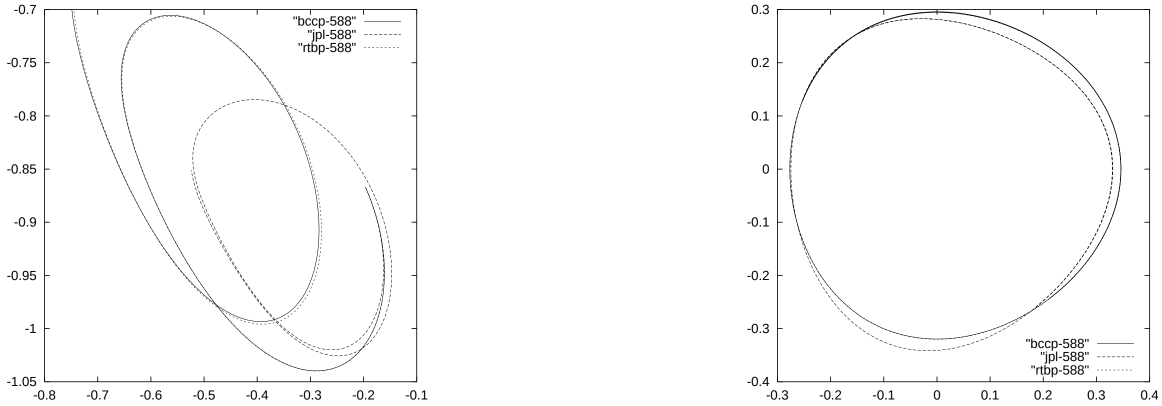

Figure C.3: Projeccions als plans (x, y) i $(z, \dot{z})$ de les òrbites de l'asteroid 588 Aquiles en els models RTBP, BCCP i JPL.

Per tal de fer un estudi de la dinàmica no-lineal al voltant d'aquesta òrbita periòdica, escrivim el Hamiltonià (C.1) de manera més convenient mitjantçant la composició de tres canvis de variable: una translació dependent del temps periòdicament (per veure l'òrbita periòdica com a punt fix), una transformació de Floquet simplèctica (per treure la dependència lineal amb el temps) i una complexificació (per diagonalitzar l'ordre 2 del Hamiltonià); i s'expandeix tot com a sèrie de Fourier-Taylor. La part lineal ve donada per $H_2 = \frac{1}{2}\omega_1(x_1^2 + y_1^2) + \frac{1}{2}\omega_2(x_2^2 + y_2^2) + \frac{1}{2}\omega_3(x_3^2 + y_3^2)$ on les freqüències són $\omega_1 = -0.08047340341466$, $\omega_2 = 0.99668687782956$ i $\omega_3 = 1.00006744139040$. Així doncs. és possible escriure el Hamiltonià expandit (en variables complexes) com:

$$H(q, p, \theta, p_\theta) = \omega_{sat} p_\theta + H_2(q, p) + \sum_{n \geq 3} H_n(q, p, \theta). \tag{C.2}$$

C.2.2.1 Forma Normal d'ordre alt

Usant el mètode de les series de Lie (l'implementació s'ha fet en C++ fent servir els mètodes de [Jor99]), transformem el Hamiltonià expandit (C.2) a una forma normal truncada a ordre 16 en les variables (q, p):

$$H = \omega_{sat} p_\theta + \sum_{n=2}^{16} H_n(qp) + \sum_{n \geq 17} H_n(q, p, \theta).$$

Acotant la norma del reste, és possible determinar una zona d'estabilitat efectiva (per un temps d'uns 5.000 milions d'anys, aproximadament) al voltant de l'òrbita periòdica. La projecció sobre el pla (x, y) d'una llesca d'aquesta zona per al temps $t = 0$ es pot veure en la figura C.3 (part superior dreta).

C.2.2.2 Integral Primera aproximada

Donada l'expansió del Hamiltonià (C.2), busquem una funció

$$F(q, p, \theta) = \sum_{n \geq 2} F_n(q, p, \theta)$$

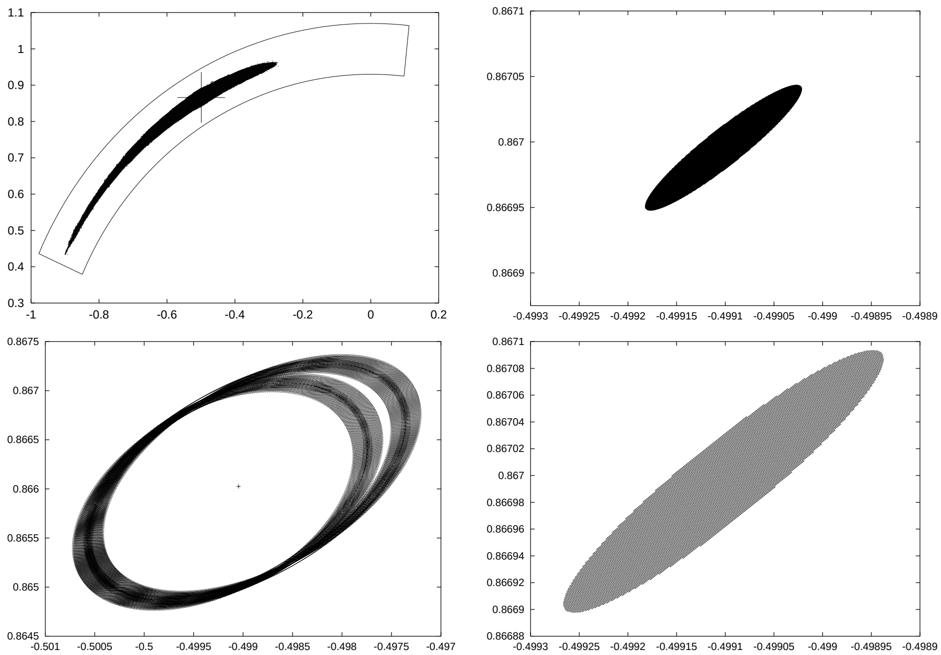

Figure C.4: Part superior esquerra: Estimació de l'estabilitat efectiva pel model BCCP a temps $t = 0$. Part superior dreta: Regió d'estabilitat efectiva per $t = 0$ a partir del càlcul de la forma normal. Part inferior esquerra: Zona d'estabilitat efectiva, al voltant de l'òrbita periòdica, calculada amb la integral primera. Part inferior esquerra: Llesca per $t = 0$ del dibuix anterior. Els eixos de tots els dibuixos corresponen a les coordenades sinòdiques x i y.

tal que $\{H, F\} = 0$. Aquesta última equació dóna una forma recursiva de calcular F. Es resol fins a ordre 16, prenent com a condició inicial $F_2 = iq_1p_1 + iq_2p_2 + iq_3p_3$.

Estimant la norma de $\dot{F}$ (això és, la part de $\{H, F\}$ que no és exactament zero), és possible trobar una zona d'estabilitat efectiva al voltant de l'òrbita periòdica. La projecció d'aquesta zona i d'una llesca d'ella per al temps $t = 0$ sobre el pla (x, y) es pot veure en la figura C.3 (part inferior esquerra i dreta, respectivament).

Així doncs, l'estudi de la forma normal del Hamiltonià proporciona un entorn d'estabilitat més petit que el de la integral primera, però ens ofereix molta més informació dels tipus de moviments que hi ha al voltant d'aquests punts (veieu, per exemple, la figura C.5.

C.3 El model Restringit El.líptic

Una altra manera de millorar (d'intentar aproximar millor la realitat) el problema restringit circular és fer-lo el.líptic, és a dir, suposar que Júpiter es mou en una òrbita el.líptica al voltant del Sol en comptes de circular. Aquest model es coneix com Problema Restringit El.líptic, ERTBP (veieu [Sze67]). En coordenades adequades, aquest model pot ser escrit com a pertorbació periòdica del RTBP. La linealització del flux al voltant dels punts triangulars del model RTBP pel cas Sol-Júpiter ve descrit per un producte

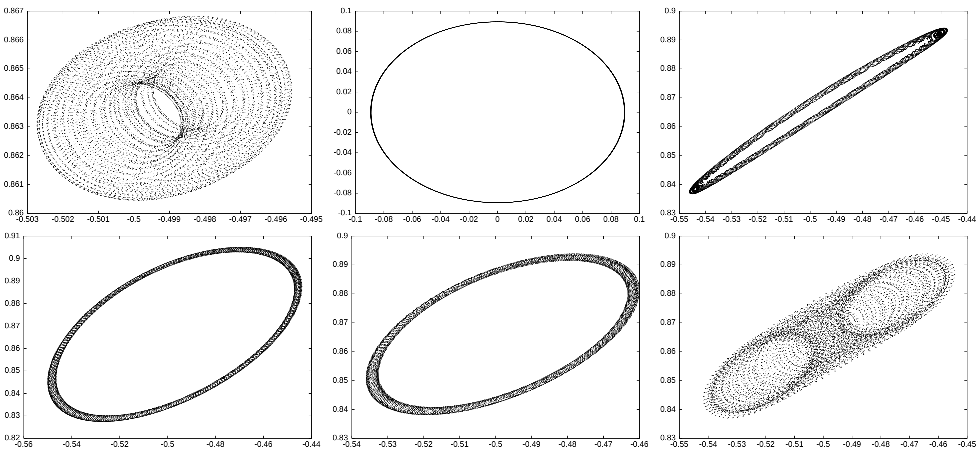

Figure C.5: Algunes projeccions de tors invariants prop de l'òrbira periòdica que substitueix el punt triangular L_5 en el sistema BCCP.

directe de tres oscil.ladors lineals, dos d'ells continguts en el pla $z = p_z = 0$ i el tercer en el pla $x = p_x = y = p_y = 0$. Un punt que cal esmentar, en aquí, és que la freqüència vertical és exactament 1, per tots els valors del paràmetre de masses μ ([Sze67]). Aquesta freqüència 1 correspon al període 2π, que a la vegada és el mateix període de revolució de Júpiter al voltant del Sol (o al revés, o dels primaris al voltant del centre de masses) en coordenades sinòdiques. Així doncs, si veiem l'efecte d'una petita excentricitat en el moviment dels primaris com una pertorbació periòdica del RTBP, llavors el període d'aquesta pertorbació és exactament 2π –el moviment el.líptic dels primaris es repeteix exactament cada revolució–. En altres paraules, es té una ressonància 1:1 exacte entre un dels modes lineal al voltant dels punts $L_{4,5}$ del RTBP i de la pertorbació provinent de l'excentricitat de Júpiter. De totes maneres, aquesta ressonància no juga cap paper important en el sistema linealitzat, ja que la pertorbació està desacoplada –a primer ordre– del "mode vertical" amb freqüència 1. La dinàmica lineal prop dels punts de Lagrange del problema el.líptic ha sigut estudiada per diversos autors (veieu [Dan64, Sze67]).

Quan un considera la dinàmica no-lineal al voltant dels punts triangulars del ERTBP, la ressonància esdevé rellevant, donant origen a tors hiperbòlics de dimensió baixa prop dels punts. Val la pena, també, mencionar que aquests tors no representen una obstrucció per l'existència de regions d'estabilitat efectiva (veieu [JS94]).

En aquest treball, es torna a estudiar el problema el.líptic, però reescrit de tal manera que la variable independent és el temps adimensional (no l'argument del periheli, tal i com es fa en l'escriptura clàssica del ERTBP). És fa un estudi de la dinàmica no-lineal mitjançant el càlcul d'una forma normal del Hamiltonià i es troba una zona d'estabilitat efectiva (en aquest cas, plana) a partir del càlcul d'una integral primera aproximada.

C.4 Els models Bianular i Tricircular coherent

En aquesta secció, es deriven dos nous models per la dinàmica al voltant dels punts de Lagrange (L_4 i L_5) del sistema Sol-Júpiter.

El primer model està basat en el càlcul de solucions quasi-periòdiques (amb dues freqüències) del problema pla de tres cossos Sol-Júpiter-Saturn (SJS) i on s'intenta ajustar alguns dels elements orbitals de Júpiter als reals. El que es pretén, doncs, és simular de manera més acurada (que en models anteriors) el moviment relatiu de Júpiter respecte el Sol. Anomenem a aquest model Problema Bianular.

El segon model és un problema restringit de cinc cossos i la seva construcció està basada en el càlcul d'una solució quasi-periòdica de dues freqüències del problema pla de quatre cossos format pel Sol, Júpiter, Saturn i Urà (SJSU). Aquest model serà conegut com el Problema Tricircular coherent.

L'última part està dedicada a l'estudi de la dinàmica local a l'entorn d'un punt de Lagrange mitjantçant tècniques semi-analítiques del model Tricircular coherent. Primer, es calcula una forma normal del Hamiltonià truncada a ordre alt al voltant de l'objecte invariant (un tor 2-D) que en aquest cas substitueix el punt L_5. Després, usem la forma normal per descriure la dinàmica no-lineal al voltant seu. En segon lloc, es calcula una integral primera aproximada del sistema i s'usa per trobar una zona d'estabilitat efectiva (mitjantçant l'estimació del reste d'aquesta quasi-integral) al voltant del tor.

C.4.1 El Problema Bianular

El Problema Bianular està basat en una solució particular del problema pla de tres cossos Sol-Júpiter-Saturn. Aquesta solució és quasi-periòdica i jeu sobre un tor 2-D. Com que el sistema és Hamiltonià, aquest tor pertany a una família de tors. El nostre objectiu és trobar un tor, dins d'aquesta família, tal que l'excentricitat de l'òrbita de Júpiter s'ajusti a la real.

C.4.1.1 El problema reduït de tres cossos

Prenem el Hamiltonià del problema pla de tres cossos escrit en coordenades de Jacobi en un sistema rotatori i fem un canvi de variables canònic (fent ús de la integral primera del moment angular) de tal manera que reduim aquest Hamiltonià de 4 a 3 graus de llibertat. S'obté:

$$\begin{aligned} H(Q_1,Q_2,Q_3,P_1,P_2,P_3) &= \frac{1}{2\alpha}\left(P_1^2+\frac{A^2}{Q_1^2}\right)+\frac{1}{2\beta}\left(P_2^2+P_3^2\right) \\ &\quad -K-\frac{\alpha}{r}-\frac{(1-\mu)m_{sat}}{r_{13}}-\frac{\mu m_{sat}}{r_{23}} \end{aligned} \tag{C.3}$$

on $\alpha=\mu(1-\mu)$, $\beta=m_{sat}/(1+m_{sat})$, $A=Q_2P_3-Q_3P_2+K$, $r=Q_1$, $r_{13}^2=(\mu Q_1-Q_2)^2+Q_3^2$ i $r_{23}^2=((1-\mu)Q_1+Q_2)^2+Q_3^2$, i K és el moment angular del sistema.

C.4.1.2 Un mètode per calcular tors invariants

Estem interessats en trobar una solució quasi-periòdica (amb dues freqüències) d'un camp vectorial donat. Reduïm aquest problema al de trobar una corba invariant per una aplicació de Poincaré determinada. Aquesta corba invariant es pot veure com una sèrie de Fourier truncada i el nostre objectiu és el de calcular una representació particular d'aquesta sèrie i el seu nombre de rotació. Seguirem molt de prop el mètode desenvolupat a [CJ00].

Càlcul numèric de corbes invariants Sigui $\dot{x} = f(x)$ $(x, f \in \mathbb{R}^n)$ un camp vectorial autònom de dimensió n (per exemple, el camp reduït (C.3)) i $\Phi(x,t) \equiv \Phi_t(x)$ el seu flux associat. Definim l'aplicació de Poincaré com el flux a temps T, $\Phi_T(\cdot)$, on T és un valor prefixat ($T = T_{sat}$, el periode relatiu de Saturn en el sistema Sol-Júpiter, en el cas que ens ocupa).

Sigui ω el nombre de rotació de la corba invariant. Sigui, també, $\mathcal{C}(\mathbb{T}^1, \mathbb{R}^n)$ l'espai de funcions continues de $\mathbb{T}^1$ a $\mathbb{R}^n$, i sigui l'aplicació lineal $T_\omega : \mathcal{C}(\mathbb{T}^1, \mathbb{R}^n) \to \mathcal{C}(\mathbb{T}^1, \mathbb{R}^n)$ la translació per ω, $(T_\omega \varphi)(\theta) = \varphi(\theta + \omega)$.

Definim $F : \mathcal{C}(\mathbb{T}^1, \mathbb{R}^n) \to \mathcal{C}(\mathbb{T}^1, \mathbb{R}^n)$ com

$$F(\varphi)(\theta) = \Phi_T(\varphi(\theta)) - (T_\omega \varphi)(\theta) \qquad \forall \varphi \in \mathcal{C}(\mathbb{T}^1, \mathbb{R}^n). \tag{C.4}$$

És clar que els zeros de F en $\mathcal{C}(\mathbb{T}^1, \mathbb{R}^n)$ corresponen a corbes invariants amb nombre de rotació ω. L'equació satisfeta és

$$\Phi_T(\varphi(\theta)) = \varphi(\theta + \omega) \quad \forall \theta \in \mathbb{T}. \tag{C.5}$$

El mètode que es resumeix en aquí consisteix en buscar numèricament un zero de F. Així doncs, escrivim $\varphi(\theta)$ com una sèrie de Fourier,

$$\varphi(\theta) = A_0 + \sum_{k>0} (A_k \cos(k\theta) + B_k \sin(k\theta)) \quad A_k, B_k \in \mathbb{R}^n \quad k \in \mathbb{N}.$$

Fixem, a priori, un valor de truncament de les sèries N_f (l'elecció d'aquest valor es discuteix més endavant), i provem de determinar (una aproximació a) els $2N_f + 1$ coeficients desconeguts A_0, A_k i B_k, $1 \le k \le N_f$. Construïm, doncs, una versió discretitzada de la F de la següents forma: primer, seleccionem una xarxa de $2N_f + 1$ punts sobre $\mathbb{T}^1$,

$$\theta_j = \frac{2\pi j}{2N_f + 1} \quad 0 \le j \le 2N_f, \tag{C.6}$$

i hi avaluem la funció (C.4). Sigui F_{N_f} aquesta discretizació de F:

$$\Phi_T(\varphi(\theta_j)) - \varphi(\theta_j + \omega), \quad 0 \le j \le 2N_f. \tag{C.7}$$

Així doncs, donat un conjunt de coeficients de Fourier (coneguts) A_0, A_k i B_k $(1 \le k \le N_f)$, podem calcular els punts $\varphi(\theta_j)$, $\Phi_T(\varphi(\theta_j))$ i seguidament els punts $\Phi_T(\varphi(\theta_j)) - \varphi(\theta_j + \omega)$, $0 \le j \le N_f$. A partir d'aquestes dades, es pot, immediatament, obtenir els coeficients de Fourier de $\Phi_T(\varphi(\theta)) - \varphi(\theta + \omega)$.

A l'aplicar el mètode de Newton per tal de resoldre l'equació $F_{N_f} = 0$, necessitem també calcular explícitament la diferencial de F_{N_f}. Això es pot fer fàcilment aplicant la regla de la cadena al procés usat per calcular F_{N_f}. Noteu que el nombre d'equacions a resoldre és $(2N_f + 1)n$ i que les incògnites són $(A_0, A_1, B_1, \ldots, A_{N_f}, B_{N_f})$, ω i el temps T pel qual es defineix l'aplicació de Poincaré associat al flux $(\Phi_T(\cdot))$. Per tant, hem de trobar $(2N_f + 1)n + 2$ incògnites. En cada pas del mètode de Newton, es resol un sistema lineal rectangular mitjançant un mètode de mínims quadrats. Aquest sistema és degenerat, a menys de que prefixem, durant els càlculs, algunes incògnites.

Error de discretització Un cop s'ha resolt l'equació (C.7) amb una certa tolerància (error en el mètode de Newton; es pren típicament 10^{-11}), no es té encara informació sobre l'error de l'aproximació de la corba invariant. La raó, tal i com queda explicat a [CJ00], és que no s'ha estimat l'error de discretització; és a dir, l'error que es produeix quan es passa de l'equació (C.5) a l'equació (C.7).

Per tal d'estimar el valor d'aquest error, calculem

$$E(\varphi,\omega) = \max_{\theta\in\mathbb{T}} |\Phi_T(\varphi(\theta,z)) - \varphi(\theta+\omega,z)|$$

en una xarxa 100 vegades més fina que la xarxa (C.6).

Si $||E||_\infty > 10^{-9}$, la solució no es considera prou bona i se'n calcula una altra amb la mateixa condició inicial pel mètode de Newton, però amb un ordre de discretització N_f més gran. El procés es repeteix fins que la norma sub-infinit de l'error de discretització sigui més petit que 10^{-9}.

C.4.1.3 Com trobar el tor desitjat?

Una bona aproximació inicial pel mètode de Newton ve donada per la linealització de l'aplicació de Poincaré al voltant del punt fix corresponent a l'òrbita periòdica (pel flux) del problema Bicircular coherent (veure l'apartat C.2).

És fàcil veure que existeixen dues direccions normals (no neutres) a l'òrbita periòdica i, per tant, tindrem dues famílies de tors invariants que hi "neixen".

Mitjantçant el mètode descrit a l'apartat C.4.1.2, es calculen dos primers tors corresponents a cada família i posteriorment, s'usen aquests tors per tal de continuar les famílies a les quals pertanyen. Aquestes famílies poden ser parametritzades pel moment angular que, a la vegada, està estretament relacionat amb els elements orbitals de les òrbites dels planetes. Així doncs, es continuen les famílies intentant trobar un tor pel qual l'excentricitat de Júpiter sigui la real. Aquest objectiu s'aconsegueix en una de les famílies, i aquest tor particular (solució quasi-periòdica del problema de tres cossos) és anomentat Solució Bianular. Aquest tor pot ser parametritzat amb els dos angles $(\theta_1,\theta_2) = (\omega_1 t + \theta_1^0, \omega_2 t + \theta_2^0)$, on les freqüències són $\omega_1 = \omega_{sat} = 0.597039074021947$ i $\omega_2 = \frac{\omega_1\bar{\omega}}{2\pi} = 0.194113943490717$ ($\bar{\omega}$ és el nombre de rotació de la corba invariant), i $\theta_{1,2}^0$ les fases inicials. Podeu veure, en la figura C.6, la projecció en els espai de configuracions (rotatori i no rotatori) d'aquesta òrbita.

C.4.1.4 El Hamiltonià del model Bianular

Finalment, és possible obtenir les equacions de moviment d'una partícula que es mou sota l'atracció gravitatòria dels tres cossos primaris, suposant que aquests estan en la solució Bianular. El Hamiltonià corresponent és:

$$\begin{aligned}
H_{BAP} &= \omega_1 p_{\theta_1} + \omega_2 p_{\theta_2} + \frac{1}{2}\alpha_1(\theta_1,\theta_2)(p_x^2+p_y^2+p_z^2) \\
&\quad +\alpha_2(\theta_1,\theta_2)(xp_x+yp_y+zp_z) \\
&\quad +\alpha_3(\theta_1,\theta_2)(yp_x-xp_y)+\alpha_4(\theta_1,\theta_2)x \\
&\quad +\alpha_5(\theta_1,\theta_2)y - \alpha_6(\theta_1,\theta_2)\left[\frac{1-\mu}{q_S}+\frac{\mu}{q_J}+\frac{m_{sat}}{q_{sat}}\right],
\end{aligned}$$

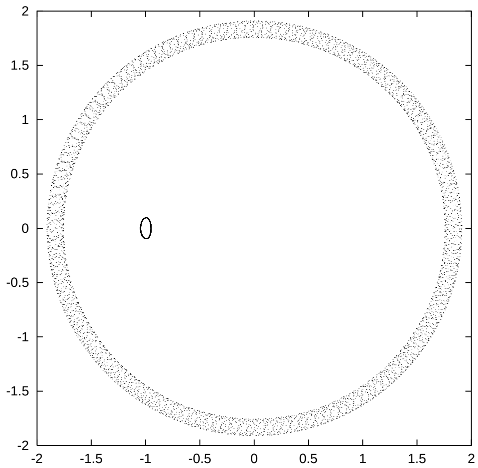

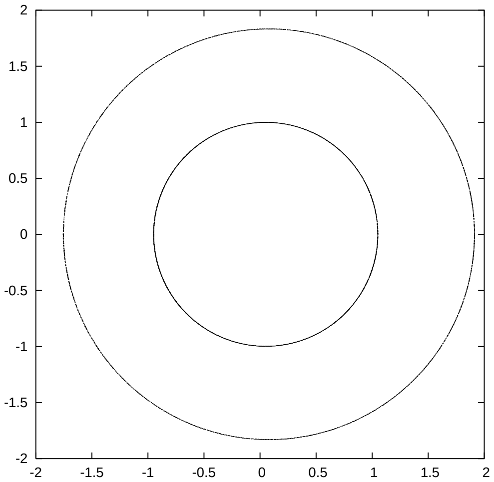

Figure C.6: Projecció a l'espai de configuracions de la solució Bianular del problema pla de tres cossos Sol-Júpiter-Saturn en un sistema de referència rotatori (esquerra) i inercial (dreta).

on $q_S^2 = (x-\mu)^2 + y^2 + z^2$, $q_J^2 = (x-\mu+1)^2 + y^2 + z^2$, $q_{sat}^2 = (x - \alpha_7(\theta_1,\theta_2))^2 + (y - \alpha_8(\theta_1,\theta_2))^2 + z^2$, $\theta_1 = \omega_1 t + \theta_1^0$, $\theta_2 = \omega_2 t + \theta_2^0$, i p_{θ_1} i p_{θ_2} són els moments corresponents als angles θ_1 i θ_2, respectivament.

Les funcions auxiliars $\alpha_i(\theta_1,\theta_2)_{\{i=1\div 10\}}$ són funcions quasi-periòdiques calculables a partir d'un anàlisi de Fourier de la solució Bianular.

C.4.2 El model Tricircular coherent

El model Tricircular coherent està basat en el càlcul d'una solució quasi-periòdica del problema (pla) de quatre cossos Sol, Júpiter, Saturn i Urà. Per a calcular aquesta solució, s'utilitza el mètode descrit a l'apartat C.4.1.2.

C.4.2.1 El problema reduït de quatre cossos SJSU

Prenem el Hamiltonià del problema pla de quatre cossos escrit en coordenades generalitzades de Jacobi (figura C.7) en un sistema rotatori i fem un canvi de variables canònic (fent ús de la integral primera del moment angular) de tal manera que reduïm aquest Hamiltonià de 6 a 5 graus de llibertat. S'obté:

$$\begin{aligned} H &= \frac{1}{2\alpha}\left(P_1^2 + \frac{A^2}{Q_1^2}\right) + \frac{1}{2\beta}\left(P_2^2 + P_3^2\right) + \frac{1}{2\gamma}\left(P_4^2 + P_5^2\right) - K - \frac{\alpha}{r} \\ &\quad -\frac{(1-\mu)m_{sat}}{r_{13}} - \frac{\mu m_{sat}}{r_{23}} - \frac{(1-\mu)m_{ura}}{r_{14}} - \frac{\mu m_{ura}}{r_{24}} - \frac{m_{sat}m_{ura}}{r_{34}}, \end{aligned} \tag{C.8}$$

on $\alpha = \mu(1-\mu)$, $\beta = m_{sat}/(1+m_{sat})$, $\gamma = (1+m_{sat})m_{ura}/(1+m_{sat}+m_{ura})$, $A = Q_2P_3 - Q_3P_2 + Q_4P_5 - Q_5P_4 + K$, $r = Q_1$, $r_{13}^2 = (Q_2 - \mu Q_1)^2 + Q_3^2$, $r_{23}^2 = (Q_2 + (1-\mu)Q_1)^2 + Q_3^2$,

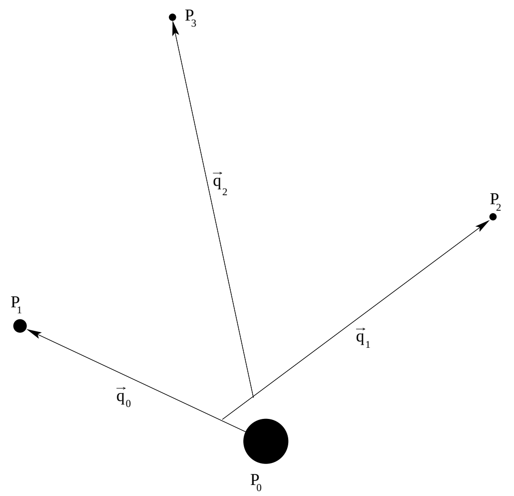

Figure C.7: Coordenades de Jacobi pel problema de quatre cossos Sol, Júpiter, Saturn i Urà.

$r_{14}^2 = (Q_5 + \beta Q_3)^2 + (Q_4 + \beta Q_2 - \mu Q_1)^2$, $r_{24}^2 = (Q_5 + \beta Q_3)^2 + (Q_4 + \beta Q_2 + (1-\mu)Q_1)^2$ i $r_{34}^2 = (Q_5 - (1-\beta)Q_3)^2 + (Q_4 - (1-\beta)Q_2)^2$, i K és el moment angular del sistema.

C.4.2.2 Càlcul del primer tor

Com a primera aproximació, suposarem que Urà té massa zero i que s'està movent al voltant del Sol en una òrbita Kepleriana. Llavors, no és massa difícil, usant el mètode de càlcul de corbes invariants descrit a l'apartat C.4.1.2, trobar un primer tor per al cas SJSU.

Si suposem que, a $t = 0$, el Sol, Júpiter, Saturn i Urà estan en una configuració colineal particular, és fàcil obtenir una condició inicial aproximada, pel mètode de Newton, prenent la Kepleriana per Urà i l'òrbita periòdica del problema BCCP (apartat C.2) pel sistema Sol-Júpiter-Saturn. Com ja hem vist, el periode d'aquesta òrbita és $T = T_{sat} = \frac{2\pi}{\omega_{sat}}$, on $\omega_{sat} = 0.5970390740 21947$. Aquesta serà la primera freqüència de l'òrbita quasi-periòdica que es busca.

A l'integrar aquestes condicions inicials pel flux corresponent al Hamiltonià (C.8) en l'interval de temps $t \in [0, T_{sat}]$, s'obté que la part corresponent a Sol, Júpiter i Saturn tanca (es tracta d'una òrbita periòdica) i l'òrbita d'Urà gira una volta i escaig (veieu la Figura C.8).

És fàcil veure que l'angle en que Urà sobrepassa una volta és molt proper al següent nombre:

$$\tilde{\omega} = \frac{2\pi\omega_{ura}}{\omega_{sat}} (\mod 2\pi) = 2.750807556, \tag{C.9}$$

on $\omega_{ura} = 0.858425538978989$ és la freqüència relativa d'Urà en el sistema sinòdic Sol-Júpiter. Així doncs, si imposem que $\tilde{\omega}$ sigui el nombre de rotació de la corba invariant, obtindrem que la segona freqüència del tor invariant 2-D que estem buscant és la freqüència d'Urà, ω_{ura}.

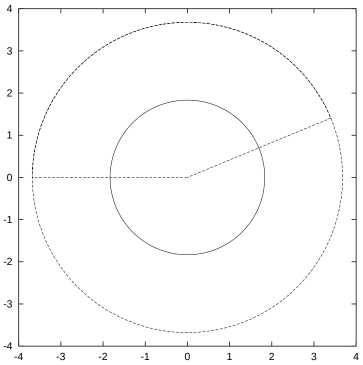

Figure C.8: Aproximació heurística del moviment d'Urà (orbita exterior). Les linies rectes mostren els punts inicial i final d'aquesta òrbita en un interval de temps de T_{sat}.

C.4.2.3 La solució Tricircular del problema SJSU

Un cop s'ha calculat el tor invariant pel cas $m_{ura} = 0$, s'utilitza un mètode de continuació per augmentar el paràmetre de masses fins al seu valor real. Durant la continuació, les dues freqüències del tor, $\omega_1 = \omega_{sat}$ i $\omega_2 = \omega_{ura}$ es mantenen constants. Així doncs, obtenim finalment un tor 2-D que es pot parametritzar amb els angles $\theta_1 = \omega_1 t + \theta_1^0$ i $\theta_2 = \omega_2 t + \theta_2^0$). Hem anomenat a aquesta solució, solució Tricircular del problema de quatre cossos SJSU. En la figura C.9, podeu veure les projeccions d'aquesta solució en l'espai de configuracions rotatori i inercial.

C.4.2.4 El Hamiltonià del model Tricircular coherent

Finalment, és possible escriure les equacions de moviment d'una partícula que es mou sota la influència dels quatre primaris (SJSU), suposant que aquests estan sobre l'òrbita quasi-periòdica Tricircular coherent. El Hamiltonià corresponent és:

$$\begin{aligned} H_{TCCP} &= \omega_1 p_{\theta_1} + \omega_2 p_{\theta_2} + \frac{1}{2}\alpha_1(\theta_1,\theta_2)(p_x^2+p_y^2+p_z^2) + \alpha_2(\theta_1,\theta_2)(xp_x+yp_y+zp_z) + \alpha_3(\theta_1,\theta_2)(yp_x - xp \\ &\quad +\alpha_4(\theta_1,\theta_2)x + \alpha_5(\theta_1,\theta_2)y - \alpha_6(\theta_1,\theta_2)\left[\frac{1-\mu}{q_S} + \frac{\mu}{q_J} + \frac{m_{sat}}{q_{sat}} + \frac{m_{ura}}{q_{ura}}\right], \end{aligned}$$

on $q_S^2 = (x-\mu)^2 + y^2 + z^2$, $q_J^2 = (x-\mu+1)^2 + y^2 + z^2$, $q_{sat}^2 = (x-\alpha_7(\theta_1,\theta_2))^2 + (y-\alpha_8(\theta_1,\theta_2))^2 + z^2$, $q_{ura}^2 = (x-\alpha_9(\theta_1,\theta_2))^2 + (y-\alpha_{10}(\theta_1,\theta_2))^2 + z^2$, $\theta_1 = \omega_{sat}t + \theta_1^0$, $\theta_2 = \omega_{ura}t + \theta_2^0$, i p_{θ_1} i p_{θ_2} són els moments corresponents als angles θ_1 i θ_2, respectivament.

Les funcions auxiliars $\alpha_i(\theta_1,\theta_2)_{\{i=1\div 10\}}$ són també quasi-periòdiques i poden ser calculades a partir d'un anàlisi de Fourier de la solució Tricircular calculada a l'apartat C.4.2.3.

C.4.3 Estudi semi-analític del model Tricircular coherent

En aquesta secció, fem un estudi semi-analític del Hamiltonià del problema Tricircular coherent prop dels punts triangulars.

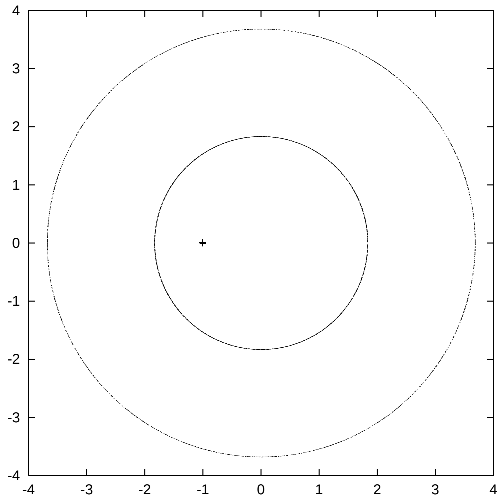

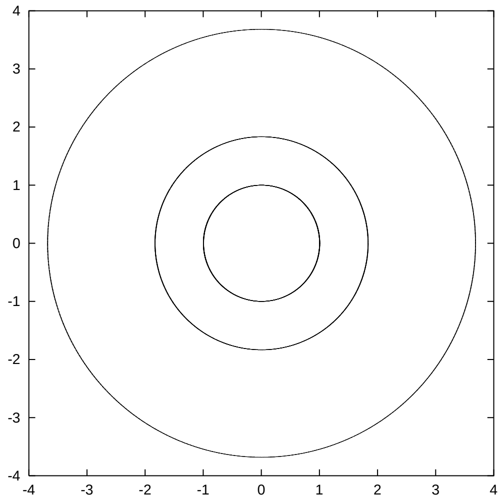

Figure C.9: Solució tricircular del problema de quatre cossos Sol-Júpiter-Saturn-Urà. L'òrbita externa correspon a la d'Urà, la intermitja a Saturn i la interna (vista com un puntet en el dibuix de l'equerra) al moviment relatiu Sol-Júpiter. El dibuix de l'esquerra correspon a un sistema de referència rotatori i el de la dreta a un d'inercial.

Primer, ens centrarem en la construcció d'una forma normal a ordre alt per tal de descriure la dinàmica no-lineal al voltant de L_4 i L_5. El procediment consisteix en una generalització d'alguns dels càlculs realitzats a l'apartat C.2.2 pel cas periòdic a els models de dues freqüències. Els passos a seguir són: i) Transformació del punt triangular a un tor 2-D, ii) Reducció de la part lineal del Hamiltonià a coeficients constants, iii) Forma normal d'ordre més gran que 2, i iv) Càlcul del canvi de variables composició dels anteriors com a sèrie de Fourier-Taylor truncada. Usant aquesta forma normal a ordre alt, és facil donar una descripció de la dinàmica no-lineal al voltant del tor invariant que substitueix L_5.

Més tard, usem l'expansió del Hamiltonià, escrita en forma normal fins a ordre 2, per a calcular una integral primera aproximada del sistema. Amb això, sóm capaços de trobar una zona d'estabilitat efectiva (qualitativament diferent a totes les trobades anteriorment) prop del punt triangular.

C.4.3.1 El tor invariant que substitueix L_5

Es pot provar, sota condicions adequades (veure [JS96]), que en el model TCCP (pertorbació quasi-periòdica amb dues freqüències del RTBP), els punts d'equilibri del restringit es transformen en tors invariants 2-D.

En aquest cas, hem calculat el tor que substitueix el punt Lagrangià L_5 mitjantçant l'adaptació al cas no-autònom del mètode de càlcul de corbes invariants descrit anteriorment. Anomenarem a aquest tor T_5. En la figura C.10 es poden veure les seves projeccions als plans (x, y) i (p_x, p_y).

És possible, també amb el mètode anterior, veure que aquest tor invariant és totalment el.líptic.

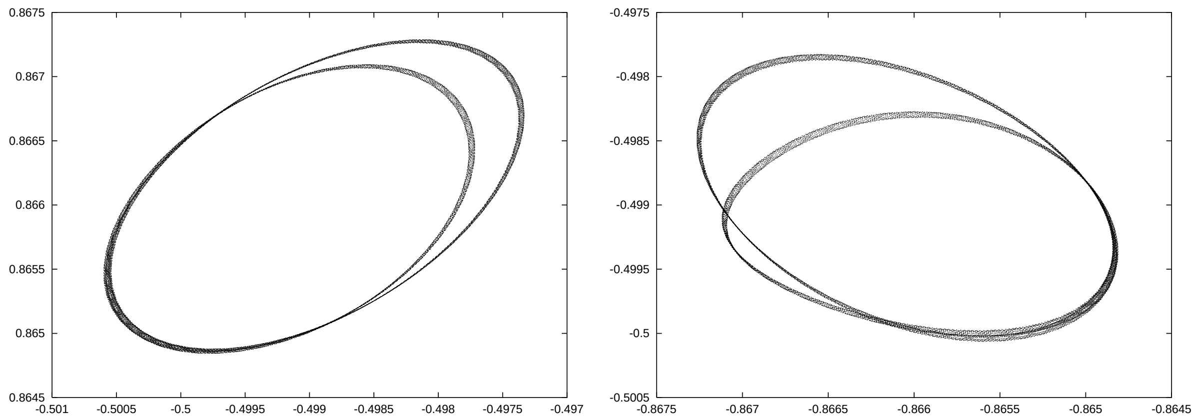

Figure C.10: Projeccions als plans (x, y) i (p_x, p_y) del tor invariant 2-D que substitueix L_5: l'hem anomenat T_5.

C.4.3.2 Forma normal d'ordre 2

Acabem de derivar, doncs, una translació dependent del temps quasi-periòdicament (traslladant l'origen a T_5 per cada instant de temps) que cancela l'ordre 1 del Hamiltonià. Ara, ens centrarem en trobar un canvi lineal (que també depèn del temps quasi-periòdicament) que transforma l'ordre 2 del Hamiltonià a una forma més convenient. Això és, essencialment, la transformació de Floquet quasi-periòdica, però tenint present l'estructura simplèctica del problema. Per simplificar passos següents, apliquem un altre canvi de variables que escriu els termes de grau dos en forma diagonal i expandim el Hamiltonià en sèries de Fourier-Taylor.

El canvi de Floquet quasi-periòdic simplèctic El flux lineal corresponent al camp TCCP al voltant del tor invariant T_5 ve donat per un sistema lineal d'equacions diferencials:

$$\begin{aligned} \dot{z} &= Q(\theta_1, \theta_2) z, \qquad \text{(C.10)} \\ \dot{\theta}_1 &= \omega_{sat}, \\ \dot{\theta}_2 &= \omega_{ura}. \end{aligned}$$

És possible trobar un canvi de variables real, simplèctic i quasi-periòdic, que podem escriure $z = P^r(\theta_1, \theta_2)x$, tal que redueixi l'equació (C.10) a un sistema lineal a coeficients constants real:

$$\dot{x} = Bx, \quad B \neq B(t). \qquad \text{(C.11)}$$

Per tal de construir aquest canvi, usem fortament el resultat de [Jor01], on es veu com (i sota quines condicions) es pot reduïr el "skew product" quasi-periòdic

$$\begin{aligned} \bar{z} &= A(\theta) z, \\ \bar{\theta} &= \theta + \omega, \end{aligned}$$

on $\theta \equiv \theta_2$ i $\omega = 2\pi\left(\frac{\omega_{ura}}{\omega_{sat}} - 1\right) = 2.75080755611202$ és el nombre de rotació de la corba invariant corresponent al tor T_5, a coeficients constants:

$$\bar{y} \;=\; \Lambda y, \tag{C.12}$$

mitjantçant el canvi lineal $z = C(\theta)y$. Λ és una matriu diagonal 6×6 complexa a coeficients constants i satisfà, juntament amb $C(\theta)$, la següent equació:

$$A(\theta)C(\theta) = C(\theta + \omega)\Lambda. \tag{C.13}$$

Si definim l'operador $T_\omega : \Psi(\theta) \in \mathcal{C}(\mathbb{T}^1, \mathbb{C}^n) \to \Psi(\theta+\omega) \in \mathcal{C}(\mathbb{T}^1, \mathbb{C}^n)$ i si anomenem $\Psi_j(\theta)$ la columna j-èssima de la matriu $C(\theta)$, podem escriure el sistema (C.13) per columnes com un problema de valors propis generalitzat:

$$A(\theta)\Psi_j(\theta) = \lambda_j T_\omega \Psi(\theta). \tag{C.14}$$

Calculant els valors i vectors propis d'aquest problema, és possible obtenir tan la matriu B del sistema reduït (C.11) com el canvi quasi-periòdic que m'hi porta $P^r(\theta_1, \theta_2)$.

Implementant aquest canvi de variables, l'ordre dos del Hamiltonià del TCCP queda:

$$H_2^r(x, y) = \frac{1}{2}\omega_1(x_1^2 + y_1^2) + \frac{1}{2}\omega_2(x_2^2 + y_2^2) + \frac{1}{2}\omega_3(x_3^2 + y_3^2), \tag{C.15}$$

on les freqüències prenen els següents valors:

$$\begin{aligned} \omega_1 &= -0.080473064872369, \\ \omega_2 &= 0.996680625156409, \\ \omega_3 &= 1.00006269133083. \end{aligned}$$

De la mateixa manera que en el cas periòdic, no podem usar el teorema de Lagrange-Dirichlet per a deduir-ne l'estabilitat no-lineal, degut als diferents signes pels valors de les freqüències.

Complexificació Com és usual en aquest tipus de càlculs, per tal d'escriure (C.15) en forma diagonal, es complexifica el sistema mitjantçant el canvi de variable (lineal i simplèctic)

$$x_j = \frac{q_j + ip_j}{\sqrt{2}}, \quad y_j = \frac{iq_j + p_j}{\sqrt{2}}, \quad j = 1, 2, 3.$$

Així doncs, després de composar els tres canvis lineals i simplèctics (translació de l'origen sobre T_5, canvi de Floquet quasi-periòdic i complexificació), el grau 2 del Hamiltonià del TCCP queda:

$$H_2^c(q, p) = i\omega_1 q_1 p_1 + i\omega_2 q_2 p_2 + i\omega_3 q_3 p_3, \qquad (q, p) \in \mathbb{C}^6. \tag{C.16}$$

Expansió del Hamiltonià Usant la recurrència dels polinomis de Legendre, és possible expandir el Hamiltonià del TCCP en sèries de Fourier-Taylor. Si prèviament s'han realitzat els canvis que deixen l'ordre 2 en forma normal diagonal, l'expansió, en les variables complexes que acabem de definir, queda:

$$H(q,p,\theta,p_\theta) = \langle \varpi, p_\theta \rangle + H_2(q,p) + \sum_{n\geq 3} H_n(q,p,\theta), \qquad (q,p) \in \mathbb{C}^6\ ,\ \theta \in \mathbb{T}^2, \tag{C.17}$$

on H_2 ve donat per (C.16), $\varpi = (\omega_{sat}, \omega_{ura})$, $\langle \cdot, \cdot \rangle$ és el producte escalar estàndard i $p_\theta = (p_{\theta_1}, p_{\theta_2}) \in \mathbb{C}^2$ són les variables conjugades (moments ficticis) a $\theta = (\theta_1, \theta_2)$.

C.4.3.3 Forma Normal i dinàmica no-lineal

Usant el mètode de les sèries de Lie (en la manera com s'explica a [Jor99]), transformem el Hamiltonià (C.17) a una forma normal truncada a ordre alt ($N = 12$):

$$H = \mathcal{N}(q_1p_1, q_2p_2, q_3p_3) + \mathcal{R}(q_1, q_2, q_3, p_1, p_2, p_3, \theta_1, \theta_2), \tag{C.18}$$

on $\mathcal{N}$ denota la forma normal (que només depèn de ls productes q_jp_j) i $\mathcal{R}$ és el reste (d'ordre més gran que N).

Escrivint (C.18) en variables acció-angle, es té que la forma normal només depèn de les accions (i, per tant, aquesta part és trivialment integrable):

$$\mathcal{N} = \sum_{|k|=1}^{[N/2]} h_k I_1^{k_1} I_2^{k_2} I_3^{k_3}, \qquad k \in \mathbb{Z}^3, \quad h_k \in \mathbb{R}. \tag{C.19}$$

D'altra banda, també calculem el canvi de variables que transforma punts de l'espai (sinòdic) inicial a l'espai on viu la forma normal. L'escrivim com a sèrie de Fourier-Taylor truncada.

Els tipus de moviments, prop del tor L_5, descrits per (C.19) són òrbites quasi-periòdiques que, vistes en l'espai (sinòdic) inicial, corresponen a tors de 3, 4 i 5 dimensions. En la figura C.11, n'hi ha alguns exemples.

C.4.3.4 Integral primera i difusió

Per tal de trobar una regió d'estabilitat efectiva al voltant del tor invariant T_5 en el sistema TCCP, calculem una integral primera aproximada del sistema. Si escrivim aquesta integral primera com una sèrie de Fourier-Taylor

$$F(q,p,\theta_1,\theta_2) = \sum_{n=2}^{N} F_n(q,p,\theta_1,\theta_2),$$

on, F_n és un polinomi homogeni de grau n escrit en les variables complexes (q,p), i amb coeficients que són, a la vegada, sèries de Fourier (truncades) en els angles θ_1 i θ_2:

$$F_n(q,p,\theta_1,\theta_2) = \sum_{|k|=n} \sum_{j=(j_1,j_2)} \left(f_{n,j}^k e^{i(j_1\theta_1 + j_2\theta_2)} \right) q^{k^1} p^{k^2},$$

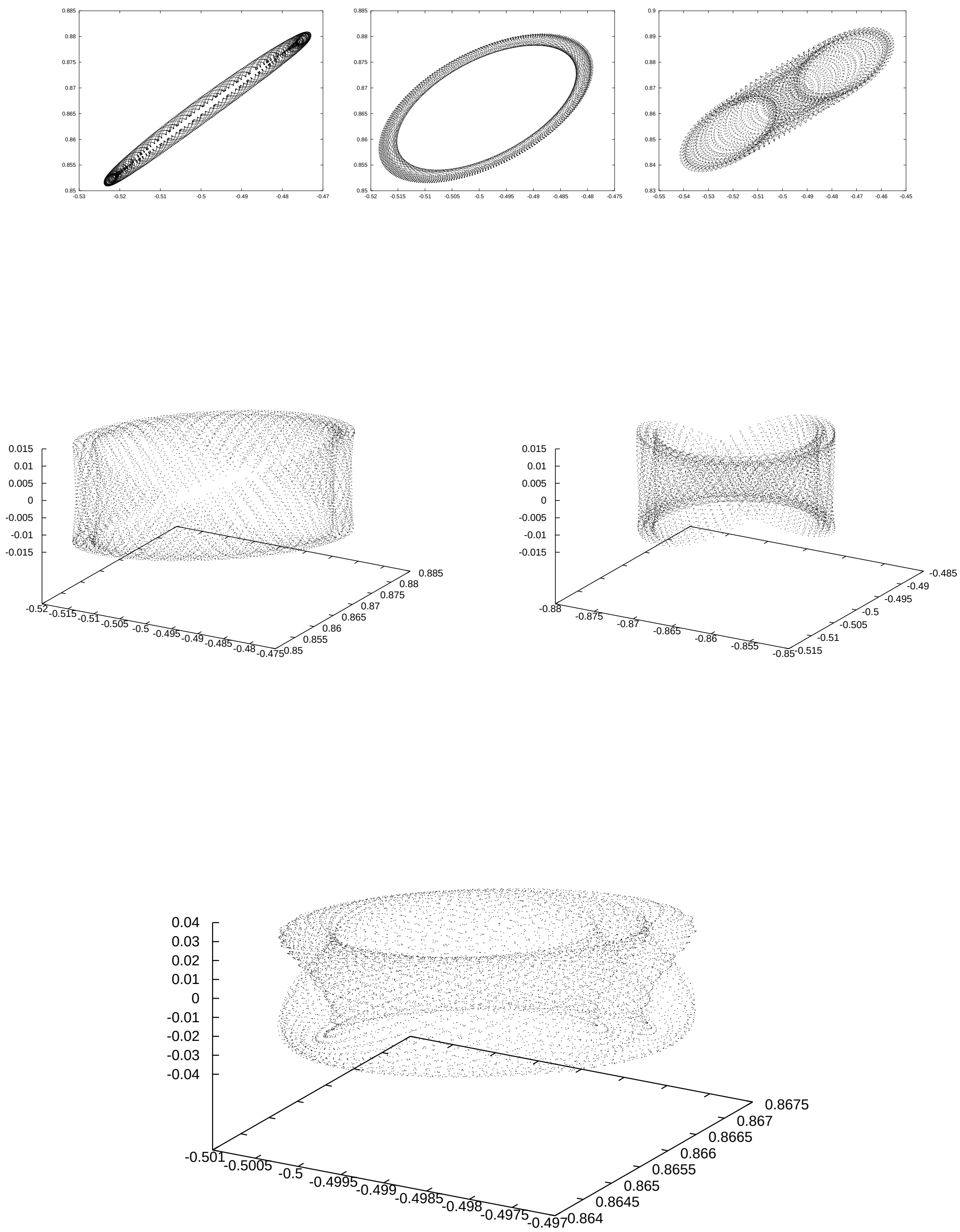

Figure C.11: Diversos tors invariants de 3, 4 i 5 dimensions prop de T_5

llavors l'equació $\{H, F\} = 0$, on H és el Hamiltonià expandit (C.2), ens dóna una recurrència per anar trobant els coeficients de F:

$$f_{n,j}^k = \frac{i c_{n,j}^k}{j_1 \omega_{sat} + j_2 \omega_{ura} - \langle k^2 - k^1, \omega \rangle},$$

on $\omega = (\omega_1, \omega_2, \omega_3)$ i $c_{n,j}^k$ és conegut.

Zona d'estabilitat efectiva Acotant el reste de l'expansió

$$\dot{F} = \{F(x, y, \theta), H(x, y, \theta, p_\theta)\},$$

és possible trobar dominis D_{ρ_0} i D_ρ, on

$$D_\rho = \{(x, y) \in \mathbb{R}^6 \; ; \; (x_1^2 + y_1^2) + (x_2^2 + y_2^2) + (x_3^2 + y_3^2) \leq \rho^2\},$$

tals que si una partícula està dins de D_{ρ_0} a $t = 0$, durant un temps de com a mínim $T = 3 \times 10^9$ ($\sim$ 5 milions d'anys) romandrà dins del domini D_ρ. Els valors trobats per aquests radis són: $\rho_0 = 1.7565 \times 10^{-4}$ i $\rho = 4.9666 \times 10^{-4}$.

C.5 El sistema solar extern

En la última part d'aquest treball, hem realitzat un estudi purament numèric de la dinàmica dels asteroids Troians, mitjantçant el mètode de l'anàlisi de freqüències ([Las93, Las99]). Com a model base usem el sistema solar extern (o OSS), que està format pel Sol, Júpiter, Saturn, Urà, Neptú i la partícula (sense massa) en qüestió.

L'òrbita de cada asteroid és generada integrant numèricament les seves posicions i velocitats real (preses de la base de dades [Bow]) durant uns 5 milions d'anys. El mètode d'integració que s'usa es deu a J. Laskar i P. Robutel ([LR01]) i pertany a la família d'integradors simplèctics. L'ús d'un integrador de tipus simplèctic és recomanable en integracions tan llargues, ja que d'altres integradors (no-simplèctics) podrien incloure "soroll" numèric al sistema i introduir un efecte artificial en el valor de les freqüències. Una de les maneres de mirar l'eficiència d'un mètode d'integració sobre camps conservatius en intervals de temps molt grans és veure com es comporta l'energia (en camps Hamiltonians s'hauria de conservar). Els mètodes simplèctics integren exactament un Hamiltonià proper al que es pretén integrar i, d'aquesta manera, s'obté la conservació d'una energia molt propera a la del sistema (les diferències, en el nostre cas, són aproximadadment de 10^{-13}). Aquest fenòmen no es dóna típicament en altres mètodes d'integració no simplèctics.

Normalment, quan es realitza aquest tipus d'estudi d'una òrbita d'un asteroid, apareixen varies freqüències bàsiques. D'una banda, tenim tres freqüències per cada planeta. La freqüència ràpida (deguda al moviment de rotació al voltant del Sol) i dues de seculars (o lentes) que són degudes a les precessions del periheli i del node. D'altra banda, cada asteroid té també tres freqüències pròpies: la freqüència (ràpida, de període 150 anys) anomenada de libració al voltant del punt triangular, i dues de seculars que provenen dels moviments propis del periheli i del node. Així doncs, es tenen 14 freqüències bàsiques (15-1, perquè la freqüència secular de Júpiter corresponent al node es pot fer zero, veieu [Las90])

C.N.	Name	$\nu\,(deg)$	$g\,(sec)$	$s\,(sec)$
588	Achilles	2.434	344.40	-11.02
617	Patroclus	2.350	310.62	-6.76
624	Hektor	2.316	335.74	-12.99
659	Nestor	2.467	355.01	-16.48
884	Priamus	2.424	353.41	-12.24
911	Agamemnon	2.290	317.35	-8.69
1143	Odysseus	2.439	365.38	-10.91
1172	Aneas	2.366	331.54	-7.92
1173	Anchises	2.371	378.19	-23.67
1208	Troilus	2.199	258.54	-0.45
1404	Ajax	2.310	334.43	-15.15
1437	Diomedes	2.213	331.25	-20.05
1583	Antilochus	2.181	282.18	-10.79
1647	Menelaus	2.438	359.34	-9.96
1749	Telamon	2.421	366.33	-13.79
1867	Deiphobus	2.233	286.24	-5.76
1868	Thersites	2.316	345.09	-20.48
1869	Philoctetes	2.382	388.78	-20.44
1870	Glaukos	2.429	363.50	-9.48
1871	Astyanax	2.311	401.29	-25.28

Table C.1: Freqüències propies dels 20 primers asteroids Troians, calculades en el model OSS. En les dues primeres columnes es pot veure el nombre de catàleg i el nom de l'asteroid, en la segona columna hi ha la freqüència de libració al voltant del corresponent punt de Lagrange i les dues últimes corresponen a les dues freqüències seculars (periheli i node, respectivament).

en el moviment d'un asteroid Troià en el OSS. En la Taula C.1, es mostren les freqüències pròpies dels primers 20 Troians amb nom.

Finalment, també es realitza un anàlisi de freqüències de les òrbites dels Troians en diversos models semi-analítics: el RTBP, BCCP, ERTBP i TCCP, i es comparen els diferents resultats obtinguts. Una de les conclusions que se n'extreu és que tots els models semi-analítics són molt propers entre ells i que, per exemple, donen resultats semblants en la freqüència de libració. Una altra conclusió, més esperable, és que no simulen massa bé el moviment secular ja que les freqüències corresponents a aquest moviment no es detecten massa acuradament.

Un possible treball pel futur seria veure com modificar (o com construir de nou) aquests models per tal de que simulin de manera més acurada el moviment secular, que bàsicament és degut a l'efecte indirecte de les pertorbacions dels planetes sobre Júpiter.

C.6 Conclusions

Els estudis usuals sobre la dinàmica dels asteroids Troians poden ser dividits, a "grosso" modo, en diverses categories segons el model usat per a la seva descripció. Alguns d'aquests treballs fan servir el RTBP. La forma tancada d'aquest model permet que se li puguin aplicar eines analítiques ([GDF$^+$89]) i semi-analítiques ([Sim89, CG91]), per tal de poder concloure'n resultats que són (o propers a) proves matemàtiques.

Alguns altres treballs usen el model OSS. Degut a la seva complexitat, aquest model ha sigut només usat en estudis numèrics, basats en integracions a temps molt grans de les òrbites dels asteroids. Noteu que, genèricament parlant, per deduïr resultats d'estabilitat–analítica–per un asteroid en el OSS requereix un resultat d'estabilitat–analítica–pel mateix OSS, cosa que sembla un problema difícil.

En aquest escenari, hi ha dues maneres de millorar l'estudi de la dinàmica dels ateroids Troians en models realístics:

a) Avenços teòrics: necessitem una teoria d'estabilitat de l'entorn d'una solució quasi-periòdica, preparada per a ser usada en aplicacions pràctiques.

b) Avenços computacionals: necessitem tècniques numèriques per aproximar el moviment dels asteroids Troians, amb un alt grau de precisió.

Recentment, hi ha hagut avenços en ambdues direccions que, aparentment, fan més factible aquest objectiu. D'un costat, tenim resultats de teoria KAM que no requereixen variables acció-angle i que poden ser aplicats lluny dels punts d'equilibri.[1] Només cal poder calcular una òrbita quasi-periòdica aproximada (més algunes condicions tècniques, veieu [Gon02] pels detalls). D'altra banda, avenços recents en tècniques computacionals permeten el càlcul de trajectòries quasi-periòdiques de sistemes Hamiltonians de forma acurada (veieu, per exemple, [RL01] o els capítols previs d'aquesta memòria).

El treball que es presenta pot ser vist com el principi d'un projecte a llarg termini que té com a objectiu omplir el buit que hi ha entre desenvolupaments teòrics sobre estabilitat

[1] Això s'ha fet a [JV98], però usant encara variables acció-angle, que fan que els càlculs siguin extremadament feixucs.

de sistemes Hamiltonians i el càlcul numèric d'òrbites regulars. El fi últim és el de calcular solucions quasi-periòdiques per un asteroid Troià[2] i usar un resultat del tipus contingut a [Gon02] per concloure'n la seva estabilitat per un temps de vida estimat de l'edat del sistema solar.

En aquest treball, hem intentat desenvolupar alguns passos bàsics en aquesta direcció. Primer, s'han construït alguns models que poden ser vistos com a correccions del RTBP per tal d'apropar-nos al OSS. Després, hem dissenyat mètodes numèrics i software per tal de calcular solucions quasi-periòdiques, la seva teoria de Floquet simplèctica, formes normals (i integrals primeres aproximades) fins a ordre alt, i procediments per tal d'acotar els seus restes i, així poder deduir regions d'estabilitat efectiva al voltant d'aquestes òrbites. Ho hem fet de forma gradual, des de models més simples (BCCP) fins a models més complexes (BAP i TCCP).

C.6.1 Sobre els models periòdics

En C.2, hem desenvolupat un model pel moviment d'un asteroid sota l'atracció gravitatòria del Sol, Júpiter i Saturn. Aquest model està basat en el càlcul, en coordenades adequades, d'una òrbita periòdica d'aquest problema de tres cossos. Aquest model és l'extensió natural del RTBP per tal d'incloure tres primaris, en el sentit de que es mouen en la solució més simple de tipus planetari. Llavors, suposant que el Sol, Júpiter i Saturn es mouen en aquesta òrbita, no és difícil escriure les equacions de moviment per l'asteroid; això és el que anomenem BCCP. En coordenades adequades, el BCCP és una pertorbació periòdica del ben conegut RTBP.

En el BCCP, els punts de Lagrange $L_{4,5}$ són reemplaçats per òrbites periòdiques. Així doncs, hem realitzat un estudi de la dinàmica al voltant d'aquesta òrbita periòdica. Mitjantçant la construcció d'una forma normal a ordre alt, és possible calcular al seu voltant aproximacions a tors invariants (de dimensions 2, 3 i 4). És més, usant estimacions adequades del reste d'aquest forma normal, hem calculat una regió per la qual el temps necessari per tal d'escapar-se'n és més gran que l'edat del sistema solar. Hem usat, també, una segona aproximació per calcular aquesta zona d'estabilitat efectiva: la construcció d'una integral primera adequada. Hem vist que la integral primera produeix una zona d'estabilitat efectiva un pèl més gran, però, d'altra banda, no proporciona una descripció completa de la dinàmica dins d'aquesta regió, tal i com sí fa la forma normal.

L'apartat C.3 pot ser vist com una aplicació de les eines desenvolupades en l'apartat previ. Els resultat obtinguts no són completament nous (veieu [JS94]); tot i que el procés de construcció difereix lleugerament (nosaltres hem usat el temps físic com a variable independent mentre que en [JS94] s'usa l'anomalia verdadera) i també hem calculat una integral primera aproximada. Un dels interessos principals d'aquest model és que inclou la ressonància (exacte) 1:1 entre un dels modes verticals de l'òrbita periòdica que reemplaça L_5 i la freqüència de la pertorbació.

[2]Evidentment, els Troians pels quals la dinàmica no és quasi-periòdica no es consideren.

C.6.2 Sobre els models quasi-periòdics

L'apartat C.4 conté, en la nostra opinió, els resultats més interessants d'aquesta memòria. Hem considerat els desenvolupaments de models millors que el BCCP, de dos maneres diferents. Primer, hem calculat una solució quasi-periòdica del problema general (pla) de tres cossos (BAP) per simular d'una millor manera el moviment de Júpiter (comparat amb el BCCP), i després hem afegit un quart cos massiu (Urà) al model (TCCP). Un altre cop, la solució que hem calculat ple sistema Sol-Júpiter-Saturn-Urà és la solució més simple de tipus planetari. En aquest sentit, el TCCP és l'extensió natural del RTBP que inclou quatre primaris.[3]

Després ens centrem en l'estudi preliminar del model TCCP. Tot i que el BAP no ha sigut estudiat en la memòria, conté aspectes interessants que el fan digne de considerar. Per exemple, la pertorbació respecte el RTBP és bastant forta, cosa que sembla produïr bifurcacions prop dels punts triangulars. Això es tracta de treball actual.

L'estudi del TCCP està basat en el càlcul de l'òrbita quasi-periòdica que substitueix el punt d'equilibri, en el canvi de Floquet simplèctic per a aquesta òrbita i en la construcció d'una forma normal per descriure la dinàmica no lineal en una zona propera a L_5. D'altra banda, s'ha usat una integral primera aproximada per trobar una zona d'estabilitat efectiva. Pensem que les eines desenvolupades en aquest capítol seran molt útils en estudis futurs d'aquest problema.

Un aspecte interessant que, pensem, cal remarcar és que les regions d'estabilitat efectiva pels diferent models no es contenen les unes a les altres. Això és degut al fet de que, quan la pertorbació és canviada, la solució que substitueix el punt de Lagrange canvia, de tal manera que la regió d'estabilitat es mou a un lloc diferent. En particular, això implica que, per exemple, les regions d'estabilitat pel BCCP i pel TCCP no són contingudes en la regió d'estabilitat del RTBP.

C.6.3 Sobre el model OSS

Per tal de discutir la qualitat dels models previs (i també per qualsevol altre model) és necessari comparar-los amb la dinàmica del sistema solar real. Amb aquesta finalitat, en l'apartat C.5, hem realitzat integracions numèriques a temps molt llarg del model OSS. Més concretament, hem calculat les freqüències pròpies de 420 asteroids Troians. Per cada asteroid, hi ha 14 freqüències que juguen algun paper: tenim 3 freqüències pròpies (una de ràpida i dues de seculars) per a cada planeta (excepte per Júpiter, pel qual una de secular es pot fer zero) i les pròpies de l'asteroid. Aquestes freqüències pròpies de l'asteroid són la freqüència de libració (al voltant del corresponent punt de Lagrange) i les dues seculars (corresponents a les precessions del node i del periheli). S'ha fet un anàlisi similar pels models RTBP, ERTBP, BCCP i TCCP.

Una conclusió general és que tots aquests models simulen d'una manera acceptable el moviment libracional però, d'altra banda, no és així pel moviment secular per cap dels models, principalment pel fet de que el moviment de Júpiter és massa llunyà al real.

Una conclusió important de tots aquests càlculs és que el RTBP no és un model prou acurat per descriure el moviment dels Troians. De fet, com que el BCCP, ERTBP i TCCP

[3]Una metodologia diferent per la constrcucció de models semi-analítics és la donada en [GMM02].

són encara massa propers al RTBP, esdevé que cap d'ells tampoc és un model acurat per la familia de Troians. De totes maneres, també volem fer notar que el nivell de precisió d'aquests models no és uniforme si no que depèn de l'asteroid que es consideri.

Tot i que sembli que els models desenvolupats no són massa propers a la realitat per tal de ser considerats interessants, creiem que és necessari desenvolupar mètodes, eines i algorismes numèrics que siguin capaços de tractar-los com a un pas previ a tractar models realistes. En aquest sentit, també pensem que algunes tènciques desenvolupades en aquesta memòria (principalment, el càlcul de la dinàmica al voltant de solucions quasi-periòdiques) poden tenir un paper rellevant en el futur.

Agraïments

Primer de tot, vull agrair molt sincerament al meu director de tesi, Àngel Jorba, pel temps i per l'esforç que m'ha dedicat durant la realització d'aquest treball. També voldria destacar la seva capacitat de mestratge que m'ha permès iniciar en l'apassionant món de la mecànica celest i aprendre una diversitat de tècniques numèriques molt útils a l'hora d'estudiar sistemes dinàmics.

Agraeixo al Departament de Matemàtica Aplicada i Anàlisi de la Universitat de Barcelona, per deixar-me els mitjans necessaris per tal de realitzar aquest treball, i a tots els companys (antics i actuals) que d'alguna manera o d'una altra m'han ajudat. Voldria mencionar especialment als amics Gerard Albà, Miquel Àngel Andreu, Imma Baldomà, Heri Coll, Àlex Haro, Xavi Massaneda, Eva Miranda, Quim Ortega, Laura Prat, Javi Rodríguez, Xavi Tolsa i Joan Vidal.

Agraeixo a Josep Maria Mondelo, per haver-me permès usar la seva rutina d'anàlisi de freqüències, que m'ha estat útil a l'hora de testejar alguns resultats.

Agraeixo a l'"Institut de Mécanique Céleste et de Calcul des Éphémerides" de Paris, per haver-me acollit en dues estades de recerca on vaig començar a aprendre les tècniques que s'han usat al Capítol 5 i molt especialment a la persona amb la qual vaig col.laborar, Philippe Robutel.

Agraeixo a la Nati, la secretaria del departament, per les múltiples tasques burocràtiques que ha realitzar per mi.

Aprofito, també, per dir dos mots d'agraïment a la persona que em va animar a entrar en el departament i que podríem fer, en part, responsable de que jo hagi realitzat aquesta tesi, però que malauradament ja no és entre nosaltres, l'August Palanques.

Ja fora de l'àmbit de feina, agraeixo als meus amics d'Avinyonet per les moltes estones de diversió que hem passat junts i als meus amics d'Efecte Bandwagon i de BeatleStones pels grans "moments musicals" que hem viscut dalt dels escenaris i, sobretot, fora d'ells.

Finalment, no tinc paraules per poder agrair tot el que han fet per mi els meus avis, els meus pares, el meu germà i la Maria. Sense el suport de tots ells, aquest treball no s'hauria pogut realitzar mai.

Bibliography

[AKN88] V.I. Arnold, V.V. Kozlov, and A.I. Neishtadt. *Dynamical Systems III*, volume 3 of *Encyclopaedia Math. Sci.* Springer, Berlin, 1988.

[And98] M.A. Andreu. *The quasi-bicircular problem.* PhD thesis, Univ. Barcelona, 1998.

[And02] M. A. Andreu. Dynamics in the center manifold around L_2 in the quasi-bicircular problem. *Celestial Mech. Dynam. Astronom.*, 84(2):105–133, 2002.

[Arn63] V.I. Arnold. Proof of A.N. Kolmogorov's theorem on the preservation of quasi-periodic motions under small perturbations of the Hamiltonian. *Russian Math. Surveys*, 18(5):9–36, 1963.

[Arn64] V.I. Arnold. Instability of dynamical systems with several degrees of freedom. *Soviet Math. Dokl.*, 5:581–585, 1964.

[AS00] M.A. Andreu and C. Simó. The quasi-bicircular problem for the Earth-Moon-Sun parameters. Preprint, 2000.

[BFG98] G. Benettin, F. Fassò, and M. Guzzo. Nekhoroshev-stability of L_4 and L_5 in the spatial Restricted Three-Body Problem. *Regul. Chaotic Dyn.*, 3(3):56–72, 1998.

[BHJ+03] H.W. Broer, H. Hanßmann, À. Jorba, J. Villanueva, and F. Wagener. Normal-internal resonances in quasi-periodically forced oscillators: a conservative approach. Preprint, 2003.

[BHS96] H.W. Broer, G.B. Huitema, and M.B. Sevryuk. *Quasi-Periodic Motions in Families of Dynamical Systems: Order amidst Chaos*, volume 1645 of *Lecture Notes in Math.* Springer, New York, 1996.

[BJ87] R. Bien and Schubart J. Three characteristic orbital parameters for the Trojan group of asteroids. *Astron. Astrophys.*, 175:292–298, 1987.

[BLH90] E. Bowell, D. H. Levy, and H. E. Holt. 1990 MB. *IAU Circ.*, 5047:3–+, July 1990.

[Bow] E. Bowell. The asteroid orbital elements database. Project funded principally by NASA grant NAG5-4741, and in part by the

Lowell Observatory endowment. For more information, visit the URL `http://www.naic.edu/~nolan/astorb.html`.

[BR01] C. Beaugé and F. Roig. A semianalytical model for the motion of the trojan asteroids: Proper elements and families. *Icarus*, 153:391–415, 2001.

[CG91] A. Celletti and A. Giorgilli. On the stability of the Lagrangian points in the spatial Restricted Three Body Problem. *Celestial Mech.*, 50(1):31–58, 1991.

[CGJ+96] V. Companys, G. Gómez, À. Jorba, J. Masdemont, J. Rodríguez, and C. Simó. Use of Earth-Moon libration points for future missions. In K.T. Alfriend, I.M. Ross, A.K. Misra, and C.F. Peters, editors, *AAS/AIAA Astrodynamics Conference*, volume 90 of *Advances in the Astronautical Sciences*, pages 1655–1666, San Diego, U.S.A., 1996. American Astronautical Society.

[CJ00] E. Castellà and À. Jorba. On the vertical families of two-dimensional tori near the triangular points of the Bicircular problem. *Celestial Mech.*, 76(1):35–54, 2000.

[CRR64] J. Cronin, P.B. Richards, and L.H. Russell. Some periodic solutions of a four-body problem. *Icarus*, 3:423–428, 1964.

[Dan62] J.M.A. Danby. *Fundamentals of Celestial Mechanics.* Willmann-Bell, Inc., Richmond, Virginia, 1962.

[Dan64] J.M.A. Danby. Stability of the triangular points in the elliptic restricted problem of three bodies. *Astron. J.*, 69:165–172, 1964.

[DDB67] A. Deprit and A. Deprit-Bartolome. Stability of the triangular Lagrangian points. *Astron. J.*, 75(2):173–179, 1967.

[DJS91] C. Díez, À. Jorba, and C. Simó. A dynamical equivalent to the equilateral libration points of the real Earth-Moon system. *Celestial Mech.*, 50(1):13–29, 1991.

[dlL01] R. de la Llave. A tutorial on KAM theory. In *Smooth ergodic theory and its applications (Seattle, WA,1999)*, volume 69 of *Proc. Sympos. Pure Math.*, pages 175–292. Amer. Math. Soc., Providence, RI, 2001.

[Dou88] R. Douady. Stabilité ou instabilité des points fixes elliptiques. *Ann. Sci. École Norm. Sup. (4)*, 21:1–46, 1988.

[FM01] E. Fontich and P. Martín. Arnold diffusion in perturbations of analytic integrable Hamiltonian systems. *Discrete Contin. Dynam. Systems*, 7(1):61–84, 2001.

[GDF+89] A. Giorgilli, A. Delshams, E. Fontich, L. Galgani, and C. Simó. Effective stability for a Hamiltonian system near an elliptic equilibrium point, with an application to the restricted three body problem. *J. Differential Equations*, 77:167–198, 1989.

[GG78] A. Giorgilli and L. Galgani. Formal integrals for an autonomous Hamiltonian system near an equilibrium point. *Celestial Mech.*, 17:267–280, 1978.

[Gio88] A. Giorgilli. Rigorous results on the power expansions for the integrals of a Hamiltonian system near an elliptic equilibrium point. *Ann. Inst. H. Poincaré Phys. Théor.*, 48(4):423–439, 1988.

[GJMS91a] G. Gómez, À. Jorba, J. Masdemont, and C. Simó. Quasiperiodic orbits as a substitute of libration points in the solar system. In A.E. Roy, editor, *Predictability, Stability and Chaos in N-Body Dynamical Systems*, pages 433–438. Plenum Press, 1991.

[GJMS91b] G. Gómez, À. Jorba, J. Masdemont, and C. Simó. A quasiperiodic solution as a substitute of l_4 in the Earth-Moon system. In *Proceedings of the 3rd International Sysmposium on Spacecraft Flight Dynamics*, pages 35–41, ESTEC, Noordwijk, Holand, 1991. ESA Publications Division.

[GJMS93] G. Gómez, À. Jorba, J. Masdemont, and C. Simó. Study of Poincaré maps for orbits near Lagrangian points. ESOC contract 9711/91/D/IM(SC), final report, European Space Agency, 1993.

[GLMS85] G. Gómez, J. Llibre, R. Martínez, and C. Simó. Station keeping of libration point orbits. ESOC contract 5648/83/D/JS(SC), final report, European Space Agency, 1985.

[GM01] G. Gómez and J.M. Mondelo. The dynamics around the collinear equilibrium points of the RTBP. *Phys. D*, 157(4):283–321, 2001.

[GMM02] G. Gómez, J. Masdemont, and J.M. Mondelo. Solar system models with a selected set of frequencies. *Astron. Astrophys.*, 390(2):733–749, 2002.

[GMS02] G. Gómez, J.M. Mondelo, and Simó S. Refined Fourier analysis: procedures, error estimates and applications. Preprint, 2002.

[Gon02] A. González. *On the existence of invariant tori for symplectic maps.* PhD thesis, Univ. Barcelona, 2002.

[GS97] A. Giorgilli and C. Skokos. On the stability of the Trojan asteroids. *Astron. Astrophys.*, 317:254–261, 1997.

[Had80] J. D. Hadjidemetriou. The restricted planetary 4-body problem. *Celestial Mechanics*, 21:63–71, January 1980.

[Jor99] À. Jorba. A methodology for the numerical computation of normal forms, centre manifolds and first integrals of Hamiltonian systems. *Exp. Math.*, 8(2):155–195, 1999.

[Jor00a] À. Jorba. A numerical study on the existence of stable motions near the triangular points of the real Earth-Moon system. *Astron. Astrophys.*, 364(1):327–338, 2000.

[Jor00b] À. Jorba. On practical stability regions for the motion of a small particle close to the equilateral points of the real Earth–Moon system. In *Proceedings of the* III International Symposium HAMSYS-98. Geometrical Methods in Hamiltonian Systems and Celestial Mechanics. *Pátzcuaro (México), December 7–11, 1998.* World Scientific, 2000.

[Jor01] À. Jorba. Numerical computation of the normal behaviour of invariant curves of n-dimensional maps. *Nonlinearity*, 14(5):943–976, 2001.

[JPL] `http://ssd.jpl.nasa.gov/horizons.html`.

[JS94] À. Jorba and C. Simó. Effective stability for periodically perturbed Hamiltonian systems. In J. Seimenis, editor, *Hamiltonian Mechanics: Integrability and Chaotic Behaviour*, volume 331 of *NATO Adv. Sci. Inst. Ser. B Phys.*, pages 245–252. Held in Toruń, Polland, 28 June–2 July 1993. Plenum, New York, 1994.

[JS96] À. Jorba and C. Simó. On quasiperiodic perturbations of elliptic equilibrium points. *SIAM J. Math. Anal.*, 27(6):1704–1737, 1996.

[JV97a] À. Jorba and J. Villanueva. On the normal behaviour of partially elliptic lower dimensional tori of Hamiltonian systems. *Nonlinearity*, 10:783–822, 1997.

[JV97b] À. Jorba and J. Villanueva. On the persistence of lower dimensional invariant tori under quasi-periodic perturbations. *J. Nonlinear Sci.*, 7:427–473, 1997.

[JV98] À. Jorba and J. Villanueva. Numerical computation of normal forms around some periodic orbits of the Restricted Three Body Problem. *Phys. D*, 114:197–229, 1998.

[JV01] À. Jorba and J. Villanueva. The fine geometry of the Cantor families of invariant tori in Hamiltonian systems. In *European Congress of Mathematics, Vol. II (Barcelona, 2000)*, volume 202 of *Progr. Math.*, pages 557–564. Birkhäuser, Basel, 2001.

[KMF+91] Z. Kneževíc, A. Milani, P. Farinella, Ch. Froeschlé, and C. Froeschlé. Secular resonances from 2 to 50 AU. *Icarus*, 93:316–330, 1991.

[Kol54] A.N. Kolmogorov. On the persistence of conditionally periodic motions under a small change of the Hamilton function. *Dokl. Acad. Nauk. SSSR*, 98(4):527–530, 1954.

[Las89] J. Laskar. Les variables de poincaré et le developpement de la fonction perturbatrice. Notes scientifiques et techniques du Bureau des Longitudes S026, Groupe de travail sur la lecture des Méthodes nouvelles de la Mécanique Céleste, 1989.

[Las90] J. Laskar. The chaotic motion of the Solar System. A numerical estimate of the size of the chaotic zone. *Icarus*, 88:266–291, 1990.

[Las93] J. Laskar. Frequency analysis for multi-dimensional systems. Global dynamics and diffusion. *Phys. D*, 67:257–281, 1993.

[Las99] J. Laskar. Introduction to frequency map analysis. In C. Simó, editor, *Hamiltonian Systems with Three or More Degrees of Freedom*, NATO ASI, pages 134–150. Kluwer, Dordrecht, 1999.

[Leo62] A.M. Leontovich. On the stability of the Lagrange periodic solutions of the restricted problem of three bodies. *Soviet Math. Dokl.*, 3:425–428, 1962.

[LR01] J. Laskar and P. Robutel. High order symplectic integrators for perturbed Hamiltonian systems. *Celestial Mech.*, 80:39–62, 2001.

[LSS97] H.F. Levison, E.M. Shoemaker, and C.S. Shoemaker. The long-term dynamical stability of Jupiter's Trojan asteroids. *Nature*, 385:42–44, 1997.

[Mar71] A.P. Markeev. Stability of the triangular Lagrangian solutions of the restricted three-body problem in the three-dimensional circular case. *Soviet Astronom. AJ*, 15:682–686, 1971.

[Mar73] A.P. Markeev. On the stability problem for the Lagrange solutions of the restricted three-body problem. *J. Appl. Math. Mech.*, 37:713–717, 1973.

[Mar80] C. Marchal. The quasi integrals. *Celestial Mech.*, 21:183–191, 1980.

[Mar90] C. Marchal. *The three-body problem.* Elsevier, 1990.

[MH92] K. R. Meyer and G. R. Hall. *Introduction to Hamiltonian Dynamical Systems and the N-Body Problem.* Springer, New York, 1992.

[Mil93] A. Milani. The Trojan asteroid belt: proper elements, stability, chaos and families. *Celestial Mech.*, 57:59–94, 1993.

[Mil94] A. Milani. The dynamics of the trojan asteroids. In *IAU Symp. 160: Asteroids, Comets, Meteors 1993*, volume 160, pages 159–174, 1994.

[MK90] A. Milani and Z. Knežević. Secular perturbation theory and computation of asteroid proper elements. *Celestial Mech.*, 49:347–411, 1990.

[MK92] A. Milani and Z. Knežević. Asteroid proper elements and secular resonances. *Icarus*, 98:211–232, 1992.

[Mos62] J. Moser. On invariant curves of area-preserving mappings of an annulus. *Nachr. Akad. Wiss. Göttingen Math.-Phys. Kl. II*, 2:1–20, 1962.

[MS86] K. R. Meyer and D. S. Schmidt. The stability of the Lagrange triangular point and a theorem of Arnold. *J. Differential Equations*, 62(2):222–236, 1986.

[Nek77] N.N. Nekhoroshev. An exponential estimate of the time of stability of nearly-integrable Hamiltonian systems. *Russian Math. Surveys*, 32:1–65, 1977.

[Nie96] L. Niederman. Stability over exponentially long times in the planetary problem. *Nonlinearity*, 9(1):1703–1751, 1996.

[NMC89] A.M. Nobili, A. Milani, and M. Carpino. Fundamental frequencies and small divisors in the orbits of the outer planets. *Astron. Astrophys.*, 210:313–336, 1989.

[PLDB99] E. Pilat-Lohinger, R. Dvorak, and CH. Burger. Trojans in stable chaotic motion. *Celestial Mech.*, 73:117–126, 1999.

[PMW+03] J. A. Pittichova, K. J. Meech, L. H. Wasserman, D. E. Trilling, R. L. Millis, M. W. Buie, S. D. Kern, K. B. Clancy, L. E. Hutchison, E. Chiang, and B. G. Marsden. 2001 QR322. *Minor Planet Circulars*, pages 55–+, January 2003.

[RL01] P. Robutel and J. Laskar. Frequency map and global dynamics in the Solar System I. *Icarus*, 152:4–28, 2001.

[Rut83] R. Ruth. A canonical integration technique. *IEEE Tran. Nucl. Sci.*, 30:2669–2671, 1983.

[SB86] J. Schubart and R. Bien. On the computation of characteristic orbital elements for the trojan group of asteroids. In *Asteroids, Comets, Meteors II*, pages 153–156, 1986.

[SB87] J. Schubart and R. Bien. Trojan asteroids - Relations between dynamical parameters. *Astron. Astrophys.*, 175:299–302, 1987.

[SD00] C. Skokos and A. Dokoumetzidis. Effective stability of the Trojan asteroids. *Astron. Astrophys.*, 367:729–736, 2000.

[SGJM95] C. Simó, G. Gómez, À. Jorba, and J. Masdemont. The Bicircular model near the triangular libration points of the RTBP. In A.E. Roy and B.A. Steves, editors, *From Newton to Chaos*, pages 343–370, New York, 1995. Plenum Press.

[Sim89] C. Simó. Estabilitat de sistemes Hamiltonians. *Mem. Real Acad. Cienc. Artes Barcelona*, 48(7):303–348, 1989.

[Sze67] V. Szebehely. *Theory of Orbits.* Academic Press, 1967.

[TDPL00] K. Tsiganis, R. Dvorak, and E. Pilat-Lohinger. Thersites: a 'jumping' Trojan? *Astron. Astrophys.*, 354:1091–1100, 2000.

[Whi52] E.T. Whittaker. *A treatise on the analytical dynamics of particles and rigid bodies: with an introduction to the problem of three bodies.* Cambridge Univ. Press, Cambridge, 1952.